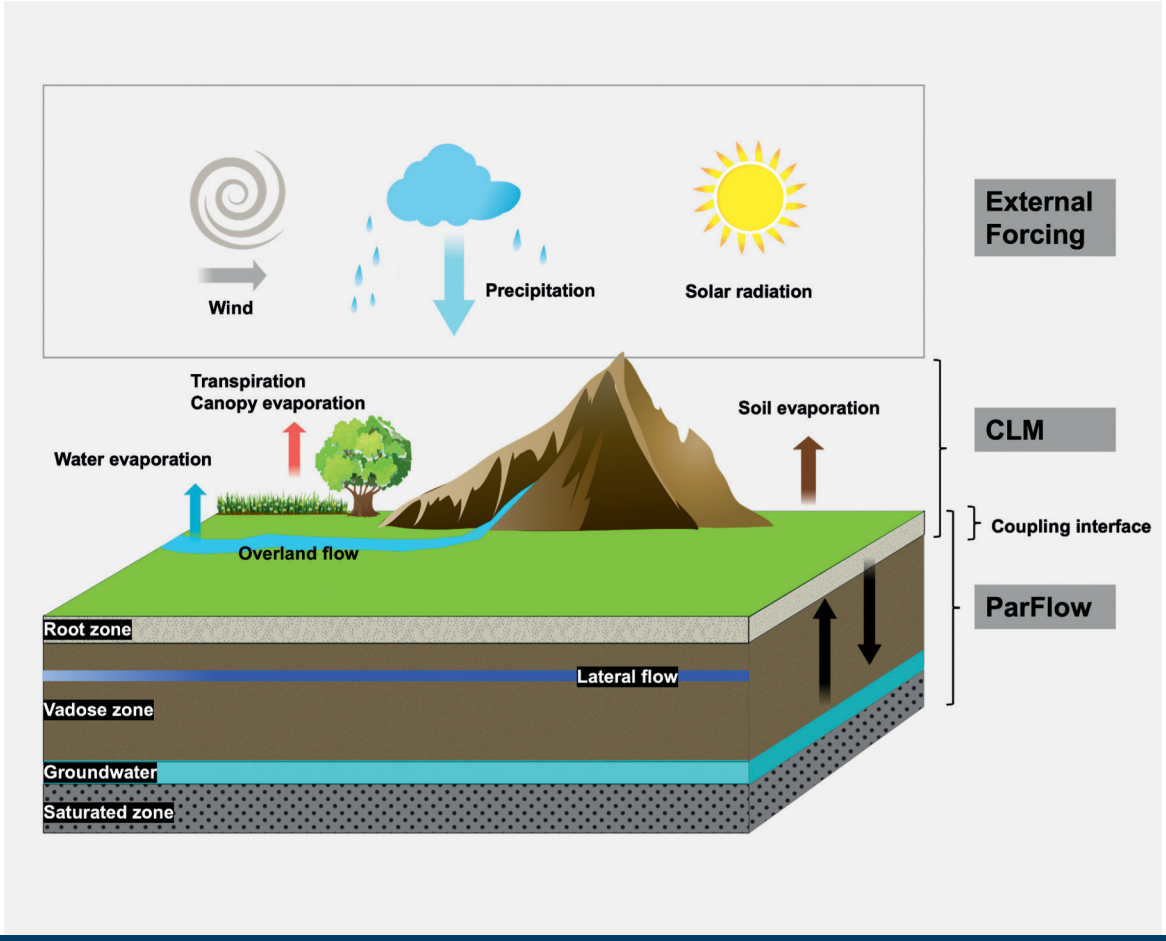

Towards improved representation of the hydrological cycle by assimilating multi-source remotely sensed soil moisture data in terrestrial system models

Haojin Zhao

Energie & Umwelt / Energy & Environment
Band / Volume 721
ISBN 978-3-95806-953-4

Mitglied der Helmholtz-Gemeinschaft

JÜLICH
Forschungszentrum

Schriften des Forschungszentrums Jülich
Reihe Energie & Umwelt / Energy & Environment Band / Volume 721

Forschungszentrum Jülich GmbH
Institut für Bio- und Geowissenschaften (IBG)
Agrosphäre (IBG-3)

Towards improved representation of the hydrological cycle by assimilating multi-source remotely sensed soil moisture data in terrestrial system models

Haojin Zhao

Schriften des Forschungszentrums Jülich
Reihe Energie & Umwelt / Energy & Environment Band / Volume 721

ISSN 1866-1793 ISBN 978-3-95806-953-4

Bibliografische Information der Deutschen Nationalbibliothek.
Die Deutsche Nationalbibliothek verzeichnet diese Publikation in der
Deutschen Nationalbibliografie; detaillierte Bibliografische Daten
sind im Internet über http://dnb.d-nb.de abrufbar.

Herausgeber und Vertrieb:	Forschungszentrum Jülich GmbH Zentralbibliothek, Verlag 52425 Jülich Tel.: +49 2461 61-5368 Fax: +49 2461 61-6103 zb-publikation@fz-juelich.de www.fz-juelich.de/zb
Umschlaggestaltung:	Grafische Medien, Forschungszentrum Jülich GmbH
Druck:	Grafische Medien, Forschungszentrum Jülich GmbH
Copyright:	Forschungszentrum Jülich 2026

Schriften des Forschungszentrums Jülich
Reihe Energie & Umwelt / Energy & Environment, Band / Volume 721

D 82 (Diss. RWTH Aachen University, 2025)

ISSN 1866-1793
ISBN 978-3-95806-952-7 (Print)
ISBN 978-3-95806-953-4 (E-Book)

Vollständig frei verfügbar über das Publikationsportal des Forschungszentrums Jülich (JuSER)
unter www.fz-juelich.de/zb/openaccess.

This is an Open Access publication distributed under the terms of the Creative Commons Attribution License 4.0, which permits unrestricted use, distribution, and reproduction in any medium, provided the original work is properly cited.

Contents

List of Figures

List of Tables

List of Acronyms

AMSR-E	Advanced Microwave Scanning Radiometer for the Earth Observing System.
AMSR2	Advanced Microwave Scanning Radiometer 2.
ASCAT	The Advanced SCATterometer.
BT	Brightness Temperature.
CATHY	CATchment HYdrology.
CDF	Cumulative Distribution Function.
CESM	Community Earth System Model.
CLM	Community Land Model.
CMEM	The Community Microwave Emission Modeling.
CoLM	Common Land Model.
COSMO	Consortium for Small-Scale Modelling.
CRNS	Cosmic-Ray Neutron Sensor.
DA	Data Assimilation.
DCA	Dual Channel Algorithm.
DGG	Discrete Global Grid.
DWD	Deutscher Wetterdienst, German Meteorological Service.
EASE2	Equal-Area Scalable Earth-2.
EC	Eddy Covariance.
ECMWF	Medium-Range Weather Forecasts.
EnKF	Ensemble Kalman Filter.
ERA5	ECMWF Reanalysis v5.
ESA	European Space Agency.
ESMF	Earth System Modeling Framework.
ET	Evapotranspiration.
FDR	frequency Domain Reflectometry.
GCOM-W1	The Global Change Observation Mission - Water 1.
GEOS-5	The Goddard Earth Observing System version 5.
GLDAS	Global Land Data Assimilation System.
ICOS	Integrated Carbon Observation System.
ISBA	Interaction Soil Biosphere Atmosphere.
LEnKF	Localised Ensemble Kalman Filter.
LETKF	Local Ensemble Transform Kalman Filter.
LPRM	The Land Parameter Retrieval Model.
LSMs	Land Surface Models.
LSTM	Long Short Term Memory network.
Merra-Land	Modern-Era Retrospective Analysis for Research and Applications Land.
Metop	Meteorological Operational Platform.
ML	Machine learning.
MODIS	Moderate Resolution Imaging Spectroradiometer.

NASA	The National Aeronautics and Space Administration.
NCAR	The National Center for Atmospheric Research.
NCL	NCAR Command Language.
NN	Nearest Neighbor.
Noah-MP	Noah-Multiparameterization Land Surface Model.
NRW	North Rhine-Westphalia.
NSIDC	National Snow and Ice Data Center.
OASIS	Ocean Atmosphere Sea Ice Soil.
ParFlow	Parallel Watershed Flow Model.
PAWS	Process-based Adaptive Watershed Simulator.
PDAF	The Parallel Data Assimilation Framework.
PIHM	Penn State Integrated Hydrologic Model.
RMSD	Root Mean Square Difference.
RNN	Recurrent Neural Network.
SMAP	Soil Moisture Active/Passive.
SMOS	Soil Moisture and Ocean Salinity.
SNR	Signal-to-Noise Ratio.
TC	Triple Collocation.
TDR	Time Domain Reflectometry.
TDT	Time Domain Transmissivity.
TERENO	TERrestrial EnviroNmental Observations.
Tibet-Obs	Tibetan Plateau Observatory of Plateau Scale Soil Moisture and Soil Temperature.
TSMP	Terrestrial System Modelling Platform.
TxSON	Texas Soil Observation Network.
ubRMSD	Unbiased Root Mean Square Difference.
ubRMSE	Unbiased Root Mean Square Error.
VIC	Variable Infiltration Capacity Model.

Abstract

Soil moisture is a key variable in the water and energy cycles at the atmosphere-land-vegetation interface. Accurate and continuous soil moisture data are essential for many applications, including water resources management, drought monitoring, and agricultural forecasting. In situ soil moisture measurements from laboratories or sensors are limited by spatial coverage and high cost. Land surface models (LSMs) can simulate soil moisture from point to large scales, but are subject to simplified parameterizations and uncertainties due to model structure and input data. For example, the role of lateral water flow is typically not represented in LSMs. The advent of remote sensing technologies has made it possible to obtain soil moisture information on a large scale and in near real-time. However, soil moisture retrievals are coarse and limited by dense vegetation, complex topography, and frozen soils. Data assimilation (DA) can use data from sources like remote sensing to improve the performance of land surface models. We evaluated LSM simulations over a temperate-climate region with complex topography and land forms in western Germany, using a variety of data types, e.g., soil moisture and evapotranspiration (ET). One objective of this PhD research was to assess the influence of considering lateral flow and the subsurface on the simulation of soil moisture and other hydrological variables, and to investigate whether the coupled land surface-subsurface model could extract more remotely sensed information in the DA process. Another objective was to gain insight into the value added by merging remotely sensed soil moisture information using different merging schemes, and to assess whether merged soil moisture datasets allow for improving land surface characterisation more than the assimilation of single remotely sensed soil moisture products.

In the first study, a cross-evaluation of land surface model results (with and without lateral flow processes), the National Aeronautics and Space Administration (NASA) Soil Moisture Active/Passive (SMAP) mission soil moisture product, and cosmic-ray neutron sensor (CRNS) measurements was carried out. A traditional land surface model (the Community Land Model (CLM) version 3.5) and a coupled land surface-subsurface model (CLM-ParFlow) were applied. Compared to CLM stand-alone simulations, the coupled CLM-ParFlow model considers both vertical and lateral water movement. In addition to standard validation metrics, a triple collocation (TC) analysis has been performed to help understand the random error variances of different soil moisture datasets. In this study, it was found that the three soil moisture datasets are consistent. The coupled and uncoupled model simulations were evaluated at CRNS sites, and the coupled model simulations showed less bias than the CLM stand-alone model (-0.02 cm^3/cm^3 vs 0.07 cm^3/cm^3), similar random errors, but a slightly smaller correlation with the measurements (0.67 vs 0.71). The TC analysis showed that CLM-ParFlow reproduced better soil moisture dynamics than CLM standalone and with a higher signal-to-noise ratio. This suggests that the representation of subsurface physics is of significant importance in land surface modeling and that coupled land surface-subsurface modeling is of high interest.

Land surface modelling combined with data assimilation provides the potential to generate highly accurate soil moisture estimates across regional and global scales. In a second study in this PhD dissertation, the CLM and the coupled land surface subsurface model CLM-ParFlow, which considers lateral surface and subsurface flows, were applied on the study region. The soil moisture retrievals from the Soil Moisture Active/Passive (SMAP) mission were assimilated with the Localized Ensemble Kalman Filter (LEnKF) (with and without parameter estimation) using an ensemble size of 32 realizations. The simulated soil moisture, ET, and groundwater level were evaluated using in situ observations from a CRNS network, Eddy Covariance (EC) stations, and groundwater measurement wells. The results showed that the assimilation of remotely sensed soil moisture product improved the correlation from 0.71-0.78 to 0.79-0.82 and decreased the unbiased Root Mean Square Error (ubRMSE) from 0.062-0.048 cm^3/cm^3 to 0.058-0.045 cm^3/cm^3. The characterisation of ET showed a limited improvement with the highest ubRMSE reduction of 5%. The assimilation did not improve the groundwater level characterization. In addition, the joint state-parameter update did not give a better performance than updating the states alone, suggesting that SMAP retrievals do not provide sufficient information to update the parameters.

Microwave remote sensing technology has emerged to provide valuable products to monitor and assess soil moisture content at regional or global scales. However, each soil moisture product exhibits different advantages and shortcomings. Data fusion could help improve accuracy by merging information from different sources. In a third study in this PhD thesis, a traditional TC-based method and a novel Long Short Term Memory network (LSTM) were used to merge soil moisture products from the SMAP mission, Advanced Microwave Scanning Radiometer 2 (AMSR2) and The Advanced SCATterometer (ASCAT). This research reveals that the LSTM outperforms the traditional TC-based method for data fusion when evaluated against field measurements. The study identifies that both climate forcing and physiographic attributes significantly influence the spatial and temporal variations observed in the LSTM prediction scheme. Consequently, the study highlights the considerable potential of the LSTM method for large-scale integration of remote sensing soil moisture data.

The comparative efficacy of assimilating microwave retrievals from different missions remains unclear. A fourth study in this dissertation investigated the effectiveness of assimilating soil moisture retrievals from both active and passive microwave instruments and their merged soil moisture datasets into the CLM using an ensemble Kalman filter (EnKF) approach. In-situ observations from the TERrestrial EnviroNmental Observations (TERENO) network were employed to evaluate the modelled soil moisture by different sets of experiments: (1) individual assimilation of each product and (2) assimilation of combined active and passive retrievals by arithmetic mean, TC-based method, and LSTM scheme. Results showed that the assimilation generally improved the model performance in terms of Pearson r and ubRMSE. The SMAP and ASCAT products were more informative than the AMSR product, with a median improved Pearson r of 0.08 and 0.09 and a reduction in ubRMSE of 28.5% and 27.3% compared to open loop runs, respectively. The similar performance for SMAP and ASCAT demonstrated that they may be complementary tools. The assimilation of merged datasets gave a similar performance to SMAP and ASCAT retrieval and a slightly better performance than ASCAT retrieval.

This dissertation aims to investigate the use of coupled land surface subsurface models to enhance the performance of LSMs through DA. However, the results indicate that the improvements for other compartments are limited, and many challenges remain. For the complex LSMs, a multivariate and multi-scale approach needs to be explored, which considers the integration of information from multiple observation types (e.g., soil moisture, leaf area index, total water storage) and their spatial mismatch with the model grid. Furthermore, it is observed that assimilating a merged product of microwave soil moisture retrievals hardly gives better results than assimilating single retrievals. In the DA scheme, a uniform observation error was applied, which might be unrealistic. A temporally and spatially variable observation error could be used to help DA assign higher weights to more accurate information and lower weights to unreliable information. Meantime, a more accurate remote sensing product (Sentinel-1 at 1 km) might be preferable for constraining the high-resolution model.

ZUSAMMENFASSUNG

Die Bodenfeuchte ist eine Schlüsselvariable in den Wasser- und Energiekreisläufen an der Schnittstelle zwischen Atmosphäre, Landoberfläche und Vegetation. Für viele Anwendungen ist es unerlässlich, dass Bodenfeuchtedaten sowohl genau als auch über einen längeren Zeitraum verfügbar sind. Zu solchen Anwendungen gehören die Bewirtschaftung von Wasserressourcen, die Dürreüberwachung, sowie die Vorhersage landwirtschaftlicher Erträge. Der Nutzen von in-situ-Bodenfeuchtemessungen in Labors oder auf dem Feld ist durch eine geringe räumliche Abdeckung und hohe Kosten begrenzt. Landoberflächenmodelle (LSMs) können helfen, da sie Bodenfeuchte auf verschiedenen Maßstäben simulieren können. Damit liefern Landoberflächenmodelle die Möglichkeit lokale Messungen für regionale und kontinentale Vorhersagen zu nutzen. Allerdings unterliegen LSMs einigen Unsicherheitsquellen, darunter vereinfachte Parametrisierungen der physikalischen Prozesse und mögliche Fehler in der Modellstruktur oder den Eingabedaten. So wird zum Beispiel lateraler Wasserfluss in LSMs in der Regel nicht berechnet. Die Einführung von Fernerkundungstechnologien hat es ermöglicht, Bodenfeuchteinformationen auf sehr großem Maßstab und nahezu in Echtzeit zu erhalten. Die Bodenfeuchtedaten, die durch Fernerkundung gewonnen werden, sind jedoch grob und in ihrer Interpretierbarkeit durch das Vorhandensein dichter Vegetation, komplexer Topografie und gefrorener Böden begrenzt. Die Datenassimilation (DA) kann Daten aus Quellen wie der Fernerkundung nutzen, um die Vorhersagekraft von Landoberflächenmodellen zu verbessern. Wir haben die LSM-Simulationen über einer gemäßigten Klimaregion mit komplexer Topografie und Landform in Westdeutschland bewertet und dabei eine Vielzahl von Datentypen, z. B. Bodenfeuchte und Evapotranspiration (ET), assimiliert. Ein Ziel dieser Doktorarbeit war es, den Einfluss der Berücksichtigung der lateralen Strömung und eines besseren Untergrundmodells im Allgemeinen auf die Simulation der Bodenfeuchte und anderer hydrologischer Variablen zu bewerten und zu untersuchen, ob ein gekoppeltes Landoberflächen-Untergrund-Modell bei der DA mehr Informationen aus Fernerkundungsdaten gewinnen kann. Ein weiteres Ziel war es, einen Einblick in den Mehrwert zu gewinnen, der durch gemeinsame Assimilation von Bodenfeuchtedaten aus lokalen und Fernerkundungsmessungen entsteht. Dabei wurden verschiedene Methoden für diese gemeinsame Assimilation genutzt. Schließlich wird bewertet, ob solche aus mehreren Quellen zusammengesetzte Bodenfeuchte-Datensätze eine bessere Charakterisierung der Landoberfläche ermöglichen als die Assimilation reiner Fererkundungsdatensätze.

In der ersten Studie der Doktorarbeit wurden die Ergebnisse des Landoberflächenmodells (mit und ohne laterale Strömungsprozesse), das Bodenfeuchteprodukt der Soil Moisture Active/Passive (SMAP) Mission der National Aeronautics and Space Administration (NASA) und Messungen aus Cosmic-Ray Neutron Sensors (CRNS) miteinander verglichen. Es wurden ein weithin anerkanntes Landoberflächenmodell (das Community Land Model (CLM) Version 3.5) und ein gekoppeltes Landoberflächen-Untergrundmodell (CLM-ParFlow) verwendet. Im Vergleich zu den CLM-Einzelsimulationen berücksichtigte das gekoppelte CLM-ParFlow-Modell sowohl die vertikale als auch die laterale Wasserbewegung. Zusätzlich zu den Standard-Validierungsmetriken wurde eine dreifache Kollokationsanalyse (TC) durchgeführt, um die zufälligen Fehlervarianzen verschiedener Bodenfeuchtigkeitsdatensätze zu verstehen. In dieser Studie wurde festgestellt, dass die drei Bodenfeuchtedatensätze konsistent sind. Die gekoppelten und ungekoppelten Modellsimulationen wurden an CRNS-Standorten ausgewertet, und die gekoppelten Modellsimulationen zeigten eine geringere Verzerrung als das CLM-Einzelmodell (-0.02 cm^3/cm^3 gegenüber 0.07 cm^3/cm^3), ähnliche zufällige Fehler, aber eine etwas geringere Korrelation mit den Messungen (0.67 gegenüber 0.71). Die TC-Analyse zeigte, dass CLM-ParFlow die Dynamik der Bodenfeuchte besser und mit weniger Hintergrundrauschen wiedergab als nur CLM. Dies deutet darauf hin, dass die Darstellung der Untergrundphysik bei der Modellierung der Landoberfläche von großer Bedeutung ist und dass die gekoppelte Modellierung von Landoberfläche und Untergrund von großem Interesse ist.

Die Landoberflächenmodellierung in Verbindung mit Datenassimilation bietet das Potenzial, hochgenaue Schätzungen der Bodenfeuchtigkeit auf regionaler und globaler Ebene zu erstellen. In einer zweiten Studie im Rahmen dieser Dissertation wurden das gemeinschaftliche Landmodell CLM und das gekoppelte Landoberflächen-Untergrundmodell CLM-ParFlow, das laterale Oberflächen- und Untergrundströmungen berücksichtigt, auf die Untersuchungsregion angewendet. Die Bodenfeuchtigkeitsdaten der Soil Moisture Active Passive (SMAP) Mission wurden mit dem Localized Ensemble Kalman Filter (LEnKF) (mit und ohne Parameterschätzung) mit einer Ensemblegröße von 32 Realisierungen assimiliert. Die simulierte Bodenfeuchte, die Evapotranspiration (ET) und der Grundwasserspiegel wurden mit In-situ-Beobachtungen eines Netzes von Cosmic Ray Neutron Sensoren (CRNS), Eddy Covariance (EC) Stationen und Grundwassermessstellen verglichen. Der Vergleich zeigte, dass die Assimilation von fernerkundeten Bodenfeuchteprodukten die Korrelation von 0.71-0.78 auf 0.79-0.82 verbesserte und den unbiased Root Mean Square Error

(ubRMSE) von 0.062-0.048 cm^3/cm^3 auf 0.058-0.045 cm^3/cm^3 reduzierte. Die Charakterisierung von ET zeigte eine begrenzte Verbesserung mit einer höchsten ubRMSE-Reduktion von 5%. Die Assimilation führte nicht zu einer Verbesserung der Grundwasserstandsbeschreibung. Darüber hinaus ergab die gemeinsame Anpassung von Zustandsvariablen und Parametern keine besseren Ergebnisse als die Anpassung der Zustände allein. Dieser Umstand deutet darauf hin, dass die SMAP-Bodenfeuchtedaten keine ausreichenden Informationen zur Anpassung der Parameter liefern.

Die Mikrowellenfernerkundungstechnologie liefert Datenprodukte, die einen Beitrag zur Beschreibung und Anpassung der Bodenfeuchtigkeit auf regionaler oder globaler Ebene leisten. Allerdings weist jedes Bodenfeuchteprodukt unterschiedliche Vorteile und Mängel auf. Eine Datenfusion könnte eine verbesserte Gesamtgenauigkeit ergeben, indem Informationen aus verschiedenen Quellen zusammengeführt werden. In einer dritten Studie im Rahmen dieser Doktorarbeit wurden ein traditionell angewandtes Verfahren auf der Grundlage der dreifachen Kollokation (TC) und ein neu eingeführtes Long Short Term Memory network (LSTM) verwendet, um Bodenfeuchteprodukte der Mission Soil Moisture Active Passive (SMAP), des Advanced Microwave Scanning Radiometer 2 (AMSR2) und des Advanced SCATterometer (ASCAT) gemeinsam zu nutzen. Die Studie zeigt, dass das LSTM die Felmessungen besser annähert als die traditionelle TC-basierte Methode. Ein weiteres Ergebnis der Studie ist, dass sowohl klimatische als auch die physiografische Faktoren einen erheblichen Einfluss auf die räumlichen und zeitlichen Schwankungen haben, die in der LSTM-Methode beobachtet werden. Insgesamt unterstreicht die Studie das beträchtliche Potenzial der LSTM-Methode für die groß angelegte Integration von Bodenfeuchtedaten aus der Fernerkundung.

Die Leistungsfähigkeit verschiedener Assimilationen in Abhängigkeit von Mikrowellenmessdaten aus verschiedenen Missionen blieb zu klären. Eine vierte Studie in dieser Dissertation untersuchte die Leistungsfähigkeit der Assimilierung von Bodenfeuchtigkeitsdaten von (1) aktiven Mikrowelleninstrumenten, (2) passiven Mikrowelleninstrumenten und (3) deren zusammengefassten Bodenfeuchtigkeitsdatensätzen in das gemeinschaftliche Landmodell (CLM) unter Verwendung eines Ensemble-Kalman-Filters (EnKF). In-situ-Beobachtungen aus dem TERENO-Netz wurden zur Bewertung der modellierten Bodenfeuchte in verschiedenen Versuchsreihen eingesetzt: (1)/(2) individuelle Assimilierung jedes Produkts und (3) Assimilation kombinierter aktiver und passiver Abrufe durch arithmetisches Mittel (3a), TC-basierte Methode (3b) und LSTM-Schema (3c). Die Modelläufe zeigten, dass jede Art der Assimilation die Metriken Pearson r und ubRMSE der Modellergebnisse verbesserte. Die SMAP- und ASCAT-Produkte waren informativer als das AMSR-Produkt, mit einem mittleren verbesserten Pearson r von 0.08 und 0.09 und einer Verringerung des ubRMSE von 28.5% bzw. 27.3% im Vergleich zu Läufen ohne Assimilation. Die ähnlichen Ergebnisse von SMAP und ASCAT zeigen, dass diese Datenprodukte sich gegenseitig ergänzen können. Die Assimilation zusammengefasster Datensätze lieferte ähnliche Ergebnisse wie die SMAP- und ASCAT-Produkte und eine etwas bessere Leistung als das ASCAT-Produkt.

In dieser Dissertation soll der Einsatz von gekoppelten Landoberflächen-Untergrundmodellen untersucht werden, um die Ergebnisse von LSMs durch DA zu verbessern. Die Ergebnisse zeigen jedoch, dass die Verbesserungen für andere Teile eines Erdsystemmodells begrenzt sind und viele Herausforderungen bestehen bleiben. Für die komplexen LSM muss ein multivariater und multiskaliger Ansatz erforscht werden, der die Integration von Informationen aus verschiedenen Beobachtungsarten (z. B. Bodenfeuchte, Blattflächenindex, Gesamtwasserspeicherung) und deren räumliche Nichtübereinstimmung mit dem Modellgitter berücksichtigt. Darüber hinaus wird festgestellt, dass die Assimilierung eines zusammengefassten Produkts von Mikrowellen-Bodenfeuchtedatensätzen kaum bessere Ergebnisse liefert als die Assimilation von Einzeldatensätzen. Für die DA wurde ein homogener Beobachtungsfehler zugrunde gelegt, was unrealistisch sein könnte. Ein zeitlich und räumlich variabler Beobachtungsfehler könnte zu einer besseren Wichtung der Datensätze beitragen. In der Zwischenzeit könnte ein genaueres Fernerkundungsprodukt (Sentinel-1 bei 1 km) zur Bestimmung eines hochauflösenden Modells besser geeignet sein.

1

Introduction

Soil moisture is a key state variable that supports terrestrial ecosystem functioning and atmosphere-land interactions. It governs the partitioning of surface net radiation between latent and sensible heat fluxes, thereby regulating land–atmosphere energy and water exchanges (Dirmeyer 2011; Koster et al. 2004; Schwingshackl et al. 2017; Small et al. 2003). Climatic related changes in soil moisture influence evapotranspiration, air temperature, and precipitation, linking hydrological and climatic extremes such as droughts and heatwaves (Berg et al. 2014; Grillakis 2019; Lorenz et al. 2010; Seneviratne et al. 2010; Teuling et al. 2006; Zhou et al. 2024). At the ecosystem level, soil moisture controls regulates plant water uptake, constrains plant transpiration, leaf and root respiration, and the photosynthesis process (Havranek et al. 1978; Trugman et al. 2018). It also modulates the growth and development of microorganisms, affecting microbiological and biochemical activities, nutrient cycling, and greenhouse gas emissions (Borowik et al. 2016; Tiemann et al. 2011). Therefore, accurate soil moisture information is essential for weather forecasting, water resources management, climate change research, and agricultural applications such as irrigation scheduling.

Soil moisture can be measured using various methods operating across different spatial and temporal scales. One of the most common and direct methods is the gravimetric method, which dries soil samples in an oven until no further mass loss occurs, after which the sample is weighed again. Despite its precision, this technique is labour-intensive and unsuitable for large-scale or continuous monitoring. Alternative indirect methods estimate soil water content by establishing relationships between soil water content and soil properties, such as dielectric constant, electrical conductivity, or thermal capacity (e.g., Robinson et al. 2008). Among these, the Time Domain Reflectometry (TDR) method is widely used, which works by sending a high-frequency electromagnetic pulse through a soil probe and measuring the time it takes for the pulse to travel back to the instrument (Rajkai et al. 1992). The travel time of the pulse is affected by the dielectric constant of the soil, which is directly related to the soil moisture content. The TDR probes are inserted into the soil at the desired depth and at the desired locations. Other similar methods include Time Domain Transmissivity (TDT) (Will et al. 2013), tensiometers (Hubbell et al. 1998) and capacitance probes (Dean et al. 1987). A more recent technique, called Cosmic-Ray Neutron Sensor, has emerged as a promising method for measuring soil moisture at an intermediate scale of approximately 240 m (Zreda et al. 2008). The penetration depth depends on the soil moisture content, ranging from 15 cm (wet soils) to 55 cm (dry soils) (Schrön et al. 2017b). However, these ground-based measurements are typically point-based and limited in their ability to capture the spatial variability of soil moisture at large scales (e.g., Dobriyal et al. 2012; Robock et al. 2000; Walker et al. 2004).

Remote sensing techniques can provide spatially continuous, large-scale soil moisture information (e.g., Jackson et al. 1996; Mohanty et al. 2017). Two key satellite missions operating at the L-band microwave frequency are the Soil Moisture and Ocean Salinity (SMOS) launched by the European Space Agency (ESA) in 2009 (Kerr et al. 2001) and the The National Aeronautics and Space Administration (NASA)'s Soil Moisture Active/Passive (SMAP) launched in 2015 (Entekhabi et al. 2010a). These missions provide global surface soil moisture observations with spatial resolutions ranging from about 9 to 50 km and revisit intervals of 1–3 days (Kerr et al. 2010; O'Neill et al. 2010). The low-frequency microwave sensors have a penetration depth of approximately 3-5 cm; although retrievals are still affected by surface roughness, vegetation density, frozen soils, and complex topography (Mishra et al. 2018).

Land surface models (LSMs) complement satellite observations by providing continuous and physically consistent estimates of soil moisture through the simulation of coupled energy, water, and carbon processes (Bonan 1998; Lawrence et al. 2019). LSMs resolve the exchanges of energy (net radiation, sensible and latent heat), water (precipitation, infiltration, runoff, and evapotranspiration), and carbon (photosynthesis, respiration, and decomposition) between the land surface and the atmosphere (Bonan et al. 2018; Sellers et al. 1997). LSMs can operate at hyper-resolution (<1 km) for catchment or regional studies (Wood et al. 2011) or at coarser (10-100 km) resolutions for global applications (Blyth et al. 2021). Modern LSMs now include explicit representations of vegetation dynamics, carbon–nitrogen cycling, and plant hydraulics, enabling better simulation of drought responses and ecosystem feedbacks (Clark et al. 2011; Fisher et al. 2018; Lawrence et al. 2019). However, LSM predictions remain sensitive to parameterization and input uncertainties, particularly meteorological forcing, soil texture, and vegetation characteristics (Dumedah et al. 2014; Hossain et al. 2005).

Data assimilation (DA) is a robust method for enhancing the reliability of LSMs by integrating observations, and it has been used to improve the accuracy of soil moisture in LSMs for several decades (Blankenship et al. 2016; Houser et al. 1998; Kumar et al. 2022; Ni-Meister 2008; Nair et al. 2022; Reichle et al. 2008a; Zhou et al. 2020). One commonly used DA algorithm in LSMs is Ensemble Kalman Filter (EnKF) (Evensen 1994), a sequential data assimilation algorithm capable of addressing various sources of modelling errors in combination with complex non-linear system models. Many studies have effectively employed EnKF and its variants to refine large-scale soil moisture predictions by assimilating remote sensing brightness temperature observations or soil moisture retrievals (Blyverket et al. 2019; Fairbairn et al. 2015; Huang et al. 2008; Naz et al. 2019; Reichle et al. 2008b; Renzullo et al. 2014; Xu et al. 2015). However, studies have reported improvements in related fluxes such as evapotranspiration and other variables (e.g., runoff) often remain limited (Chen et al. 2011; Hostache et al. 2020; Naz et al. 2019; Strebel et al. 2024). This limitation partly stems from structural simplifications in many LSMs, in which soil water flow is treated as one-dimensional, and the coupling between soil moisture and groundwater dynamics is neglected. Recent studies have demonstrated that including three-dimensional hydrological processes (lateral flow and groundwater interactions) leads to more realistic soil moisture distributions and improved simulation of transpiration and ground evaporation fluxes (Kim et al. 2017; Maxwell et al. 2016; Yang et al. 2021b).

In recognition of the importance of surface and subsurface lateral flows, a growing body of research has focused on integrating groundwater processes with LSMs. Maxwell et al. (2005) coupled the Common Land Model (CoLM) and a variably saturated groundwater flow model (ParFlow) and demonstrated that the soil moisture and groundwater table depth simulated by the coupled model performed better when evaluated against observations. Shi et al. (2013) incorporated a land surface scheme Flux into the PIHM (Penn State Integrated Hydrologic Model), which is capable of simulating lateral water flow and deep groundwater at fine resolution. Riley et al. (2014) and Ji et al. (2015) coupled the Community Land Model (CLM 4.0) with the Process-based Adaptive Watershed Simulator (PAWS). The coupled model CLM+PAWS computes two-dimensional overland flow, one-dimensional channel network flow, and quasi-three-dimensional subsurface flow. Niu et al. (2014a) find that the coupling of CATchment HYdrology (CATHY) and Noah-Multiparameterization Land Surface Model (Noah-MP) outperforms the one-dimensional Noah-MP, and the improvement is attributed to the incorporation of groundwater table depth into the coupled modeling framework, highlighting the influence of groundwater dynamics on energy balance partitioning. Moreover, an atmosphere-land surface-subsurface Terrestrial System Modelling Platform (TSMP) was developed by Shrestha et al. (2014), where the CLM 3.5, ParFlow, and Consortium for Small-scale Modeling (COSMO) models are coupled through the Ocean Atmosphere Sea Ice Soil (OASIS) coupler. The component ParFlow model solves the three-dimensional Richards' equation to simulate the three-dimensional movement of subsurface water. However, only in a few studies (Gebler et al. 2019; Lahmers et al. 2022; Sawada 2020) were soil moisture measurements assimilated into the coupled model. It remains uncertain whether accounting for lateral flows and coupling a groundwater component could enhance DA skill in LSMs.

The effectiveness of data assimilation is determined by the relative magnitude of errors in the remote sensing retrievals and the model itself. It is expected that more accurate and informative remote sensing retrievals can lead to higher benefits of DA (Gevaert et al. 2018). The satellite soil moisture products from both active (Brocca et al. 2010, 2011; Draper et al. 2011; Loizu et al. 2018; Renzullo et al. 2014) and passive microwave sensors (Ahmad et al. 2022; Chakrabarti et al. 2014; Kolassa et al. 2017b; Larue et al. 2018; Lievens et al. 2015; Pinnington et al. 2021; Sawada et al. 2015; Al-Yaari et al. 2014; Zhou et al. 2020) have been assimilated to LSMs. The passive sensors are more sensitive to soil dielectric properties than the active sensors. However, the passive sensors are limited by their coarse spatial resolution and high sensitivity to surface parameters, such as temperature. Soil moisture retrievals can be obtained from multiple microwave frequencies, including L-band (1.4 GHz), C-band (6 GHz), and X-band (10 GHz), regardless of whether the microwave sensors are active or passive. Among these, L-band is considered more advantageous for soil moisture retrieval because of its greater penetration depth and reduced sensitivity to dense vegetation and atmospheric conditions (Konings et al. 2017; Schmugge 1978). Beyond the single-sensor retrieval products, synergistic retrieval approaches have emerged to leverage the complementary strengths of microwave observations from multiple sensors in the DA process.

Draper et al. (2012) investigated the potential benefits of assimilating data from both the active microwave Advanced Scatterometer (ASCAT) and the passive Advanced Microwave Scanning Radiometer for the Earth Observing System (AMSR-E) together. In a follow-up study, Kolassa

et al. (2017a) used the same sensors as Draper et al. (2012) and further investigated merging strategies for DA, evaluating the performance of both joint and separate retrieval assimilation techniques. These studies demonstrate that assimilating merged retrievals yields comparable to, or even better than, assimilating individual retrievals. Other similar studies (Gevaert et al. 2018; Kim et al. 2018; Lievens et al. 2017b; Liu et al. 2016; Xu et al. 2017) conclude that joint assimilation of multiple retrievals does not consistently outperform separate retrieval approaches. Despite the growing use of multiple soil moisture information sources in DA processes, limited research has explored diverse approaches for effectively combining these data and examined how DA benefits from remote sensing soil moisture across different schemes.

The objective of this PhD thesis is to:

(a) Explore the effects of the lateral flow process and incorporation of subsurface components in the spatial and temporal distribution of simulated soil moisture by LSMs.

(b) Investigate whether coupling of groundwater components improves model performance more than extracting information through assimilating remote sensing retrievals, and whether this leads to improved predictions for soil moisture and other hydrological variables, such as Evapotranspiration (ET) and groundwater level.

(c) Develop a methodology to effectively merge the remote sensing soil moisture information from multiple microwave sensors and improve the characterization of soil moisture over large scales.

(d) Investigate whether the assimilation of merged microwave soil moisture retrievals can further improve the prediction than single retrieval assimilation, and assess whether the merging scheme yields a significant difference in the skill of the assimilation output.

Chapter 2 presents a comprehensive overview of the integrated TSMP platform used in this research. This chapter also introduces DA schemes and the Triple Collocation (TC) method. It also briefly introduces the research area and the remote sensing soil moisture retrievals from the SMAP mission.

Chapter 3 conducts a comparative evaluation of two land surface models within the TSMP framework, the CLM model and the coupled CLM-ParFlow model, which considers both vertical and lateral water movements. This chapter conducts a cross-evaluation that includes model simulations, soil moisture data derived from the SMAP mission, and cosmic-ray neutron sensor (CRNS) measurements, based on the TC method. The study area is located in Western Germany, which has a temperate climate and diverse vegetation.

Chapter 4 examines the assimilation of SMAP soil moisture data into the CLM and CLM-ParFlow models. As argued before, only a few studies explored the influence of lateral water flow on the DA process. The assimilation effects on the soil moisture and ET characterization are evaluated with in situ measurements. Given the strong coupling between soil moisture and groundwater, particularly when groundwater levels are shallow, we also explored the impact of assimilating soil moisture data on CLM-ParFlow groundwater level simulations. Additionally, two DA strategies are compared: one that updates only the model states, and another that includes parameter estimation.

Chapter 5 explores different methods to integrate multiple remote sensing soil moisture retrievals from SMAP, the Advanced Microwave Scanning Radiometer 2 (AMSR2), and ASCAT. The merging schemes include a straightforward arithmetic mean technique, a TC-based approach, and an innovative Long Short-Term Memory (LSTM) neural network model. The performance of the merged datasets and each remote sensing product is evaluated against in situ measurements to assess their accuracy and reliability. We compare the results and identify the most effective approach for data fusion.

Chapter 6 compared (i) the assimilation of joint active and passive retrievals (the fusion dataset by Chapter 5) and (ii) the assimilation of the separate soil moisture products by using the CLM model. The results for different assimilation strategies are compared and validated using CRNS measurements.

Finally, chapter 6 summarizes the main results and provides an insight for future research.

2

Methods and materials

2.1 Integrated Terrestrial Systems Modelling Platform (TSMP)

Previous work by Shrestha et al. (2014) has introduced the TSMP. The platform consists of an atmospheric model (Consortium for Small-Scale Modelling, COSMO) (Baldauf et al. 2011), a land surface model (the NCAR CLM version 3.5) (Oleson et al. 2008), and a three-dimensional variably saturated groundwater flow model (ParFlow) (Kollet et al. 2006). An external coupler (Ocean Atmosphere Sea Ice Soil, version 3.0, OASIS3) (Valcke 2013) is used to couple the three models through a multi-executable and multi-data approach, allowing for independent executions of the three models while maintaining data exchange. The TSMP simulates the exchange of water and energy between the lower atmospheric boundary layer, the land surface, and the subsurface.

In the TSMP, atmospheric variables (e.g., air temperature, air pressure, wind speed, specific humidity, incoming short- and long-wave radiation, precipitation) from the lowest COSMO layer are provided to the CLM. The land surface mass and energy balance components are calculated in CLM. Then the land surface-atmosphere exchange fluxes, momentum flux, albedo, and outgoing long-wave radiation are sent back to COSMO. ParFlow is coupled to CLM over the upper ten vertical soil layers. The land surface model CLM sends the net infiltration flux, taking into account precipitation and evapotranspiration, and which can be negative for the top 10 layers to ParFlow; in turn, ParFlow sends the updated subsurface relative saturation and pressure values for the top 10 layers to CLM. TSMP offers a flexible configuration mode, supporting fully coupled operation (COSMO + CLM + ParFlow), partial coupling (COSMO + CLM or CLM + ParFlow), and standalone runs of individual modules (COSMO, CLM, or ParFlow). In this work, the partly coupled configuration with CLM and ParFlow is used. A more detailed overview of the CLM and ParFlow models is given in the following sections.

2.1.1 Community Land Model (CLM), version 3.5

The CLM, developed by the NCAR, is the land component of the Community Earth System Model (CESM). CLM calculates land surface mass and energy balance, including infiltration, interception, surface runoff, snow, and evapotranspiration (Oleson et al. 2004; Oleson et al. 2008). The codes were originally written by Yongjiu et al. (1997), and their features include the unevenly spaced layers for simulating soil temperature and soil moisture, the representation

of liquid water and ice mass, the snow process, and the runoff parameterization following the TOPMODEL concept. Further developments have been implemented, including in the areas of carbon cycling, vegetation dynamics, and river routing. CLM version 2.0 was released (Bonan et al. 2003). CLM version 3.0 differs from previous releases, particularly from a software engineering perspective. Following this release, several modifications are introduced to alleviate previous biases, e.g., new parameterizations for canopy integration and interception, frozen soil, subsurface runoff, and evapotranspiration (Oleson et al. 2008). CLM version 3.5 represents significant improvements over CLM 3.0, particularly in its representation of the hydrological cycle. The CLM version 5.0 (Lawrence et al. 2019) represents a large advancement over earlier model versions, including improved representations of bio-geophysical and biochemical processes. Despite these advantages, CLM 3.5 coupled with ParFlow remains valuable for studies requiring detailed lateral subsurface flow and groundwater surface water interactions at fine spatial scales; therefore, this configuration is used in this study. The model is driven using COSMO-REA6 (Bollmeyer et al. 2024) atmospheric forcing data, which provide high-resolution regional meteorological inputs suitable for hydrological simulations over Europe.

The spatial heterogeneity of the land surface in CLM is represented as a three-level sub-grid hierarchy, including specific land units (including glaciers, lakes, wetlands, urban areas, and vegetated areas), columns, and 16 plant functional types (PFTs) (Oleson et al. 2004). PFTs include evergreen needle-leaf (boreal or temperate), deciduous needle-leaf (boreal), evergreen broad leaf (temperate or tropical), deciduous broad leaf (boreal, temperate, or tropical), deciduous shrub (boreal or temperate), evergreen shrub (temperate), grass (C3 Arctic, C3, and C4), and crop. Each plant type has its own definition of leaf and stem optical properties and photosynthetic parameters. The vertical soil/snow profile is represented by 10 soil layers and up to 5 snow layers.

In CLM, the one-dimensional vertical water flow in the soils is calculated based on a modified Richards equation:

$$\frac{\partial \theta}{\partial t} = \frac{\partial}{\partial z}\left[k\left(\frac{\partial \psi}{\partial \theta}\frac{\partial \theta}{\partial z} + 1\right)\right] \tag{2.1}$$

where θ is the volumetric soil water content ($L^3 \cdot L^{-3}$), t is the time, and z is the height (L) (positive upwards), k represents the hydraulic conductivity ($L \cdot T^{-1}$), and p is the hydraulic potential (L). The hydraulic conductivity k_i ($L \cdot T^{-1}$) and the soil matric potential ψ_i (L) for each layer i vary with soil water content θ and soil texture (% sand and % clay) and their calculations based on the work of Clapp et al. (1978) and Cosby et al. (1984). The hydraulic conductivity is defined at the interface between two adjacent layers $z_{h,i}$ and calculated as:

$$k[z_{h,i}] = \begin{cases} k_{sat}[z_{h,i}]\left[\frac{0.5(\theta_{liq,i}+\theta_{liq,i+1})}{0.5(\theta_{sat,i}+\theta_{sat,i+1})}\right]^{2B_i+3} & 1 \leq i \leqslant 9 \\ k_{sat}[z_{h,i}]\left[\frac{\theta_{liq,i}}{\theta_{sat,i}}\right]^{2B_i+3} & i = 10 \end{cases} \tag{2.2}$$

where the θ_{liq} represents the liquid water content, and the saturated hydraulic conductivity $k_{sat}[z_{h,i}$ ($\mathrm{L{\cdot}T^{-1}}$) is calculated by:

$$k_{sat}[z_{h,i}] = 0.0070556 \times 10^{-0.884+0.0153(\%sand)_i} \left[exp(-\frac{z_{h,i}}{z_*}))\right] \tag{2.3}$$

where $z_* = 0.5$ m is the length scale for the decrease in $k_{sat}[z_{h,i}]$. The water content at saturation (θ_{sat}, porosity) and the exponent B are given by:

$$\theta_{sat,i} = 0.489 - 0.00126\,(\%sand)_i \tag{2.4}$$

$$B_i = 2.91 + 0.159\,(\%clay)_i \tag{2.5}$$

The land-atmosphere exchange fluxes are described by the Monin-Obukhov similarity theory (Oleson et al. 2010). The evapotranspiration in CLM is defined as the sum of evaporation from ground and vegetation. For the non-vegetated surfaces, the evaporation from ground E_g is calculated as:

$$E_g = -\frac{\rho_{atm} * (q_{atm} - q_g)}{r_{aw}} \tag{2.6}$$

where ρ_{atm} is the atmospheric air density ($\mathrm{M{\cdot}\ L^{-3}}$), q_{atm} is the atmospheric specific humidity ($\mathrm{M \cdot M^{-1}}$), q_g is the specific humidity of the soil surface ($\mathrm{M \cdot M^{-1}}$), and r_{aw} is the aerodynamic resistance to water vapor transfer ($\mathrm{T \cdot L^{-1}}$). For the vegetated columns, the water fluxes from the ground and the vegetation E_v are calculated as follows:

$$E_g = -\rho_{atm}\frac{(q_s - q_g)}{r_{aw}{}'} \tag{2.7}$$

where $r_{aw}{}'$ is the aerodynamic resistance ($\mathrm{T \cdot L^{-1}}$) to water vapor transfer between the ground and the canopy air and q_s is the canopy specific humidity ($\mathrm{M \cdot M^{-1}}$).

$$E_v = -\rho_{atm}\frac{(q_s - q_{sat}^{T_v})}{r_{total}} \tag{2.8}$$

where $q_{sat}^{T_v}$ is the saturated specific humidity ($\mathrm{M \cdot M^{-1}}$) at the vegetation temperature T_v, r_{total} is the total resistance to water vapor transfer from the canopy to the canopy air, caused by both the leaf boundary layer and stomatal resistance.

2.1.2 ParFlow

The integrated, parallel, and three-dimensional variably saturated subsurface flow model ParFlow has been developed over a long period by multiple institutions. The current development is led by a collaboration between Princeton University, Lawrence Livermore National Laboratory, Forschungszentrum Jülich, Colorado School of Mines, University of Bonn, Washington State University, and other universities and institutes. It is multi-platform and runs with a common I/O structure from laptops to supercomputers with excellent efficiency, which can handle a wide range of applications, from small-scale hill-slope studies to high-resolution large-scale hydrologic simulations (Maxwell et al. 2015). ParFlow was initially developed for simulating saturated fluid flow and chemical transport in three-dimensional heterogeneous media (Ashby et al. 1996) and has since expanded its capabilities. A two-dimensional distributed overland flow simulator was incorporated into ParFlow, and the numerical methods were also improved (Kollet et al. 2006). A terrain-following grid transform with variable vertical discretizations was implemented by Maxwell (2013) to improve the model resolution in the shallow soil layers. ParFlow has been widely used to study the coupling process between surface and subsurface flow. Many studies analyzed the dynamic behaviour of groundwater and surface–subsurface inter-connectivity for small catchments (e.g., less than 30 km^2) (Kollet et al. 2006), larger catchments (e.g, over 600 km^2)(Condon et al. 2013, 2014, 2019; Kollet et al. 2008; Soltani et al. 2022), to the continental scale (Condon et al. 2015; Furusho-Percot et al. 2019; Naz et al. 2023; O'neill et al. 2021). The model's capabilities extend to complex terrains as demonstrated in applications for the Rocky Mountain National Park, Colorado, USA (Engdahl et al. 2015), and even subsurface–surface and atmospheric coupling (Rahman et al. 2015; Shrestha et al. 2014; Xu et al. 2023). ParFlow was found to provide accurate results for the simulation of flows in surface and subsurface systems. The ParFlow model can simulate in three different modes: variably saturated, steady-state saturated and integrated watershed flows.

Variably saturated flow is calculated based on the following formulations of the Richards equation (Celia et al. 1990):

$$S_s S_{(p)} \frac{\partial p}{\partial t} + \phi \frac{\partial S_{(p)}}{\partial t} = \nabla \cdot \mathbf{q} + q_s \tag{2.9}$$

$$\mathbf{q} = -k_{sat} k_r(p) \nabla (p - z) \tag{2.10}$$

where S_s is the specific storage coefficient (L^{-1}), $S_{(p)}$ is the relative saturation as a function of the pressure head p (L), t is time, ϕ is porosity, $\mathbf{q}$ is Darcy flux ($L{\cdot}T^{-1}$), q_s is a general source/sink term (T^{-1}) (including wells and surface fluxes), k_{sat} is saturated hydraulic conductivity ($L{\cdot}T^{-1}$), and k_r is relative permeability, and z represents the depth below the surface (L). The coupled free-surface flow and subsurface flow in combination with heterogeneity are simulated under variably saturated flow conditions (Kollet et al. 2010). An overland flow boundary condition is employed when simulating surface and subsurface flow:

$$\frac{\partial \psi_s}{\partial t} = \nabla \cdot (\boldsymbol{v} \psi_s) + q_s \tag{2.11}$$

where ψ_s is the surface ponding depth (L), $\boldsymbol{v}$ is the depth-averaged velocity vector ($\mathrm{L{\cdot}T^{-1}}$). Considering the vertical flow, the equation (2.11) can be modified to include an exchange rate with the subsurface q_e, as:

$$\frac{\partial \psi_s}{\partial t} = \nabla \cdot (\boldsymbol{v}\psi_s) + q_s + q_e \tag{2.12}$$

The implicit system is solved with the inexact Newton-Krylov method. More details can be found in previous studies (Kollet et al. 2006).

An advantageous feature of ParFlow is that it transforms the topography into a structured grid using the terrain-following grid formulation. The transformation incorporates a topographic slope component to Darcy's law:

$$\begin{aligned} q_x &= k\sin(\theta_x) + k\frac{\partial p}{\partial x}\cos(\theta_x), \text{ and} \\ q_y &= k\sin(\theta_y) + k\frac{\partial p}{\partial y}\cos(\theta_y) \end{aligned} \tag{2.13}$$

where q_x and q_y represent Darcy flux components, $k = k_{sat}k_r$, and the topographic slopes S_x and S_y in the x and y directions may be presented as $\theta_x = \tan^{-1} S_x$ and $\theta_y = \tan^{-1} S_y$, respectively, where θ represents the local angle of topographic slope (Maxwell 2013).

2.2 Data assimilation

2.2.1 Ensemble Kalman Filter (EnKF)

The EnKF emerged as an advanced generalization of the traditional Kalman Filter (Evensen 1994), specifically for handling high-dimensional nonlinear systems. Based on a Monte Carlo methodology, EnKF generates an ensemble of model trajectories, facilitating the estimation of the temporal evolution of the probability density functions associated with model states and the corresponding error covariances.

The EnKF methodology involves two main steps: the forecast step ^{f} and the update step ^{a}. The forecast and analysis model state ensembles ($\mathbf{X}^f$ and $\mathbf{X}^a$) are given as:

$$\mathbf{X}^f = \left[\mathbf{x}_1^f, \mathbf{x}_2^f, ...\mathbf{x}_N^f\right] \tag{2.14}$$

$$\mathbf{X}^a = [\mathbf{x}_1^a, \mathbf{x}_2^a, ...\mathbf{x}_N^a] \tag{2.15}$$

where N represents the number of ensemble members. For each ensemble member, the forecast step at time t is calculated as follows:

$$\mathbf{x}^{f,t} = \mathbf{M}\left(\mathbf{x}^{t-1}, \mathbf{p}, \mathbf{q}^t\right) \tag{2.16}$$

The model is represented by $\mathbf{M}$, the parameter vector is denoted by $\mathbf{p}$, and the model forcing vector is represented by $\mathbf{q}$. The ensemble of model states is generated by an integrative perturbation of model parameters $\mathbf{p}$ (e.g., soil texture) and model forcings $\mathbf{q}$ (e.g., precipitation). This forecast step is repeated N times for each ensemble member. Then the model state vector is updated by:

$$\mathbf{x}^{a,t} = \mathbf{x}^{f,t} + \mathbf{K}\left(\mathbf{y}^t - \mathbf{y}^{f,t}\right) \tag{2.17}$$

where $\mathbf{K}$ is the Kalman gain, $\mathbf{y}^t$ is the observation vector, and $\mathbf{y}^{f,t}$ is the vector with the forecast observations. The Kalman gain is calculated according to:

$$\mathbf{K} = \mathbf{C}^f\mathbf{H}^\mathbf{T}\left(\mathbf{H}\mathbf{C}^f\mathbf{H}^\mathbf{T} + \mathbf{R}\right)^{-1} \tag{2.18}$$

where $\mathbf{C}$ denotes the forecast error covariance, representing the uncertainty in the model, and $\mathbf{R}$ is the observation error covariance, representing measurement uncertainty as specified by the user. $\mathbf{H}$ is the observation operator that maps the model state space to the observation space.

We calculate $\mathbf{C}$ by:

$$\mathbf{C}^f = \frac{1}{N-1}\sum_{i=1}^{N}\left(\mathbf{x}_i^t - \bar{\mathbf{x}}^t\right)\left(\mathbf{x}_i^t - \bar{\mathbf{x}}^t\right) \tag{2.19}$$

where $\bar{\mathbf{x}}^t$ represents the average over the ensemble members.

Besides updating states, one can update both model parameters and states (Hendricks Franssen et al. 2008). In this case, the augmented state vector is constructed by combining the unknown model states $\mathbf{x}^t$ and unknown model parameters $\mathbf{p}^t$. Let n_x denote the dimension of the state vector and n_p the dimension of the parameter vector, while n_y represents the number of observations, such that:

$$\mathbf{x}^* = \begin{bmatrix}\mathbf{x}\\ \mathbf{p}\end{bmatrix} \in \mathbb{R}^{(n_x+n_p)} \tag{2.20}$$

Accordingly, the augmented forecast error covariance matrix $\mathbf{C}^*$ is:

$$\mathbf{C}^* = \begin{bmatrix}\mathbf{C}_{xx} & \mathbf{C}_{xp}\\ \mathbf{C}_{px} & \mathbf{C}_{pp}\end{bmatrix} \in \mathbb{R}^{(n_x+n_p)\times(n_x+n_p)} \tag{2.21}$$

Here, the matrix $\mathbf{C_{xx}}$ and $\mathbf{C_{pp}}$ denote the covariance among states and parameters, respectively, while $\mathbf{C_{xp}}$ and its transpose $\mathbf{C_{px}}$ represent the cross-covariance between states and parameters. The observation operator $\mathbf{H}^*$ and Kalman gain $\mathbf{K}^*$ are also extended to account for both states and parameters:

$$\mathbf{H}^* = \begin{bmatrix} \mathbf{H}_x & \mathbf{H}_p \end{bmatrix} \in \mathbb{R}^{n_y \times (n_x + n_p)} \tag{2.22}$$

$$\mathbf{K}^* = \begin{bmatrix} \mathbf{K}_x \\ \mathbf{K}_p \end{bmatrix} \tag{2.23}$$

The $\mathbf{H}_p$ represents the sensitivity of observations to model parameters, and is often assumed to be zero. $\mathbf{K}_x \in \mathbb{R}^{n_x \times n_y}$ $\mathbf{K}_p \in \mathbb{R}^{n_p \times n_y}$, and $\mathbf{K}_p$ describe the contributions of the innovation to the updates of states and parameters, respectively. After each analysis step, the updated parameters are written back to the model parameter fields and propagated using a persistence (constant) model. In the case of soil moisture assimilation with a standalone land surface model, the updated sand and clay fractions are updated to recalculate the soil hydraulic properties for the next forecast cycle.

In some cases, a damping factor (α) is applied on the parameters to reduce the filter inbreeding (Hendricks Franssen et al. 2008), which refers to the underestimation of the ensemble variance due to a limited number of ensemble members. The updated equation for the joint state-parameter estimation is:

$$\mathbf{x}^{a,t*} = \mathbf{x}^{f,t*} + \boldsymbol{\alpha}\mathbf{K}\left(\mathbf{y}^t - \mathbf{y}^{f,t}\right) \tag{2.24}$$

where $\boldsymbol{\alpha}$ is a diagonal matrix with values between 0 and 1.

2.2.2 TSMP-PDAF

The Parallel Data Assimilation Framework (PDAF) (Nerger et al. 2005) has been coupled to the TSMP by Kurtz et al. (2016), enabling efficient data assimilation with numerical models within a parallelized data assimilation system. PDAF enables full parallelization of the data assimilation framework by parallelizing both the forward ensemble simulations and the analysis step. TSMP allows data assimilation for the land-surface model CLM and the subsurface/surface flow model ParFlow. An online coupling approach is used to improve computational efficiency by exchanging relevant states and fluxes between the ensemble and filter in memory, making it suitable for large-scale problems. More technical background can be found in Kurtz et al. (2016). Several filters are currently available for data assimilation, such as the EnKF, Local Ensemble Kalman Filter (LEnKF), and Local Ensemble Transform Kalman Filter (LETKF). In TSMP, several observations can be used for assimilation, including soil moisture and pressure. In addition, a joint state-parameter update is also developed to estimate spatially distributed fields of the Manning's roughness parameter or saturated hydraulic conductivities (Kurtz et al. 2016) and other van Genuchten parameters (Brandhorst et al. 2023).

Kurtz et al. (2016) explored the potential for large-scale applications of high-resolution models, which are extremely computationally intensive. Studies by Baatz et al. (2017), Gebler et al.

(2019), Naz et al. (2019), and Li et al. (2024) show that soil moisture estimates are improved after assimilation of in-situ observations or satellite retrievals. Zhang et al. (2018) investigates the assimilation of groundwater level alone or together with soil moisture in synthetic experiments, Hung et al. (2022) and Li et al. (2023) further applied the methodology in real-world cases and found that assimilating groundwater level and soil moisture improved the characterisation of the subsurface status. Given the demonstrated effectiveness and reliability of the TSMP-PDAF, we also used it in this study to perform hydrological simulations and data assimilation experiments.

2.3 Triple Collocation (TC) method

The TC analysis was initially introduced and applied in meteorology by Stoffelen (1998), which enables the estimation of systematic and random errors in data obtained from three distinct sources without requiring a reference dataset. The methodology assumes a linear relationship between the soil moisture observations and the actual ground truth value θ (Gruber et al. 2017).

$$SM_i = \beta_i \theta + \alpha_i + \varepsilon_i \tag{2.25}$$

where $i \in [x, y, z]$ is one of the three collocated soil moisture datasets, α_i and β_i represent the additive and multiplicative biases of dataset i, respectively, while ε_i denotes the zero-mean random error. Accordingly, the covariances between the two soil moisture datasets would be given by

$$\begin{aligned} Cov\left(SM_x, SM_y\right) &= E\left(SM_x SM_y\right) - E\left(SM_x\right) E\left(SM_y\right) \\ &= \beta_x \beta_y \sigma_\theta^2 + \beta_x Cov\left(\theta, \varepsilon_y\right) \\ &+ \beta_y Cov\left(\theta, \varepsilon_x\right) + Cov\left(\varepsilon_x, \varepsilon_y\right) \end{aligned} \tag{2.26}$$

Considering the following assumptions by Yilmaz et al. (2014), orthogonality of errors $Cov\left(\theta, \varepsilon_x\right) = 0$, independence of errors $Cov\left(\varepsilon_x, \varepsilon_y\right) = 0$, and an expected error $E\left(\varepsilon_x\right) = 0$, the equation (2.26) can be reduced to:

$$\begin{aligned} Q_{xy} &= Cov\left(SM_x, SM_y\right) \\ &= \begin{cases} \beta_x \beta_y \sigma_\theta^2 & \text{for } x \neq y \\ \beta_x^2 \sigma_\theta^2 + \sigma_{\varepsilon_x}^2 & \text{for } x = y \end{cases} \end{aligned} \tag{2.27}$$

Given that we have seven unknowns (β_x, β_y, β_z, $\sigma_{\varepsilon_x}^2$,$\sigma_{\varepsilon_y}^2$, $\sigma_{\varepsilon_z}^2$, σ_θ) in a system of six equations, by introducing a new variable $\lambda_x = \beta_x \sigma_\theta$, the equation can be written as:

$$Q_{xy} = Cov\left(SM_x, SM_y\right) = \begin{cases} \lambda_x \lambda_y & \text{for } x \neq y \\ \lambda_x^2 + \sigma_{\varepsilon_x}^2 & \text{for } x = y \end{cases} \tag{2.28}$$

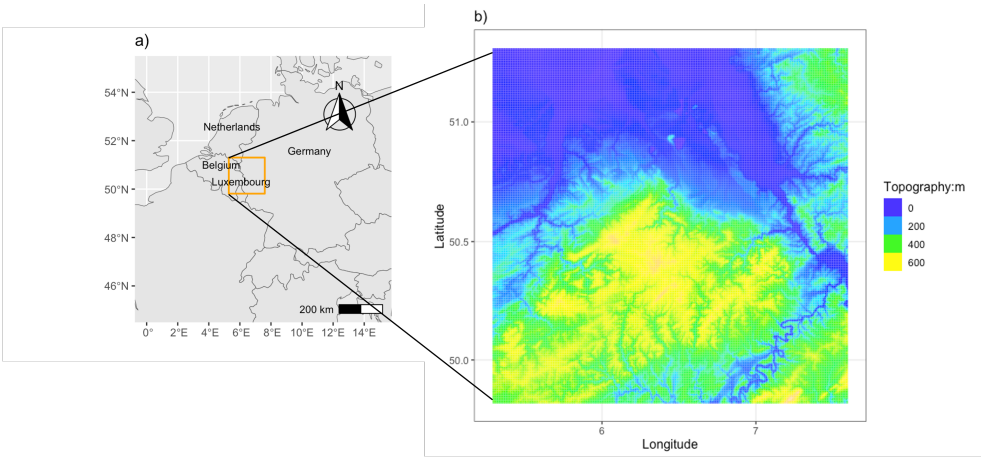

Figure 2.1: Overview of the research area a) location and b) topography.

2.4 Study area

The domain covers an area of 150 km × 150 km, including parts of western Germany (DE, Deutschland), parts of Belgium (BE), the Netherlands (NL) and Luxembourg (LUX) (see Fig.2.1). The climate in this region is controlled by the Atlantic Ocean, resulting in relatively mild conditions in spite of its latitude. Figure 2.2 shows the mean monthly daily maximum and minimum temperature together with precipitation data from 27 weather stations in North Rhine-Westphalia [Source: WorldData.info, retrieved on 10/03/2024, https://www.worlddata.info/europe/germany/climate-north-rhine-westphalia.php]. All data are monthly averages of the last 20 years. The model domain has very heterogeneous topography and land cover types. The central and southern parts of the domain are characterized by the hilly terrain of the Eifel regions with mountain ridges that are separated by narrow valleys. In contrast, the northern and northwestern parts of the domain are characterized by flat lowland regions. The elevation ranges from the plains at around 14 m a.s.l to the mountainous regions at around 735 m. The variability in topography influences the spatial distribution of precipitation. While the mountainous regions receive an average yearly precipitation of up to 1300 mm in the Eifel region (southwest) and up to 1600 mm in the Bergisches Land (northeast), the flat areas have an average yearly precipitation between 600 and 900 mm. Agriculture is the major land use type in this research domain, especially in the lowland areas. Major crops include winter wheat, maize, and sugar beet. The forest areas are mainly distributed in the mountainous areas, such as the Eifel region and Bergisches Land. Urban areas are mainly located along the Rhine Valley. Based on the FAO-UNESCO Soil Map of the World classification, clay loam is the most predominant soil texture in this model domain, followed by loam (e.g., Rhine Valley and Eifel regions), sand (the northwestern part of the domain), and clay. This study area was selected due to its heterogeneity in topography and soil properties, which provide a suitable test-bed for an integrated land surface-subsurface modelling. Furthermore, this region is well instrumented with a dense network of in situ observations. COSMOS-Europe (Bogena et al. 2022) stations and distributed in situ soil

moisture sensors offer valuable soil moisture information at multiple spatial scales. In addition, several Integrated Carbon Observation System (ICOS) sites are available within the domain, providing high-quality measurements of land-atmosphere fluxes. This observational data supports comprehensive model evaluation.

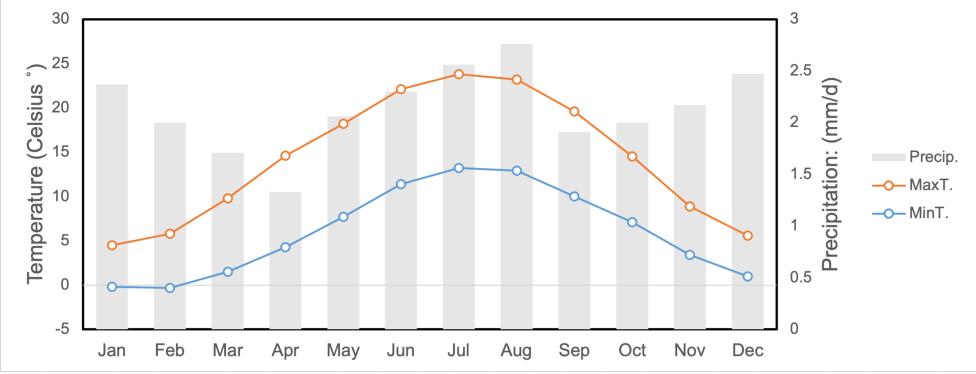

Figure 2.2: The mean monthly daily maximum temperature (red) and mean monthly daily minimum temperature (blue) and precipitation collected from 27 weather stations in North Rhine-Westphalia for the period 2003 to 2023.

2.5 Soil Moisture Active Passive (SMAP)

The Soil Moisture Active Passive (SMAP) satellite, launched in January 2015, is an Earth science satellite designed to provide high-resolution global measurements of soil moisture and freeze-thaw conditions (Entekhabi et al. 2010a). SMAP was originally designed with both a radar and a radiometer; however, following the radar failure in July 2015, soil moisture retrievals have relied solely on the radiometer. The SMAP radiometer measures brightness temperature at a spatial resolution of approximately 36 km. Using radiative transfer models, the soil moisture is retrieved and can be enhanced to 9 km through interpolation techniques. The SMAP satellite provides near-global coverage every 2-3 days, with an exact 8-day orbit (Entekhabi et al. 2010a). This data is valuable for a variety of applications, including hydrological modelling, land surface modelling, and climate research.

SMAP products are available in four different levels. Level 1 (L1) data are instrument data (from radar or radiometer) based on half orbits. Level 2 (L2) data are geophysical retrievals from L1 (Colliander et al. 2017). Level 3 (L3) products are global daily composites. The L4 products are value-added products generated through the integration of a land surface model and the assimilation of the SMAP data. Following the radar failure, the SMAP Enhanced Passive Soil Moisture products (L2_SM_P_E and L3_SM_P_E) are developed using radiometer brightness temperature observations and the Backus–Gilbert optimal interpolation technique to improve spatial resolution (Chan et al. 2018). L3_SM_P_E is a daily composite product, which is generated from L2_SM_P_E over a one-day composite.

In this Ph.D. research, we used the L3_SM_P_E product, which provides soil moisture data on a 9 km grid (National Snow and Ice Data Center (NSIDC), https://nsidc.org/data/smap/smap-data.html). The temporal coverage spans from April 2015 to the present. The performance of this enhanced product has been evaluated against long-term in situ soil moisture observations, with a mean Unbiased Root Mean Square Error (ubRMSE) (ubRMSE) of approximately 0.055 cm^3 / cm^3 (Chan et al. 2018; Kim et al. 2018; Li et al. 2018a; Stillman et al. 2018; Wang et al. 2021). Comparative studies have generally shown that the performance of the SMAP mission outperforms the SMOS mission in many regions and conditions (Chen et al. 2018; Chen et al. 2017b; Ma et al. 2019). This advantage is also reflected in DA studies, where SMAP products have demonstrated a greater potential to improve LSM simulations compared to SMOS data (Blyverket et al. 2019; Mousa et al. 2020a).

3

The importance of subsurface processes in land surface modeling over a temperate region: An analysis with SMAP, Cosmic Ray Neutron Sensing and Triple Collocation analysis.

*adapted from: Zhao, H., Montzka, C., Baatz, R., Vereecken, H., & Franssen, H. J. H. (2021). The importance of subsurface processes in land surface modeling over a temperate region: An analysis with SMAP, Cosmic Ray Neutron Sensing, and Triple Collocation analysis. Remote Sensing, 13(16), 3068.

3.1 Introduction

Soil moisture exerts an important control on the water and energy cycles in the atmosphere-land surface-subsurface continuum. Therefore, improving soil moisture estimation is beneficial for understanding the partitioning of water and energy fluxes. Soil moisture variability in the unsaturated zone is affected by water exchanges between the unsaturated zone, atmosphere, and groundwater. Studies have been focused on the effects of groundwater dynamics on land surface processes, showing the role of the groundwater in the water and energy cycles (Hidayat et al. 2017; Sulis et al. 2018). Results indicate that groundwater has little impact on soil moisture in deep groundwater regions; however, in districts with shallow groundwater, such as wetlands and river valleys, groundwater can become a major source of soil water (Chen et al. 2004; Ochoa et al. 2009; Zipper et al. 2015). The groundwater table depths and hydraulic gradients between saturated and unsaturated soils can cause capillary rise and make groundwater a constant water supply, leading to altered runoff and evaporation rates (Appels et al. 2017; Johnson et al. 2010). The land surface energy balance is affected by soil moisture states and land surface temperature (Alkhaier et al. 2009, 2012; Martínez-de la Torre et al. 2019).

Despite the importance of subsurface flow, most current LSMs neglect the lateral flow between grid cells or at sub-grid scales and only consider the water exchange in the vertical direction. Such models include the Variable Infiltration Capacity (VIC) model, the Interaction Soil Biosphere Atmosphere (ISBA) land surface scheme, Noah Land Surface Model(CLM). Recently, some works have considered the role of lateral subsurface flow and developed three-dimensional hydrological models coupled with LSMs, such as CATHY (CATchment HYdrology), NoahMP (Niu et al.

2014a), VIC-MD (MODFLOW) (Sridhar et al. 2018), and CLM-ParFlow (Kollet et al. 2008). These models aim at simulating the subsurface water and energy cycles more realistically than uncoupled models. However, model predictions are affected by errors given the uncertainty of the many required input parameters, e.g., atmospheric forcing, soil texture, and vegetation properties (Dumedah et al. 2014). Precise soil hydraulic parameter data and land cover type information are hard to obtain, as most areas lack sufficient land surveys. Also, the model structure and further assumptions influence the simulation performance. A large number of parameters used in land surface models are hard-coded as constants, although they are calculated by linear regression from preliminary studies using a limited amount of data and known to be uncertain (Cuntz et al. 2016).

Soil moisture can be measured via automated techniques such as gravimetric methods, nuclear techniques (such as neutron scattering, Gamma ray attenuation), electromagnetic methods (e.g., the time domain reflectometry TDR and the frequency domain reflectometry FDR), tensiometers, and hygrometry (Babaeian et al. 2019; Hanson 2009; Walker et al. 2004). However, most sensors monitor soil moisture at point scales (radius less than 1 m) only. As soil moisture is very heterogeneous in space and time, one usually needs to collect data from multiple locations in a specific area (Montzka et al. 2020). To reduce the scale gap between remote sensing products and modelling results and to obtain area-averaged soil moisture, a new technology has emerged with the CRNS. It measures neutron count intensity and determines soil moisture in a non-invasive and continuous way (Franz et al. 2012b). The omnipresent cosmic radiation produces neutrons that interact with the atmosphere and ground. These secondary neutrons include fast neutrons, which are generated by collisions between high-energy neutrons and nuclei. Fast neutrons are easily moderated by hydrogen atoms. As soil is the main source of hydrogen, the variations of fast neutrons are strongly related to soil moisture changes. The process of moderation can be captured and counted by cosmic-ray neutron sensors (Zreda et al. 2008, 2012). The large spatial footprint makes it suitable for agricultural water resources management and remote sensing product validation (Montzka et al. 2017).

Two innovative satellite missions that include L−band (1200-1400 MHz) passive microwave systems have already been launched, including SMOS (The Soil Moisture and Ocean Salinity mission, launched in November 2009) (Kerr et al. 2010) and SMAP (The Soil Moisture Active Passive mission, launched in January 2015 and starting operations in April 2015) (Entekhabi et al. 2010a). Both SMOS and SMAP aim to measure soil moisture globally. After SMAP radar stopped operation in July 2015, an enhanced product was developed to give high-resolution observations at 9 km resolution. This enhanced product was evaluated by comparing it with long-term in situ soil moisture data (Chan et al. 2017; Zhang et al. 2019c). It was found that the average ubRMSE (unbiased Root Mean Square Error) in L2_SM_P_E (Level 2 Enhanced Passive Soil Moisture) product and L3_SM_P_E (Level 3 Enhanced Passive Soil Moisture) product are between $0.040 \sim 0.055$ cm^3 / cm^3 (Colliander et al. 2017, 2021; Zhang et al. 2019c), which barely meets the accuracy requirements of the SMAP mission. A number of previous studies have compared SMAP products and/or model simulations with in-situ observations. El Hajj et al. (2018) evaluated SMAP soil moisture products at sites in Southwestern France and found that the average bias over stations was about -0.032 cm^3 / cm^3, indicating SMAP

moderately underestimates the soil moisture compared to in situ observations. Walker et al. (2019) compared SMAP soil moisture with validation sites in the South Fork River watershed in Iowa, U.S., and found that the bias could be up to -0.04 cm^3 / cm^3 in early-spring and late fall and improve to -0.02 cm^3 / cm^3 in the summer time. At global scale, a study indicated that SMAP shows a dry bias (Kim et al. 2018). Recently, a new COSMOS network is developed to provide a unified, standardized, publicly available, traceable and objective validation procedure that is operational in ISMN and the QA4SM online validation service for soil moisture products (Bayat et al. 2021). In this platform, soil moisture from ERA5, ERA5-Land, and GLDAS are provided for validation, but subsurface processes are not considered (Bayat et al. 2021). As mentioned, SMAP was only compared to soil moisture simulated by stand-alone land surface models that have a rather simple subsurface structure and do not consider the role of groundwater and lateral flows (Bi et al. 2016; Li et al. 2018a; Pan et al. 2016), which could lead to systematic deviations. Studies show that soil moisture can be overestimated when the representation of topography in LSMs is simplified or insufficient (Forrester et al. 2020; Soulis et al. 2000). Also, previous studies focused mostly on large scales and simulations at a coarser spatial resolution (Albergel et al. 2012; Duygu et al. 2019; Montzka et al. 2017).

To find relative error estimates for different products, the Triple Collocation (TC) method is used, which is an error magnitude estimation approach for inter-comparison among three or more independent observed or modelled datasets (Stoffelen 1998). The method was first used for ocean wind studies and then developed and widely used in other areas, such as land surface hydrology (Caires et al. 2003; Chen et al. 2016; Gruber et al. 2017, 2016; McColl et al. 2014; Roebeling et al. 2012). It has been proven to be a useful tool to understand the random error variances of remote sensing time series. It assumes one of these datasets as a reference to relative re-scaling, and further assumes truth-error orthogonality and zero error cross correlation between datasets to obtain a bias-free TC analysis (Chen et al. 2016; Gruber et al. 2017; Yilmaz et al. 2014). Here, we present simulated soil moisture by CLM and the CLM-ParFlow coupled model and compared it with CRNS observations and SMAP enhanced soil moisture datasets using the TC method. Compared to the CLM model, CLM-ParFlow considers three-dimensional water flow in the subsurface (soil and aquifer) and a two-dimensional overland flow module. It is investigated whether a better subsurface representation can improve soil moisture estimates. The research area has various land use types, and various pedological, hydrological, and hydrogeological site conditions were observed. These small-scale hydrological processes can provide insights for large-scale modelling. This research aims to understand the performance and limitations of the subsurface role in land surface model simulations, which might recall the need to consider hydrogeology (including complex 3D geology and critical parameters like hydraulic conductivity and storage coefficients) in soil-vegetation-atmosphere processes, and to obtain more accurate soil moisture and groundwater level data.

3.2 Materials and methods

3.2.1 Study area

The study area is located in central Europe, encompassing parts of North Rhine-Westphalia and Rhineland-Palatinate in western Germany and parts of Belgium, the Netherlands, and Luxembourg, covering an area of 150 km × 150 km (see Figure 3.1). This region has a sub-Atlantic oceanic climate. Summers are mild, while winters are humid and relatively mild. The average monthly temperatures are highest in July (18 °C) and lowest in January (3 °C). There is a large spatial variability in precipitation due to topography. In the rather flat Lower Rhine area in the North of the study region, the yearly precipitation is between 600 mm and 900 mm (Kreklow et al. 2020). In the southern low mountain ranges, the average yearly precipitation is locally 1600 mm in the Bergisches Land (North East) and 1300 mm in the Eifel (South West). The rainfall is frequent and evenly distributed over the seasons. The elevation in this area ranges from the plains at around 14 m a.s.l. to the mountainous areas at around 735 m.

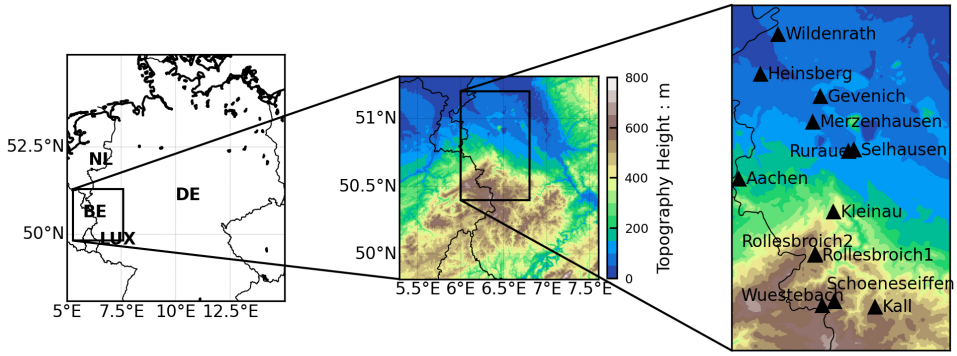

Figure 3.1: The research area and thirteen CRNS locations (denoted as black triangles).

The land use is a mixture of agricultural areas, forests, urban and rural areas, water, grassland, industry, and mining (Sulis et al. 2018). The dominant land use is agriculture, covering more than 60 % of the area (shown in Figure 3.2). The major crops are winter wheat, maize, and sugar beet. Forests cover nearly 20 % of this area and are mainly located in the south, i.e., Eifel, Bergisches Land, and Sauerland. The dominant soil textures are sandy loam, loam, and clay loam, and our simulations are based on the FAO/UNESCO Soil Map (Batjes 1997). Sandy soils with low water holding capacities are mainly located in the Northwest region.

This research area has three solid rock areas of regional importance (Herrmann et al. 2015). The largest part is Palaeozoic rocks located in the southern and eastern part, having the dominant aquifer typology “schist and shales” that includes folded and partly metamorphosed clastic sedimentary rocks. This part has a low hydraulic conductivity. The north-eastern part is mainly occupied by unconsolidated rocks of the Cenozoic era, including alternating sequences of clastic sedimentary rocks horizontally. In this region, hydraulic conductivity varies significantly

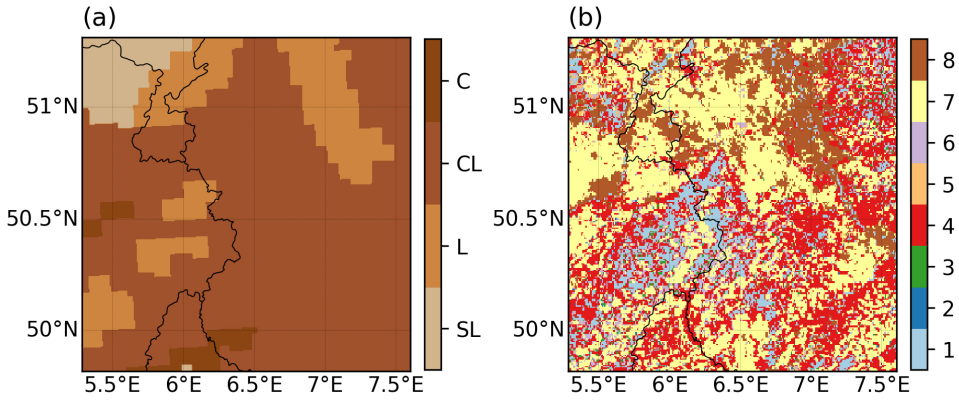

Figure 3.2: Map of the North Rhine-Westphalia (NRW) domain for (a) soil texture and (b) plant functional types. The soil textures are divided into sandy loam (SL), loam (L), clay loam (CL), and clay (C). The PFT´s are defined as: 1- needle-leaf evergreen tree (NET), 2-needle-leaf deciduous tree (NDT), 3-broad-leaf evergreen tree (BET), 4-broad-leaf deciduous tree (BDT), 5-broad-leaf deciduous shrub (BDS); 6-grassland (GRASS), 7-crop (CROP), 8-barren soil (BARE).

depending on the composition and arrangement of the different sediment layers. In the western part, the dominant aquifer rocks are mostly consolidated, weakly permeable material from the Mesozoic.

Soil moisture validation activities have been performed in this area before based on in situ and CRNS data (Hasan et al. 2014; Kerr et al. 2010; Montzka et al. 2013, 2016) as well as simulation and data assimilation experiments (Baatz et al. 2017; Han et al. 2014, 2013; Shrestha et al. 2014).

3.2.2 Data

3.2.2 (a) Land surface modelling

Soil moisture was simulated by the land surface model CLM and the coupled land surface-subsurface model CLM–ParFlow. The CLM model was developed by the The National Center for Atmospheric Research (NCAR). In the CLM 3.5 model, the soil is discretized into 10 unevenly distributed soil layers (see Table 3.1). Soil hydraulic properties are estimated internally from soil texture (sand fraction and clay fraction) using pedo-transfer functions according to Clapp et al. (1978) and Cosby et al. (1984). A simplified Richards equation is used in CLM to calculate the vertical water movement in the unsaturated zone:

$$\frac{\partial \theta}{\partial t} = \frac{\partial}{\partial z}\left[k_{sat} \cdot \frac{\partial(\varphi + z)}{\partial z}\right] + q_s \tag{3.1}$$

where $\frac{\partial\theta}{\partial t}$ is the soil moisture [-] change over time, k_{sat} represents the saturated hydraulic conductivity [L·T^{-1}], φ is the soil matric potential pressure head (unit is defined as length [L], z as the vertical coordinate [L] and q_s is the source / sink term (i.e., the soil water removed due to evaporation). A main limitation of CLM 3.5 is that lateral flows are not considered, and groundwater is not represented, although groundwater can strongly influence soil moisture conditions.

Table 3.1: Soil layer depth in CLM model.

Layer	1	2	3	4	5	6	7	8	9	10
Depth (m)	0.010	0.035	0.075	0.135	0.235	0.400	0.650	1.050	1.650	2.500

ParFlow (Maxwell et al. 2005) is a numerical, integrated hydrological model that simulates subsurface groundwater flow and water flow in soils, as well as overland flow. Both retention and relative permeability curves are represented by the van Genuchten relationships (Van Genuchten 1980). ParFlow does not include land surface processes (e.g, evaporation), nor does it have a parameterization scheme for frozen soil and ice processes. In addition to the DEM dataset used in CLM, the topographic slopes need to be specified for ParFlow. When coupled with CLM, ParFlow replaces the one-dimensional CLM soil moisture characterization by the three-dimensional approach in CLM-ParFlow, considering the redistribution of soil moisture, and integrating vertical and lateral flow of groundwater and surface water.

$$S_s S_p \frac{\partial p}{\partial t} + \phi \frac{\partial S_p}{\partial t} - \nabla \cdot [k_{sat} k_r(p) \nabla (p - z)] = q_s \tag{3.2}$$

In this equation, S_s is the specific storage coefficient (L^{-1}), S_p is the relative saturation, ϕ is the porosity, k_r is the relative permeability [-]. The subsurface is discretized into 30 layers, with 10 vertically layered near the surface (2 – 100 cm) and 20 constant levels (135 cm depth) that reach up to 30 m below the surface. The physically based coupled model (CLM-ParFlow) can better simulate the role of groundwater in terrestrial systems, and the interaction between surface water and subsurface (Maxwell et al. 2005).

To represent the high spatial heterogeneity of the land surface, the simulation domain was discretized into grid cells of 500 m × 500 m. The plant functional types (PFTs) were based on MODIS land cover data. The hilly areas are mostly covered by broad-leaf forest and needle-leaf forest, while the other flat regions are covered by crops and urban areas. Soil texture information was taken from the FAO/UNESCO Soil Map (Batjes 1997) with the scale of 1: 5,000,000 (see Figure 3.2). Most of the model domain is dominated by clay-loam (35 % clay, 35 % sand, 30 % silt). Sandy loam (10 % clay, 65 % sand, 25 % silt) and loam (20 % clay, 40 % sand, 40 % silt) are dominant in the north-western part. Clay (45 % clay, 15 % sand, 40 % silt) is found in the northwestern corner of the domain. The van Genuchten water retention parameters and the hydraulic conductivity used in CLM-ParFlow are calculated by the Rosetta pedo-transfer function (Schaap et al. 2001), summarized in Table 3.2.

To drive the model, the high-resolution reanalysis dataset (COSMO-REA6) (Bollmeyer et al. 2015) was used as meteorological forcing. This dataset covers the period 1995 – 2020 and is continuously

Table 3.2: Subsurface hydraulic properties used in CLM-ParFlow simulations.

Parameter	Clay	Clay loam	Loam	Sandy loam
k_{sat} (m h^{-1})	0.0062	0.0034	0.0050	0.0158
α (m^{-1})	2.1	2.1	2.0	2.7
n	2.0	2.0	2.0	2.0
θ_{sat}	0.4701	0.4449	0.4386	0.4071
θ_{res}	0.21	0.17	0.15	0.10

supported by DWD (Deutscher Wetterdienst, German Meteorological Service). It uses ERA-Interim data as a boundary condition and is generated by assimilating observed meteorological data into the atmospheric model COSMO (the Consortium for Small-scale Modelling) (Baldauf et al. 2011). The dataset comprises air temperature, precipitation, humidity, incoming shortwave and longwave radiation. A 2-year spin-up period was applied for CLM, and the initial conditions for CLM-ParFlow were taken from previous studies (Shrestha et al. 2014; Sulis et al. 2018). Both simulations with CLM and CLM-ParFlow started from a near-equilibrium condition. Thus, different spin-up treatments do not have an influence on results. In total, a period of two years (2017-2018) was simulated with a time step of 3600 s. In case of convergence issues, the time steps are reduced until convergence can be achieved.

The simulated soil moisture for the upper 5 cm layer (SM_{5cm}) and the upper 20 cm (SM_{20cm}) were derived by vertically averaging the model output ($H2OSOI_i$, where i is the index denoting the soil layer) across the corresponding depth intervals. The weights are based on the fractional contribution of each soil layer to the target depth, accounting for the thickness of each model layer:

$$SM_{5cm} = 0.14 \times \ H2OSOI_1 + 0.56 \times H2OSOI_2 + 0.30 \times \ H2OSOI_3 \tag{3.3}$$

$$\begin{aligned} SM_{20cm} =& 0.0165 \times \ H2OSOI_1 + 0.0651 \times H2OSOI_2 + \\ & 0.1451 \times \ H2OSOI_3 + 0.2770 \times \ H2OSOI_4 \end{aligned} \tag{3.4}$$

3.2.2 (b) CRNS observations

The CRNS is an emerging technology to monitor soil moisture at the intermediate scale (Franz et al. 2012b; Zreda et al. 2008). The measured neutron count intensity provides an estimate of soil moisture content for a radius of around 240 m, at sea level and dry bare soil conditions. The radius is a function of air density, air humidity, and vegetation density (Köhli et al. 2015). The penetration depth of the CRNS measurements varies from 15 cm (wet soils) to 55 cm (dry soils) (Schrön et al. 2017b). The neutron count intensity is mainly sensitive to the number of hydrogen atoms in the soil, but is also influenced by changes in atmospheric pressure, vapor pressure, and incoming cosmic radiation. These factors are considered in the standard correction process (Baatz et al. 2015; Jakobi et al. 2018).

Several studies have been conducted to investigate the accuracy of the CRNS measurements and found that CRNS provides reliable soil moisture estimates when calibrated properly (Bogena et al. 2013; Tian et al. 2016; Zhu et al. 2016). Bogena et al. (2018) found that even for a densely

vegetated and wet site, the RMSE of daily soil moisture estimated by CRNS is only 0.03 cm^3 / cm^3. In our work, thirteen CRNS stations are used to evaluate SMAP and soil moisture model products (see Figure 3.1). The datasets are collected in the context of the TERENO project (Bogena 2016) and passed quality assurance procedures. We acknowledge that the effective depth of CRNS is dependent on soil moisture and also on the depth of the calibration dataset. Our CRNS calibration and validation used individual support volumes of samples from 5 cm, 20 cm, and 50 cm based on the gravimetric method. We calculate the penetration depth based on a previous study (Franz et al. 2013) and found that the effective penetration depth is mostly between 15 cm $\sim$ 30 cm in our research area and period. The mean and median of penetration depth are 20.3 cm and 18.6 cm, respectively. Hence, we assumed that the CRNS has an effective penetration depth of 20 cm. Table 3.3 provides more information about the CRNS stations.

Table 3.3: Coordinates, altitude (m), average annual precipitation (mm y^{-1}), land use type information for 13 sites.

Name	Lat.	Lon.	Alt. (m)	Precip. (mm)	Land use	Clay (%)	Sand (%)	Bulk density (g cm^{-3})
Merzenhausen	50.9303	6.29747	94	825	Crop	22	21	1.39
Aachen	50.7986	6.02472	232	952	Crop	23	22	1.20
Selhausen	50.8659	6.44719	–	–	Crop	24	16	1.26
Heinsberg	51.0411	6.10424	57	814	Grassland, crop	19	18	1.27
Wüstebach	50.5049	6.33092	605	1401	Spruce	23	19	0.83
Gevenich	50.9892	6.32355	108	884	Crop	20	22	1.31
Rollesbroich1	50.6219	6.30424	515	1307	Grassland	23	22	1.09
Rollesbroich2	50.6242	6.30514	–	–	Grassland	–	–	1.09
Ruraue	50.8623	6.42734	102	743	Grassland	26	19	1.12
Wildenrath	51.1327	6.16918	76	856	Needleleaf forest	12	65	1.15
Kall	50.5013	6.52645	504	935	Grassland	22	20	1.31
Schoeneseiffen	50.5149	6.37559	–	–	Grassland	24	16	1.11
Kleinhau	50.7224	6.37204	–	–	Grassland	25	15	1.12

3.2.2 (c) SMAP Enhanced Soil Moisture L3_SM_P_E product

SMAP provides soil moisture observations of the top 5 cm of the soil and thaw/freeze states derived from the passive microwave brightness temperature (BT). BT is recorded by a conically-scanning antenna beam at L-band with a 40° incidence angle. This results in a -3 dB antenna footprint of 40 km. To enhance the resolution of the typically 36 km SMAP radiometer data posting, the Backus-Gilbert optimal interpolation technique is used to interpolate the multiple scans of a single location. It makes the most use of the available information and provides a better representation of the original data (Chan et al. 2017).

In this study the L3_SM_P_E product (version 4) was used, which provides soil moisture on a 9 km EASE2 (Equal-Area Scalable Earth-2) grid (National Snow and Ice Data Center NSIDC, https://nsidc.org/data/smap/smap-data.html (accessed on 1 August 2021). The soil moisture baseline retrieval algorithm in L3_SM_P_E product is performed by the vertical polarization single channel algorithm (SCA-V) (https:$//$nsidc.org$/$data$/$smap$/$technical-references,

accessed on 1 August 2021). The L3_SM_P_E product is provided in the form of global daily datasets, including soil moisture measured for the 6:00 a.m. (descending) and 6:00 p.m. (ascending) orbit. Here, the soil moisture daily value is calculated by taking the average of the two datasets. To eliminate the non-high-quality pixels, the surface and quality flags are used (retrieval_qual_flag and surface_flag).

3.2.3 Methods

3.2.3 (a) Data processing

Both 2017 (normal year) and 2018 (dry year) were selected to be evaluated for all datasets. In order to avoid unreliable soil moisture observations during frozen conditions and snow cover, the winter period (December, January, and February) was excluded.

The model simulations are sampled onto the SMAP grid by nearest neighbor (NN) search. Compared to area-wide space-borne observation and model simulation results, the CRNS stations are quite sparse. As the spatial coverage of measurements by a CRNS is close to the model grid size in this work, CRNS observations are compared to a complete cell of the CLM, CLM-ParFlow, and SMAP grid containing the coordinates of the CRNS stations.

The SMAP product and the model grids are at different spatial resolutions (9 km vs. 500 m), and a comparison between SMAP soil moisture and modeled soil moisture is made at both resolutions. The fine resolution (model grid) provides a detailed assessment of the spatial variability, and the coarse resolution (SMAP grid) gives a smoothed representation, excluding local noise. The comparison at the 9 km resolution is made by taking the arithmetic average of simulated soil water content data on the 500 m grid to get modeled values at the 9 km resolution (upscaling). The comparison at the 500 m resolution is made by downscaling the SMAP data, using the nearest source to destination to remap from 9 km resolution to 0.5 km resolution. In this case, for each model grid cell, it takes the value from the nearest SMAP grid cell. This is done by ESMF (Earth System Modeling Framework) regridding function in NCL (NCAR Command Language).

3.2.3 (b) Standard evaluation metrics

Statistical performance was evaluated according to Good Practices Guidelines (Gruber et al. 2020; Montzka et al. 2020), including bias, Root Mean Square Difference (RMSD), and unbiased Root Mean Square Error (ubRMSD). The bias is given by

$$bias = \frac{1}{n}\sum_{i=1}^{n}(X_i - X_{i,ref}) \tag{3.5}$$

where X_i represents a simulated or remotely sensed product, and $X_{i,ref}$ is the referenced soil moisture dataset. The sample size is n.

The Root Mean Square Deviation (RMSD) is given by

$$RMSD = \sqrt{\frac{1}{n}\sum_{i=1}^{n}(X_i - X_{i,ref})^2} \tag{3.6}$$

and the unbiased root mean squared difference (ubRMSD) is

$$ubRMSD = \sqrt{RSMD^2 - bias^2} \tag{3.7}$$

The correlation between different soil moisture datasets (X and Y) was calculated using the Pearson correlation coefficient ($r_{X,Y}$). Here, the focus is on the dynamics of the different time series rather than absolute soil moisture values, considering the fundamental scale mismatch between the CRNS, SMAP, and LSM model grids, which cannot be adequately considered without complex scaling functions. The ubRMSD and $r_{X,Y}$ screen out the influence of bias between different amplitudes of soil moisture variation (Entekhabi et al. 2010b).

$$r_{X,Y} = \frac{cov(X,Y)}{\sigma_X \sigma_Y} \tag{3.8}$$

where $cov(X,Y)$ represents the covariance between two datasets, σ_X and σ_Y are the standard deviations for dataset X and Y.

3.2.3 (c) Triple Collocation (TC)

The method is based on the assumption that a measurement system can be understood as being composed of an additive systematic error (α_i), multiplicative systematic error (β_i), additive zero-mean random error (ε_i), and θ (the underlying truth value) Gruber et al. 2017.

$$i = \alpha_i + \beta_i\theta + \varepsilon_i, i \in [X,Y,Z] \tag{3.9}$$

X, Y, and Z denote the time series of soil moisture products to be compared. Here, the assumption is that the errors are uncorrelated with each other ($cov(\varepsilon_i, \varepsilon_j) = 0, i \neq j$) and with θ ($cov(\varepsilon_i, \theta) = 0$). It applies to both reference datasets and soil moisture products to be evaluated. Given that all observation data have errors, in this study, we assumed that X is the reliable CRNS dataset, which is well calibrated and without multiplicative (second-order) error, Z is the SMAP L3 enhanced product, and Y denotes the soil moisture in the upper 5 cm of CLM and CLM-ParFlow simulations. The β_x is set to 1, and other scaling factors are calculated according to equations 3.10 - 3.12 to eliminate the scale differences of different products. This assumption was also made in other studies (Gruber et al. 2020, 2016; Scipal et al. 2008).

$$\beta_X = 1 \tag{3.10}$$

$$\beta_Y = \frac{cov(X,Z)}{cov(Y,Z)} \tag{3.11}$$

$$\beta_Z = \frac{cov(X,Y)}{cov(Z,Y)} \tag{3.12}$$

The scaling factor can be regarded as a form of regression, by taking a third variable as a tool to resolve the relationship between the two variables (Su et al. 2014). It can be used to describe the soil moisture sensitivities. The unscaled error variances, which represent the variance of the scaled white noise of each product, can be solved by

$$\sigma^2_{\varepsilon X} = \left| var(X) - \frac{cov(X,Y)cov(X,Z)}{cov(Y,Z)} \right| \tag{3.13}$$

$$\sigma^2_{\varepsilon Y} = \left| var(Y) - \frac{cov(Y,X)cov(Y,Z)}{cov(X,Z)} \right| \tag{3.14}$$

$$\sigma^2_{\varepsilon Z} = \left| var(Z) - \frac{cov(Z,Y)cov(Z,X)}{cov(Y,X)} \right| \tag{3.15}$$

In addition, the signal-to-noise ratios (SNRs) are calculated, which provides a clearer representation of the ratio between soil moisture and uncertainty magnitude (Gruber et al. 2020). It is a combination of several information sources, including the sensitivity of the measurement system, the variability of the true value (θ^2), and the variability of the random error (ε^2)(McColl et al. 2014). SNRs are not normalized to the range from 0 to 1, but are often expressed in decibel (dB) units.

$$SNR_X = -10log(\left| \frac{var(X)cov(Y,Z)}{cov(X,Y)cov(X,Z)} - 1 \right|) \tag{3.16}$$

$$SNR_Y = -10log(\left| \frac{var(Y)cov(X,Z)}{cov(Y,X)cov(Y,Z)} - 1 \right|) \tag{3.17}$$

$$SNR_Z = -10log(\left| \frac{var(Z)cov(X,Y)}{cov(Z,X)cov(Z,Y)} - 1 \right|) \tag{3.18}$$

3.3 Results and discussions

3.3.1 Agreement between space-borne and in situ observations

Table 3.4 shows that the SMAP L3_SM_P_E product and CRNS observations have, in general, a relatively good agreement. The detailed time series of soil moisture from SMAP, CRNS, and LSMs at 13 sites are provided in Appendix 3.6. The SMAP product and CRNS show, on average, not large systematic differences, while previous studies (Colliander et al. 2021; Montzka et al. 2017) found that SMAP tends to underestimate soil moisture compared to CRNS measurements at most sites. In terms of the average r value, the SMAP is relatively well correlated to CRNS, ranging from 0.653 to 0.825, except for Ruraue station (r = 0.452). The Ruraue station is located near the Rur river, and part of the closest SMAP pixels contain some amount of open fresh water. The presence of open water introduces a soil moisture bias due to the lower brightness temperature for the grid cell. This may partly explain the low r for the Ruraue station.

However, it should be noted that local differences are large. One reason is that the CRNS footprint is still much smaller than a 9 km SMAP pixel. This spatial mismatch could lead to

Table 3.4: Comparison metrics for the SMAP L3_SM_E_P product compared to CRNS.

Name	Bias	RMSD	ubRMSD	r
Merzenhausen	0.076	0.096	0.059	0.674
Aachen	-0.003	0.049	0.049	0.768
Selhausen	0.031	0.066	0.059	0.653
Heinsberg	0.070	0.091	0.057	0.668
Wüstebach	-0.120	0.133	0.057	0.752
Gevenich	0.067	0.088	0.058	0.684
Rollesbroich1	-0.023	0.060	0.055	0.741
Rollesbroich2	-0.053	0.077	0.055	0.708
Ruraue	0.030	0.080	0.075	0.452
Wildenrath	0.133	0.143	0.053	0.654
Kall	-0.072	0.086	0.047	0.825
Schoeneseiffen	-0.055	0.079	0.056	0.718
Kleinhau	-0.018	0.051	0.048	0.789
Average	**0.005**	**0.085**	**0.056**	**0.699**

differing soil hydraulic parameters and land cover between CRNS and SMAP observations (see Tables 3.3 and 3.5), causing lower correlation between the two soil moisture datasets. It is also important to consider that the satellite observations are negatively impacted by high vegetation density, topography, frozen soil, snow cover, and volume scattering effect in the case of low soil moisture content. The retrieval under dense forest is challenging or impossible since the recorded signal (brightness temperature) originates to a large extent from the canopy instead of the soil microwave emissions (Dubois et al. 1995; Li et al. 2019). When vegetation density increases, the impact of soil moisture on changes in ground emissivity becomes invisible; hence, the contribution of the ground is less than from the canopy. A large bias is observed in Wildenrath, where the land cover type is needle leaf (forest). Moreover, topography as well as surface roughness increases the surface area and alters the total microwave emission. In addition, it is also found that areas with complex topography are prone to shadowing and adjacency effects (Mialon et al. 2008; Talone et al. 2007).

It should be noted that the soil organic matter content is high at the Wüstebach site, and there is a large difference in the bulk density between ancillary data (1.3 g/cm^3) and the actual observed value (0.83 g/cm^3). In the single-channel algorithm used by SMAP to retrieve soil moisture, the dielectric mixing model plays an important role in describing the relationship between soil moisture and microwave emissivity. The higher ancillary bulk density assumes a more mineral soil composition in the dielectric mixing model. A recent study has found that high levels of organic matter decrease the microwave effective dielectric constant and therefore cause higher brightness temperature for a particular soil moisture content (Park et al. 2019). The observed brightness temperatures may be higher than expected by the retrieval model, causing the algorithm to interpret the signal as drier soil conditions and thereby underestimate soil moisture.

Table 3.5: Ancillary datasets used in the SMAP soil moisture retrieval algorithm. Notice that altitudes differ from Table 3.3 for the sites because here we list the altitudes used by SMAP.

Name	DEM (m)	IGBP class	Clay (%)	Sand (%)	Bulk density (g cm^{-3})
Merzenhausen	79	12: Croplands	21	39	1.40
Aachen	209	12: Croplands	22	41	1.40
Selhausen	105	13: Urban and built-up lands	23	37	1.40
Heinsberg	45	13: Urban and built-up lands	21	39	1.40
Wüstebach	610	1: Evergreen needleleaf forests	20	42	1.30
Gevenich	99	12: Croplands	22	41	1.40
Rollesbroich1	520	14: Cropland/natural vegetation mosaics	20	42	1.30
Rollesbroich2	520	14: Cropland/natural vegetation mosaics	20	42	1.30
Ruraue	98	12: Croplands	22	39	1.40
Wildenrath	79	5: Mixed forests	22	41	1.40
Kall	510	14: Cropland/natural vegetation mosaics	20	40	1.30
Schoeneseiffen	567	5: Mixed forests	20	42	1.30
Kleinhau	347	5: Mixed forests	20	42	1.30

3.3.2 Comparison of model simulation and CRNS measurements

The 500 m modeled soil moisture was compared with CRNS measurements, assuming a measurement depth of 20 cm. Bias, RMSD, ubRMSD, and correlation coefficient were calculated for thirteen stations and over three seasons (see Table 3.6 and Figure 3.3). The CLM simulations tend to overestimate soil moisture with a bias of 0.070 cm^3 / cm^3, and CLM-ParFlow has a slight dry bias of -0.021 cm^3 / cm^3. The large wet bias of the models for Wildenrath is most likely related to soil texture. Soil moisture decreases faster in sand than in finer-textured soil. The sand content is high (up to 65 %), and the models seem to have too low hydraulic conductivity for this site. CLM-ParFlow shows a large bias at sites located at a higher elevation, such as Wüstebach, Rollesbroich, and Schoeneseiffen sites.

After overlooking systematic bias, ubRMSD for the CLM stand-alone model and the coupled model are not significantly different and both are below 0.06 cm^3 / cm^3, which indicates that both simulations could produce reasonable results. The correlation between CRNS observations and land surface simulations ranges from 0.576 to 0.821 for CLM stand-alone and 0.365 to 0.805 for CLM-ParFlow. Both CLM and CLM-ParFlow simulations show a strong correlation with in situ data, suggesting that the soil moisture dynamics at the 500 m scale can be relatively well captured by both models.

3.3.3 Temporal and spatial correlation between model simulations and the SMAP L3_SM_P_E product

Figure 3.4 shows daily mean soil moisture content in the upper soil layer (5 cm) over the research area for CLM and CLM-ParFlow simulations compared with the SMAP L3_SM_P_E product, together with the daily precipitation time series. The SMAP product and model simulations

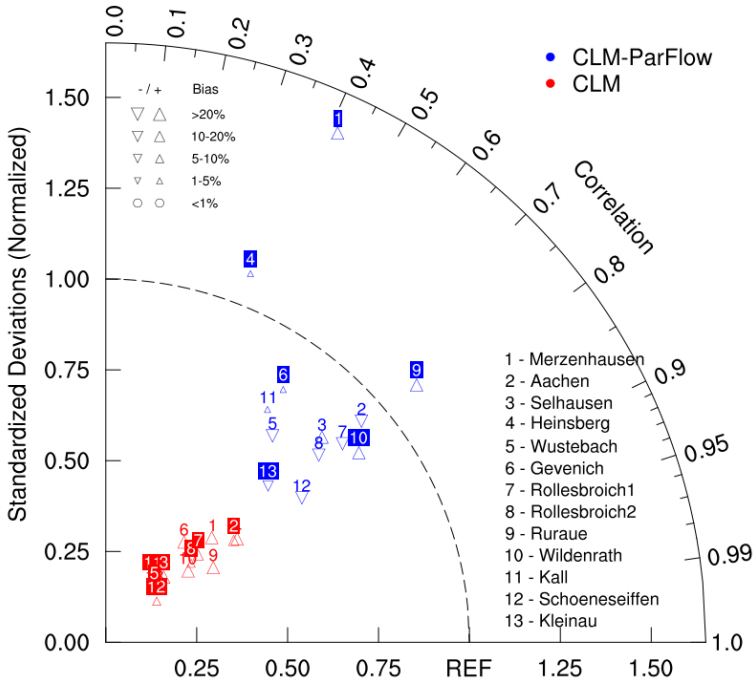

Figure 3.3: Taylor diagram of the soil moisture of CLM and CLM-ParFlow model runs as compared CRNS observations.

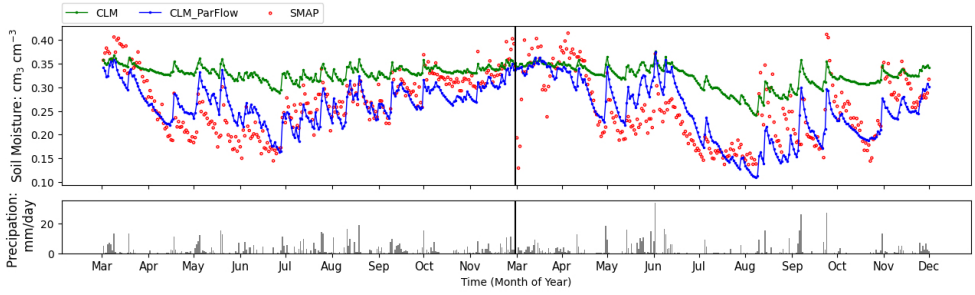

Figure 3.4: Soil moisture time series (0-5 cm) averaged over the simulation domain for 2017 and 2018 from CLM and CLM-ParFlow simulations compared with SMAP product

Table 3.6: Ancillary datasets used in the SMAP soil moisture retrieval algorithm. Notice that altitudes differ from Table 3.5 for the sites because here we list the altitudes used by SMAP.

Name	**CLM simulations**				**CLM–ParFlow simulations**			
	Bias	**RMSD**	**ubRMSD**	**r**	**Bias**	**RMSD**	**ubRMSD**	**r**
Merzenhausen	0.108	0.136	0.050	0.711	0.045	0.105	0.094	0.414
Aachen	0.126	0.058	0.047	0.782	-0.106	0.115	0.045	0.756
Selhausen	0.035	0.127	0.063	0.664	0.131	0.141	0.050	0.725
Heinsberg	0.111	0.088	0.049	0.785	0.005	0.083	0.083	0.365
Wüstebach	0.073	0.079	0.052	0.665	-0.169	0.175	0.047	0.628
Gevenich	-0.060	0.160	0.062	0.615	0.002	0.065	0.065	0.574
Rollesbroich1	0.148	0.071	0.062	0.726	-0.091	0.104	0.051	0.766
Rollesbroich2	0.036	0.070	0.068	0.733	-0.112	0.126	0.056	0.751
Ruraue	0.016	0.105	0.054	0.821	0.068	0.087	0.053	0.770
Wildenrath	0.090	0.186	0.039	0.755	0.078	0.083	0.029	0.800
Kall	0.182	0.079	0.079	0.576	0.007	0.075	0.075	0.570
Schoeneseiffen	0.008	0.077	0.070	0.778	-0.088	0.101	0.050	0.805
Kleinhau	0.031	0.103	0.076	0.675	-0.049	0.078	0.061	0.720
Average	0.070	0.103	0.059	0.714	-0.021	0.103	0.058	0.665

have different soil wetting and drying dynamics after rainfall. The near-surface soil is sensitive to precipitation because of intensive positive vertical water gradients, but tends to dry quickly after water infiltration related to evaporation (Chen et al. 2017a). Although the representation of L-band sensing depth at 5 cm has been used for remote sensing validations (Escorihuela et al. 2010; O'Neill et al. 2017; Zhang et al. 2019c), the L-band sensing depths are affected by soil moisture, and the penetration depth can be shallower when soil moisture is high (Bierkens et al. 2015). The penetration depths and vertical soil moisture gradients lead to different drying behavior. The simulations match soil moisture from SMAP well during most of the year. Generally, CLM overestimates the soil water content during summer. Compared to SMAP, CLM-ParFlow simulations show a very small wet bias of only 0.004 cm^3 / cm^3 while CLM has a larger wet bias of 0.065 cm^3 / cm^3. The RMSD for CLM and CLM-ParFlow simulations are 0.085 cm^3 / cm^3 and 0.045 cm^3 / cm^3 respectively.

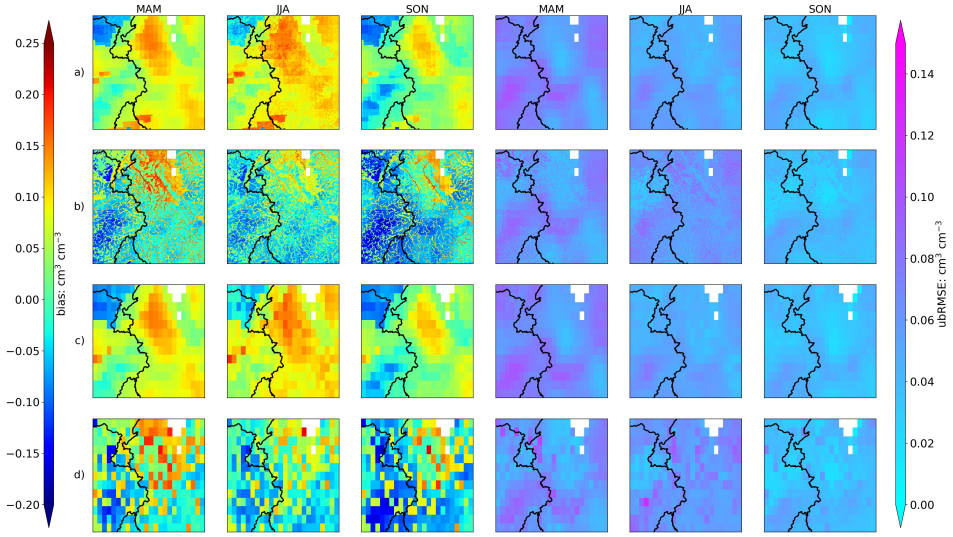

Figure 3.5: Spatial maps of bias (left three columns) and ubRMSD (right three columns) of soil moisture between SMAP and CLM model (a,c), SMAP and CLM-ParFlow model (b,d) for MAM, JJA and SON over the investigation area posted at (upper) the resolution of the model grid (500 m) and (lower) at the resolution of SMAP (9 km).

Spatial maps of performance indices are given in Figure 3.5 and illustrate the differences between model predictions and observations. For the maps at 500 m resolution, as the resolution of the simulations is finer than the satellite measurement, large differences between simulation and measurements occur in valleys and river regions because these areas are not well covered by the coarser resolution of the SMAP satellite.

In most areas, CLM has a higher soil water content than SMAP. The CLM-ParFlow model captures the spatial variability of soil water content and shows the influence of the river network. The soil moisture is close to saturation in the river valley. Meanwhile, the soil is drier in hilly areas. This is related to the difference in subsurface process representation between CLM and CLM-ParFlow. In Parflow, the Richards' equation is used to calculate 3D subsurface water flow, including both vertical and lateral water movement, which includes the lateral groundwater flow that moves water from the hilly areas towards the river valleys. In addition, lateral flow by streams and rivers is also modelled. The water flow convergence process (i.e., the lateral redistribution of water via streams and aquifers from hills to the river valleys and lowlands) can be better captured by CLM-ParFlow than by CLM, which just considers vertical water flow. In the northern flat and valley areas, the differences of soil moisture between CLM and CLM-ParFlow are smaller, where precipitation and infiltration excess are low, thus the later water flow redistribution processes have a smaller impact.

Further minor discrepancies between CLM and CLM-ParFlow simulations are related to the different estimation of soil hydraulic parameters (different pedotransfer functions). Several areas where CLM shows larger deviations with respect to SMAP soil moisture coincide with loam regions of the soil texture map, which indicates that for loam texture, CLM is probably too wet, which could be related to the default pedo-transfer function in CLM, which might underestimate hydraulic conductivity for loamy soil textures. The spatial distribution of both bias and ubRMSD also shows clear differences between the northern flat area (with larger bias) and the southern hilly area (smaller bias). This is probably related to the fact that precipitation is high in the hills and both CLM and SMAP have soil moisture values close to field capacity. Concerning CLM-ParFlow, the differences with SMAP are larger in the Rhine valley; ParFlow overestimates the influence of the river on soil moisture values in the areas next to the stream. Notice that the CLM-ParFlow model is not calibrated, and that river-groundwater interaction could be closer to real conditions by adjusting, for example, riverbed hydraulic conductivities. Both bias and ubRMSD values show that the discrepancies between model simulations and SMAP data are smallest in autumn for CLM simulations and CLM-ParFlow.

3.3.4 TC analysis

In general, the statistics of a time series triple are inherently unique, so that a comparison of different triples in a collocation analysis is not directly possible. However, the same SMAP product and CRNS data are used in this study to be compared to two different simulation results. That provides a large ability for a direct comparison. Table 3.7 shows the TC results for model simulations (as Y) and SMAP L3_SM_E_P product (as Z) compared to reference CRNS datasets (as X). By definition, the scaling factor β_X of the reference dataset is 1, while the SMAP product and model simulations are scaled to this reference product. β_Y and β_Z values larger than 1 indicate that the dynamic range of the datasets from the SMAP product and the model simulations is lower than that of the CNRS soil moisture time series, and vice versa. For CLM stand-alone simulation, the average β_Y is 4.538 and β_Z is 1.370. For CLM-ParFlow, β_Y and β_Z are quite close (1.453 and 1.242, respectively). The scaling factors larger than 1 indicate that both SMAP L3_SM_P_E and the land surface model simulations have underestimated the soil moisture dynamics at the CRNS sites, and probably in the complete research area. Compared to CLM stand-alone simulations, the β_Y of the coupled model is closer to 1, indicating less need to scale. In terms of β_Z, it should be noted that the scaling factors for Wüstebach and Wildenrath are lower than for other stations, indicating that the dynamics range of retrieved soil moisture needs to be reduced to match the scale of CRNS observations and model simulation time series. For these two stations, some additional problems (see Section 3.3.1) seem to influence the soil moisture retrieval results. Although the soil moisture datasets used in the TC correspond to different depths (SMAP for the upper 5 cm and the other two datasets for the upper 20 cm), no obvious relationship between the penetration depth differences and soil moisture dynamics is detected. Table 3.7 also provides the absolute TC error standard deviation. The ranges for $\sigma_{\varepsilon Y}$ are 0.010 to 0.026 (CLM) and 0.028 to 0.080 (CLM-ParFlow), respectively. In general, the SMAP soil moisture product provides similar error standard deviations with $\sigma_{\varepsilon Z} \leq 0.060$ in both triples.

Table 3.7: Triple collocation comparison results for model simulations (as Y) and SMAP L3_SM_E_P product (as Z) compared to reference CRNS datasets (as X).

Name	Z: CLM						Z: CLM-ParFlow					
	$\sigma_{\varepsilon X}$	$\sigma_{\varepsilon Y}$	$\sigma_{\varepsilon Z}$	β_Y	β_Z	SNR_Y	$\sigma_{\varepsilon X}$	$\sigma_{\varepsilon Y}$	$\sigma_{\varepsilon Z}$	β_Y	β_Z	SNR_Y
Merzenhausen	0.016	0.024	0.061	3.015	1.285	-1.397	0.021	0.080	0.056	1.134	1.088	-7.456
Aachen	0.020	0.025	0.057	2.610	1.270	1.485	0.023	0.037	0.050	1.199	1.025	6.576
Selhausen	0.017	0.015	0.061	5.669	1.556	-2.082	0.011	0.045	0.059	1.415	1.441	2.622
Heinsberg	0.013	0.026	0.056	2.346	1.391	3.351	0.015	0.060	0.054	1.980	1.283	-11.020
Wüstebach	0.028	0.008	0.055	5.941	0.783	1.330	0.028	0.036	0.055	1.526	0.780	-1.414
Gevenich	0.020	0.024	0.060	3.520	1.376	-3.166	0.040	0.041	0.052	1.257	1.052	4.035
Rollesbroich1	0.023	0.024	0.058	3.698	1.455	-1.250	0.030	0.038	0.050	1.267	1.144	8.143
Rollesbroich2	0.019	0.023	0.059	3.858	1.579	-0.489	0.039	0.038	0.050	1.322	1.192	8.099
Ruraue	0.008	0.019	0.065	2.806	1.691	6.315	0.038	0.058	0.068	1.383	2.164	0.826
Wildenrath	0.018	0.010	0.057	3.689	0.889	4.258	0.021	0.028	0.056	1.072	0.831	7.878
Kall	0.006	0.017	0.049	7.141	1.443	-6.570	0.023	0.058	0.046	1.825	1.337	-4.374
Schoeneseiffen	0.011	0.010	0.061	7.090	1.429	2.879	0.010	0.036	0.060	1.774	1.383	4.907
Kleinhau	0.026	0.014	0.061	7.607	1.664	-2.779	0.023	0.040	0.057	1.730	1.424	3.800
Average	0.017	0.018	0.058	4.538	1.370	0.145	0.025	0.046	0.055	1.453	1.242	1.740

3.3.5 Effect of lateral water flow on soil moisture

Previous research indicated that the lateral flow is important in land surface modelling, especially when the resolution is fine (Yair 2008). The spatial patterns of modelled soil moisture show that the CLM-ParFlow has wet grid cells in the foothills and valleys. The soil moisture gradient is larger in the wet grid cells and surrounding drier grid cells. By taking account of lateral flow, soil moisture decreases in these wet areas due to lateral diffusion. Also, the lateral drainage driven by topographic gradient results in soil moisture redistribution. In view of previous studies (Senatore et al. 2015), lateral flow is expected for steep hillocks, even if slight difference in soil texture between adjoining grid cells. Also, the accumulated runoff in ParFlow, generated by infiltration excess or saturation excess, can route or reinfiltrate, while some other traditional LSMs can remove excess water from the modeled water cycle (Albergel et al. 2010). CLM-ParFlow maintains the high soil moisture in convergence areas. This confirms the importance of lateral subsurface flow on the hydrological cycle, especially in mountainous areas.

3.4 Conclusions

This study compared soil moisture data from cosmic ray neutron sensors (CRNS), passive microwave remote sensing (SMAP L3_SM_E_P product), and land surface model simulations by the Community Land Model (CLM, version 3.5) and the coupled land surface-subsurface model CLM-ParFlow over a 150 km × 150 km region in western Germany. CLM-ParFlow can better capture the impact of groundwater on soil moisture than CLM, as it has a more advanced subsurface physical process scheme. With this approach, an analysis of the impact

of the representation of subsurface processes in hydrological simulations of soil moisture was performed. The evaluation results can be summarized as follows:

Over thirteen CRNS sites, the SMAP L3_SM_E_P product shows a small bias of 0.005 cm^3 / cm^3 only compared to the CRNS observations. Nevertheless, local differences can be large (up to -0.120 cm^3 / cm^3 for the densely forested Wüstebach site) due to differing spatial resolution of the soil moisture products and errors in soil texture and land cover used to derive soil moisture from brightness temperature in the SMAP L3_SM_E_P product. Besides, the disturbing role of dense vegetation and complex topographic features influences the accuracy of the SMAP product. Overall, the unbiased root mean square error (ubRMSE) is around 0.056 cm^3 / cm^3, indicating that the SMAP L3_SM_E_P product could barely meet its mission requirement for this very heterogeneous and hilly region.

The comparison between CRNS and land surface simulations shows that CLM has a wet bias (0.070 cm^3 / cm^3) and CLM-ParFlow has a dry bias (-0.021 cm^3 / cm^3). Local biases can be large, which might be related to the uncertainty in soil texture and hydraulic conductivity, inadequate pedotransfer functions, and lack of consideration for soil bulk density in CLM model. In terms of ubRMSE, both CLM and CLM-ParFlow are below 0.06 cm^3 / cm^3 and compare well to CRNS observation dynamics. The SMAP product and CLM-ParFlow do not show a systematic difference in soil moisture, which is in contrast to most land surface models, which are wetter than SMAP.

The triple collocation (TC) validation comparison implies that both CLM and CLM-ParFlow show similar noise levels with $\sigma_{\varepsilon Z}$ below 0.056. The scaling factor of CLM-ParFlow is less than a third of CLM stand-alone, indicating that the coupled model could better capture the soil moisture dynamics over the study area and perform better with respect to CRNS measurements. This is an important aspect for future data assimilation studies, as the typical adaptation of the soil moisture climatology of model and observation becomes less mandatory. The higher SNR (Signal-to-Noise Ratio) value for the coupled model CLM-ParFlow also indicates it can provide more valuable results than the CLM stand-alone model.

It should be noted that the direct metrics (e.g., RMSE and r) do not show a clear better performance of the CLM-ParFlow model compared to the CLM stand-alone model. The TC method shows that the simulation has been improved when lateral subsurface dynamics are involved. Unlike typical performance metrics, where the assumption is that the reference data set is free of (random) errors, TC methods account for sensor and representativeness errors and can be considered more robust than conventional metrics and closer to reality (Gruber et al. 2017). With conventional evaluation metrics, we focus on the dynamics of the different time series instead of the absolute soil moisture values, because there can be a systematic bias between CRNS and SMAP measurements, as well as model simulations, which is related to different underlying assumptions for the different measurement and simulation methods. This method is also used because it is standard in the land surface modelling literature and allows, therefore an easier comparison with other papers (Albergel et al. 2010; Albergel et al. 2012; Bi et al. 2016; Ford et al. 2019).

In summary, the model structure is important for soil moisture modelling. Compared to the CLM-ParFlow model, the CLM model has a simplified representation of describing the soil moisture variability while neglecting lateral water flow. The CLM model tends to overestimate the soil moisture and provides similar soil moisture estimation in grid cells that have the same soil texture and plant functional type. The lateral subsurface process in CLM-ParFlow leads to soil water redistribution and improvements in prediction. The coupled model can describe the spatial variability of soil moisture. It is worth considering lateral subsurface flow in LSMs to have a more accurate soil moisture simulation.

However, some limitations should be noted. First, lateral subsurface flow mainly takes place in the saturated subsurface. However, there is also evidence for lateral flow in the top layer of the unsaturated zone for sloping soil due to rainfall dynamics. Nevertheless, the CRNS measurements provide, in the first place, only information on soil moisture, and are less suited to evaluate how well the influence of groundwater is represented by models. Second, the CRNS measurements might be slightly biased, caused by the limited number of observation sites, scale mismatches, and imperfect calibration. The bias is simply set aside when using the same statistical evaluation methods in order to compare these results with other remote sensing and land surface modelling studies. Finally, this study only covers three seasons for the years of 2017 (quite average conditions) and 2018 (very dry). A longer time may be desirable to better evaluate the relative performance of the model, including different weather conditions. Also, a finer soil map resolution and larger study domain would be desirable in future studies.

3.A Appendix

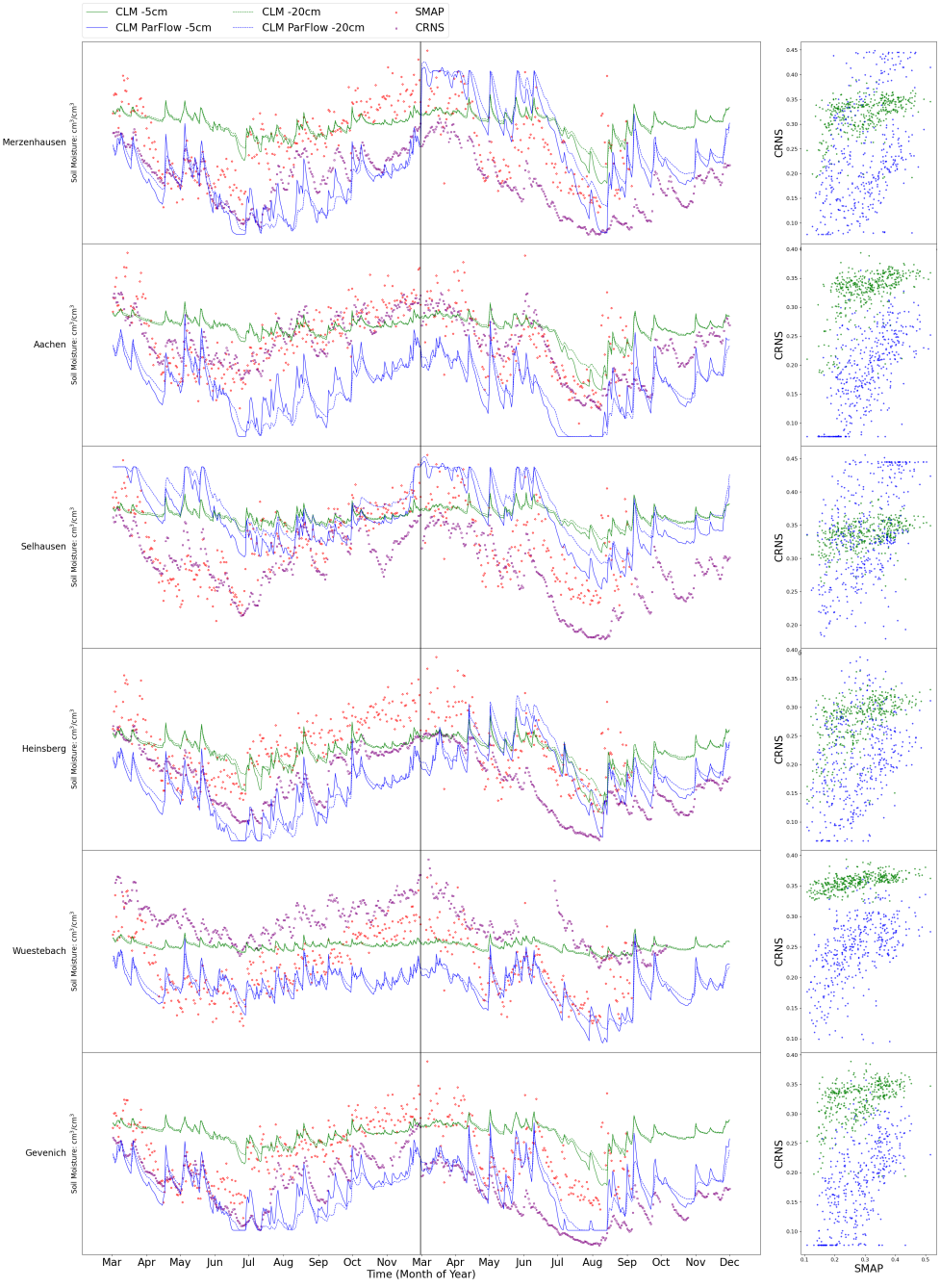
CLM -5cm
CLM ParFlow -5cm
CLM -20cm
CLM ParFlow -20cm
SMAP
CRNS
Merzenhausen
Aachen
Selhausen
Heinsberg
Wuestebach
Gevenich
Soil Moisture cm³/cm³
CRNS
SMAP
Mar Apr May Jun Jul Aug Sep Oct Nov Mar Apr May Jun Jul Aug Sep Oct Nov Dec
Time (Month of Year)

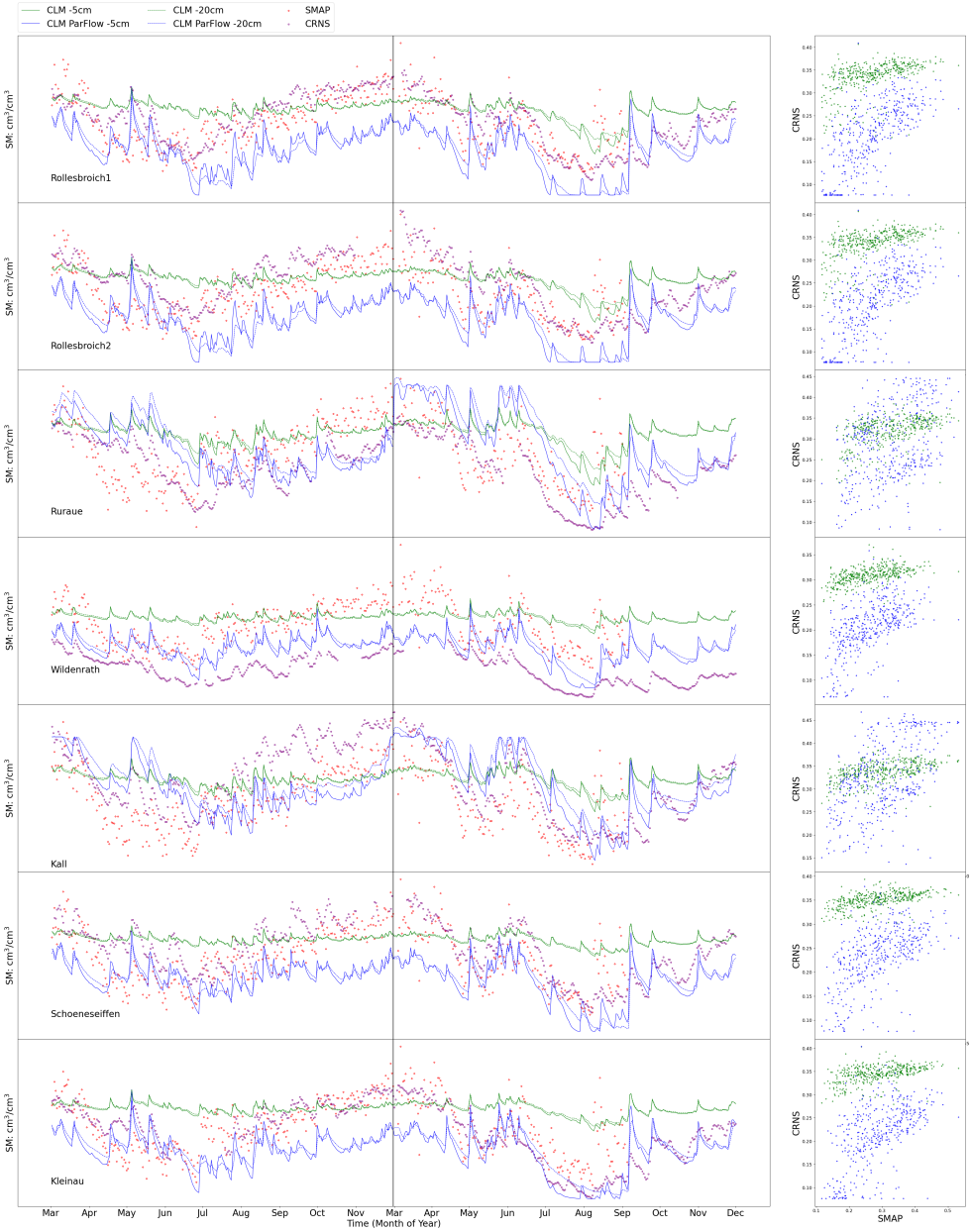

Figure 3.6: Time series and scatterplots of soil moisture from SMAP (red), CRNS (purple) and LSMs (CLM at 5 cm (green solid) and at 20 cm (green dashed); CLM-ParFlow at 5 cm (blue solid) and at 20 cm (blue dashed) at 13 sites. (CLM at 5 cm (green solid) and at 20 cm (green dashed); CLM-ParFlow at 5 cm (blue solid) and at 20 cm (blue dashed) at 13 sites.

4

Added value of lateral flow processes for assimilating SMAP soil moisture into a land surface model.

*adapted from: Zhao, H., Montzka, C., Keller, J., Li, F., Vereecken, H., & Franssen, H. J. H. (2025). How does assimilating SMAP soil moisture improve characterization of the terrestrial water cycle in an integrated land surface-subsurface model? Water Resources Research, 61, e2024WR038647. https://doi.org/10.1029/2024WR038647

4.1 Introduction

Soil moisture impacts crop yield, controls the division of precipitation into surface runoff and soil infiltration, and regulates sensible and latent heat fluxes (Babaeian et al. 2019; Seneviratne et al. 2010). Accurate and large-scale soil moisture data are essential for understanding hydrological processes, predicting weather and extreme events, and developing effective water resources management strategies. While in situ measurement networks, such as Terrestrial Environmental Observatories (TERENO) (Zacharias et al. 2011) in Germany, Texas Soil Observation Network (TxSON) (Clewley et al. 2017) in the U.S.A., and the Tibetan Plateau Observatory of Plateau Scale Soil Moisture and Soil Temperature (Tibet-Obs) (Su et al. 2011) in China, provide high-quality soil moisture observations, their spatial coverage remains limited to specific regions.

Soil moisture can be simulated using land surface models (LSMs), for example, the Community Land Model (CLM) (Oleson et al. 2008) with different spatial and temporal resolutions depending on the research question and the available computational resources. Nevertheless, the accuracy of model predictions is often compromised by uncertainties related to input data. For instance, offline LSMs must be driven by meteorological forcing datasets and are sensitive to the accuracy of the atmosphere forcing (Albergel et al. 2018). In addition, the uncertainties in soil and vegetation properties and model structure errors greatly influence the simulations (Bastidas et al. 2003; Hartley et al. 2017; Laguë et al. 2019; Li et al. 2018b).

Alternatively, remote sensing techniques provide a possibility to obtain continuous and global soil moisture data. Soil moisture data from satellites like SMOS (Soil Moisture Ocean Salinity) (Kerr et al. 2010) and SMAP (Soil Moisture Active Passive) (Entekhabi et al. 2010a) provide exhaustive information at a coarse resolution of 36 km or 9 km, respectively. These satellites

capture soil moisture information from the upper soil layer (approximately 5 cm depth), and their accuracy may be influenced by factors such as vegetation type and distribution (Jha et al. 2007; Konings et al. 2017; Zheng et al. 2018). Data assimilation, a technique that combines observations with model predictions, offers a promising approach to enhance the accuracy of LSMs. Sequential data assimilation in combination with LSMs has been used to provide better estimates for soil moisture for two decades (Han et al. 2014; Koster et al. 2018; Lievens et al. 2017a,b; Nair et al. 2019; Nie et al. 2022; Pleim et al. 2003; Reichle 2008; Reichle et al. 2002; Yang et al. 2016; Yin et al. 2015).

Several studies have assimilated remotely sensed soil moisture observations into LSMs for the improvement of predictions of soil moisture and other hydrological variables. For example, SMOS and SMAP products have been assimilated into LSMs (e.g. GEOS-5, VIC-CMEM coupled model) with EnKF and pronounced improvements in soil moisture characterization are observed (Ahmad et al. 2022; De Lannoy et al. 2016; Lievens et al. 2016, 2017a; Reichle et al. 2017). Studies using other satellite-based products (e.g. ESACCI and ASCAT) also demonstrated the potential of assimilating remotely sensed soil moisture information to improve soil moisture estimates (Nair et al. 2019; Naz et al. 2019; Pinnington et al. 2018; Zhou et al. 2022). In general, most studies indicate that while the assimilation of remotely sensed retrievals improves soil moisture estimates, the improvement is limited when it comes to characterizing land surface fluxes and estimating runoff (Ahmad et al. 2022; De Santis et al. 2021; Lu et al. 2020; Martens et al. 2016; Naz et al. 2019; Prakash et al. 2023). Traditional LSMs usually do not take into account lateral water exchange, restricting water flow to the vertical direction only. Several studies suggest that groundwater dynamics need to be considered when dealing with land surface processes (Kollet et al. 2008; Liang et al. 2003; Maxwell et al. 2005). A more detailed representation could not only improve soil moisture distribution (Kim et al. 2017), but also influence energy flux partitioning (Maxwell et al. 2016; Zhang et al. 2021b), runoff, and groundwater recharge (Holtzman et al. 2020; Wang et al. 2020). Therefore, coupled simulation platforms have been developed to examine the coupled water and energy cycles in the atmosphere-land surface-subsurface continuum (Maxwell et al. 2007; Rummler et al. 2019; Sulis et al. 2017; Tian et al. 2012). Such models include Flux with Penn State Integrated Hydrologic Model (PIHM) (Shi et al. 2013), CLM 4.0 with process-based Adaptive Watershed Simulator (PAWS) (Shen et al. 2013), CATchment HYdrology (CATHY) with Noah-Multiparameterization Land Surface Model (Noah-MP) (Niu et al. 2014b,c). Furthermore, the Terrestrial System Modelling Platform (TSMP) (Shrestha et al. 2014) was developed, consisting of three different models which are two-way coupled: the atmospheric simulation model COSMO (Consortium for Small-Scale Modelling) (Baldauf et al. 2011), the land surface model CLM 3.5 (Oleson et al. 2008) and the sub-surface hydrological model ParFlow (Kollet and Maxwell 2006). TSMP can model the water and energy cycles from the very deep subsurface to the stratosphere (Sulis et al. 2017) and is one of the few available modeling platforms that fully integrates the atmospheric, land surface, and subsurface physical processes. TSMP calculates three-dimensional flow over the entire domain and has a detailed physical modeling of the land surface fluxes (Koch et al. 2016). Despite the enhanced understanding of the LSM process, a limited number of synthetic studies have investigated the value of data assimilation when employed in conjunction with integrated land surface-subsurface models. At smaller to

catchment scales, the lateral groundwater flow can influence soil moisture and generate spatial patterns by redistributing water from uplands to lowlands (Nousu et al. 2024). These studies (Hung et al. 2022; Kumar et al. 2009; Li et al. 2024; Sawada 2020) have demonstrated that the information of soil moisture observations can be propagated to the neighbouring grid cells and in the vertical profile.

The objective of this study is to conduct, for the first time, an evaluation of assimilating remote sensing soil moisture information into the two-way coupled CLM-ParFlow model within the TSMP framework in a real-world case study. By integrating SMAP data into a high-resolution modelling system that is capable of simulating three-dimensional saturated and unsaturated groundwater flow, it allows us to examine SMAP's potential to improve soil moisture, evapotranspiration, and groundwater level characterization compared to traditional land surface models, such as CLM. While SMAP observations are limited to the top 5 cm of soil, where soil moisture dynamics are primarily influenced by vertical fluxes (e.g., infiltration and evaporation), lateral flow processes can indirectly affect surface soil moisture through subsurface moisture redistribution, particularly in regions with complex topography. We evaluate the soil moisture estimates and other predicted variables in both CLM and CLM-ParFlow in situ measurements over a temperate region in western Germany. This paper addresses the following research questions:

1. Does the SMAP soil moisture product provide effective information to improve the characterization of soil moisture states in the high-resolution coupled land surface-subsurface CLM-ParFlow model more than in the stand-alone CLM model?

2. How does assimilating remotely sensed soil moisture affect the characterization of ET in CLM-ParFlow, and can the characterization of ET be improved more than for the stand-alone CLM model?

3. How does soil moisture assimilation affect shallow and deep groundwater level predictions in the coupled land surface-subsurface model?

4. Does updating the model parameters, in addition to the states, further improve the simulation of hydrological variables?

4.2 Materials and methods

4.2.1 Study area and in situ data

In this work, SMAP soil moisture data is assimilated into the TSMP model for the so-called NRW-domain, which consists of parts of the North Rhine-Westphalia, Rhineland-Palatinate, and Hesse Federal states in western Germany, and includes also parts of Belgium, the Netherlands, and Luxembourg (Figure 4.1). The domain size is 150 km $\times$ 150 km. The elevation ranges from 13 m in the northwestern part to 735 m in the southern part. It is characterized by a high population density and urban development, while the remaining land cover is predominantly

composed of grasslands, agricultural fields, and forested regions. TSMP runs over the NRW domain have already been performed by Sulis et al. (2018) and Uebel et al. (2018).

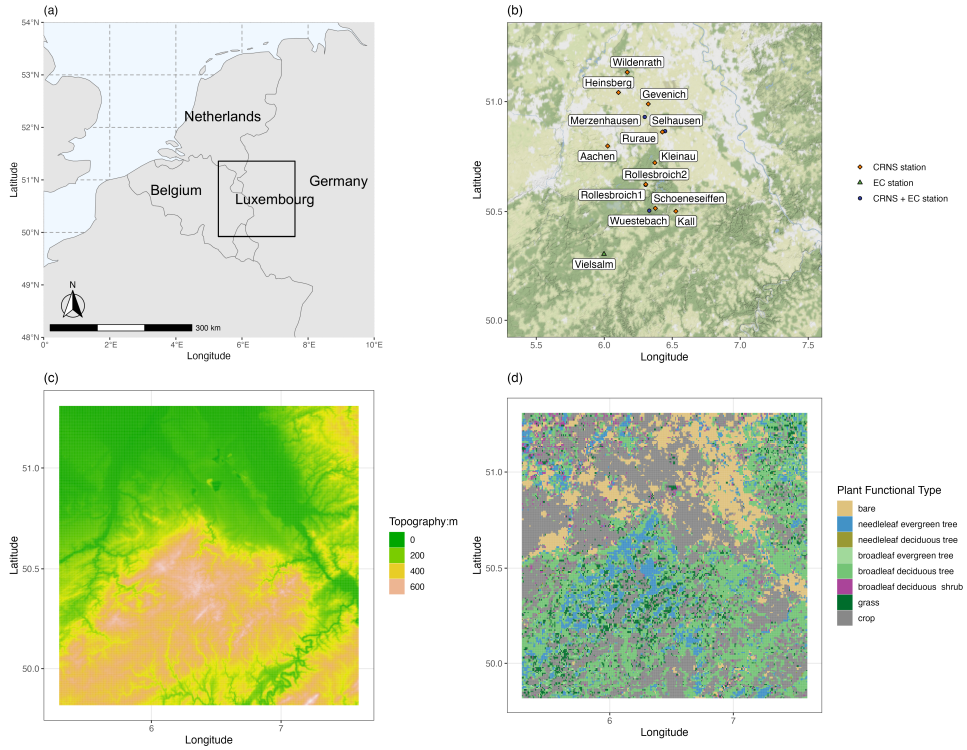

Figure 4.1: a) Location of the study area in Europe (DE=Germany; NL=Netherlands; BE=Belgium, LUX=Luxembourg); b) In situ stations for soil moisture (CRNS) and evapotranspiration (EC) in the study area; c) Elevation of the region (m) and d) The spatial distribution of plant functional types (PFTs).

The CRNS (Cosmic Ray Neutron Sensors) is an emerging technology for monitoring soil moisture at the intermediate scale. The measurement radius ranges between 130 m and 300 m as a function of factors like air density, air humidity, and vegetation density (Köhli et al. 2015; Zreda et al. 2012). The penetration depth of CRNS measurements varies from 15 cm (wet soils) to 80 cm (dry soils) (Franz et al. 2012a; Köhli et al. 2015). Several studies have been conducted to investigate the accuracy of the CRNS measurements (Jakobi et al. 2018; Tian et al. 2016; Zhu et al. 2016). In the study by Bogena et al. (2013), it is found that the RMSE of daily soil moisture data was about 0.03 cm^3/cm^3 for the forested site Wüstebach in Germany, which has, in general, very high soil moisture content. Thirteen CRNS stations are located in the research domain and are used for the verification of the simulations and data assimilation experiments. Table 4.1 provides further details. The penetration depth z^* of the CRNS measurements is calculated and given by Franz et al. (2012):

Table 4.1: CRNS and EC stations: Coordinates, altitude from digital elevation model (DEM) (m), average annual precipitation (mm y^{-1}), plant functional types and soil texture information (Baatz et al. 2017; Bogena et al. 2022; H2020_eLTER_Project Team 2019).

Name	latitude	longitude	DEM	Precip.	Plant functional type	Clay %	Sand %
Merzenhausen	50.930	6.297	91	718	crop	22	21
Aachen	50.799	6.025	232	865	crop	23	22
Selhausen	50.866	6.447	101	718	crop	24	16
Heinsberg	51.041	6.104	58	722	grassland, crop	19	18
Wüstebach	50.505	6.331	607	1180	forest	23	19
Gevenich	50.989	6.324	107	718	crop	20	22
Rollesbroich1	50.622	6.304	515	1018	grassland	23	22
Rollesbroich2	50.624	6.305	506	1018	grassland	-	-
Ruraue	50.862	6.427	100	718	grassland	26	19
Wildenrath	51.133	6.169	72	722	forest	12	65
Kall	50.501	6.526	505	857	grassland	22	20
Schoeneseiffen	50.515	6.376	611	870	grassland	24	16
Kleinau	50.722	6.372	374	614	grassland	25	15
Vielsam	50.305	5.998	493	1062	forest	-	-

$$z^* = \frac{5.8}{\theta + 0.0829} \tag{4.1}$$

where θ is the total soil water content. If the simulated soil moisture by CLM and CLM-ParFlow are taking at different depths d, the weight W_d is determined based on a linear relation:

$$W_d = \begin{cases} 1 - d/z^*, & d \leq z^* \\ 0, & d > z^* \end{cases} \tag{4.2}$$

A weighted average of soil moisture θ_{z^*} is calculated over L vertical layers with depths d_i, simulated soil moisture θ_{d_i} and weights W_{d_i}:

$$\theta_{z^*} = \frac{\sum_{i=1}^{L} W_{d_i} \cdot \theta_{d_i}}{\sum_{i=1}^{L} W_{d_i}} \tag{4.3}$$

The eddy covariance (EC) method allows for measuring ET at the field scale. Four eddy covariance sites are located in our study domain and are part of the FLUXNET2015 dataset (Pastorello et al. 2020), including Selhausen (crop land), Rollesbroich (grassland), Wüstebach (forest), and Vielsam (forest). Raw data, including fluxes of latent heat, sensible heat, CO_2 and meteorological variables, are measured every 10 or 20 seconds and are processed towards a half-hourly time step at each site. The data gaps in fluxes and meteorological time series are filled, undergo quality checks, and are aggregated to daily observations (Drought 2018 Team et al. 2019; Ukkola et al. 2017). Fig. 4.1 shows the spatial locations of the CRNS and EC stations.

The groundwater level observations are obtained from the monitoring network Geoportal NRW (https://www.geoportal.nrw) and GroundwaterTools (https://www.grondwatertools.nl). A total of 977 groundwater wells are available in this research area, providing monthly observations throughout the year 2018. Of these, only 527 wells with shallow groundwater levels (less than 30 m deep) are included in the analysis.

4.2.2 SMAP (L3_SM_P_E) product

SMAP provides soil moisture measurements of approximately the top 5 cm of the soil and thaw/freeze state that can be used in hydrological models and land surface models. The SMAP satellite completes a global soil moisture map with a revisit interval of about three days (O'Neill et al. 2021). Compared to other L-band sensors, e.g., SMOS, the assimilation of SMAP data shows higher skill (Blyverket et al. 2019; Zhang et al. 2019b).

In this study, the L3_SM_P_E product from National Snow and Ice Data Center NSIDC (https://nsidc.org/data/smap/smap-data.html) is used, which provides soil moisture on a 9 km grid for the upper 5cm soil with an error of no greater than 0.04 cm^3/cm^3 (Colliander et al. 2017). The SMAP Enhanced Passive Soil Moisture Products (L2_SM_P_E and L3_SM_P_E) were developed following the SMAP radar failure in July 2015. To enhance the resolution of SMAP radiometer data, the Backus-Gilbert optimal interpolation technique is used to make most use of the additional information and provide a better representation of the original data (Chan et al. 2017). L3_SM_P_E is a daily composite product that is generated from L2_SM_P_E over a one-day composition. This enhanced product was assessed by comparing it with long-term in situ soil moisture data, and it was found that the average ubRMSE (unbiased Root Mean Square Error) of the level 3 product is around $0.045 \sim 0.055$ cm^3/cm^3 (Chan et al. 2017; Colliander et al. 2021; Montzka et al. 2017; Zhang et al. 2019b; Zhang et al. 2019c).

4.2.3 CLM - ParFlow in TSMP

The Terrestrial Systems Modeling Platform (TSMP) consists of the atmospheric model COSMO (Baldauf et al. 2011), the land surface model CLM 3.5 (Oleson et al. 2008), and the subsurface model ParFlow (Kollet et al. 2006). These models are two-way coupled by the Ocean Atmosphere Sea Ice Soil Model Coupling Toolkit, OASIS-MCT (Valcke 2013). COSMO is the operational weather forecast model of the German weather service (Baldauf et al. 2011). TSMP provides a flexible coupling arrangement that enables fully coupled simulations (COSMO + CLM + ParFlow) as well as partially coupled simulations (COSMO + CLM or CLM + ParFlow). Additionally, each of the three models can be run independently. When simulating CLM or CLM coupled with ParFlow, external forcing data is necessary to provide the required boundary conditions.

4.2.3 (a) The land surface model - CLM

CLM 3.5 models the water and energy cycles in the soil-vegetation-atmosphere continuum, including snow packs. Five land cover types are defined in this model to characterize surface heterogeneity, including glacier, lake, wetland, urban, and vegetated. Snow accumulation is represented with up to five snow layers on top of the soil layers. Plant properties are assigned based on different plant functional types (PFTs). CLM has ten soil layers with varying thicknesses. Runoff calculation in CLM is based on the traditional TOPMODEL (Oleson et al. 2004) approach. Hydraulic conductivity and porosity are determined by soil texture (% sand and % clay) based on pedo0transfer functions (Clapp et al. 1978; Cosby et al. 1984). A simplified Richards equation is used to calculate the water movement in the unsaturated zone:

$$\frac{\partial \theta}{\partial t} = \frac{\partial}{\partial z}\left[k(\theta)\frac{\partial (p+z)}{\partial z}\right] + q_s \tag{4.4}$$

where θ represents the volumetric soil water content [$L^3 \cdot L^{-3}$], t is time [T], k is the hydraulic conductivity [$L \cdot L^{-1}$], z is height [L] and p is pressure head [L].

The hydraulic conductivity between two adjacent layers $k_{i,j}$ can be calculated as:

$$k_{i,j} = \begin{cases} k_{sat(i,j)} \left[\frac{0.5(\theta_{liq,j})+0.5(\theta_{liq,j+1})}{0.5(\theta_{sat,j})+0.5(\theta_{sat,j+1})}\right]^{2B_j+3}, & 1 \le j \le 9 \\ k_{sat(i,j)} \left[\frac{\theta_{liq,j}}{\theta_{sat,j}}\right]^{2B_j+3}, & j = 10 \end{cases} \tag{4.5}$$

and i and j are layer indices. θ_{liq} is the volumetric liquid water content and θ_{sat} is the soil moisture content at saturated state. The saturated hydraulic conductivity $k_{sat(i,j)}$ is assumed to be exponentially decreasing with depth following the TOPMODEL concept (Beven et al. 1979):

$$k_{sat(i,j)} = 0.0070556 \times 10^{-0.884+0.0153(\%sand)_j} \left[exp\left(-\frac{z_{i,j}}{z_0}\right)\right] \tag{4.6}$$

where $z_0 = 0.5$ m is the length scale for decrease in $k_{s(i,j)}$, $z_{i,j}$ represents height at the interface between i and j, and the exponent B_j is calculated as:

$$B_j = 2.91 + 0.159\,(\%clay)_j \tag{4.7}$$

The saturated water content θ_{sat} (i.e., porosity ϕ) is calculated as:

$$\theta_{sat} = 0.489 - 0.00126\,(\%sand) \tag{4.8}$$

In the CLM model, the mass transfer equation (MT) and Monin-Obukhov Similarity Theory are used to calculate evapotranspiration (ET). The ground evaporation, evaporation from interception, and transpiration are separately considered. For the vegetated areas, the water vapor flux from vegetation E_v [$M \cdot L^{-2} \cdot T^{-1}$] and from ground soil E_g [$M \cdot L^{-2} \cdot T^{-1}$] are calculated as follows:

$$E_v = -\rho_{atm}\frac{(q_s - q_{sat}^{T_v})}{r_{total}} \tag{4.9}$$

$$E_g = -\rho_{atm}\frac{(q_s - q_g)}{r_{aw}{}'} \tag{4.10}$$

where ρ_{atm} is the atmospheric air density [M·L^{-3}], q_s is the canopy specific humidity [M·M^{-1}], $q_{sat}^{T_v}$ is the saturated specific humidity [M·M^{-1}] at the vegetation temperature T_v, r_{total} [T·L^{-1}]is the total resistance to water vapor transfer from the canopy to the canopy air, caused by both the leaf boundary layer and stomatal resistance, q_g is the specific humidity of ground, and $r_{aw}{}'$ is the aerodynamic resistance [T·L^{-1}] to water vapor transfer, from the ground to the canopy air. A detailed description of the soil moisture content and ET calculation process can be found in the CLM technical description document (Oleson et al. 2004).

4.2.3 (b) The subsurface model - ParFlow

ParFlow is a numerical, integrated hydrological model that simulates subsurface flow in unsaturated and saturated porous media, as well as overland flow. ParFlow solves the pressure in the subsurface and interactions with surface water bodies. The saturated-unsaturated subsurface flow equation is solved in three dimensions according to Richards. The surface water routing scheme is based on the kinematic wave approximation of overland flow, while coupling subsurface flow and overland flow in an integrated fashion (Kollet et al. 2006). Both the soil water retention curve and relative permeability are represented in ParFlow using the van Genuchten relationships (Maxwell et al. 2005). The water retention curve and relative permeability in the Van Genuchten model are defined as follows:

$$\theta(p) = \theta_{res} + \frac{\theta_{sat} - \theta_{res}}{[1 + (\alpha|p|)^n]^m} \tag{4.11}$$

$$k_r(p) = \frac{\left[1 - (\alpha|p|)^{n-1}\left(1 + (\alpha|p|)^n\right)^{-m}\right]^2}{(1 + (\alpha|p|)^n)^{m/2}} \tag{4.12}$$

Where $m = 1 - \frac{1}{n}$, p is the suction pressure [L] and k_r is the relative permeability [-]. α (α >0) [L^{-1}] and n (n >1) are soil parameters that are related to air entry suction for drying/wetting and slopes in van Genuchten curves. θ_{sat} and θ_{res} represent saturated water content and residual water content respectively (L^3·L^{-3}). More details of this model can be found in Kollet et al. (2006) and Maxwell (2013).

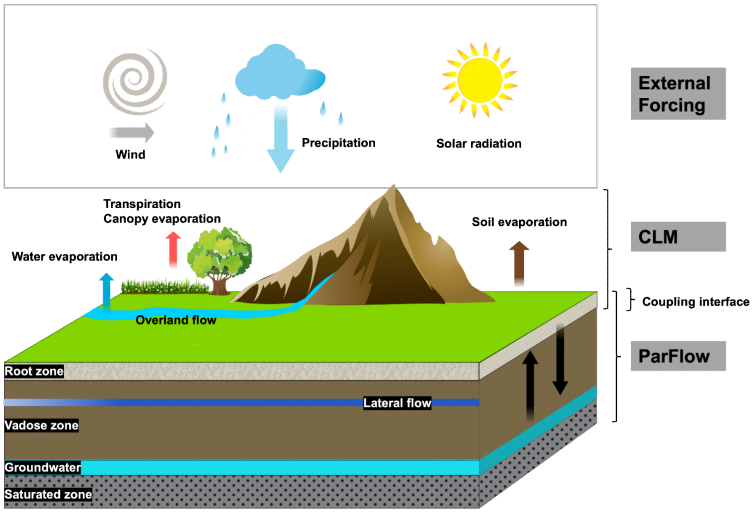

Figure 4.2: Schematic diagram of CLM-ParFlow in TSMP.

4.2.3 (c) The integrated CLM-ParFlow

The coupled CLM-ParFlow model is used in this work. A schematic representation of CLM-ParFlow in TSMP is shown in Fig. 4.2. The offline atmospheric forcing drives the CLM to model land surface processes. ParFlow replaces the one-dimensional soil hydrology of CLM with a three-dimensional approach. The models are coupled via net infiltration (CLM calculates net infiltrating water for ParFlow), soil evaporation and transpiration (including root water uptake) (CLM calculates water to be extracted by ParFlow), and ParFlow provides CLM with saturation and pressure for the top ten layers simultaneously (Shrestha et al. 2014).

4.2.4 Data assimilation

The data assimilation framework PDAF (Nerger et al. 2013, 2005) has already been coupled to TSMP (Kurtz et al. 2016). TSMP-PDAF includes data assimilation algorithms like the Ensemble Kalman Filter (Evensen 1994) and its variants, e.g, the localized Ensemble Kalman Filter (LEnKF) (Ott et al. 2004) and the local ensemble transform Kalman filter (LETKF) (Hunt et al. 2007). In this study, the EnKF is used to assimilate SMAP soil moisture data into TSMP. EnKF has already been proven to be robust and computationally efficient, suitable for large-scale non-linear models (Zamani et al. 2010).

4.2.4 (a) Ensemble Kalman filter

The first step in the EnKF is the forecast step, where the model $\mathbf{M}$ calculates the state $\mathbf{x}^t$ at time t:

$$\mathbf{x}^t = \mathbf{M}\left(\mathbf{x}^{t-1}, \mathbf{p}, \mathbf{q}\right)^t \tag{4.13}$$

where $\mathbf{p}$ is the vector with parameters and $\mathbf{q}$ is the vector with model forcing. This forecast step is carried out N times, for each of the ensemble members j. The different ensemble members can have different atmospheric forcing, model parameters, and initial conditions, which should adequately capture the uncertainty in these variables. In this study, the soil moisture observations θ are assimilated through the observation operator $\mathbf{H}$, which maps the model states into the observation space. The model states for each of the realizations are updated to $\mathbf{x}^{t,a}$ by combining forecasts and the observations $\mathbf{y}^t$:

$$\mathbf{x}^{t,a} = \mathbf{x}^t + \mathbf{K}\left(\mathbf{y}^t - \mathbf{H}\mathbf{x}^t\right) \tag{4.14}$$

where $\mathbf{H}$ is the operator that links measurements and model states, and the Kalman gain $\mathbf{K}$ is defined as follows:

$$\mathbf{K} = \mathbf{C}^f\mathbf{H}^\mathbf{T}\left(\mathbf{H}\mathbf{C}^f\mathbf{H}^\mathbf{T} + \mathbf{R}\right)^{-1} \tag{4.15}$$

where $\mathbf{C}$ is the covariance matrix of the model states and $\mathbf{R}$ is the measurement error-covariance matrix. We calculate $\mathbf{C}$ by:

$$\mathbf{C}^f = \frac{1}{N-1}\sum_{j=1}^{N}\left(\mathbf{x}_j^t - \bar{\mathbf{x}}^t\right)\left(\mathbf{x}_j^t - \bar{\mathbf{x}}^t\right) \tag{4.16}$$

where $\bar{\mathbf{x}}^t$ represents the matrix with the ensemble mean of the model states at time t. N is the number of ensemble members.

In some cases, the model parameters $\mathbf{p}$ are estimated together with the state variables by augmenting the vector $\mathbf{x}$ (Hendricks Franssen et al. 2008). The augmented state vector for updating both states and parameters is given by :

$$\mathbf{x}^{t*} = \begin{pmatrix}\mathbf{x}^t \\ \mathbf{p}^t\end{pmatrix} \tag{4.17}$$

The model covariance matrix $\mathbf{C}$ is then also composed of the cross covariances between the model states and the model parameters, as well as the covariances among the parameters.

$$\mathbf{C}^f = \begin{pmatrix}\mathbf{C_{xx}} & \mathbf{C_{xp}} \\ \mathbf{C_{px}} & \mathbf{C_{pp}}\end{pmatrix} \tag{4.18}$$

4.2.4 (b) Localization

In the EnKF data assimilation, localization reduces the size of the matrix to be inverted to minimize the influence of distant observations and removes spurious long-distance correlations (Houtekamer et al. 1998). Here, localization is applied to the model error covariance matrix $\mathbf{C}$. The standard covariance matrix $\mathbf{C}$ is replaced by $\boldsymbol{\rho}^{\circ}\mathbf{C}$. $\boldsymbol{\rho}$ is defined as a correlation matrix with local support, which means that this function is only non-zero in a local (small) region and zero elsewhere. $^{\circ}$ is the Schur (elementwise) product. Note that $\boldsymbol{\rho}$ and $\mathbf{C}$ have the same dimensions. Therefore, the Kalman gain in the LEnKF scheme is calculated as follows:

$$\mathbf{K} = \left[\boldsymbol{\rho}^{\circ}\mathbf{C}_j^f\mathbf{H}^{\mathbf{T}}\right]\left[\mathbf{H}\boldsymbol{\rho}^{\circ}\mathbf{C}^f\mathbf{H}^{\mathbf{T}} + \mathbf{R}\right]^{-1} \tag{4.19}$$

and $\boldsymbol{\rho}^{\circ}$ is calculated using a fifth-order polynomial function (Gaspari et al. 1999).

4.3 Experimental setup

4.3.1 Input Data

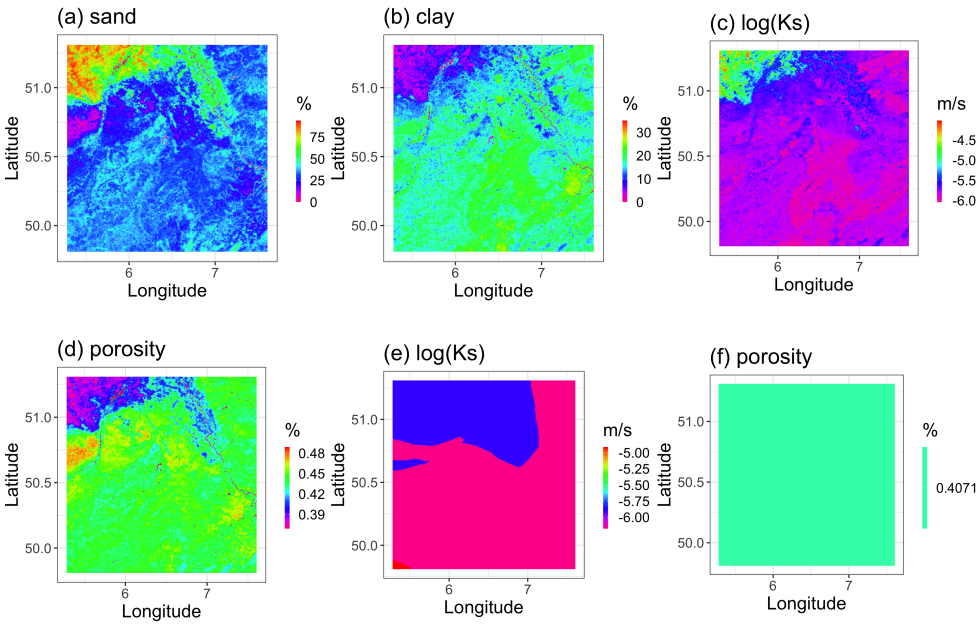

Figure 4.3: (a) and (b) Percentages of sand and clay used in the CLM stand-alone model. (c) and (d) Saturated hydraulic conductivity k_{sat} and porosity for the surface layer (0 - 3 m depth) in the CLM-ParFlow model. (e) and (f) show the same for the bottom layer (3 - 30 m depth).

The spatial model resolution is 500 m × 500 m in the lateral horizontal direction. The soil depth in the CLM stand-alone model reaches 2.5 m with 10 near-surface layers, and in CLM-ParFlow to 30 m depth, with 10 near-surface layers with increasing thicknesses from 0.02 m to 1 m and 20 vertical layers with a thickness of 1.35 m each. The input data for CLM consist of topography (Fig. 4.1), plant functional types (Fig. 4.1), associated plant physiological parameters, and soil properties (Fig. 4.3). The soil texture information is taken from SoilGrids (Hengl et al. 2014, 2017) and remapped to the model grid. The plant functional types and leaf area index are extracted from the Moderate Resolution Imaging Spectroradiometer (MODIS) product, and details can be found in Shrestha et al. (2014).

To keep the consistency between the CLM and CLM-ParFlow models, a Rosetta model (Zhang et al. 2017) is used to estimate the saturated hydraulic conductivity in the surface layers (0 m to 3 m below the surface) of CLM-ParFlow. The Rosetta model takes the soil texture information from CLM. The porosity (ϕ) in the surface layers of CLM-ParFlow is calculated based on the same function that is used in the CLM model. For lower layers (3 m to 30 m), the permeability information was taken from a global geological dataset (Gleeson et al. 2011), and for details see Shrestha et al. (2014). Other van Genuchten water retention parameters (e.g, α and n) are assigned constant, spatially uniform values that are adopted from previous studies (Shrestha et al. 2014; Sulis et al. 2017). The soil texture in CLM and hydraulic parameters in CLM-ParFlow for the surface layers (a-d) and bottom layers (e-f) are shown in (Fig. 4.3). Sandy soils are mainly located in the northwestern corner of the research domain, leading to a high hydraulic conductivity there. An impermeable boundary condition is defined for the lateral borders of the subsurface.

Atmospheric forcing is extracted from the high-resolution reanalysis dataset COSMO-REA6 (Bollmeyer et al. 2015) and used as input for CLM. COSMO-REA6 was created by assimilating observed meteorological data into the atmospheric model COSMO at 6 km resolution over the European continent. In the COSMO-REA6, ERA-interim data (Dee et al. 2011) are used as lateral boundary conditions. Compared to other datasets, such as ERA-interim (at 80 km resolution) and ERA5 (at 25 km resolution), the COSMO-REA provides a higher resolution atmospheric reanalysis. It is shown that the high-resolution reanalysis provides additional value compared to coarse-scale reanalysis and leads to a better representation of small-scale variability (Bollmeyer et al. 2015). A subset of highly requested variables can be directly downloaded from the open data server at DWD (ftp://opendata.dwd.de/climate_environment/REA/COSMO_REA6), including essential variables which were used in this study, e.g., wind speed, air humidity, air pressure, air temperature, precipitation, downward short wave radiation, and downward long wave radiation.

4.3.2 Experiment set up and analyses

The localized EnKF scheme is used in the data assimilation experiments with an ensemble of N = 32 members. To characterize the uncertainty of the land surface-subsurface simulations, random perturbations are introduced for each ensemble member, including (a) atmospheric forcings for both the CLM stand-alone model and the CLM-ParFlow model, (b) soil texture for the CLM

stand-alone model, and (c) hydraulic conductivity and porosity for the soil (0-3 m depth) of the CLM-ParFlow model. Four atmospheric variables, including precipitation, air temperature, long-wave radiation, and short-wave radiation, are perturbed in a spatially and temporally homogeneous manner with correlations among the four variables defined by a correlation matrix (shown in Table 4.2). The mean value and standard deviation of the perturbation of precipitation, air temperature, long-wave radiation, and short-wave radiation are (0, 0 K, 0 W/m^2, 0) and (0.15, 1.5 K, 30 W/m^2, 0.15) respectively. While the noise (lognormally distributed) for precipitation and shortwave radiation perturbations is introduced multiplicatively, the noise for longwave radiation and temperature perturbations is additive. Precipitation is multiplied by log-normally distributed noise, and a bias has been introduced in the back transformation (Han et al. 2013) as the expectation of a log-normal distribution is greater than its median. To quantify the effect, we compared the long-term annual mean precipitation summed over all time steps between the perturbed and the original forcing data. The results showed that the ensemble mean precipitation is systematically overestimated by approximately 5 % relative to the reference. To account for this bias, a constant correction factor (0.95) is applied to each of the ensemble members.

In the CLM stand-alone simulations, soil texture is perturbed by adding a spatially uniform noise to both % sand and % clay (±10 %). The sum of sand and clay percentages is constrained to be smaller than 100 % for each ensemble member. For CLM-ParFlow experiments, the ensemble of soil texture data used in CLM is transformed into input parameters for CLM-ParFlow in the surface layers. Hydraulic conductivity realizations are generated using the Rosetta model, while porosity realizations are calculated using Eq. 4.8. Consequently, the perturbation of hydraulic conductivity and porosity is also spatially uniform. The hydraulic conductivity and porosity for the bottom aquifer layers are not perturbed.

To initiate model simulations with the CLM stand-alone model, the model is first spun up using atmospheric forcing data from the years 2015 - 2017. CLM-ParFlow, on the other hand, has a more comprehensive characterisation of the terrestrial water cycle, and a dynamic equilibrium needs to be reached to have a more proper model initialization (Ajami et al. 2014). It is spun up with initial states from a previous study (Sulis et al. 2017) and then using forcing data of the year 2017 until a dynamic equilibrium is reached.

Soil moisture from SMAP products is quality controlled to exclude observations under dense vegetation, water bodies, and frozen soils. The penetration of SMAP is considered to be at a depth of 5 cm. The localisation radius is set to 20 grid cells (10 km) to take into account the approximate size of the Backhus-Gilbert optimal interpolated original SMAP footprints. The year 2018 is used for the DA experiments. The measurement error is set to 0.04 cm^3/cm^3, which is the target accuracy of the SMAP mission. The assimilation experiments are run with a one-hour time step, while soil moisture data assimilation is performed daily. In this study, six simulation experiments are conducted using the TSMP-PDAF framework: (a) CLM-OL: an open-loop simulation (without data assimilation) using the CLM stand-alone; (b-c) assimilation of SMAP L3_SM_P_E soil moisture into the CLM model, employing either state-only update (CLM-DA) or state and parameter update (CLM-DA-SP); (d) CLM-PFL-OL: an open-loop simulation with the CLM-ParFlow; (e-f) CLM-PFL-DA and CLM-PFL-DA-SP, similar to (b-c) but with

the CLM-ParFlow model. When updating both states and parameters in the CLM-ParFlow model, a damping factor of 0.1 is employed to limit the intensity of the hydraulic conductivity perturbations (Hung et al. 2022; Li et al. 2024).

Table 4.2: Correlation matrix of perturbed atmospheric forcing variables.

Variable name	precipitation	shortwave radiation	longwave radiation	temperature
precipitation	1	-0.8	0.5	0.0
shortwave radiation	-0.8	1.0	-0.5	0.4
longwave radiation	0.5	-0.5	1.0	0.4
temperature	0.0	0.4	0.4	1.0

4.3.3 Evaluation metrics

To assess the influence of the assimilation, statistical performance measures were evaluated, including bias, the root mean square error (RMSE), unbiased root mean square error (ubRMSE), Pearson's correlation coefficient (r) (Gruber et al. 2020), and a normalized error reduction index (NER):

$$bias = \frac{1}{T}\sum_{i=1}^{T}(X_{t_i} - Y_{t_i,obs}) \tag{4.20}$$

$$RMSE = \sqrt{\frac{1}{T}\sum_{i=1}^{T}(X_{t_i} - Y_{t_i,obs})^2} \tag{4.21}$$

$$ubRMSE = \sqrt{RMSE^2 - bias^2} \tag{4.22}$$

$$r_{X,Y} = \frac{cov\,(X,Y)}{\sigma_X \sigma_Y} \tag{4.23}$$

$$NER = 100 \times (1 - \frac{E_{DA}}{E_{OL}}) \tag{4.24}$$

where T is the total number of time steps, X_{t_i} is the modelled ensemble mean variable (soil moisture, ET, or groundwater level), and $Y_{t_i,obs}$ is the corresponding observed value, both at time step t_i. $cov(X,Y)$ is the covariance between model-simulated values and observed values, σ_X is the standard deviation of model-simulated values, and σ_Y is the standard deviation of observed values. The E_{DA} and E_{OL} represent the RMSE from the data assimilation and open-loop runs.

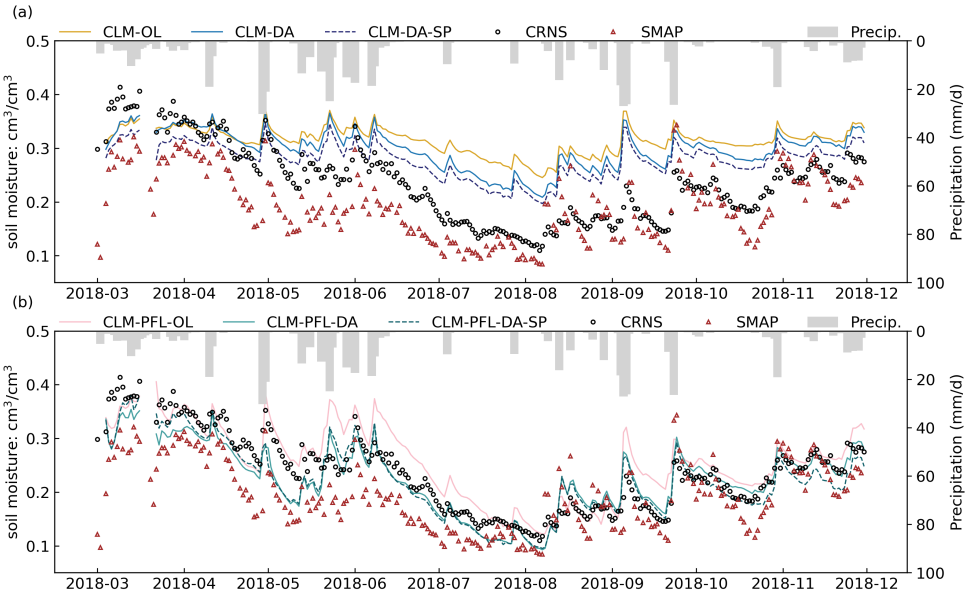

Figure 4.4: Time series of simulated daily soil moisture (at the depth corresponding to the CRNS) average over thirteen CRNS sites from (a) CLM-OL, CLM-DA and CLM-DA-SP and (b) CLM-PFL-OL, CLM-PFL-DA and CLM-PFL-DA-SP) along with soil moisture measurements by SMAP (green triangles) and CRNS (black circles), and precipitation for the simulation period of 2018.03.01 - 2018.11.30. The CRNS observations are shown in black circles and SMAP observations are shown in red triangles.

4.4 Results and discussion

4.4.1 Evaluation with in situ soil moisture measurements

Fig. 4.4 compares the soil moisture time series simulated by CLM and CLM-PFL for the OL, DA, and DA-SP experiments, with in situ measurements and SMAP observations. Fig. 4.4 shows the seasonal dynamics in both observations and simulated datasets, with the highest soil moisture in early spring and a distinct dry-down from May into the summer time. The simulated soil moisture from CLM-OL is systematically higher than the measurements. Data assimilation corrects the overestimation of soil moisture, especially under drier conditions in the summer season. In general, the simulated soil moisture from CLM-ParFlow shows better temporal consistency with in situ measurements and the SMAP retrievals.

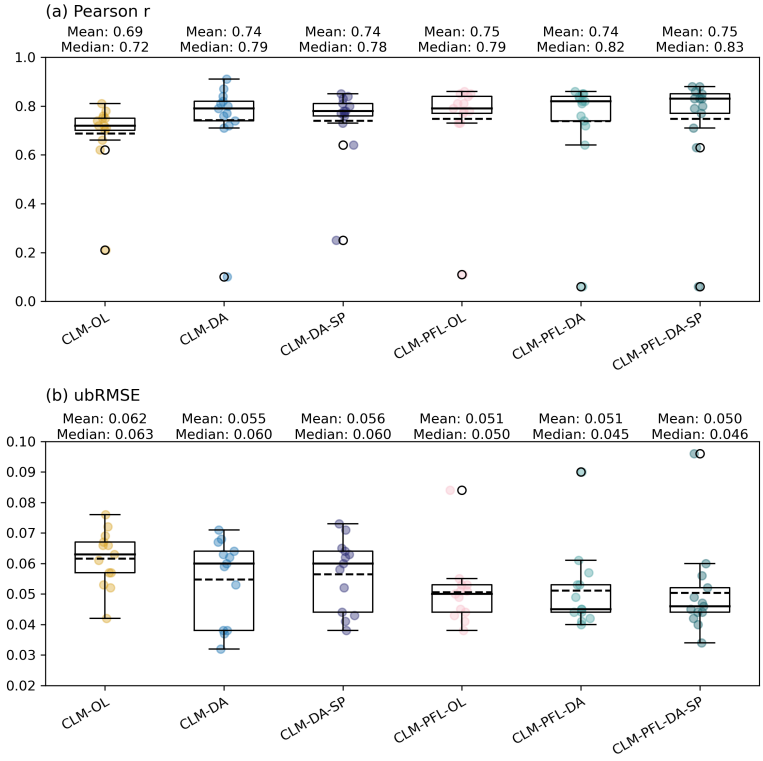

Figure 4.5: Boxplots of (a) r and (b) ubRMSE for the simulated soil moisture CLM-OL, CLM-DA and CLM-DA-SP and CLM-PFL-OL, CLM-PFL-DA and CLM-PFL-DA-SP compared to CRNS measurements for the simulation period of 2018.03.01 - 2018.11.30. The box plot shows the 10, 25, 50, 75, and 90% quantiles, with the dashed line representing the mean values and circle marks representing the outliers.

Fig. 4.5 summarizes the evaluation metrics for CLM and CLM-PFL, with and without data assimilation experiments, compared with thirteen CRNS observations. It shows that both CLM-

DA and CLM-DA-SP experiments are closer to in situ soil moisture measurements in terms of ubRMSE and R than the open loop runs. The median ubRMSE decreases from 0.063 cm^3/cm^3 to 0.060 cm^3/cm^3 for CLM-DA and 0.060 cm^3/cm^3 for CLM-DA-SP, meanwhile, the median R increases from 0.72 to 0.79 and 0.78, respectively. For CLM-PFL, the median ubRMSE and R for OL and two DA scenarios are 0.050 cm^3/cm^3, 0.045 cm^3/cm^3, and 0.046 cm^3/cm^3, 0.78, 082 and 0.83, respectively. Overall, compared to the OL runs, assimilation with the CLM and CLM-PFL models leads to small but improved estimates of soil moisture in terms of Pearson r and ubRMSE. It is important to note that while improvements are observed in the median values for Pearson r and ubRMSE, the mean values do not demonstrate a significant improvement for the CLM-ParFlow model. This discrepancy suggests an increased variability in site-specific performance, with some locations exhibiting a deterioration following assimilation. One potential explanation for this is the scale mismatch between the high-resolution model (500 m) and the coarser resolution of the SMAP data (9 km). In the assimilation process, multiple sites are located within the same SMAP grid cell, leading to homogenised updates that may not reflect the finer-scale dynamics captured by CLM-ParFlow.

The performance of the CLM and CLM-PFL models in simulating soil moisture varies across the thirteen sites (see Fig. 4.6, Fig. 4.12, and Fig. 4.13). For example, at the Heinsberg and Gevenich sites, the DA runs with CLM and CLM-PFL show the best agreement with the CRNS measurements, with R values above 0.83 and ubRMSE values below 0.041 cm^3/cm^3. At the Merzenhausen site, the performance of the CLM-PFL-DA and CLM-PFL-DA-SP simulations is somewhat lower than CLM-DA and CLM-DA-SP. The assimilation behaves poorly for some stations like Wüstebach, where the ubRMSE of the OL is lower than for the DA runs. The soil in the Wüstebach site has high organic matter content, resulting in a high porosity, which is not considered by the pedo-transfer functions used for both models. In general, the coupled model CLM-PFL with data assimilation tends to result in the lowest ubRMSE value and highest correlation across most sites. The site-to-site variability can be attributed to the limited footprint of CRNS measurements, which have a radius of approximately 130–300 meters. While this footprint is relatively close to the model grid resolution, it only partially covers a model grid cell. This partial overlap introduces additional uncertainty when comparing observed and simulated soil moisture, particularly in regions where soil moisture exhibits high spatial variability. Furthermore, factors such as dense vegetation cover, soil texture, and topographical features are known to impact SMAP observations, thereby affecting their integration into SM simulations.

4.4.2 Spatial analysis of OL and DA and SMAP observations

In the following, we analyze the assimilation effects on spatial patterns of soil moisture (for the upper 5 cm) for different assimilation scenarios. Fig. 4.7 shows the spatial patterns of modelled soil moisture and their differences with SMAP observations for the simulation period. The CLM-OL simulation consistently produces higher soil moisture than SMAP observations over most of the study area, indicating a systematic positive bias in the CLM model. This overestimation is also present in the CLM-DA and CLM-DA-SP simulations, but the deviations are reduced. This suggests that data assimilation is effective in reducing biases and introducing a

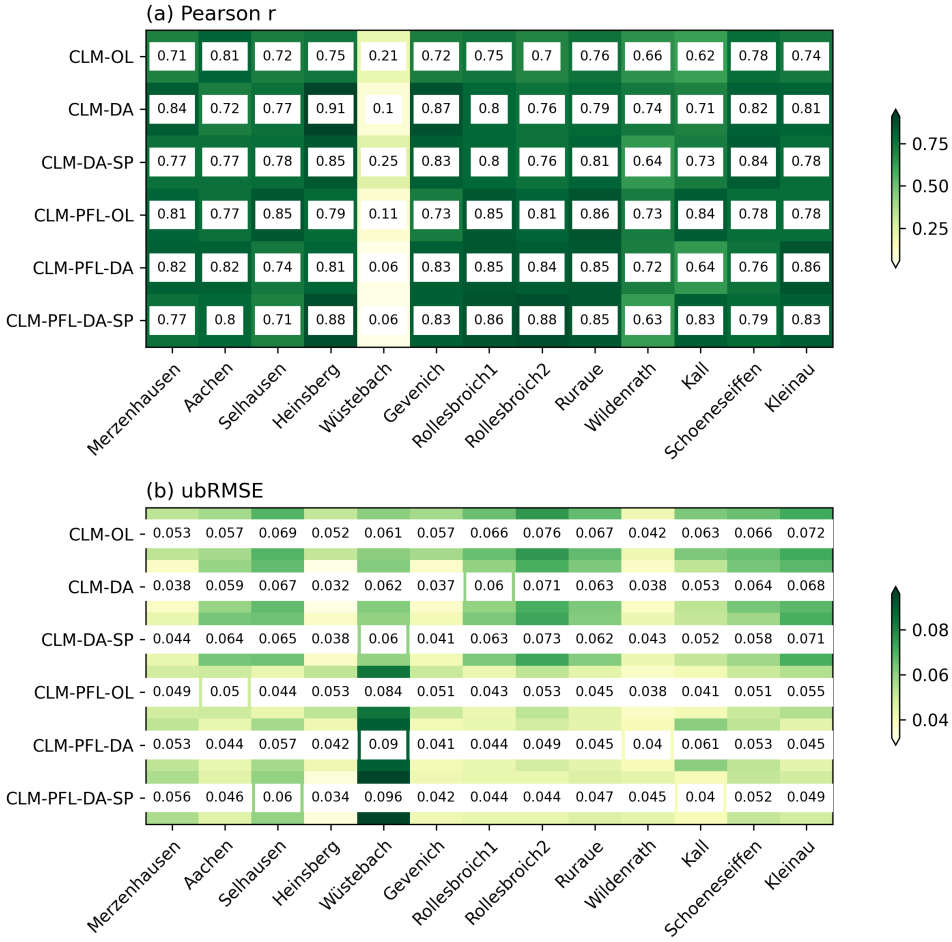

Figure 4.6: Performance metrics of (a) r and (b) ubRMSE for the simulated soil moisture CLM-OL, CLM-DA and CLM-DA-SP and CLM-PFL-OL, CLM-PFL-DA and CLM-PFL-DA-SP compared to CRNS measurements for the simulation period of 2018.03.01 - 2018.11.30.

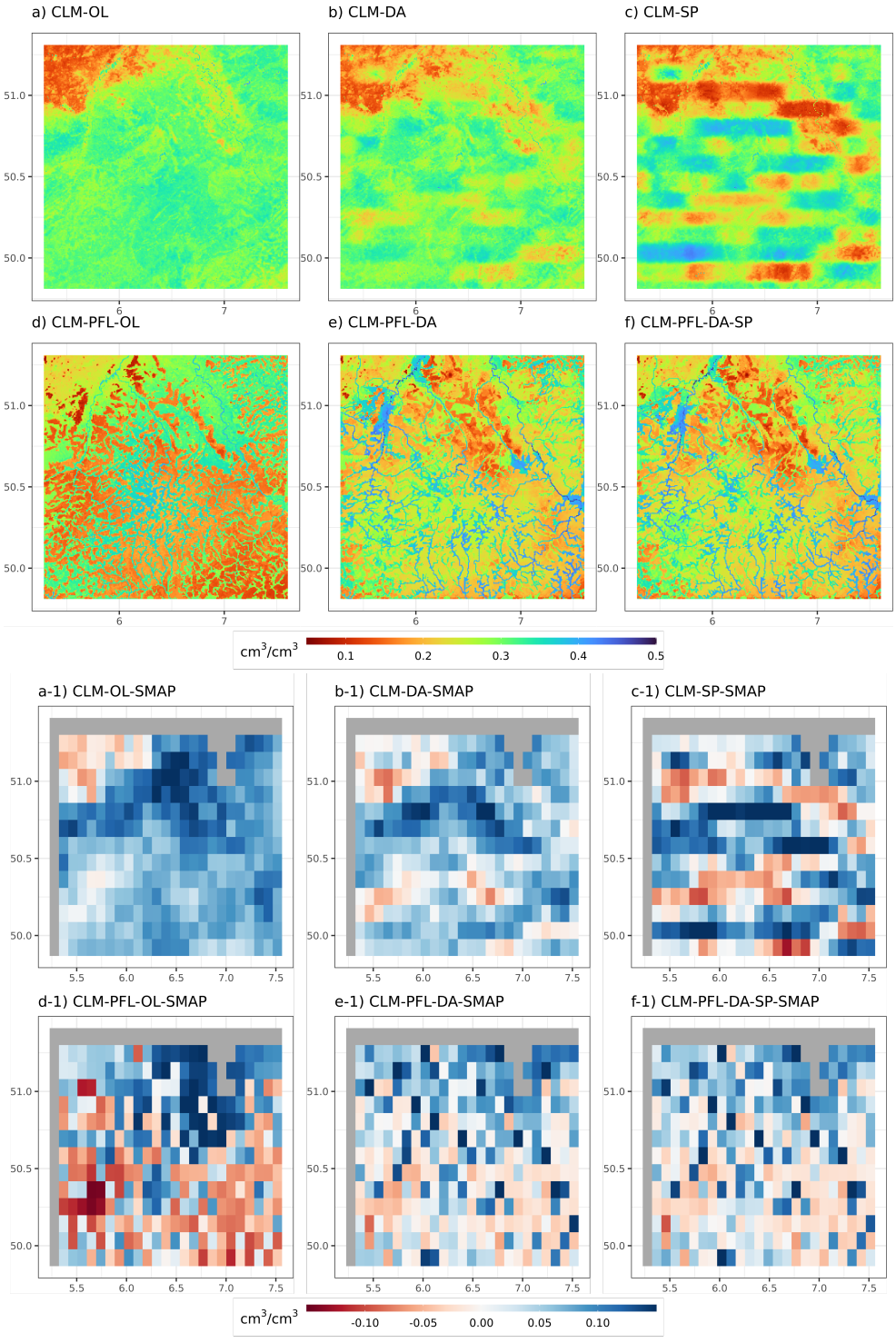

Figure 4.7: Temporally averaged soil moisture over the simulation period of 2018.03.01 - 2018.11.30 for (a and e) SMAP, (b) CLM-OL, (c) CLM-DA, (d) CLM-DA-SP, (f) CLM-PFL-OL, (g) CLM-PFL-DA and (h) CLM-PFL-DA-SP for MAM (March, April and May), JJA (June, July and August) and SON (September, October and November)

degree of spatial heterogeneity into the model's output. However, localized assimilation schemes seem to lead to the formation of artificial soil moisture patterns that are related to SMAP footprints.

In contrast, all CLM-ParFlow configurations exhibit a more pronounced spatial heterogeneity in soil moisture compared to CLM and its data assimilation variants. This enhanced heterogeneity reflects the ability of CLM-ParFlow to simulate lateral flow processes that contribute to a more realistic representation of soil moisture distribution, particularly in areas with complex topography. The assimilation of SMAP data in the CLM-PFL-DA and CLM-PFL-DA-SP experiments further modifies the soil moisture patterns, resulting in a more localized variability of soil moisture that aligns better with SMAP observations. Note that the reductions in discrepancies are spatially heterogeneous; for instance, southern areas with complex topography, where lateral flow dominates, tend to benefit more.

Interestingly, the performance of CLM-PFL-DA and CLM-PFL-DA-SP is very similar, illustrating that parameter estimation does not clearly improve simulation results. This could be attributed to the inherent strengths of the CLM-ParFlow model, which already captures key hydrological processes such as lateral flow in soil moisture redistribution. Additionally, the lack of parameter updates for deep subsurface layers in the assimilation process may limit the potential for further improvements in soil moisture.

4.4.3 Evaluation of in situ evapotranspiration (ET) measurements

The influence of soil moisture DA on ET modelling is also investigated. Fig. 4.8 shows the temporal dynamics of daily ET at four EC sites. The simulated ET agrees well with the observations at most EC sites. A seasonal pattern is visible, with higher values corresponding to the growing season with higher incoming radiation and increased vegetation activity. The observed ET shows significant temporal variability, with occasional spikes, which could be due to natural variability in weather patterns, vegetation responses, or measurement errors. The quantitative evaluation metrics of R and ubRMSE are shown in Table 4.3, where no significant impact of data assimilation is found. For the CLM model, the average r are 0.73, 0.73, and 0.74, and the average ubRMSE are 0.71, 0.71, and 0.70 mm/d for the OL, DA, and DA-SP, respectively. The coupled CLM-PFL model exhibits similar performance, yielding r values of 0.76, 0.74, and 0.72, and average ubRMSE are observed to be 0.70, 0.71, and 0.73 mm/d for the OL, DA, and DA-SP, respectively.

At the Selhausen site, the consistent underestimation of ET by both models during the growing season suggests a potential misrepresentation of the crop cycle dynamics. In situ observations reveal a sharp decline in ET rates following senescence and summer harvesting in combination with very dry conditions at that time. This decline is not captured by either of the models, owing to the absence of harvest-related information in the model scheme and, in the case of CLM, a stand-alone also an overestimation of the soil moisture content. By comparing Fig. 4.8 and Fig. 4.6, we find that ET and soil moisture are strongly correlated, with changes in soil moisture typically being reflected in corresponding changes in ET. The high ET simulated by

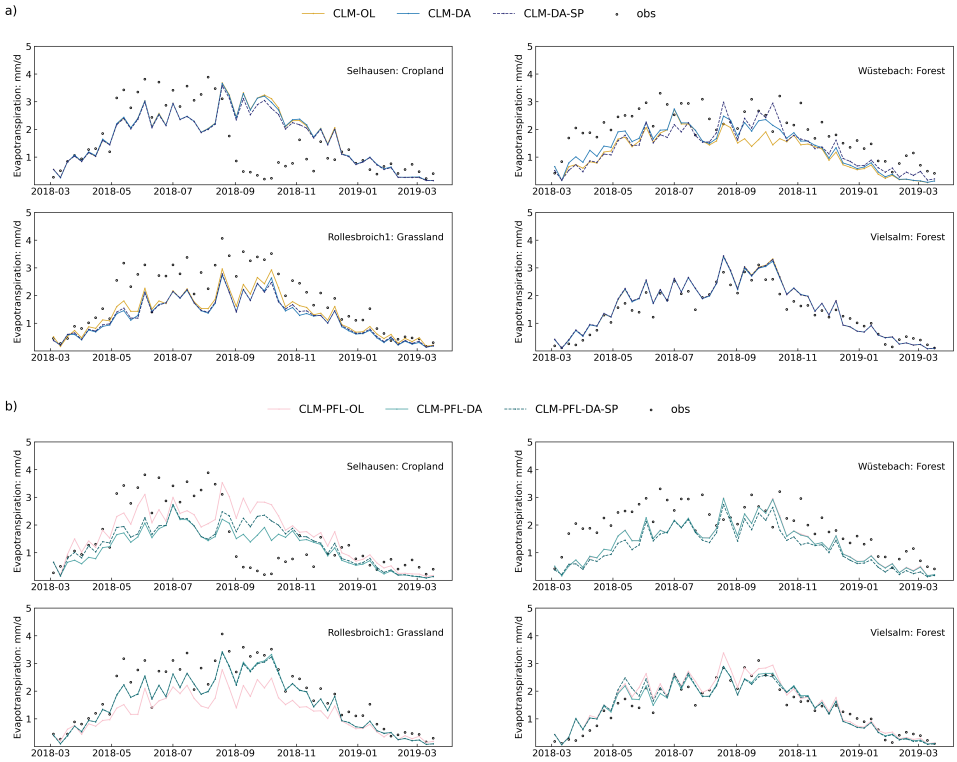

Figure 4.8: Time series of weekly evapotranspiration simulated by (a) CLM-OL, CLM-DA, CLM-DA-SP, (b) CLM-PFL-OL, CLM-PFL-DA, and CLM-PFL-SP compared to in situ measurements at four eddy-covariance (EC) sites (a) Selhausen, (b) Wüstebach, (c) Rollesbroich1, and (d) Vielsalm. Black dots represent flux tower observations.

Table 4.3: Comparison metrics of Pearson r and ubRMSE (mm/d) for the simulated evapotranspiration from CLM-OL, CLM-DA, CLM-DA-SP, CLM-PFL-OL, CLM-PFL-DA and CLM-PFL-SP at four EC sites for the period of 2018.03.01 - 2018.11.30

Station	**Run**	**r**	**ubRMSE**	**Run (PFL)**	**r**	**ubRMSE**
Selhausen	CLM-OL	0.47	1.22	CLM-PFL-OL	0.47	0.94
	CLM-DA	0.47	1.21	CLM-PFL-DA	0.47	1.11
	CLM-DA-SP	0.49	1.17	CLM-PFL-DA-SP	0.49	1.12
Wüstebach	CLM-OL	0.63	0.75	CLM-PFL-OL	0.62	0.75
	CLM-DA	0.63	0.75	CLM-PFL-DA	0.62	0.75
	CLM-DA-SP	0.63	0.75	CLM-PFL-DA-SP	0.62	0.75
Rollesbroich1	CLM-OL	0.92	0.47	CLM-PFL-OL	0.87	0.69
	CLM-DA	0.93	0.48	CLM-PFL-DA	0.91	0.59
	CLM-DA-SP	0.92	0.48	CLM-PFL-DA-SP	0.89	0.64
Vielsalm	CLM-OL	0.90	0.40	CLM-PFL-OL	0.89	0.42
	CLM-DA	0.90	0.40	CLM-PFL-DA	0.90	0.41
	CLM-DA-SP	0.90	0.40	CLM-PFL-DA-SP	0.89	0.42

CLM-PFL-OL at Selhausen is reduced as soil moisture decreases by the assimilation, which reduces latent heat flux and increases sensible heat flux. The finding aligns with previous research (Martens et al. 2016; Peters-Lidard et al. 2011), which established a strong correlation between the improved or degraded representation of ET fields and the corresponding changes in simulated soil moisture induced by assimilating remote sensing soil moisture products. The only limited improvements in ET characterization related to soil moisture data assimilation could be partly due to the limited value of absolute soil moisture data to estimate energy fluxes with land surface models. Other factors, such as incoming shortwave radiation, vegetation schemes, and roughness length parameterization, also have a significant impact on the modelled latent and sensible heat fluxes.

4.4.4 Evaluation of groundwater level simulated by CLM-PFL

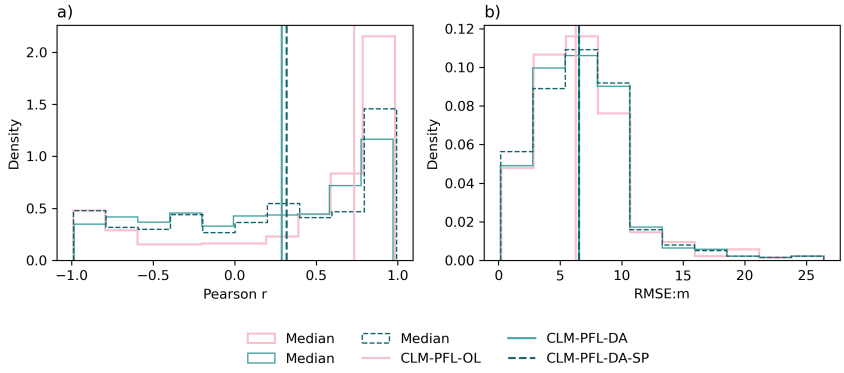

Figure 4.9: Comparison of model performance metrics across three CLM-PFL scenarios for monthly groundwater level simulations at 527 sites: (a) Pearson r (b) RMSE).

During the assimilation process, the pressure head is updated based on the Mualem-van Genuchten model (Van Genuchten 1980), which has an impact on the simulated groundwater levels. The simulated groundwater levels are spatially interpolated from model grid points to the closest location of the monitoring well. Figure. 4.9 illustrates the validation results of mean monthly groundwater levels (in terms of Pearson correlation and RMSE evaluated across 527 sites) for the three simulations with the CLM-ParFlow model. The median Pearson r value for the OL (0.73) is notably higher compared to the value for the DA (0.29) and DA-SP (0.32) experiments, suggesting that the OL experiment without data assimilation already captures the monthly groundwater variation well at many sites. Contrary to the correlation results, the OL, DA and DA-SP have similar median RMSE values of 6.25 m, 6.54 m, and 6.54 m, respectively, suggesting that soil moisture assimilation is not able to improve groundwater depth characterisation. One potential explanation is that groundwater wells may be subject to localised influences, which may be related to land use and human activities. The remotely sensed soil moisture data, however, have a relatively coarse resolution and are therefore unable to capture this information. The DA-SP experiment appears to have a slightly higher median ubRMSE compared to DA; however,

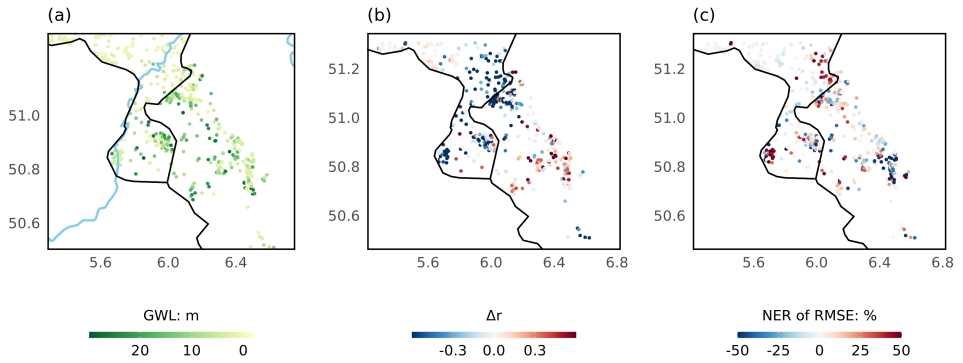

Figure 4.10: The spatial distribution of (a) observed annual mean groundwater levels, and (b) and (c) the performance of CLM-PFL-SP simulations compared to CLM-PFL-OL. Performance is evaluated in terms of changes in Pearson r (Δr) and reduction in RMSE (NER: %).

the DA-SP experiment shows a tighter distribution, which suggests that the results are more consistent across different sites.

To further investigate the impact of data assimilation, we present the spatial distribution of Δr and RMSE reduction (NER) for the CLM-PFL-SP compared to CLM-PFL-OL experiments in Fig. 4.10. As there are only minor differences in the performances of CLM-PFL-DA and CLM-PFL-SP, we do not show CLM-PFL-DA here. The spatial analysis of Δr and NER of RMSE shows that only a small portion of sites benefit from data assimilation, indicated by both increased Δr and decreased NER. At most sites, however, the two metrics display an inverse relationship. Regions with decreased Pearson r often coincide with areas where RMSE is notably reduced. One possible explanation is that the groundwater level characterization improves gradually over time, during the simulation period. However, for the overall time series, this results in a worse representation of seasonal dynamics (due to the gradual adjustments over time by DA) with an associated worse correlation between simulated and measured values, compared to the OL run.

4.5 Discussion

The performance metrics show the relatively better performance of data assimilation runs compared to the open-loop runs for both CLM and CLM-ParFlow. The SMAP retrievals are characterized by a spatial resolution of 9 kilometers yet exhibit discontinuities in both spatial and temporal coverage. In contrast, both CLM and CLM-ParFlow are run at a high-resolution scale of 500 m, generating continuous predictions. This study supports that SMAP products have significant skill to improve the accuracy and consistency of soil moisture estimations. However, the improvement in soil moisture characterization for CLM-ParFlow is less significant than the

improvement for CLM stand-alone in the time series plot (Figure 4.4). This may be due to the fact that the coupled CLM-ParFlow already simulates soil moisture very well, leaving less room for further improvement. It is important to note that the footprints of SMAP are much larger than the model resolution. In this study, the SMAP soil moisture data are assigned to the nearest model grid cell, and the other surrounding grid cells within a local radius are updated via the covariance. Another possibility is to implement multi-scale assimilation for remote sensing soil moisture products like SMAP. This would allow for the updating of multiple model grid cells covered by a satellite footprint (Montzka et al. 2012). In multi-scale assimilation, the average simulated soil moisture within a satellite footprint is compared with the satellite soil moisture observations, which may result in improved assimilation results for the CLM and CLM-ParFlow models. The spatial variability in soil moisture simulated by CLM is limited due to the CLM model structure, which does not account for lateral water flow processes between adjacent grid cells. The absence of lateral flow processes restricts CLM's ability to capture the influence of topographic features and subsurface heterogeneities on the soil moisture distribution, resulting in spatially uniform soil moisture patterns that deviate from reality.

The results from ET validation generally agree with previous assimilation studies (Gebler et al. 2017; Martens et al. 2016; Peters-Lidard et al. 2011) and also for the same model (Hung et al. 2022; Li et al. 2024), that is, the assimilation of soil moisture only marginally improves the estimation of ET. Larger improvements are found under drier conditions (during the summer period). Note that the southern modelling area is predominantly characterized as energy-limited rather than water-limited due to the relatively low temperatures, global radiation, and high annual precipitation. ET in such an environment may approach the potential ET, and is mostly controlled by energy availability (e.g., temperature and radiation) rather than soil moisture. The findings align with Baatz et al. (2017) and Li et al. (2024), where they also found that soil moisture assimilation had minimal effect on ET in the southern part of the area. Studies concluded that uncertainties in soil moisture characterization are mainly influenced by soil texture, whereas ET predictions are predominantly affected by uncertainties in forcing data (Nearing et al. 2016, 2018). While our findings in the southern part could support this, we also find that soil moisture exerts a more important control on ET in the northern part.

In the CLM model, ET is simulated as a function of soil moisture and vegetation parameters, which makes the model more suitable for water-limited conditions. However, to effectively simulate both water- and energy-limited conditions, a scheme should be introduced to consider maximum ET based on available solar radiation. Such a scheme would allow for a better representation of energy-limited environments where ET is predominantly driven by energy availability rather than soil moisture. Moreover, the spatial variability as shown here underscores the critical need for a deeper understanding and improved quantification of the transition between energy-limited and water-limited conditions in LSMs. Such transitions are influenced by the complex interplay of drivers, including meteorological factors and vegetation status (leaf area index).

In addition, the ET calculation is also largely influenced by uncertainties in atmospheric forcing and vegetation parameters, which control root water uptake and stomata closure. To improve

ET estimation, it may be beneficial to assimilate other data types such as ET or LAI. Studies have shown that multivariate assimilation of remotely sensed soil moisture and ET (Gavahi et al. 2020) or LAI observations (Albergel et al. 2017; Fairbairn et al. 2017; Rahman et al. 2022) at finer resolutions contributes significantly to improved ET characterization.

Few studies investigate the influence of assimilating soil moisture on groundwater level predictions in a coupled modelling framework at the larger regional scale. A comparison of the modelled groundwater levels with observations from 527 wells revealed that the assimilation of SMAP soil moisture did not result in improvements in the RMSE. An important aspect is the spatial mismatch between the model resolution and SMAP observations; therefore, it may not be appropriate to evaluate the accuracy of the groundwater level simulations based on the well measurements. On the other hand, the groundwater level is controlled by recharge, the aquifer transmissivity, the aquifer geometry, and, to some extent, the topography itself (Haitjema et al. 2005). In this mountainous modelling domain, regional flow is generally stronger than perpendicular flow and is mainly influenced by the ratio of recharge to hydraulic conductivity (Gleeson et al. 2008). SMAP measures surface soil moisture, which shows a weak correlation with deeper groundwater aquifers. Therefore, its effectiveness in updating parameters in the deep aquifers is very limited. Additionally, the relatively coarse spatial resolution of SMAP data limits its ability to capture variations caused by lateral flow in the CLM-ParFlow model. This finding is also consistent with Hung et al. (2022), while our real-world case presents more complexity. In the future, better results may be obtained by using a model resolution of 100 m instead of 500 m, which allows for better representation of small valleys. The CLM-ParFlow model is constrained to a vertical depth of 30 meters, and this simplification does not fully account for the complexity of real-world aquifer systems. Consequently, measurements in deeper aquifers are excluded from the analysis. In future work, extending the vertical depth of the model could enhance the realism of the simulations. Nevertheless, this objective would require a more detailed representation of three-dimensional geological structure to accurately represent the complex layering and interactions within the subsurface.

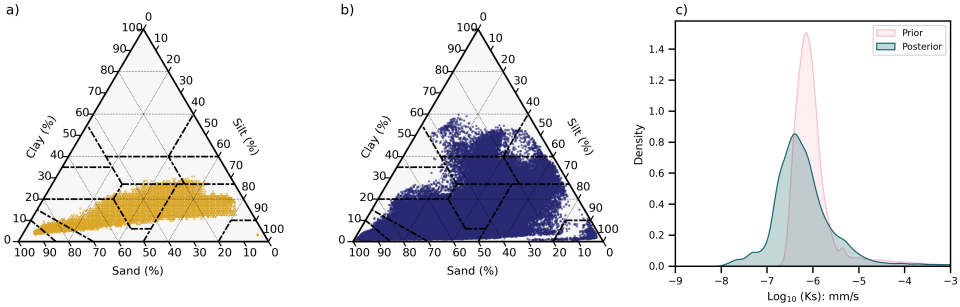

Figure 4.11: Ternary diagram of (a) prior (open loop runs) (b) posterior (parameter update after soil moisture assimilation) soil texture at 5 cm depth in CLM model, and probability density functions of prior (pink) and posterior (blue) hydraulic conductivity k_r at the same depth in CLM-ParFlow model.

In both model configurations, we find that jointly updating the parameters and states does not

provide better results than only updating the states, suggesting that there may be difficulties in updating parameters in the high-resolution real-world cases with the remote sensing soil moisture information. The parameter spread (uncertainty) is still large after the assimilation (see Fig. 4.11). Prescribing an inaccurate soil structure could result in deteriorated soil moisture estimates, particularly in sites like Wildenrath, which is characterized by dense forest cover. In such circumstances, the accuracy of SMAP retrieval is subject to large uncertainty. Studies (Zhao et al. 2023) have demonstrated that the retrieval of soil physical properties through the assimilation of remote sensing information is unlikely to enhance the accuracy of modelled soil moisture. Assimilating high-quality soil moisture measurements, e.g, CRNS observations, probably can provide more accurate parameters for the hydrological models (Baatz et al. 2017; Li et al. 2024). In this study, as the soil moisture is updated on a daily basis, the updated values may be in close alignment with the SMAP observations. Consequently, only minor changes in the soil properties are observed. Hung et al. (2022) assimilated soil moisture in the CLM-ParFlow model with an ensemble size of 64 for a virtual case, and the results show that parameter estimation only gives an additional slight improvement compared to updating soil moisture alone. Brandhorst et al. (2022) also investigated the impact of parameter updates with soil moisture assimilation and found that a small spread in the ensembles impedes parameter updates. Hendricks Franssen et al. (2008) suggested that 200-500 realizations may be sufficient for successful joint state-parameter estimation with hydrological models. However, a larger ensemble size in this work was not feasible because of the required computational resources when running the coupled land surface-subsurface model at high resolution. For instance, running the CLM-ParFlow model with 32 ensemble members for one year simulation required 250,000 CPU core hours. In the future, a hybrid machine learning (ML) data assimilation approach with an approximation of the model by a ML-based emulator could allow the simulation of larger ensemble sizes which could improve the performance of the data assimilation and parameter estimation. However, we feel that the remotely sensed information might also not be accurate enough to estimate model parameters, especially because the observation is at a coarse scale and limited to the upper few cm of the soil.

One challenge of this study was trying to maintain the consistent configurations between the CLM and CLM-ParFlow model despite their different representations of the subsurface. To address this, we perturbed the percentages of sand and clay content in a homogeneous manner in the CLM model and employed the Rosetta pedo-transfer function to convert these parameters into hydraulic conductivity for the CLM-ParFlow model. The perturbation is spatially uniform and could be improved to better consider the spatial variability of soil characteristics. Additionally, previous studies (Ryu et al. 2009) suggest that input parameters and forcing data can have complicated feedback in the model process, leading to unintended effects of the ensemble perturbation. Investigating more advanced ways to create ensembles for different variables is necessary, but beyond the scope of this study. Additionally, it has been suggested that other parameters (α and n in the van Genuchten model) can be estimated (Chaudhuri et al. 2018; Yetbarek et al. 2020), which was not considered in our study. However, the estimation of α and n would bring more instabilities, considering our limited number of ensemble members and the complexity of real-world cases.

It should be noted that the quality check for SMAP retrievals was primarily based on the retrieval quality flag, which did not fully consider the impact of dense vegetation. SMAP suggests that data with a Vegetation Water Content (VWC) less than 5 kg/m^2 is optimal for retrieval. However, as the research area is largely covered by dense vegetation, observations with a VWC between 5-10 kg/m^2 were also used in the assimilation process. As the observations are spatially uniform, this introduces additional uncertainty into the model and affects the predictions, as evidenced by the example of the Wüstebach site. Accurate estimation of observation errors can improve the benefits of assimilating remote sensing products(Degelia et al. 2023; Terasaki et al. 2024). A possible future work is to consider the spatial patterns of the microwave soil moisture retrievals in order to quantify the observational errors, taking into account sensitivities to vegetation and other atmospheric conditions.

The EnKF is an example of a sequential algorithm, which makes it well-suited to real-time forecasting applications, including hydrological studies, weather prediction, and other modelling tasks. However, the EnKF relies on several underlying assumptions (Evensen 2003) that may not always hold in practical applications, particularly in complex, high-dimensional land surface systems. A critical aspect of improving EnKF performance—and DA in general—is achieving an optimal balance among model structure, model parameters, observation data and assimilation technique. Research indicates that misrepresentation of model errors (Jafarpour et al. 2011; Pathiraja et al. 2018; Reichle et al. 2002) can significantly impact the effectiveness of DA. A study assessing the assimilation of satellite-derived SM retrievals over irrigated areas in the U.S. demonstrated that the success of DA largely depended on the model bias (Kumar et al. 2015). Additionally, LSMs often misrepresent the coupling between SM and ET or runoff, leading to reduced DA performance in constraining water fluxes using SM observations (Crow et al. 2024). Future research should focus on enhancing the understanding and refinement of LSMs parameterization to further improve DA efficiency

4.6 Summary

In this study, the remote sensing SMAP soil moisture product is assimilated into the Community Land Model (CLM 3.5) and the coupled land surface-subsurface model CLM-ParFlow (CLM-PFL) over a region of size 22.500 km^2 in western Germany for the year of 2018. A total of 32 ensemble members is generated by perturbing the atmospheric forcings (for both the CLM and CLM-ParFlow model), soil texture properties (for CLM) and hydraulic conductivity and porosity (for CLM-ParFlow). The DA experiments are carried out with the Localized Ensemble Kalman Filter (LEnKF) and SMAP data are assimilated daily. The characterization of soil moisture and other hydrological variables are then assessed with in situ measurements. The key messages from this study and the recommendations for future research are as follows:

1. The assimilation of SMAP soil moisture observations into the CLM and CLM-ParFlow generally improves the soil moisture characterisation with an increase of the median Pearson correlation from 0.72 to 0.79 (CLM) and 0.79 to 0.83 (CLM-PFL) and a reduction of the median ubRMSE from 0.063 to 0.060 cm^3/cm^3 (CLM) and 0.050 to 0.046 cm^3/cm^3

(CLM-PFL). The coupled model shows greater soil moisture spatial variability that is closer to reality, showing that the consideration of lateral flow dynamics is crucial for a realistic simulation of soil moisture. These advantages cannot be fully offset by assimilating soil moisture in CLM.

2. However, the assimilation of soil moisture data does not improve the ET characterisation compared to the open loop runs for both CLM and CLM-ParFlow, which may be attributed to the energy-limited conditions within the modelling domain. When compared to monthly groundwater level measurements, the assimilation does not reduce the RMSE and the correlation between simulated and measured groundwater levels even decreases. This outcome suggests that assimilating surface soil moisture alone is insufficient to improve groundwater level simulations, likely due to the inherent complexity of groundwater systems and the multitude of controlling factors beyond recharge. It is assumed that more accurate soil moisture data will provide more information to the models. The impact of assimilation of passive and active microwave soil moisture data, either individually or in combination, on the predictive skills of the models can be evaluated. Furthermore, we acknowledge the importance of a higher spatial resolution of soil moisture observations, which indicates the need to investigate the assimilation of data from sources such as Sentinel-1 or downscaled SMAP products. On the other hand, a single measurement type (in this case, soil moisture) may not be sufficient to infer other model states in a complex coupled model. Building on previous studies, which have demonstrated the effectiveness of multivariate data assimilation in land surface models, future research will explore the integration of additional variables—such as Leaf Area Index (LAI) or Total Water Storage (TWS)—to further constrain multiple model variables and enhance performance within a coupled land surface-subsurface framework.

3. In this work, we also assimilated soil moisture, including parameter estimation, and found that joint state parameter estimation does not improve predictions compared to state estimation alone. This might point to the difficulty of using the remotely sensed soil moisture information to improve parameter estimates over a large domain with a complex topography. It would be beneficial to further investigate by utilising larger ensemble sizes and a more refined computational model once enhanced computational efficiency has been achieved.

4.A Appendix

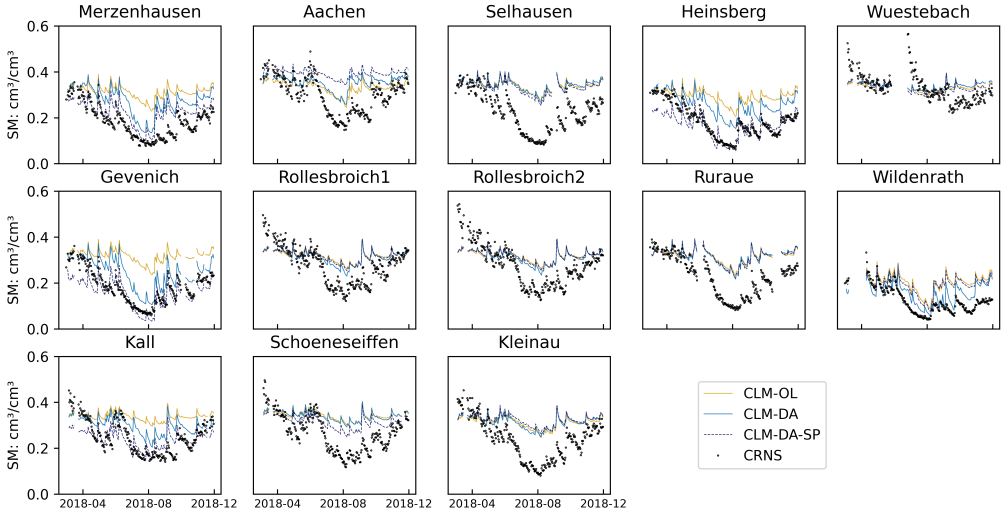

Figure 4.12: Time series of simulated daily soil moisture (at the depth corresponding to the CRNS) at thirteen CRNS sites for the CLM-OL, CLM-DA and CLM-DA-SP simulation experiments and the period 2018.03.01 - 2018.11.30. The CRNS observations are shown in black circles.

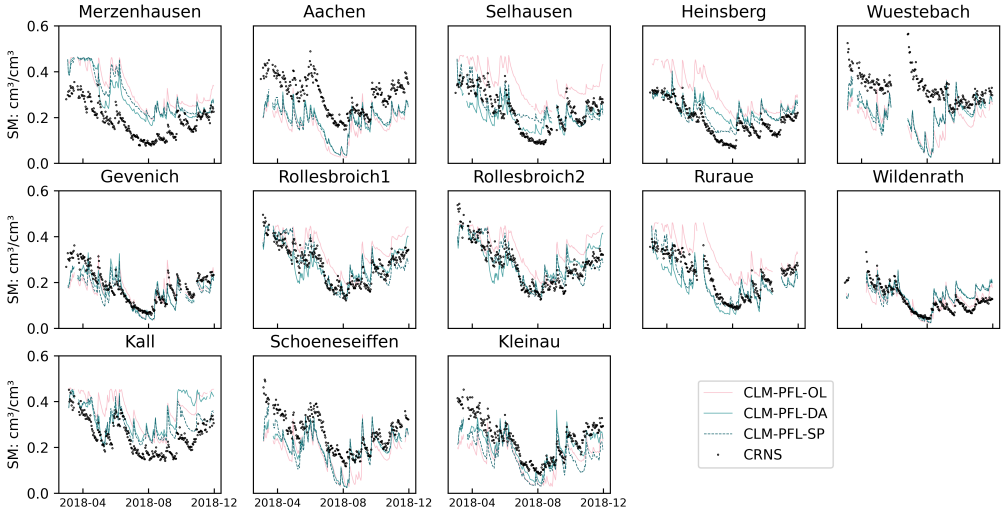

Figure 4.13: Time series of simulated daily soil moisture (at the depth corresponding to the CRNS) at thirteen CRNS sites for the CLM-PFL-OL, CLM-PFL-DA and CLM-PFL-DA-SP simulations and for the period 2018.03.01 - 2018.11.30. The CRNS observations are shown in black circles.

5

A Comparative Analysis of Remote Sensing Soil Moisture Data-sets Fusion Methods: Novel LSTM Approach versus Widely-Used Triple Collocation Technique.

*adapted from: Zhao, H., Montzka, R., Vereecken, H., & Franssen, H. J. H. (2023). A comparative analysis of remote sensing soil moisture datasets fusion methods: novel LSTM approach versus widely used triple collocation technique. IEEE Journal of Selected Topics in Applied Earth Observations and Remote Sensing 17 (2024): 16659-16671.

5.1 Introduction

Soil moisture is a fundamental parameter with broad implications for agricultural production, hydrological processes, and climate studies (Henderson-Sellers 1996; Seneviratne et al. 2010). Precise and timely estimation of soil moisture at regional and global scales is essential for effective management of water resources (Dobriyal et al. 2012). Here, microwave remote sensing offers an effective way to retrieve soil moisture information due to its sensitivity to the dielectric properties of the soil (Engman 1991; Mohanty et al. 2017).

Microwave remote sensing operates at different frequencies, namely L-band (1-2 GHz), C-band (4-8 GHz), and X-band (8-12 GHz), and has been widely employed in soil moisture retrievals. Each frequency exhibits unique interactions with the soil surface and subsurface (Zhao et al. 2021b). Satellites based on X-band and C-band include Advanced Microwave Scanning Radiometer for Earth Observing System (AMSR-E) (Njoku et al. 2003), and the successor Advanced Microwave Scanning Radiometer 2 (AMSR2) (Imaoka et al. 2010), and the Advanced Scatterometer (ASCAT) from Meteorological Operational platform series (Metop-A, Metop-B, and Metop-C) (Bartalis et al. 2007; Brocca et al. 2017). Over the past decade, L-band has been commonly considered favorable for large-scale soil moisture monitoring with its reduced sensitivity to vegetation cover and atmospheric interference. Additionally, it has a greater signal penetration depth into the soil profile, allowing for a more comprehensive assessment of soil moisture conditions (Baur et al. 2018; Ma et al. 2023; Wigneron et al. 2017). Satellites operating at L-bands include the Soil Moisture and Ocean Salinity (SMOS) (Kerr et al. 2001) and the Soil Moisture Active Passive (SMAP) (Entekhabi et al. 2010a).

The remote sensing soil moisture products derived from multiple instruments exhibit notable disparities, not only caused by different microwave frequencies but also from orbits, polarization methods, and retrieval algorithms (Barrett et al. 2009; Dobson et al. 1986; Karthikeyan et al. 2017). These discrepancies emphasize each soil moisture product's distinct strengths and limitations and potentially result in inconsistent findings. Therefore, there is a need to combine remote sensing data to reduce uncertainties from any individual datasets and provide a more accurate estimation of soil moisture.

The arithmetic mean is the common method to merge information from multiple satellites, and its effectiveness has been demonstrated in various applications (Peng et al. 2021; Zhang et al. 2019a; Zhang et al. 2021a). Other, more sophisticated linear weighting methods could assign the weights to each dataset based on their prediction errors, commonly evaluated against reference datasets. Kim et al. (2015, 2016) developed a method to merge two satellite soil moisture products by maximizing their correlation with reference datasets from ERA-Interim (ECMWF Reanalysis-Interim) and Merra-Land (Modern-Era Retrospective Analysis for Research and Applications Land) and showed the improved performance for the merged dataset when comparing with in-situ observations. However, they found that the reference dataset can impact the fusion process as the set of weights is governed by the correlation among the parent datasets and the used reference. Triple collocation (TC) is a mathematical technique to assess the error statistics of three or more products without relying on ground truth measurements (Gruber et al. 2016; Scipal et al. 2010; Su et al. 2014). For example, Yilmaz et al. (2012) applied the TC method to merge modeled and remote sensing soil moisture data, and subsequently, the method gained widely usage (Anderson et al. 2012; Gruber et al. 2017; Kang et al. 2021; Kim et al. 2018; Kim et al. 2020; Li et al. 2022; Min et al. 2022; Xie et al. 2022). The European Space Agency Climate Change Initiative (ESA CCI) soil moisture product also applies TC-based uncertainty characterization and weighted merging approaches to combine soil moisture retrievals from multiple satellite sensors into a long-term consistent climate data record (Dorigo et al. 2017; Gruber et al. 2019). In general, the linear weighting methods are easy to understand, straightforward to use, and can be applied to various datasets.

Machine learning (ML) technique has recently been implemented to merge remote sensing information from various instruments because of its remarkable learning abilities. The ML algorithms are capable of handling large and noisy datasets and extracting spatial and temporal features from multiple data sources, making it a valuable approach to enhance the data fusion accuracy and efficiency (Babaeian et al. 2021; Salcedo-Sanz et al. 2020). The success of ML in soil moisture fusion has been demonstrated in previous studies (Babaeian et al. 2021; Batchu et al. 2023; Karthikeyan et al. 2021; Nguyen et al. 2022), including increased correlations and decreased unbiased root mean square error.

This study focuses on merging soil moisture retrievals obtained from three distinct satellite sources using the traditional TC-based merging method and the Long Short-Term Memory (LSTM) technique. The primary aim is to assess the possibility of LSTM as a data fusion approach and compare its performance against the TC-based merging scheme. Additionally, we aim to explore the potential benefits of the LSTM merging scheme in terms of temporal and spatial soil

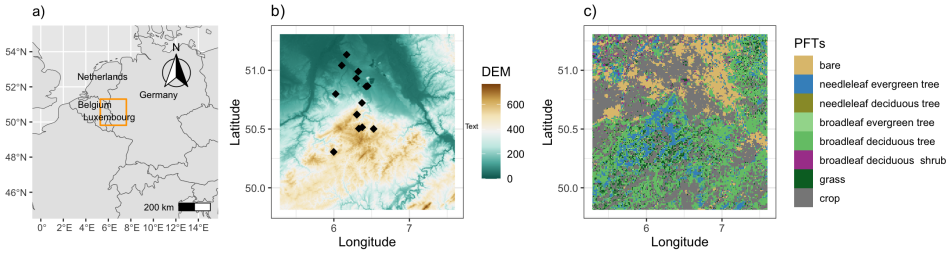

Figure 5.1: (a) Location of the research area in Europe, (b) Digital Elevation Model (DEM: m), and (c) Plant Functional Types (PFTs) over the research area. The diamonds indicate the locations of the CRNS sites.

moisture estimation. Furthermore, we investigate the impact of different parameter setups in the LSTM scheme across various scenarios to gain insights into the respective contributions of these parameters to the soil moisture merging process.

5.2 Study area and data

5.2.1 Study area

The study area is situated in western Europe, encompassing regions within Germany, Belgium, Luxembourg, and the Netherlands and covering an area of 150 km × 150 km (Fig. 5.1). It consists of a diverse range of land-use types and distinct geographical features, including main crops in the flat terrain and deciduous and coniferous forests in the upland regions (Herrmann et al. 2015). The study area exhibits a temperate marine climate. The annual precipitation patterns vary across the region and are influenced by terrain elevation, with the northern part experiencing an average precipitation of 600-900 mm and the southern part receiving higher amounts, reaching up to 1600 mm annually (Zhao et al. 2021a).

5.2.2 Remote sensing soil moisture products

In this study, three different soil moisture products are employed for the data fusion scheme, including the SMAP Enhanced Level 3 Radiometer Soil Moisture (SPL3SMP_E), Version 5 (O'Neill et al. 2021), the AMSR2/GCOM-W1 surface soil moisture L3 product (Owe et al. 2014), and ASCAT Surface Soil Moisture Climate Data Record 7 Extension 12.5 km sampling (H119) (Saf, H 2021). Additionally, the multi-mission passive soil moisture product Version 6.1 from ESA CCI (Dorigo et al. 2017; Gruber et al. 2019; Preimesberger et al. 2020) serves as the reference dataset to evaluate the merged soil moisture.

The SMAP L-band SPL3SMP_E product, first released in December 2016, provides a global daily composite soil moisture estimate at a spatial resolution of 9 km using the Equal-Area Scalable Earth Grid (EASE-Grid) (Chan et al. 2018). It is generated with the Backus-Gilbert

optimal interpolation technique, which extracts information from antenna temperatures and converts them to brightness temperatures (Chan et al. 2018). The final soil moisture estimates are then derived through the Dual Channel Algorithm (DCA).

AMSR2 is deployed on the Global Change Observation Mission - Water 1 (GCOM-W1) satellite, using the Land Parameter Retrieval Model (LPRM) and providing daily measurements of soil moisture at 25 km resolution (Du et al. 2017). The AMSR2 data archive consists of two distinct products: ascending (daytime) and descending (nighttime) acquisitions. It offers two available bands, namely C-band and X-band, for soil moisture measurements (Parinussa et al. 2015). Both the descending and ascending C-band (6.93 GHz) soil moisture products from AMSR2 are utilized in the analysis.

The ASCAT H119 product is generated by data from the Advanced Scatterometer (ASCAT) instrument on board the MetOp-A, MetOp-B, and MetOp-C satellites (Wagner et al. 2013). ASCAT measures the back-scattered radar signals from the Earth's surface, which are utilized to estimate soil moisture. The H119 product provides long-term soil moisture monitoring capabilities, with data available starting from January 2007 (Brocca et al. 2017). It has a sampling resolution of 12.5 km on the Discrete Global Grid (DGG) and a temporal resolution of approximately 1-3 days (Brocca et al. 2017). The soil moisture information derived from ASCAT is expressed in the degree of saturation (%), which is subsequently converted to volumetric soil moisture content (cm^3/cm^3) by multiplication with the soil porosity data retrieved from the Global Land Data Assimilation System (GLDAS-2.1) (also within the ASCAT datasets). Only measurements with a soil moisture noise designation below 20% are retained for analysis.

The ESA CCI SM v 6.1 Passive product is retrieved using the Land Parameter Retrieval Model (LPRA) (Owe et al. 2008) algorithm. This particular product is derived from Level2 data obtained from various satellite missions, including SMAP, SMOS, AMSR2, AMSR-E, among others. The merged passive product provides a global coverage of soil moisture at the spatial resolution of 0.25° and temporal resolution of 1 day. Note that the ESA CCI dataset is mainly used as a reference for visual comparison due to its widespread use in hydrological studies (Chakravorty et al. 2016; Gruber et al. 2017; Ma et al. 2019; Xu et al. 2021).

It is worth noting that both SMAP and AMSR2 are passive sensors. However, the soil moisture products are largely influenced by other factors, e.g, the microwave frequencies, orbits, retrieval, and ancillary data such as soil texture and land cover classes. Several studies (Burgin et al. 2017; Cui et al. 2017; Kim et al. 2018; Wang et al. 2021) have validated the SMAP and AMSR2 soil moisture data at regional and global scales and revealed that they have distinct soil moisture trends and spatial patterns. Moreover, Montzka et al. (2017) validated the SMAP, AMSR2 over the same research region using both standard validation methods and the TC approach and revealed structural quality differences between SMAP and AMSR2 retrievals. Consequently, we assume that the SMAP and AMSR2 are independent products in the subsequent research.

Given the different spatial resolutions of these remote sensing soil moisture products, it is necessary to rescale them prior to the application of merging schemes. In this study, we rescale the data sets to a 500 m × 500 m resolution using the Nearest Neighbor Method.

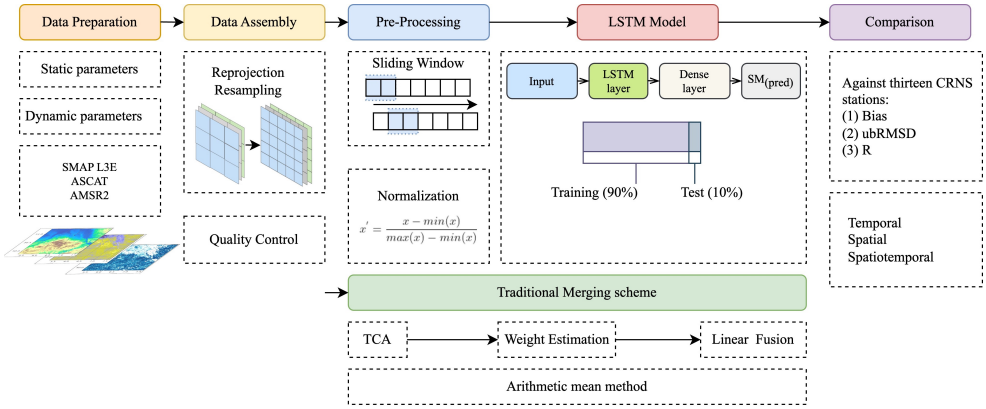

Figure 5.2: A flow diagram of the study, comprising five major steps.

5.2.3 In situ soil moisture observations

Thirteen cosmic-ray neutron sensing (CRNS) stations (Zreda et al. 2012) from the Terrestrial Environmental Observations (TERENO) network (Zacharias et al. 2011) are used for measuring soil moisture at the field scale. Fig. 5.1 shows the locations of CRNS stations. The diameter of the CRNS footprint varies between 260 and 480 meters (Köhli et al. 2015). Previous studies (Köhli et al. 2015; Schrön et al. 2017a) proved that the CRNS effective penetration depth follows an exponential function, ranging from 12 to 76 cm depending on the soil moisture. The remote sensing soil moisture retrievals are typically assumed to be uniform for the penetration depth of the sensor, and non-uniformity as a function of depth is not considered. Studies (Baatz et al. 2014; Bogena et al. 2013) have demonstrated that the RMSE of our CRNS measurements is generally below 0.03 cm^3/cm^3 despite the diverse characteristics of the sites (e.g., land use, biomass, meteorological conditions, soil texture). In general, both CRNS measurements and satellite soil moisture products exhibit similar sensitivity to the soil moisture within the first few centimeters. The CRNS method for measuring soil moisture content has been employed for validation of remote sensing datasets on soil moisture, and its reliability has been demonstrated in a number of studies (Colliander et al. 2017; Montzka et al. 2020, 2017; Zhao et al. 2020). This indicates that the CRNS is suitable for validating remote sensing soil moisture retrievals as well as being targeted in the LSTM training. When used for validating the remote sensing soil moisture datasets, the CRNS are resampled onto the satellite grid using a Nearest Neighbor Search. Original data processing methods and detailed information regarding the thirteen stations can be downloaded and found in previous studies (Bogena et al. 2022; Bogena et al. 2018).

5.3 Methods

The remote sensing soil moisture data merging scheme is depicted in Fig. 5.2.

5.3.1 TC-based merging scheme

The TC analysis was initially introduced and applied in meteorology by Stoffelen (1998), which enables the estimation of systematic and random errors in data obtained from three distinct sources without requiring a reference dataset. The methodology assumes a linear relationship between the soil moisture observations and the actual ground truth value θ (Gruber et al. 2017).

$$SM_i = \beta_i \theta + \alpha_i + \varepsilon_i \tag{5.1}$$

where $i \in \{x, y, z\}$ is one of the three collocated soil moisture datasets, α_i and β_i represent the additive and multiplicative biases of dataset i, respectively, while ε_i denotes the zero-mean random error. Accordingly, the covariances between the two soil moisture datasets would be given by

$$\begin{aligned} Cov\left(SM_x, SM_y\right) &= E\left(SM_x SM_y\right) - E\left(SM_x\right) E\left(SM_y\right) \\ &= \beta_x \beta_y \sigma_\theta^2 + \beta_y Cov\left(\theta, \varepsilon_y\right) \\ &+ \beta_x Cov\left(\theta, \varepsilon_x\right) + Cov\left(\varepsilon_x, \varepsilon_y\right) \end{aligned} \tag{5.2}$$

Considering the following assumptions (Yilmaz et al. 2014), orthogonality of errors $Cov\left(\theta, \varepsilon_i\right) = 0$, for all $i \in \{x, y, z\}$, independence of errors $Cov\left(\varepsilon_i, \varepsilon_j\right) = 0$, for $i \neq j.$, and an expected error of zero $E\left(\varepsilon_i\right) = 0$, the equation (5.2) can be reduced to:

$$\begin{aligned} Q_{xy} &= Cov\left(SM_x, SM_y\right) \\ &= \begin{cases} \beta_x \beta_y \sigma_\theta^2 & \text{for } x \neq y \\ \beta_x^2 \sigma_\theta^2 + \sigma_{\varepsilon_x}^2 & \text{for } x = y \end{cases} \end{aligned} \tag{5.3}$$

Given that we have seven unknowns (β_x, β_y, β_z, $\sigma_{\varepsilon_x}^2$,$\sigma_{\varepsilon_y}^2$, $\sigma_{\varepsilon_z}^2$, σ_θ) in a system of six equations, by introducing a new variable $\lambda_x = \beta_x \sigma_\theta$, the equation could be written as:

$$Q_{xy} = Cov\left(SM_x, SM_y\right) = \begin{cases} \lambda_x \lambda_y & \text{for } x \neq y \\ \lambda_x^2 + \sigma_{\varepsilon_x}^2 & \text{for } x = y \end{cases} \tag{5.4}$$

Then the error standard deviations for the three independent datasets can be calculated based on the following equations:

$$\sigma_\varepsilon = \begin{cases} \sqrt{Q_{xx} - \frac{Q_{xy} Q_{xz}}{Q_{yz}}} \\ \sqrt{Q_{yy} - \frac{Q_{xy} Q_{yz}}{Q_{xz}}} \\ \sqrt{Q_{zz} - \frac{Q_{xz} Q_{yz}}{Q_{xy}}} \end{cases} \tag{5.5}$$

The linear weight fusion method based on least square error can be employed to calculate the

weight value for each pixel in each soil moisture product, and for each grid cell.

$$\begin{cases} w_1 \\ w_2 \\ w_3 \end{cases} = \begin{cases} \frac{1/\sigma^2_{\varepsilon_x}}{1/\sigma^2_{\varepsilon_x}+1/\sigma^2_{\varepsilon_y}+1/\sigma^2_{\varepsilon_z}} \\ \frac{1/\sigma^2_{\varepsilon_y}}{1/\sigma^2_{\varepsilon_x}+1/\sigma^2_{\varepsilon_y}+1/\sigma^2_{\varepsilon_z}} \\ \frac{1/\sigma^2_{\varepsilon_z}}{1/\sigma^2_{\varepsilon_x}+1/\sigma^2_{\varepsilon_y}+1/\sigma^2_{\varepsilon_z}} \end{cases}, w_1 + w_2 + w_3 = 1 \tag{5.6}$$

By using the calculated weight for three remote sensing soil moisture products, the merged soil moisture value at a given grid cell is obtained by:

$$SM_{TC} = w_1 * SM_x + w_2 * SM_y + w_3 * SM_z \tag{5.7}$$

5.3.2 LSTM

The LSTM model, which belongs to the Recurrent Neural Network (RNN) architectures class, has demonstrated notable performances in capturing patterns within sequential data (Siami-Namini et al. 2018). Unlike conventional RNNs, LSTM models effectively address the inherent difficulties of modeling long sequential data. The solution employed by the LSTM model involves using gating mechanisms to regulate the memory retention process (Hochreiter et al. 1997).

As illustrated in Fig. 5.3, a single LSTM layer comprises a sequential arrangement of cell states, each corresponding to a specific time step t. The gating mechanism is incorporated within each cell state, encompassing a forget gate for determining the exclusion of information from the preceding time step, an input gate for selecting and storing new information from the current time step, and an output gate for determining the information to be output from the current time step. During the training phase, the LSTM model incorporates four weight matrices, namely W_f, W_i, W_o, and W_c, along with four bias vectors denoted as b_f, b_i, b_o, and b_c. These weight matrices and bias vectors pertain to the forget, input, output, and candidate gates. These sets of weights are updated through an iterative learning process using the stochastic gradient descent during training. In the case where there are multiple input variables, the LSTM model processes each variable independently. The weight matrices (W_f, W_i, W_o, and W_c) generated for all input variables at a given time step are concatenated and used as input for the next time step. Thus, the LSTM model can capture the relationships between different input variables.

$$f_t = \sigma(W_f \cdot [h_{t-1}, x_t] + b_f) \tag{5.8}$$

$$i_t = \sigma(W_i \cdot [h_{t-1}, x_t] + b_i) \tag{5.9}$$

$$o_t = \sigma(W_o \cdot [h_{t-1}, x_t] + b_o) \tag{5.10}$$

$$C_t = f_t \otimes C_{t-1} + i_t \otimes \tilde{C}_t \tag{5.11}$$

$$\tilde{C}_t = \tanh(W_c \cdot [h_{t-1}, x_t] + b_c) \tag{5.12}$$

$$h_t = o_t \otimes \tanh(C_t) \tag{5.13}$$

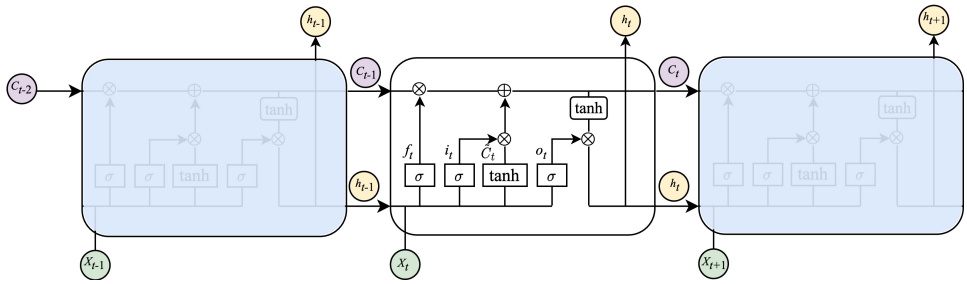

Figure 5.3: Schematic diagram of the LSTM neural network structure. f, i, o represent the values of forget gate, input gate, and output gate, respectively. The symbols C, X, and h refer to the cell state, current input and hidden state, respectively. The symbols σ and tanh represent the sigmoid and hyperbolic tangent activation functions, $\otimes$ means multiplication by weights. (Hochreiter et al. 1997)

5.3.2 (a) Input and target data

For the LSTM model, the training targets are the CRNS observations from thirteen stations. The input data consists of remote sensing soil moisture observations from SMAP L3E, AMSR2, and ASCAT. Additional relevant parameters are categorized into static attributes and dynamic parameters. The static attributes include sand, clay, and silt percentages, bulk density, and altitude from the Digital Elevation Model (DEM). Soil parameters are derived from SoilGrids (Poggio et al. 2021), a global digital soil mapping system based on soil profile observations from the WoSIS database (Batjes et al. 2017). Temporal atmospheric forcing data are obtained from regional reanalysis COSMO-REA6 (Bollmeyer et al. 2015), which includes precipitation, air temperature, global radiation, air humidity, and wind speed time series. The time series of Leaf Area Index (LAI) data is extracted from MCD15A2H Version 6 Moderate Resolution Imaging Spectroradiometer (MODIS) Level 4 (R.B.Myneni, Y.Knyazikhin, T. Park. 2015), and this dataset provides an 8-day composite LAI with a pixel size of 500 meters.

5.3.2 (b) Experimental setups

The training and validation period is from 1 January 2015 to 31 December 2017, with a training-test ratio of 0.1. In order to facilitate the model's ability to recognize temporal relationships and understand patterns over multiple time steps (as illustrated in Fig. 5.3), a sliding window approach is employed during data processing, creating overlapping sub-sequences of input data with a window size of 10 days. The architecture of the LSTM model comprises a single LSTM layer followed by a dense layer. The LSTM layer is configured with a hidden state feature size of 256. The input data is represented as a matrix with dimensions equal to the number of features $\times$ the number of time steps.

The LSTM model is trained with soil moisture retrievals, with and without static and dynamic features, to simulate the target soil moisture measured by CRNS at a single grid pixel. Then the trained model is applied to thirteen CRNS stations as well as other grid cells for another

Table 5.1: Summary of performance metrics in the LSTM model training period (2015 to 2017)

	RMSE: cm^3/cm^3	
	Training (90%)	Validation (10%)
LSTM	0.055	0.045
LSTM_DFSF	0.058	0.052
LSTM_DT	0.056	0.045
LSTM_ST	0.063	0.064

independent year, specifically from 10 January to 31 December 2018. Four scenarios are considered in the analysis: LSTM, which includes both static and dynamic data in the input; LSTM_DFSF, where both static and dynamic data are excluded; LSTM_DT and LSTM_ST, representing scenarios where only dynamic or static data is present, respectively.

The performance of the LSTM model is evaluated over the training and validation period. A summary of the model performance in the training period (2015 - 2017) is provided below. An agreement is observed between the CRNS measurements and the predicted soil moisture in both the training and validation datasets in most scenarios. A smaller RMSE is observed in the validation set than in the training dataset, suggesting that the training strategy reduces over-fitting and enables model generalization to the validation period. The observed smaller RMSE in the validation dataset can be attributed, at least in part, to the smaller size of the validation set. A smaller dataset can, for example, exhibit less variation in the data, which may result in capturing less extreme values that would otherwise contribute to a higher RMSE. Furthermore, an early stopping mechanism is incorporated into the model training process to prevent over-fitting of the training data and to enhance the generation of reliable results for unseen data.

5.3.3 Performance metrics

The validation is conducted for satellite soil moisture products, as well as for the merged dataset. At each CRNS site, the bias, RMSE, unbiased root mean square error (ubRMSE), and Pearson correlation coefficient (r) are calculated. θ_i represents the corresponding satellite retrieval or merged dataset, θ_{crns} represents the CRNS soil moisture measurements, and $E[\cdot]$ is the expectation operator. σ_i and σ_{crns} are the time-variances of the estimated (retrieval or merged dataset) and observed soil moisture for the pixel, respectively.

$$\text{Bias} = E(\theta_i) - E(\theta_{crns}) \tag{5.14}$$

$$\text{RMSE} = \sqrt{E\left[(\theta_i - (\theta_{crns}))\right]^2} \tag{5.15}$$

$$\text{ubRMSE} = \sqrt{E\left[(\theta_i - E(\theta_i)) - (\theta_{crns} - E(\theta_{crns}))^2\right]} \tag{5.16}$$

$$\text{R} = \frac{\sqrt{E\left[(\theta_i - E(\theta_i)) \cdot (\theta_{crns} - E(\theta_{crns}))\right]}}{\sigma_i \sigma_{crns}} \tag{5.17}$$

5.4 Results and discussions

5.4.1 Evaluation of remote sensing products

Fig. 5.4 summarizes the error metrics for remote sensing soil moisture products compared to CRNS observations at thirteen stations between 11 January 2018 and 31 December 2018. The SMAP L3E has the best performance, with median bias of -0.014 cm^3/cm^3, median ubRMSD of 0.057 cm^3/cm^3 and median R of 0.77. For AMSR2 and ASCAT, the median ubRMSD is 0.064 cm^3/cm^3 and 0.098 cm^3/cm^3, respectively, while median R are 0.67 and 0.64. The SMAP L3E, AMSR2, and ASCAT show negative bias compared to CRNS, which could be attributed to the vertical depth mismatch between remote sensing products and CRNS observations. However, the ESA CCI passive dataset gives a wet bias of approximately 0.09 cm^3/cm^3, the finding is consistent with previous studies (Yang et al. 2021a; Zhu et al. 2019). The large difference between in-situ observations and ASCAT and AMSR2 might be attributed to the soil porosity data obtained from LDAS, which converts soil saturation into volumetric soil moisture. The key to improving the accuracy of volumetric soil moisture measurements obtained from AMSR2 and ASCAT systems lies in acquiring high-quality soil porosity data characterized at high spatial resolution. The time series of satellite-based soil moisture retrievals and corresponding ground soil moisture averaged over thirteen sites are presented in Fig. 5.5. Here, we present the average in order to reduce the influence of spatial heterogeneity, which might be introduced by scale mismatches between remote sensing products and in situ measurements. SMAP L3E, ASCAT, and ESA CCI passive exhibit the ability to represent the seasonal variations approximately. Nevertheless, the soil moisture range observed in the AMSR2 data exhibits significant damping.

5.4.2 Comparison of LSTM performance with different setups

Fig. 5.6 shows the spatial patterns of the merged soil moisture derived from different LSTM setups. It is found that the LSTM merged soil moisture demonstrates an integration of the distinctive attributes found in both LSTM_ST and LSTM_DT; on the contrary, the LSTM_DFSF exhibits the lowest spatial variability. In order to evaluate the accuracy of the different LSTM setups and compare the influence of different features, we compare evaluation metrics for different LSTM setups with respect to reproducing measured soil moisture at CRNS stations in Fig. 5.7. It is found that the LSTM gives the best performances, with a relatively low median bias of -0.013 cm^3/cm^3, median ubRMSD of 0.052 $^3/cm^3$ and high median R values of 0.77. Conversely, the LSTM_DT model exhibits the poorest performance, characterized by a larger positive median bias of 0.136 cm^3/cm^3 and median ubRMSD value of 0.106 cm^3/cm^3, along with the lowest median R value of 0.55. In terms of all evaluation metrics, LSTM_ST demonstrates superior performance compared to LSTM_DFSF, indicating that the soil moisture at finer resolution is mostly influenced by the static parameters. Previous studies demonstrated that the small-scale variability of soil moisture is primarily influenced by topography and soil textural parameters. Meteorological variables, on the other hand, exhibit a significant impact on soil

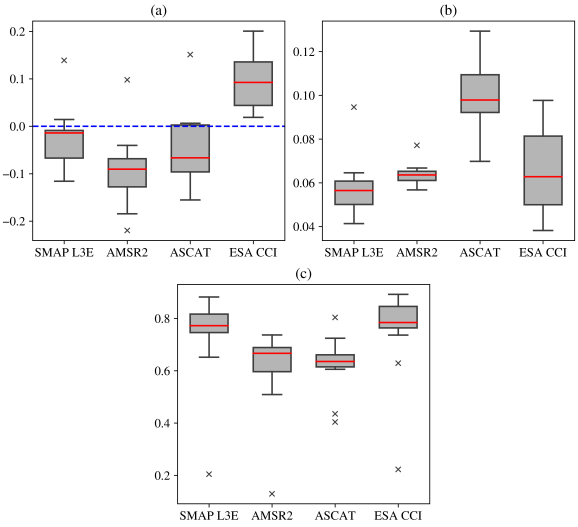

Figure 5.4: Box plots of statistical metrics for comparison between remote sensing soil moisture and CRNS soil moisture at thirteen stations. The metrics are calculated for the period from January 10, 2018 to December 31, 2018: (a) Bias; (b) ubRMSD; (c) R

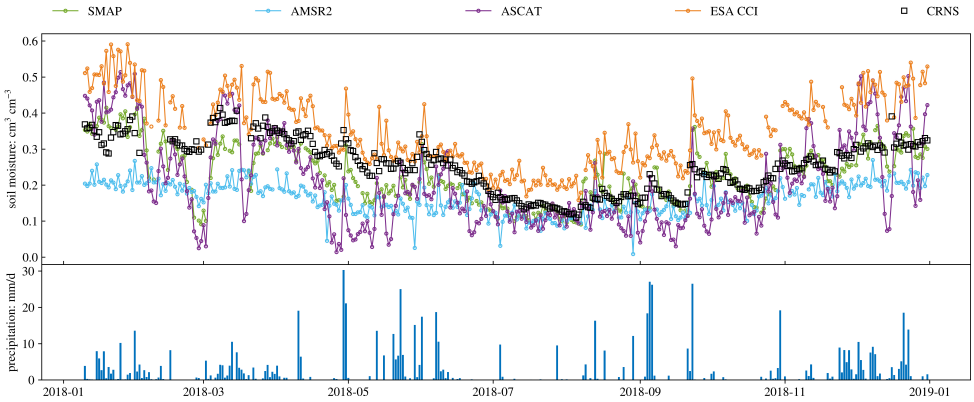

Figure 5.5: Time series of soil moisture of in situ observations (black square), SMAP L3E (green dots), AMSR (cyan dots), ASCAT (purple dots), and ESA CCI (orange dots) over thirteen stations for 10 January 2018 – 31 December 2018. The bottom graph represents the daily time series of precipitation forcing from COSMO-REA6.

moisture variability mostly at regional or watershed scales (Crow et al. 2012; Karthikeyan et al. 2021). The poor performance of the LSTM_DFSF scenario compared to the LSTM scenario also illustrates that both dynamic parameters and static features play an important role while predicting soil moisture at finer spatial scales.

To study the temporal dynamics of the soil moisture, the in situ data and merged soil moisture datasets derived from different LSTM setups are compared in Fig. 5.8. The LSTM and LSTM_ST

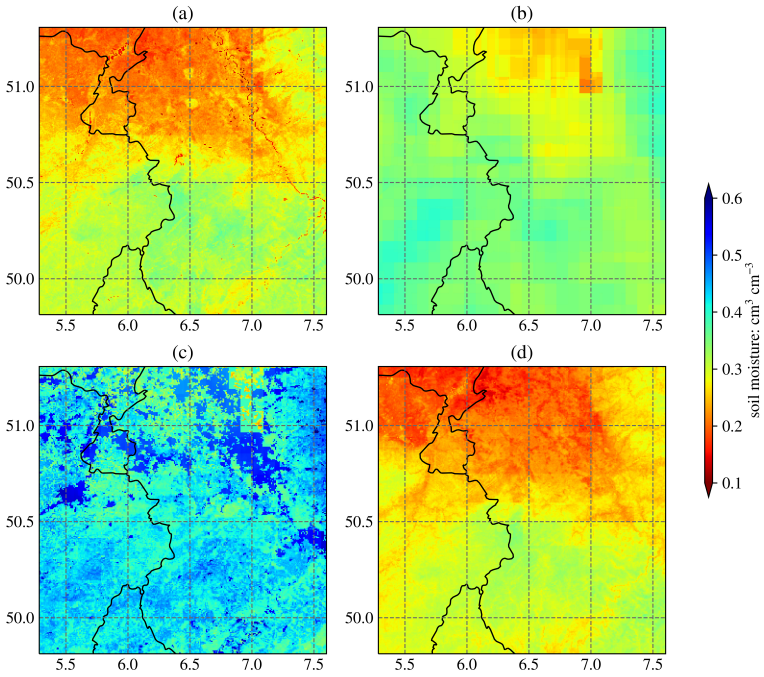

Figure 5.6: Comparison of spatial soil moisture maps from different LSTM scenarios. Shown are average soil moisture distributions for the period from January 10, 2018, to December 31, 2018: (a) LSTM; (b) LSTM_DFSF; (c) LSTM_DT; (d) LSTM_ST

merged datasets exhibit consistent agreement with observed dry-down and wetting-up patterns, demonstrating their ability to capture precipitation intensities accurately. The LSTM_DFSF and LSTM_DT merged datasets can hardly capture the temporal soil moisture variations, especially during soil moisture dry-down events, which usually happen during a period following the precipitation events. In contrast to LSTM_DFSF, LSTM_DT exhibits a more pronounced overestimation, arising from the duplication of precipitation data present in both the dynamic features and the remote sensing soil moisture datasets. This demonstrates that the LSTM model learns the features of various soil textures and captures the soil dry-down patterns over time.

5.4.3 Evaluation of merged soil moisture by TC

The relative weights of SMAP L3E, AMSR2 and ASCAT calculated by the TC-based method are shown in Fig. 5.9. The weights are assigned to each dataset as a function of the magnitudes of their error variances. Lower error variances will be associated with higher weights, whereas higher error variances are associated with lower weights. In general, the ASCAT has low weights (below 0.2), implying that the merged soil moisture product receives larger weights from SMAP

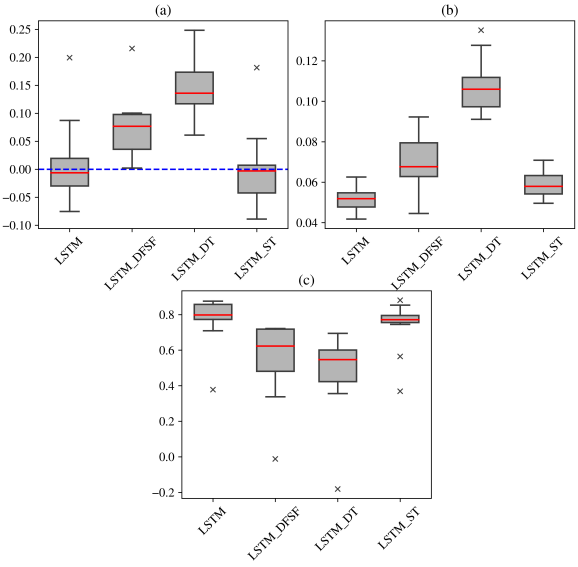

Figure 5.7: Box plots of statistical metrics by comparing soil moisture from the LSTM scenario and measured by CRNS evaluated at thirteen CRNS stations. The metrics are calculated for the period from January 10, 2018, to December 31, 2018: (a) Bias; (b) ubRMSD; (c) R

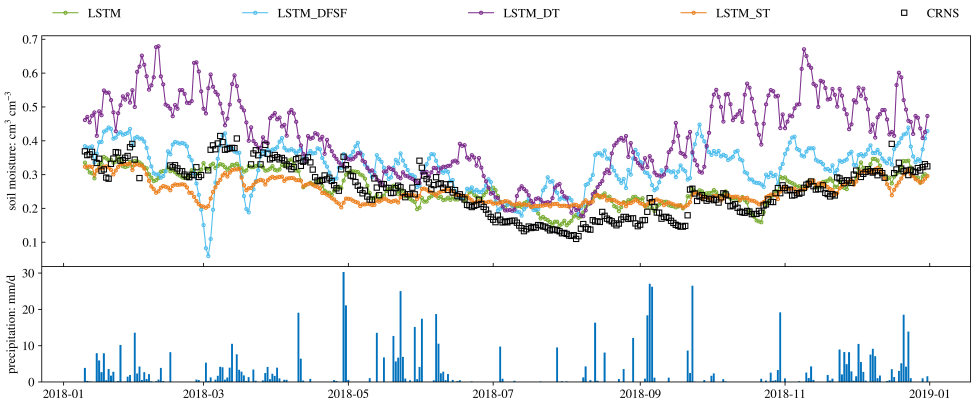

Figure 5.8: Time series of soil moisture in situ observations (black square), LSTM (green dots), LSTM_DFSF (cyan dots), LSTM_DT (purple dots), and LSTM_ST (orange dots) over thirteen stations for 10.January 2018 – 31. December 2018. The bottom graph represents the daily time series of precipitation forcing from COSMO-REA6.

L3E and AMSR2. SMAP L3E exhibits high weights in southern regions, which are predominantly characterized by dense forests and complex topographic features. This indicates that the SMAP L3E demonstrates the least variability in error estimates within areas of high vegetation density. This finding is consistent with previous studies, that SMAP could capture the soil moisture

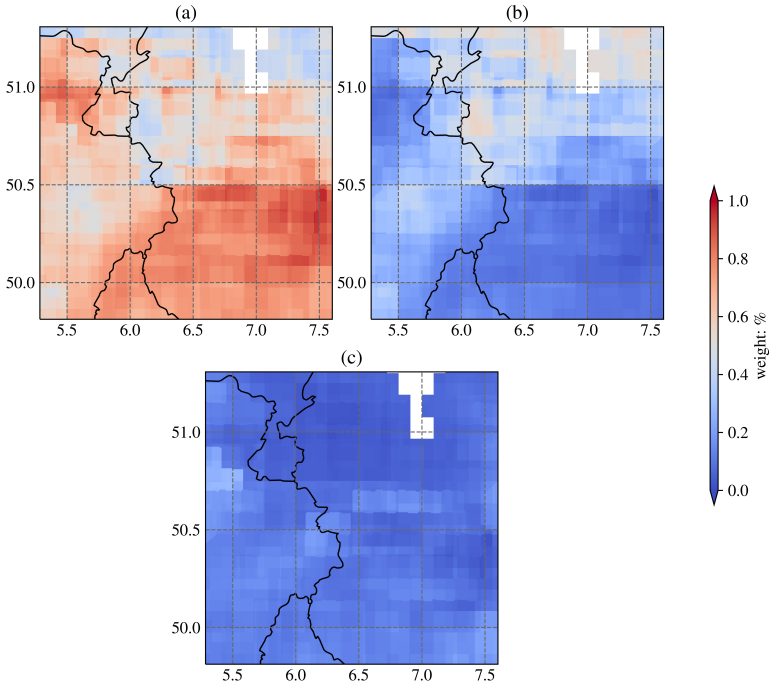

Figure 5.9: The spatial distribution of the weights of (a) SMAP L3E; (b) AMSR2 and (c) ASCAT estimated using triple collocation for data fusion of soil moisture.

under conditions of dense vegetation coverage (Andreadis et al. 2022; Ayres et al. 2021; Chan et al. 2018; Cui et al. 2017).

Fig. 5.10 shows the spatial distribution of soil moisture over the simulation domain. The TC combined dataset is derived from the original products, which, in theory has the potential to reduce the random retrieval errors observed in the original products. Our results reveal distinct spatial patterns among the individual products, whereas the merged product exhibits wet and dry patterns similar to the SMAP L3E product. Specifically, the figure shows high levels of soil moisture in southwestern areas, accompanied by a general decrease in wetness in central northern regions.

5.4.4 Comparison of merged soil moisture datasets from TC-based, Mean and LSTM scenario

The boxplot (Fig. 5.11) summarizes the comparison between the LSTM merged product, TC merged product and the simple arithmetic average dataset (equal weights for each parent dataset). It shows that the LSTM merged product and TC merged product have similar performance in terms of median ubRMSD and R (ubRMSE = 0.052 cm^3/cm^3 and 0.052 cm^3/cm^3, R = 0.79 and 0.80, respectively). However, the TC merged product has a larger bias than the LSTM

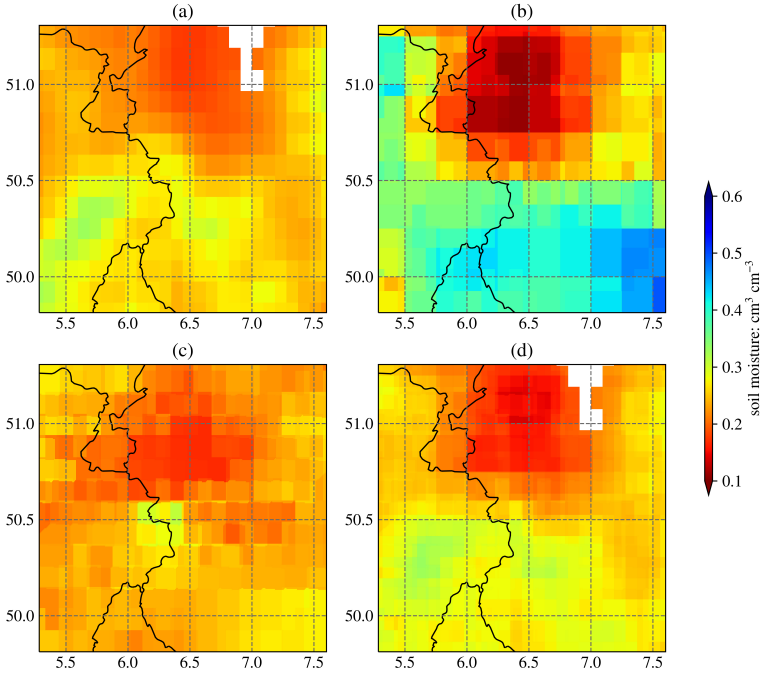

Figure 5.10: Spatial soil moisture distributions derived from original and merged datasets. Shown are average soil moisture distributions for the period from January 10, 2018 to December 31, 2018: (a) SMAP L3E; (b) AMSR2; (c) ASCAT; (d) TC merged.

merged product (-0.041 cm^3/cm^3 compared to -0.006 cm^3/cm^3). The arithmetic average product shows the worst performance, with the largest bias of -0.058 cm^3/cm^3, a median ubRMSE of 0.058 cm^3/cm^3 and a median R of 0.76. The three merged soil moisture datasets show better performance than the ESA CCI passive in terms of all evaluation metrics. Recall from previous sections, the median bias, median ubRMSD and median R are 0.093 cm^3/cm^3, 0.063 cm^3/cm^3, and 0.75, respectively.

Fig. 5.12 gives the spatial patterns of the three merged soil moisture products. It reveals that the merged products incorporated the characteristics of the original products. In theory, the merged soil moisture products should reduce the random retrieval error associated with remote sensing instruments, algorithms, and other factors. The spatial pattern of each merged soil moisture product shows similar spatial distributions, exhibiting elevated soil moisture levels in the southern mountainous regions and lower soil moisture levels in the northern regions. Some discrepancies are observed between the TC merging approach and the arithmetic average method in the southeast and northeast areas. Notably, the weight assigned to the SMAP L3E product exceeds 0.6 in these areas (see Fig. 5.9). The LSTM merged soil moisture exhibits significant

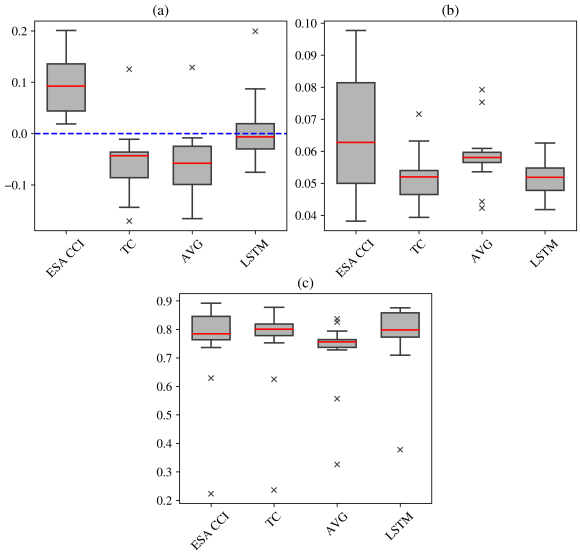

Figure 5.11: Box plots of statistical metrics for comparison between merged soil moisture products at thirteen CRNS stations: (a) Bias; (b) ubRMSD; (c) R.

spatial heterogeneity, as it integrates fine-scale resolution information derived from both static and dynamic parameters.

To have a comprehensive understanding of the performance of different data fusion methods, the soil moisture time series are visually presented in Fig. 5.13. It is found that the TC and arithmetic mean merged products exhibit generally comparable variability, particularly in scenarios characterized by minimal discrepancies between the original products. However, the TC method demonstrates superior performance under low soil moisture conditions compared to the simple averaging method. Nevertheless, the TC-based method should be preferred over the simple arithmetic mean method, as it could yield optimal weighing factors and result in a better merged product. The LSTM merged product agrees well with the temporal dynamics of in-situ measurements, indicating its capability to capture the relationship between remote sensing observation and CRNS soil moisture measurement, considering the influence of penetration depth.

5.5 Discussions

As shown in Fig.5.12 and Fig. 5.13, the LSTM-based merged product exhibits more variability in spatial patterns and a closer alignment with CRNS measurements compared to the TC-based merging dataset. The TC merged dataset exhibits more sensitivity to the extreme events (e.g, wetting and drying conditions) that are subject to similar performance in the parental remote sensing products. This might be attributed to the limited information constrained in the remotely sensed soil moisture penetration depth, which lacks information about the deeper soil. In

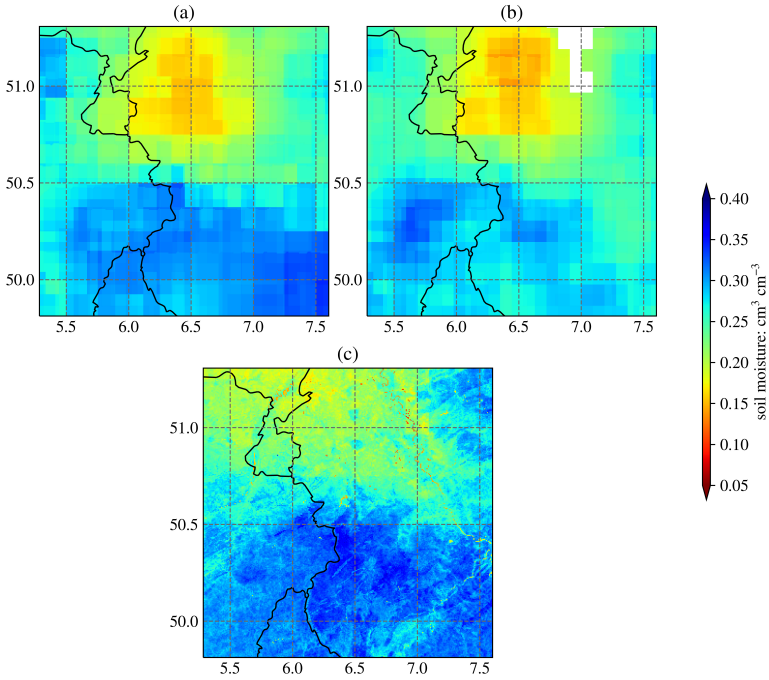

Figure 5.12: Comparison of spatial soil moisture distributions derived from merged datasets. Shown are average soil moisture distributions for the period from January 10, 2018 to December 31, 2018: (a) Arithmetic average method; (b) TC-based method; (c) LSTM scenario.

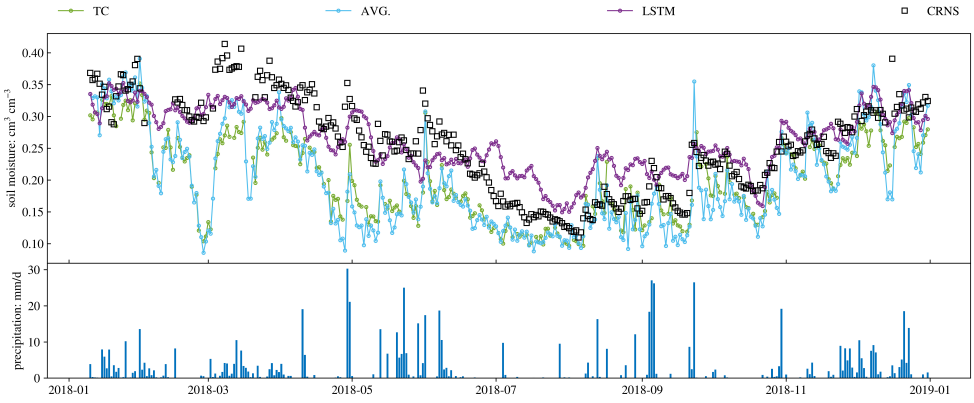

Figure 5.13: Time series of soil moisture in situ observations (black square) and merged soil moisture from TC (green dots), merged soil moisture by arithmetic mean (cyan dots), and merged soil moisture by LSTM (purple dots) over thirteen stations for 10 January 2018 – 31 December 2018. The bottom graph represents the daily time series of precipitation forcing from COSMO-REA6.

contrast, the LSTM is capable of exploiting this temporal information from CRNS during the training process. Additionally, its window size mechanism allows the model to learn long-term dependencies and effectively capture the soil moisture memory.

While complete independence of in situ measurements would be optimal for validation purposes, the acquisition of such data may be constrained by the fact that only thirteen in situ stations are located in the research area. Some validation sites, in particular those with high bulk density or dense vegetation cover, exhibited unique performance characteristics. Therefore, we proposed that the inclusion of training data across a range of conditions could enhance the robustness of the LSTM model. Alternatively, we implemented an evaluation strategy, which involves training the model on data spanning from 2015 to 2017 and evaluating on an entirely independent year (2018), which was characterized by significant dryness. This allows us to assess the generalizability of the model across different conditions.

Our findings demonstrate that LSTM can be an effective approach to merge soil moisture observations from active and passive satellite microwave sensors; however, there are some limitations in the approach. The LSTM model targets in situ data with parameter tuning. In contrast, the TC merging scheme relies solely on error calculations. Thus, the comparison with TC-based merging datasets may not be entirely fair. Despite this, we present our findings to demonstrate the applicability of the LSTM model and encourage further research in this direction. The LSTM model application can be hindered in the areas where the in-situ soil moisture measurements are sparse, such as Africa. A spatial mismatch exists between the LSTM grid and in situ sampling, which increases the uncertainty in the training process. In addition, the LSTM merging scheme generates a higher resolution merged dataset by leveraging information from high-resolution static and dynamic feature datasets, but its effectiveness can be limited in complex landscapes. In addition, there is also a vertical mismatch between the remote sensing products and the CRNS measurement, which could affect the comparability of the merged product with the CRNS soil moisture datasets. Although the CNRS shows advantages for the validation of the near-surface soil moisture products (Fersch et al. 2018; Howells et al. 2021; Montzka et al. 2017), the higher penetration depth of the CRNS should be considered (Bayat et al. 2020; Montzka et al. 2017).

Previous studies (Yilmaz et al. 2012) have demonstrated that the TC merging scheme does not always produce a superior product to the simple arithmetic mean method. Peng et al. (2021) have confirmed this finding and demonstrated that TC-based approaches provide better results when the parent products exhibit large differences. The results obtained in this study align with those studies and show that the TC merged product exhibits superior performance in terms of smaller bias, lower ubRMSE, and higher Pearson r when compared to the arithmetic mean soil moisture product. The TC merging scheme could be further improved to optimally retain both spatial and temporal information by taking into account the spatial and temporal non-stationary errors (Zhou et al. 2021). This would facilitate a more accurate comparison with other machine learning merging methodologies.

Future research can enhance the predictive capacity of the model and evaluate its performance in areas that are not included in the training, which could be done by increasing the training data

or using transfer learning techniques. Moreover, related physical constraints can be introduced into the LSTM model to guide the training process. Studies (Singh et al. 2023; Wang et al. 2023) have shown that the performance of physics-informed machine learning can be significantly improved in scenarios traditionally challenging for traditional machine learning methods, such as sparse datasets and extreme values.

5.6 Conclusions

The acquisition of high-quality soil moisture data at high spatial and temporal resolution is of importance for hydrological and meteorological applications. In this study, we select a region in western Europe exhibiting very heterogeneous land use and topographical variations. In the research area, multiple sources of soil moisture products are accessible, from either satellite retrievals (e.g., SMAP L3E, AMSR2 and ASCAT) or field measurements by Cosmic Ray Neutron Sensors (CRNS). We train a Long Short-Term Memory (LSTM) model with retrievals and a limited number of in-situ measurements. Subsequently, we employ the pre-trained LSTM model to make predictions in research areas where in-situ measurements are not attainable. Our investigation includes the assessment of various parameter configurations within the LSTM model. A TC-based merging scheme and the arithmetic mean method are also employed to merge the different satellite soil moisture products and generate a merged soil moisture product.

Results for the different scenarios of the LSTM model illustrate the importance of incorporating both static and dynamic data in the soil moisture merging scheme at finer spatial resolution. Static data like soil texture information influences the spatial soil moisture variation not only by the high-resolution information, but also by its role in the soil drying process over time. Accurate static information at high spatial resolution exerts an important influence on enhancing the correlation between the merged soil moisture dataset and in situ measurements.

The LSTM and TC merged soil moisture datasets exhibit the ability to effectively integrate soil moisture information derived from diverse remote sensing products. They demonstrate comparable performance in terms of ubRMSE and R when compared to in-situ measurements, better than a soil moisture dataset based on the simple arithmetic mean of the different remote sensing products. Notably, the LSTM approach demonstrates reduced bias and superior handling of spatial and temporal variations than the TC merged dataset, owing to its intricate weighting calculations by incorporating information from both static and dynamic parameters at a finer resolution. This demonstrates the potential of LSTM as a robust tool for soil moisture prediction, characterization, and scaling.

6

Fusion of multiple microwave soil moisture products for data assimilation in land surface models

*adapted from: Zhao, H., Montzka, & Franssen, H. J. H. (2024). Fusion of multiple microwave soil moisture products for data assimilation in land surface models, in preparation.

6.1 Introduction

Soil moisture plays an important role in the water and energy cycles at the catchment, regional, and global scale, by controlling the division of net radiation into sensible and latent heat fluxes (Entekhabi et al. 1996; Seneviratne et al. 2010). Additionally, it controls the distribution of precipitation between surface runoff and subsurface infiltration (Eltahir 1998; Liu et al. 2011a) and has a significant influence on the carbon cycle (Falloon et al. 2011; Green et al. 2019).

Satellite-based soil moisture monitoring has become an effective method for obtaining regional-to-global soil moisture estimates with a temporal resolution of 1 to 2 days (Babaeian et al. 2019). The microwave instruments are well-suited for soil moisture estimation due to their high sensitivity to the dielectric properties of soil (Dobson et al. 1986; Schmugge et al. 1986). The Soil Moisture and Ocean Salinity (SMOS) mission (Kerr et al. 2010) and the Soil Moisture Active Passive (SMAP) mission (Entekhabi et al. 2010a) were launched specifically to monitor soil moisture. These missions operate at L-band (1.4 GHz), which is very sensitive to soil moisture and less affected by vegetation and atmospheric conditions (Wang et al. 1981). Prior to these missions, soil moisture products have been retrieved from other microwave sensors that were designed for multiple purposes and operational applications. The passive microwave Advanced Microwave Scanning Radiometer (AMSR-E) was launched in 2002 and operated at 6.7 GHz, 10.7 GHz, and 18.9 GHz to provide information on soil moisture, sea surface temperature, sea ice concentration, and other variables (Njoku et al. 2003). The Advanced Microwave Scanning Radiometer 2 (AMSR2) is a successor to the AMSR-E, providing continuity of soil moisture data (Imaoka et al. 2010; Imaoka et al. 2012). Another widely used mission is the Advanced Scatterometer (ASCAT), operated at C-band (5.3 GHz), providing wind over water surfaces and soil moisture observations (Wagner et al. 2013).

In previous studies, soil moisture from different microwave instruments on separate platforms has already been successfully merged based on different data fusion methods. For example, Liu et al. (2011b) proposed a cumulative distribution function (CDF) matching approach to rescale the AMSR2 and ASCAT soil moisture values against a reference land surface model dataset. Based on this, Liu et al. (2012) further blended the soil moisture products from four different microwave products. Follow-up research explored the development of new data fusion schemes for merging soil moisture data, based on both traditional mathematical methods and more advanced neural network (NN) techniques. Gruber et al. (2017) found that combining soil moisture datasets using triple collocation (TC) analysis outperformed each individual product in almost all cases. Kolassa et al. (2017a) used the NN retrieval algorithm to merge the ASCAT and AMSR-E and found that the merging yielded a more accurate soil moisture prediction product. These results were in line with other similar findings (Kim et al. 2020; Mousa et al. 2020b; Xie et al. 2022), demonstrating the motivation for the development of improved soil moisture datasets by blending satellite-based retrievals from multiple frequencies and multiple sensors.

Soil moisture from various satellite missions can also be combined with land surface models (LSMs) through data assimilation. By merging additional information, the LSMs can have a better prediction of soil moisture as well as other hydrological variables at a finer spatial and temporal scale (Houser et al. 1998). Some studies have investigated the benefits of assimilating blended soil moisture datasets. Gevaert et al. (2018) found that joint assimilation of L- and C-band retrievals outperformed individual assimilation of C-band retrievals in the Australian Landscape Water Balance model (AWRA-L) (Wallace et al. 2013). Nair et al. (2019) assimilated the soil moisture products from AMSR2 and ASCAT missions and showed that merging the blended products has more advantages at capturing the dynamics of soil moisture over large areas at daily temporal resolutions. Similar results were also found by Draper et al. (2012) and Kolassa et al. (2017b). The integration of different microwave sensor data is anticipated to lead to a higher benefit of data assimilation, but the extent of this benefit and the influence of merging techniques remain to be demonstrated.

In this study, we assimilate soil moisture retrievals from three different missions, namely SMAP, AMSR2, and ASCAT and their merged datasets in the Community Land Model (CLM, version 3.5) using an Ensemble Kalman Filter (EnKF). The assimilation experiments build on the work of Zhao et al. (2024) to investigate different data fusion strategies for merging active and passive remotely sensed soil moisture information in data assimilation. We compare 1) the assimilation of the separate soil moisture products and 2) the assimilation of merged soil moisture products from Zhao et al. (2024). The merging schemes include the commonly used arithmetic mean method and the Triple Collocation (TC) based method, as well as a novel Long-Short Term Memory (LSTM) algorithm. We aim to investigate whether combining information from different missions leads to added value in data assimilation skills. Additionally, we investigate the differences between the merging strategies in terms of their performance in data assimilation experiments and evaluate whether the benefit of assimilation depends on the quality of merged products.

6.2 Materials and Methods

6.2.1 Data

6.2.1 (a) Remote sensing soil moisture products

This study uses soil moisture products from three space-borne sensors: passive microwave products from Soil Moisture Active Passive (SMAP) at L-band, Advanced Microwave Scanning Radiometer 2 (AMSR2) at C-band, and an active microwave product from Advanced Scatterometer (ASCAT) at C-band. The three different soil moisture products have different spatial resolutions and penetration depths (Brocca et al. 2017; Entekhabi et al. 2010a; Njoku et al. 2003; Ulaby et al. 1982). The SMAP SPL3SMP_E product boasts a superior spatial resolution of 9 km, whereas the AMSR2 GCOM-W1 L3 and ASCAT H119 products exhibit a coarser resolution of 25 km. The quality control procedures are performed before data assimilation by excluding soil moisture data where snow cover, frozen soil, and dense vegetation are found. Daily composite retrievals are generated by averaging observations from both descending and ascending overpasses and then resampled to a 500 m $\times$ 500 m grid using the Nearest Neighbour approach.

6.2.1 (b) Merged soil moisture products

Merged soil moisture products are calculated using three different strategies, referred to as (1) Avg (Average), (2) TC (Triple Collocation), and (3) LSTM (Long Short-Term Memory), respectively. The Avg method employs a simple arithmetic mean of the three parental soil moisture products. The merged soil moisture $\mathrm{SM_{avg}}$ is obtained as:

$$\mathrm{SM_{avg}} = 1/3 \cdot \mathrm{SM_{SMAP}} + 1/3 \cdot \mathrm{SM_{AMSR2}} + 1/3 \cdot \mathrm{SM_{ASCAT}} \tag{6.1}$$

The TC method employs TC analysis, giving weights to each soil moisture product as functions of their error covariances. This analysis is based on the principle that the error structures of the three datasets are independent. The merged product $\mathrm{SM_{TC}}$ can be calculated as:

$$\mathrm{SM_{TC}} = w_1 \cdot \mathrm{SM_{SMAP}} + w_2 \cdot \mathrm{SM_{AMSR2}} + w_3 \cdot \mathrm{SM_{ASCAT}} \tag{6.2}$$

where the w_1, w_2 and w_3 are the relative weights for SMAP, AMSR2 and ASCAT retrievals. One dataset is selected as the reference, and its weight is proportional to the uncertainty of the other two datasets and can be written as:

$$w_1 = \frac{\sigma_2^2 \sigma_3^2}{\sigma_1^2 \sigma_2^2 + \sigma_1^2 \sigma_3^2 + \sigma_2^2 \sigma_3^2} \tag{6.3}$$

$$w_1 = \frac{\sigma_1^2 \sigma_3^2}{\sigma_1^2 \sigma_2^2 + \sigma_1^2 \sigma_3^2 + \sigma_2^2 \sigma_3^2} \tag{6.4}$$

$$w_1 = \frac{\sigma_1^2 \sigma_2^2}{\sigma_1^2 \sigma_2^2 + \sigma_1^2 \sigma_3^2 + \sigma_2^2 \sigma_3^2} \tag{6.5}$$

where the σ_1^2, σ_2^2 and σ_3^2 represent error variances for SMAP, AMSR2 and ASCAT data.

The LSTM approach is trained using the three remotely sensed soil moisture products as input and in-situ observations as the target. Following training with years of data from 2015 to 2017, the estimated soil moisture values are generated for an independent period spanning from 10 January 2018 to 31 December 2018 with a spatial resolution of 500 m × 500 m. The merging process can be expressed as:

$$\mathrm{SM_{LSTM}} = \mathbf{LSTM}(\mathrm{SM_{SMAP}}, \mathrm{SM_{AMSR2}}, \mathrm{SM_{ASCAT}}, \mathrm{F_{static}}, \mathrm{F_{dynamic}}) \tag{6.6}$$

where the $\mathrm{F_{static}}$ and $\mathrm{F_{dynamic}}$ denote static and dynamic features, respectively. The static features include soil texture information and altitude from the Digital Elevation Model (DEM). Dynamic features include the temporal meteorological forcing from the COSMO-REA6 reanalysis product (Bollmeyer et al. 2015) and Leaf Area Index (LAI) from Moderate Resolution Imaging Spectroradiometer (MODIS). For more information regarding the merging scheme, the reader is referred to Zhao et al. (2024).

6.2.1 (c) In situ soil moisture measurements

The in situ soil moisture data are obtained from the TERENO observation network Bogena 2016. There are thirteen CRNS stations in the research area (see Figure. 6.1), measuring the soil moisture with a radial footprint of 150 $\sim$ 240 m size (Köhli et al. 2015; Zreda et al. 2012). The penetration depth of CRNS is inversely proportional to soil moisture content and can be expressed in terms of Franz et al. 2012a:

$$z^* = \frac{5.8}{\theta + 0.0829} \tag{6.7}$$

where θ represents the total soil water content. Data are provided as hourly measurements and aggregated to daily mean soil moisture. The original data processing methods and comprehensive information regarding the thirteen stations are accessible through previous publications (Bogena et al. 2022).

6.2.2 Model and data assimilation system

6.2.2 (a) The Community Land Model (CLM)

The Community Land Model (CLM) is a land surface model that simulates the exchange of energy, water, and carbon between the land surface and the atmosphere (Oleson et al. 2008). CLM represents the land surface as a collection of sub-grid cells that do not interact with each other. Each sub-grid cell has its own set of parameters that represent the biophysical properties

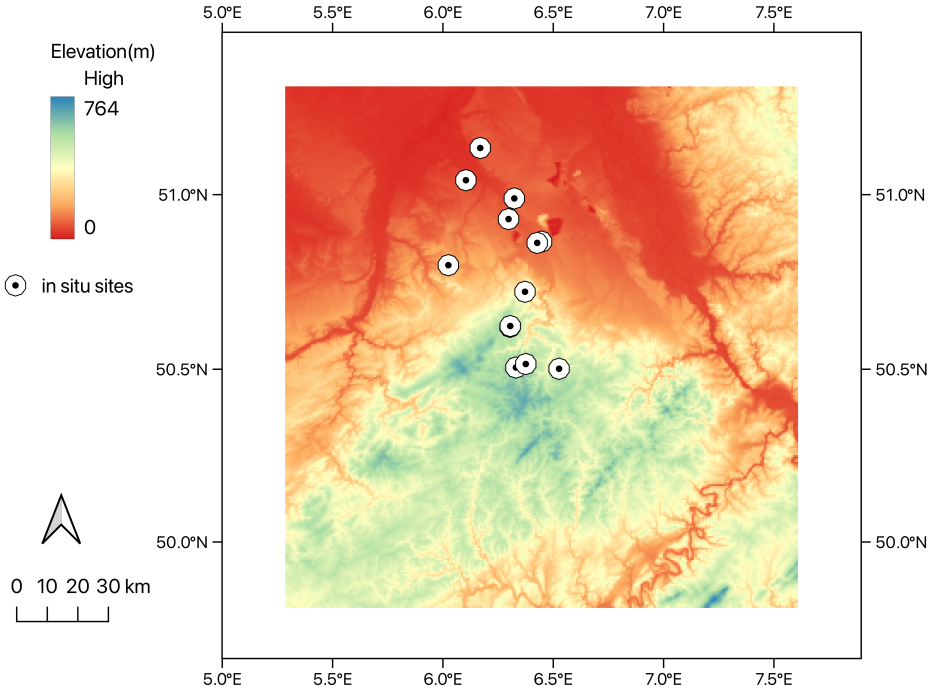

Figure 6.1: Overview of the research area in North Rhine-Westphalia, Germany, with elevation and the location of thirteen CRNS stations.

of the land surface, such as vegetation type, soil texture, and topography (Dai et al. 2003). CLM simulates land surface processes, such as evapotranspiration, water infiltration, photosynthesis, and respiration. The fluxes are calculated using the Monin-Obukhov similarity theory (Oleson et al. 2004). The simulation of soil water flow is carried out using a simplified Richards equation (Oleson et al. 2004).

The CLM soil profile is discretised into 15 layers, with hydrological states and fluxes calculated for the top 10 layers (Oleson et al. 2010). The soil hydraulic parameters are calculated from sand and clay fractions based on the Clapp-Hornberger pedo-transfer (Clapp et al. 1978) function together with the Brooks-Corey parameterization (Milly 1987). It is noteworthy that each grid cell is simulated independently, implying that lateral water exchange between neighbouring cells is not considered.

6.2.2 (b) Data assimilation

Data assimilation is done with the classic Ensemble Kalman Filter (EnKF), a well-established technique that distributes observed information to nearby model grid cells based on correlations

Table 6.1: Summary of performance metrics in the LSTM model training period (2015 to 2017)

Variables	Noise	Standard deviation	Cross correlation			
			P	SW	LW	T
P	multiplicative	0.15	1.0	-0.8	0.5	0.0
SW	multiplicative	0.15	-0.8	1.0	-0.5	0.4
LW	additive	30 W m-2	0.5	-0.5	1.0	0.4
T	additive	1.5 K	0.0	0.4	0.4	1.0

between the observed grid cells and neighbouring grid cells (Reichle et al. 2003). The EnKF has been extensively applied in the assimilation of remote sensing soil moisture data into land surface models (Blyverket et al. 2019; Huang et al. 2016, 2008; Patil et al. 2018; Reichle et al. 2002; Tian et al. 2022). It consists of a forecast and an analysis step. In the forecast step, an ensemble of model predictions is simulated by perturbing the model inputs, e.g., soil texture and meteorological forcing data. The ensemble represents the uncertainty in the model states. In the analysis step, the EnKF updates the model states using observations based on the magnitudes of the model error variance and the measurement error variance. The updated states for the analysis step at time t are calculated as:

$$\mathbf{x}_t^a = \mathbf{x}_t^f + \mathbf{K}(\mathbf{y}_t - \mathbf{H}_t\mathbf{x}_t^f) \tag{6.8}$$

where $\mathbf{x}_t^a$ is the model analysis, $\mathbf{x}_t^f$ is the model forecast, $\mathbf{H}_t$ is the operator that relates the model output to the measurements, and t indicates the time step. The Kalman Gain $\mathbf{K}$ is given by:

$$\mathbf{K} = \mathbf{C}\mathbf{H}^{\mathrm{T}}\left(\mathbf{H}\mathbf{C}\mathbf{H}^{\mathrm{T}} + \mathbf{R}\right)^{-1} \tag{6.9}$$

where $\mathbf{C}$ is the model error covariance matrix and $\mathbf{R}$ represents the observation error matrix.

6.2.3 Numerical experiments

In this study, the modelling domain is composed of 300 × 300 grid cells with a spatial resolution of 500 m × 500 m. The simulation period is from 10 January 2018 to 31 December 2018. The years 2015 to 2017 are used to spin up the CLM model to obtain equilibrium initial state variables. We have a total of N=32 ensemble members. To address uncertainties in atmospheric forcing and soil characteristics, both soil texture (%sand and %clay) and meteorological variables are perturbed in the CLM model. The sand and clay content are perturbed with random noise sampled from a spatially uniform distribution within a range of ± 20 %. To prevent unrealistic values of the soil parameters, the sum of the sand and clay content is constrained to be less than 100 %. Spatially homogeneous and temporally uncorrelated normally distributed perturbations are added to four atmospheric variables, including precipitation, incoming short-wave radiation, incoming long-wave radiation, and air temperature, based on previous work (Han et al. 2013; Reichle et al. 2010). Table 6.1 summarises the correlation and standard deviations of the perturbed atmospheric variables.

The model time step is 1 hour, and the temporal interval for assimilating soil moisture information is set to 1 day. Considering the computational efficiency, we select the observations with a step size of 10, meaning that the number of observations is reduced from 300 × 300 to 30 × 30. In the DA process, the state vector consists of soil moisture across all soil layers, with a size of $N_x = N_g \times n_{\text{levsoi}}$, where N_g is the number of grid cells and n_{levsoi} is the number of soil layers. The second soil layer, which most closely corresponds to the effective penetration depth of the remote sensing products, is directly constrained by the assimilated observations. The remaining soil layers are updated indirectly through the ensemble-estimated cross-layer error covariance within the EnKF framework. Montzka et al. (2017) compared remote sensing products with in situ measurements in the same region and found that the unbiased root mean square error (ubRMSE) for SMAP, AMSR2, and ASCAT were 0.050, 0.087, and 0.060 cm^3/cm^3, respectively. Zhao et al. (2024) demonstrated the effectiveness of merged soil moisture datasets from Avg, TC and LSTM schemes, which are 0.058, 0.052, and 0.052 cm^3/cm^3, respectively. These values were used as the observation error in the assimilation experiments.

The simulated soil moisture from LSMs and the remotely sensed soil moisture products often exhibit different climatologies, leading to systematic biases between model and observations. A bias correction step can be applied to ensure consistency with the unbiased error assumption of ensemble-based methods. Typical approaches include the removal of seasonal bias or cumulative distribution function (CDF) matching (Reichle et al. 2004). Here, no explicit bias correction is applied. This choice is motivated by the fact that bias correction may alter the spatial patterns of the observations and potentially remove independent information contained in the observation datasets.

The data assimilation experiments conducted in this study are organised according to three scenarios: (a) an open-loop simulation (CLM-OL, no data assimilation); (b) univariate assimilation of the different soil moisture remote sensing datasets (CLM-SMAP, CLM-AMSR2 and CLM-ASCAT); (c) assimilation of merged soil moisture datasets (CLM-Avg, CLM-TC, and CLM-LSTM). Based on the experiments, we can evaluate the benefit of merged assimilation with respect to assimilating each soil retrieval separately.

6.2.4 Evaluation metrics

Model performance is evaluated by comparing simulated soil moisture against CRNS measurements. The simulated soil moisture for the top 5 cm and for the layers corresponding to the CRNS penetration depth are estimated by linearly combining simulated outputs for different model layers. The Pearson correlation coefficient r and unbiased root mean square error ubRMSE are employed to assess the agreement between the ensemble mean of simulated soil moisture $\theta_{t,model}$ and daily averages of in situ data $\theta_{t,crns}$ during the assimilation period.

$$r = \frac{\sum_{t=1}^{T}\left(\theta_{t,model} - \bar{\theta}_{model}\right)\left(\theta_{t,crns} - \bar{\theta}_{crns}\right)}{\sqrt{\sum_{t=1}^{T}\left(\theta_{t,model} - \bar{\theta}_{model}\right)^2}\sqrt{\sum_{t=1}^{T}\left(\theta_{t,crns} - \bar{\theta}_{crns}\right)^2}} \tag{6.10}$$

Table 6.2: An overview of the evaluation metrics for open loop (CLM-OL) and assimilation experiments (CLM-SMAP, CLM-AMSR2, and CLM-ASCAT)

Station	CLM-OL		CLM-SMAP		CLM-AMSR2		CLM-ASCAT	
	r	ubRMSD	r	ubRMSD	r	ubRMSD	r	ubRMSD
Merzenhausen	0.70	0.065	0.88	0.037	0.70	0.058	0.87	0.040
Aachen	0.84	0.062	0.81	0.049	0.76	0.053	0.79	0.051
Selhausen	0.65	0.077	0.78	0.057	0.61	0.070	0.76	0.057
Heinsberg	0.81	0.058	0.90	0.034	0.55	0.069	0.85	0.043
Wuestebach	0.23	0.060	0.25	0.075	0.36	0.070	0.35	0.077
Gevenich	0.68	0.072	0.79	0.052	0.82	0.049	0.87	0.042
Rollesbroich1	0.75	0.064	0.78	0.050	0.86	0.041	0.80	0.050
Rollesbroich2	0.69	0.078	0.77	0.060	0.85	0.051	0.79	0.057
Ruraue	0.73	0.075	0.81	0.053	0.80	0.054	0.81	0.052
Wildenrath	0.73	0.043	0.79	0.042	0.56	0.051	0.65	0.051
Kall	0.71	0.065	0.85	0.041	0.87	0.038	0.85	0.041
Schoeneseiffen	0.80	0.068	0.83	0.048	0.86	0.045	0.89	0.038
Kleinau	0.77	0.074	0.85	0.052	0.84	0.052	0.85	0.047

$$ubRMSE = \sqrt{\frac{\sum_{t=1}^{T}\left(\left(\theta_{t,model} - \bar{\theta_{model}}\right) - \left(\theta_{t,crns} - \bar{\theta_{crns}}\right)\right)^2}{T}} \tag{6.11}$$

A sample size of T = 356 was obtained for each site based on daily observations during the 356-day study period (10 January 2018 to 31 December 2018). In addition to evaluating the skills of different data assimilation experiments, a normalized error reduction index (NER) is also calculated:

$$\mathrm{NER}_{\%} = 100 \times \left(1 - \frac{E_{\mathrm{DA}}}{E_{\mathrm{OL}}}\right) \tag{6.12}$$

where the E_{DA} and E_{OL} represent the data assimilation and open-loop runs. The E represents ubRMSE in this study. NER values between 0 and 1 indicate that the DA has improved the model's performance to some extent, while negative NER indicates a degradation in assimilation.

6.3 Results

This section begins by comparing the performance of assimilating individual remote sensing soil moisture products to in situ measured data, using the CLM-OL performance as a reference. Following this, the assimilation skills of the different merged soil moisture datasets are analysed.

6.3.1 Assimilating single soil moisture products

First, the performance of CLM-OL is assessed by comparing its simulated soil moisture to in situ measurements. The correlation coefficients and ubRMSE are computed for CLM-OL at each site (see Table 6.2). In general, the CLM-OL exhibits a good correlation with the observations, with

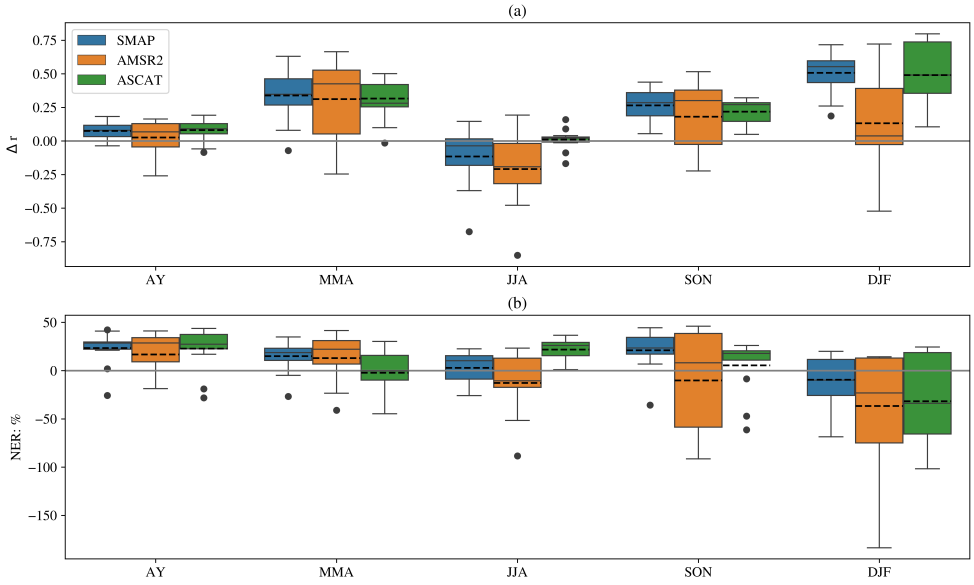

Figure 6.2: The change in correlation (Δ r and NER between simulated soil moisture and in situ measurements for the period (2018.01.10 to 2018.12.31), where Δ r and NER are calculated over the research period (AY), and spring (MAM), summer (JJA), autumn (SON) and winter periods (DJF).)

r values ranging from 0.65 to 0.80. However, the Wüstebach site shows low correlation (r = 0.23) compared to the other sites. The large discrepancy in simulated soil moisture at the Wüstebach site is primarily attributed to the low porosity in CLM, compared to the true porosity at the site. The porosity is underestimated as the pedotransfer functions in CLM3.5 do not take organic matter content into account for calculating porosity. The ubRMSE for CLM-OL varies across sites, and ranges from 0.043 to 0.077 cm^3/cm^3.

The skill of assimilating retrievals compared to CLM-OL is also compared in Figure. 6.2. The assimilation generally enhances the agreement between modelled soil moisture and CRNS measurements. The correlation coefficient r increased up to 0.19 compared to the CLM-OL scenario. The assimilation of SMAP soil moisture and ASCAT soil moisture both have a significant impact, with a median correlation improvement Δ r of 0.08 and median NER of 28.5 % for SMAP and median Δ r = 0.09 and median NER = 27.3 % for ASCAT. This is followed by the assimilation of AMSR2 soil moisture (median Δ r = 0.07 and median NER = 28.7 %). The performance of data assimilation varies across different sites (see Table 2). Assimilation of SMAP yields the most significant improvement in r at 5 out of 13 sites, and the lowest at 5 out of 13 sites. Assimilating remotely sensed soil moisture from ASCAT or AMSR2 gives the largest improvement in soil moisture characterization for 4 out of 13 sites.

To investigate the influence of seasonality on the effectiveness of soil moisture assimilation, the assimilation period is divided into four seasons, namely MAM (March-April-May), JJA (June-July-August), SON (September-October-November), and DJF (December-January-February).

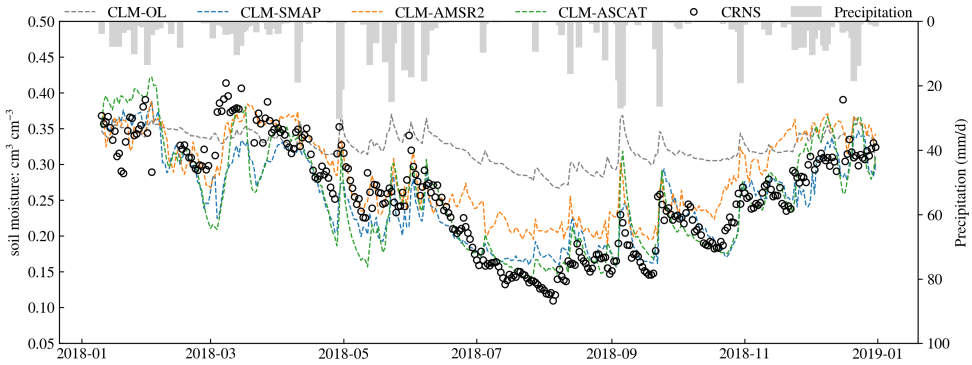

Figure 6.3: Time series of the daily soil moisture derived from model open loop and assimilation experiments and in situ measurements. The corresponding daily precipitation rate from forcing data is also presented.

The assimilation of soil moisture data from SMAP and ASCAT improves the Pearson r most significantly during the winter period (DJF). In contrast, the assimilation of AMSR2 soil moisture data primarily enhances r during the transitional periods (MAM and SON). A slight decrease in r is observed for all three experiments during the summer season (JJA). The ubRMSE analysis shows that assimilation significantly enhances soil moisture estimation primarily during transitional periods across all scenarios, while modest improvements are observed in summer, and no advancements are evident during the winter season.

The time series of modelled soil moisture averaged over thirteen sites are also shown in Figure. 6.3. The soil moisture simulated by CLM-OL replicates the temporal patterns of precipitation but does not correctly capture the temporal fluctuations observed by the in situ measurements. The CLM-OL scenario consistently overestimates soil moisture throughout the year. Data assimilation effectively corrects this bias, resulting in soil moisture estimates that are close to in situ observations. The improvement is most pronounced in the summer seasons (JJA). During winter, the CLM-OL more closely matches the in situ measurements, suggesting limited room for improvement. The assimilation of SMAP data results in a good agreement between the simulated temporal variation of soil moisture and in situ observations, and captures the variation in both the shape and magnitude of soil moisture fluctuations. The CLM-ASCAT scenario is more sensitive to dry down and precipitation events due to ASCAT's sensitivity to changes in soil moisture. This is because ASCAT has a shallower penetration depth, ranging from 0.5 to 2.0 cm in the topsoil (Seo et al. 2021).

Figure. 6.4 shows the spatial pattern of average soil moisture for the upper soil layer (5 cm) for different data assimilation experiments. Spatial soil moisture patterns for the open loop and three DA experiments show higher soil moisture in the southern region and lower soil moisture in the northern region, as southern areas typically experience higher precipitation compared to northern regions. However, large discrepancies are observed in the north-western corner, where soil texture is characterized by a high sand content. The CLM-OL simulation generally produces

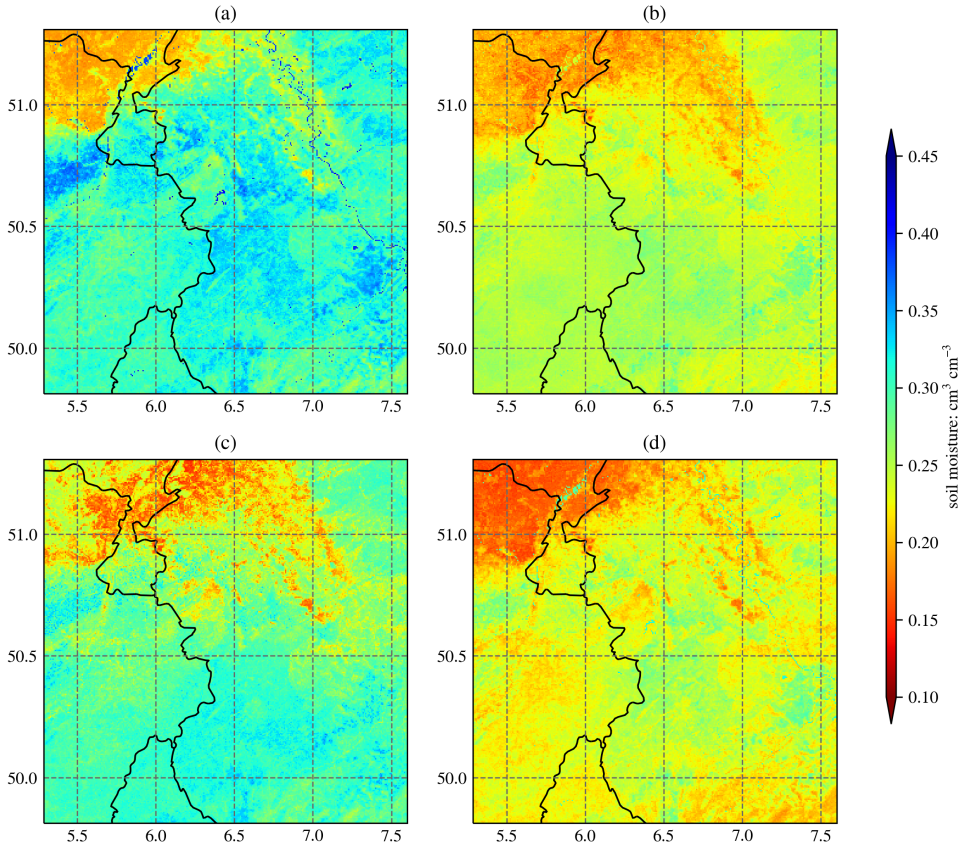

Figure 6.4: Spatial distribution of soil moisture (5 cm) from (a) CLM-OL, (b) CLM-SMAP, (c) CLM-AMSR2, (d) CLM-ASCAT for the period 2018.01.10-2018.12.31.

slightly higher soil moisture estimates compared to other scenarios over most parts of the research area. The assimilation of ASCAT soil moisture exhibits more spatial variability.

The number of available observations differs strongly across the remotely sensed soil moisture products. The SMAP dataset provides 11 to 457 observations per day for 354 days, the AMSR2 dataset provides 50 to 70 observations per day for 343 days, and the ASCAT dataset provides 144 observations per day for 356 days. The coverage of different soil moisture datasets has an impact on the data assimilation results.

6.3.2 Evaluation of the added value of merged dataset assimilation

The assimilation of the merged soil moisture products CLM-Avg and CLM-TC gives similar results, in terms of median improvements of r 0.09 and 0.08, and median ubRMSE reduction of 31.34% and 28.80%, respectively. However, the assimilation of CLM-LSTM shows less improvement (median improvement of r = 0.04, and median NER = 19.64%). The performance of different

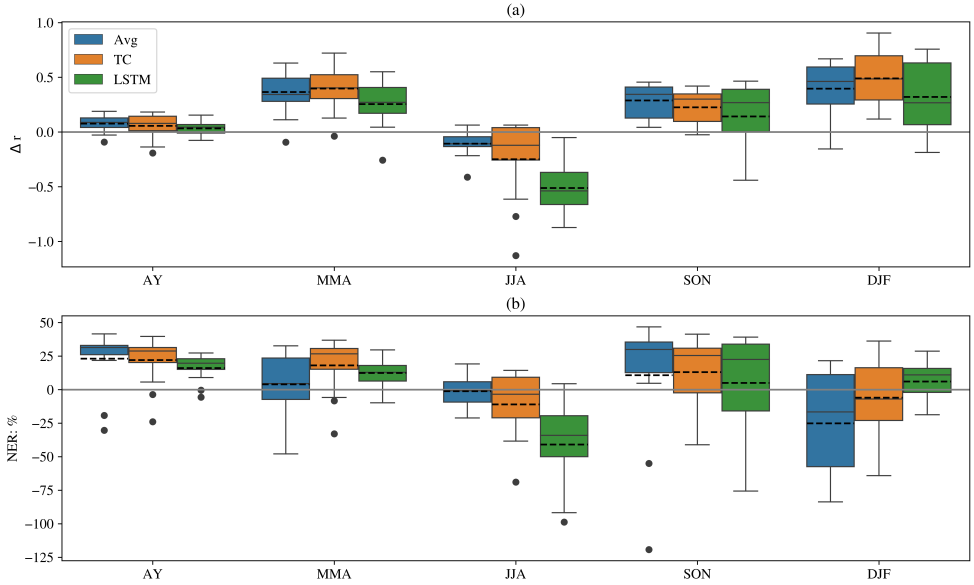

Figure 6.5: The change in correlation (Δ r and NER between simulated soil moisture and in situ measurements for the period (2018.01.10 to 2018.12.31), where Δ r and NER are calculated over the research period (AY), and spring (MAM), summer (JJA), autumn (SON) and winter periods (DJF).

assimilation scenarios varies across sites and time periods (see Figure. 6.5). The assimilation of merged soil moisture datasets demonstrates the most significant improvement in the Pearson correlation coefficient (r) during the winter period (DJF), followed by the transitional periods (MAM and SON). A pronounced reduction in ubRMSE is observed during transitional periods (MAM and SON), aligning with the assimilation of SMAP and ASCAT data. Notably, the assimilation of LSTM merged datasets exhibits superior performance in reducing ubRMSE during the winter season.

To evaluate the potential benefit of the assimilation of merged soil moisture products, the assimilation of merged datasets is compared with assimilating individual soil moisture products. The result (Figure. 6.6) indicates that the joint assimilation is superior to assimilating retrievals from AMSR2 individually. On average, the assimilation scenarios for CLM-Avg, CLM-TC and CLM-LSTM improve the Pearson r by 0.05, 0.03 and 0.01, respectively, compared to AMSR2. However, it shows only slight improvement or no improvement compared to assimilating soil moisture products from SMAP or ASCAT alone. In comparison to assimilating the SMAP product, assimilating the merged datasets resulted in no change in r for CLM-Avg and a slight decrease in r of 0.02 and 0.04 for CLM-TC and CLM-LSTM, respectively. Similarly, compared to using the ASCAT product, assimilating the merged datasets resulted in no change in r for CLM-Avg and a slight decrease in r of 0.02 and 0.05 for CLM-TC and CLM-LSTM, respectively.

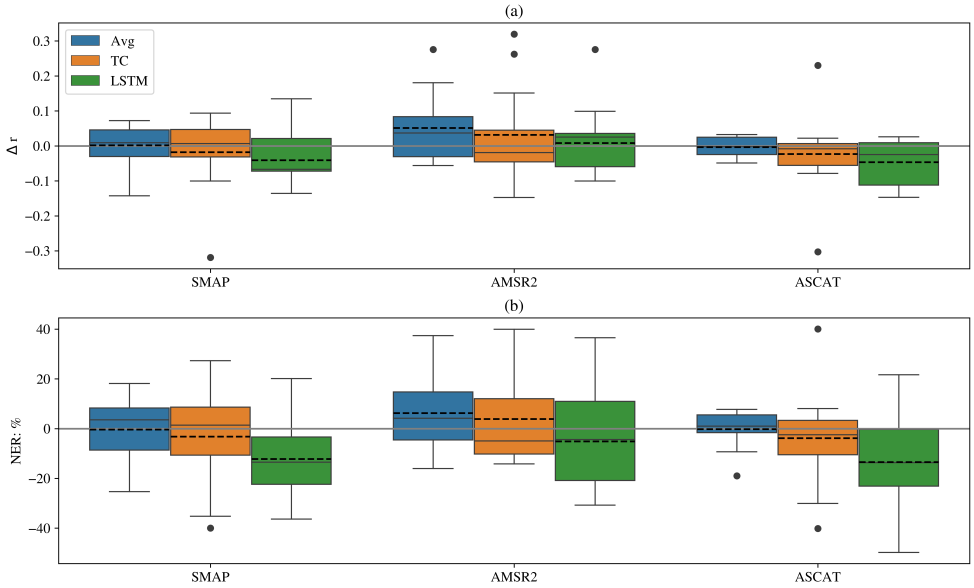

Figure 6.6: The difference in correlation (Δ r and NER between assimilating merged datasets and assimilating single retrieval for the period (2018.01.10 to 2018.12.31).

6.4 Discussions

Previous studies have shown that the SMAP soil moisture products perform best when evaluated with in situ measurements. As expected, the assimilation of datasets with higher accuracy generally provides more information. Here, we show that assimilation of the SMAP dataset leads to the most improved estimates, compared to ASCAT and AMSR2. Interestingly, the assimilation of ASCAT soil moisture products also gives a comparable performance to the assimilation of SMAP retrievals. This can be attributed to the different settings of the observation errors, which affect the Kalman gain in the assimilation process. The comparable performances for assimilating different products also indicate the potential for substitution within data assimilation systems with minimal impact on model performance. This finding holds significance for long-term land surface modelling applications where transitions are needed between different microwave sensors.

The assimilation of merged soil moisture datasets usually has similar performance to assimilating individual retrievals like SMAP and ASCAT, but improves the model performance compared to assimilating individual, less accurate products like AMSR2. The assimilation of merged datasets from Avg. and TC gives similar performance and better than LSTM. This may be related to the fact that the LSTM merged datasets were only trained with a limited number of stations, introducing uncertainties in other areas. The merged products appear to leverage the useful information from retrievals. In line with previous studies (Draper et al. 2012; Gevaert et al. 2018; Kolassa et al. 2017a), our results support that joint assimilation of active and passive microwave soil moisture products can achieve similar model performance when compared to assimilation of

individual products. Kolassa et al. (2017a) found that the skill of assimilation experiments is not only related to the skill of the assimilated products but also related to observation errors specified in the assimilation process.

In this study, the observation errors are set to be spatially and temporally uniform for each soil moisture product, which could lead to unrealistic spatial patterns in the observation error and have an influence on the assimilation results. Given the significant influence of topography and dense vegetation on satellite retrievals, their weighting in mountainous regions should be reduced. A refined approach to observation error specification could enhance the identification of reliable information and improve remotely sensed soil moisture assimilation.

It is important to note that the data assimilation period is restricted to the year 2018, a very dry year. Long-term soil moisture assimilation experiments would likely yield different assimilation results. For example, for an average year, the LSTM would probably perform better than for the very dry year 2018, as the training period did not include a very dry year. The other merged soil moisture products (from average and TC-based merging schemes) are probably less impacted by the specific conditions during the year. The present study evaluates soil moisture estimations at only 13 stations. This limited number of sites is insufficient for capturing the large variability in soil, land cover types, and slope patterns. With the availability of satellite and in situ data, the data assimilation strategy employed in this study could be extended to the EURO-CORDEX domain to acquire accurate soil moisture over the continental scale.

6.5 Conclusions

In this study, the land surface model Community Land Model (CLM) version 3.5, coupled to the Parallel Data Assimilation Framework (PDAF), CLM-PDAF, was used to assimilate soil moisture retrievals from active (ASCAT) and passive (SMAP and AMSR2) microwave sensors and their merged datasets for an area in Western Germany for the very dry year 2018. The retrievals, as well as merged datasets, were subject to quality control and remapped to the same spatial resolution. The merging schemes included arithmetic averaging, triple collocation, and the machine learning method LSTM (Long Short-Term Memory). The different open-loop and data assimilation scenarios were evaluated against in situ soil moisture measurements by CRNS stations.

Data assimilation enhances the accuracy of soil moisture simulations, leading to an improvement of the Pearson correlation coefficient r evaluated on the basis of a comparison with in situ observations (Δ r ranging from 0.04 to 0.19) and a reduction of the ubRMSE between 2% and 42% depending on the assimilated datasets, and always compared to open loop simulations. The assimilation is more informative during transitional periods (spring and autumn). Overall, the soil moisture from SMAP shows the best agreement with in situ observations; this is consistent with previous studies (Gevaert et al. 2018; Seo et al. 2021).

The assimilation of merged soil moisture products (by arithmetic averaging and triple collocation) shows similar performance as the assimilation of single soil moisture products. It improves model

performance more in the transitional seasons (MMA and SON). The assimilation demonstrated relatively minor or no improvements in the simulation of soil moisture during the winter season, which could be attributed to the presence of snow and frozen soil Kumar et al. (2009). The LSTM merged dataset assimilation does not improve or even deteriorate performance, particularly during the summer season, suggesting its inability to effectively merge soil moisture information retrieved under dry conditions that are not included in the training period.

Compared to the single retrieval assimilation, the assimilation of merged datasets results in a better performance than assimilating the less informative retrieval of AMSR2. However, assimilating merged soil moisture products does not give better results compared to assimilating SMAP or ASCAT individually.

7

Summary and outlook

Soil moisture plays a crucial role in regulating the Earth's water and energy cycles by influencing the partitioning of water between infiltration, runoff, and evapotranspiration, and the partitioning of incoming solar radiation into latent and sensible heat fluxes at the land-atmosphere interface. Soil moisture information can be obtained from in situ observations, remote sensing techniques, and land surface modelling (LSM). However, each of these methods has its own advantages and limitations. Advances in data assimilation (DA) techniques make it possible to merge remote sensing observations and model simulations to improve the model's accuracy and reliability. However, most traditional LSMs often have simplified representations of subsurface processes and neglect lateral water movement. One aspect of this PhD research was to assess whether a coupled land surface-subsurface model (CLM-ParFlow) can derive more information from DA than a stand-alone land surface model (CLM). Another objective was to explore the potential of merging active and passive remote sensing retrievals to further improve DA performance.

The thesis evaluated the performance of CLM compared to the CLM-ParFlow model for accurate soil moisture prediction at regional scales and highlighted the importance of considering lateral flow dynamics. Multiple regional and continental. Consistent with previous studies (Naz et al. 2019; Shrestha et al. 2018), CLM tends to overestimate soil moisture and fails to capture short-term dynamics on daily to weekly timescales. Our results indicated that the coupled model improves the representation of soil moisture variability by accounting for lateral surface and subsurface distribution. This is in line with recent studies (Ji et al. 2017; Rummler et al. 2019), demonstrating that subsurface lateral flow plays an important role in controlling soil moisture patterns and hydrological connectivity, especially in areas with complex hydrological processes. Including these processes enhances the physical consistency of the simulated terrestrial water cycle and improves the realism of soil moisture dynamics.

This thesis further tested and compared the performance of CLM and CLM-ParFlow for extracting information from remote sensing soil moisture (SMAP L3_SM_P_E product) via the Localized Ensemble Kalman Filter (LEnKF) assimilation scheme. While data assimilation improved soil moisture estimates relative to in situ observations, the impact on other variables, such as evapotranspiration (ET) and groundwater levels, remained limited. Improvements were more pronounced for CLM than for CLM–ParFlow, likely because the latter already provides a more physically realistic representation of subsurface processes, leaving less room for correction through assimilation. Moreover, the strong influence of topography-driven lateral flow in CLM–ParFlow, particularly at high spatial resolution (e.g., 500 m), reduces the effectiveness of assimilating coarse-resolution satellite observations $\sim$ 9 km) and propagating the information horizontally

across other model grid cells. Both models exhibited comparable performance in terms of ET, as they shared the same ET parameterization scheme. The sensitivity of ET to soil moisture was more evident under water-limited conditions than under energy-limited conditions. In contrast, groundwater simulations did not benefit from soil moisture assimilation in CLM–ParFlow. This may be attributed to the fact that the spatial distribution of groundwater dynamics is governed by deeper subsurface processes, which are indirectly linked to surface soil moisture. In addition, the spatial distribution of groundwater is highly heterogeneous, and in situ well measurements are often influenced by local effects (e.g., soil properties, pumping, and small-scale hydrogeological features). It was also found that the assimilation of coarse-resolution remote sensing retrievals may not enhance model performance.

This work proposed a novel LSTM method and a traditional TC-based method to merge soil moisture retrievals from spaceborne active and passive microwave sensors, including SMAP, AMSR2, and ASCAT. The merged products were evaluated against in situ observations and benchmarked against the ESA CCI soil moisture dataset. Results showed that the LSTM-based product achieved improved agreement with ground measurements in terms of bias and ubRMSE, while both LSTM and TC approaches outperformed the ESA CCI dataset. The superior performance of the LSTM can be attributed to its ability to integrate both static and dynamic features and to learn complex nonlinear relationships from the training data. The TC-based method calculated the weights by taking into account the error characteristics of the parental data sets. It is important to note that the LSTM model may not fully capture regional effects due to the limited number of in situ stations, and its application is also hampered in areas where in situ stations are sparse. In addition, the TC merging scheme could be improved by considering the seasonal variability of weights.

The thesis further investigated the assimilation of individual and merged soil moisture products into the CLM model using a data assimilation framework. Different assimilation scenarios were evaluated against in situ soil moisture measurements at thirteen sites. DA generally had a positive impact on the characterization of surface soil moisture with increased Pearson r and decreased ubRMSE. Assimilating SMAP and ASCAT resulted in slightly better performance compared to assimilating AMSR2, but the differences between the assimilation of SMAP and ASCAT are not significant. The consistency observed between soil moisture retrievals from SMAP and ASCAT indicated a potential benefit for long-term assimilation studies, especially when relying on data from multiple sensors or platforms. The assimilation of merged products did not consistently outperform the assimilation of individual datasets. For example, the LSTM-based merged product led to degraded performance in some cases. This can be explained by the fact that data assimilation systems rely not only on the accuracy of the input data but also on the consistency of their error characteristics with the model assumptions. While the LSTM product performs well in a direct comparison with observations, it may exhibit altered error structures that are not properly represented in the assumed observation error model. As a result, the assimilation may introduce suboptimal updates. Furthermore, the limited generalization capability of the LSTM under conditions not represented in the training period (e.g., the dry conditions in 2018) reduces its effectiveness as an assimilation input. In contrast, the TC-based product, despite being simpler, preserves the statistical properties of the original datasets more

consistently, making it more compatible with the assumptions of the DA framework.

From these studies, we conclude that the assimilation of remotely sensed soil moisture information helps improve the characterisation of hydrological processes in LSMs. In particular, the stand-alone CLM is known to exhibit a systematic wet bias in soil moisture, which can be effectively reduced through data assimilation. In addition, the coupled CLM–ParFlow model demonstrates an enhanced capability to utilize observed information by redistributing soil moisture laterally through subsurface flow processes. This lateral connectivity allows observational information to propagate across neighboring grid cells, which is not represented in the stand-alone CLM. However, the benefits of assimilating surface soil moisture are largely confined to the upper soil layers and do not consistently translate into improvements in the full soil column or in related fluxes such as ET. As previously stated, the information obtained from a single data source (e.g., remote sensing soil moisture data) may not be sufficient for the desired improvements in other model compartments. Many studies (Heyvaert et al. 2024; Khaki et al. 2020; Rahman et al. 2022; Scherrer et al. 2023; Tangdamrongsub et al. 2020) have demonstrated that the integration of additional information (e.g., total water storage or leaf area index) can further constrain the model's physical process and enhance the predictive capabilities of the model. In light of advanced satellite retrievals and in situ observation networks, multiple source DA needs to be explored further. Better ET predictions can be expected by assimilating leaf area index and estimating vegetation parameters. The results also revealed the difficulty of improving subsurface characterization in the real-world case, as also shown in previous studies (Hung et al. 2022). A follow-up study can consider including the groundwater level measurements in the assimilation scheme. In addition to hydraulic conductivity and porosity, more van Genuchten parameters (such as α and n) can be considered for estimation.

In this dissertation, bias refers to the systematic discrepancy between model-simulated states and observations that arises from structural model errors, observation uncertainties, or representativeness mismatches. Classical state update approaches, such as the EnKF, assume unbiased errors so that innovations are zero-mean and can be interpreted as random noise. The presence of systematic bias may therefore degrade the optimality of the assimilation updates. Nevertheless, in our case, state updating alone gives reasonable improvements for the CLM model. This may be explained by the fact that the satellite observations provide useful information regarding the temporal variability of soil moisture, allowing the assimilation to correct short-term deviations from the model trajectory. At the same time, our findings indicate that parameter estimation using remotely sensed measurements is challenging. Few previous studies have shown that parameter estimation using remotely sensed information can lead to better soil moisture characterisation, either in the synthetic case (Brandhorst et al. 2017; Montzka et al. 2011) or at coarser model resolution (close to or larger than the satellite footprint) (Khaki et al. 2020; Pinnington et al. 2018; Wanders et al. 2014). Here we use the SMAP mission product, which provides full spatial coverage of the study area with a three-day revisit interval. However, the product only provides information for the upper soil (0 - 5 cm), which does not reflect well the dynamics in the deeper layers. The deeper layers benefit little from the assimilation, as the updating is controlled by the model dynamics and other parameter uncertainties. Besides, the findings may be due to model structural error and the inference of this error with model parameterization.

For instance, in a fully coupled land surface subsurface model, the errors may be attributed to a misrepresentation of subsurface processes, such as preferential flow. These model structural errors have an effect on the assimilation process, resulting in the erroneous estimation of other parameters. The preferential flow plays a significant role in soil water retention, which in turn affects the modelling of soil moisture and the estimation of hydraulic conductivity and other parameters in the assimilation process. A more accurate representation of the physical process is therefore crucial for more accurate hydrological modelling, as well as for the application of assimilation techniques.

A key limitation in this study arises from the spatial scale mismatch between remotely sensed soil moisture observations and the model grid resolution. This issue has been widely addressed in the literature through multi-scale or three-dimensional data assimilation frameworks, such as those implemented in the studies by. Here, our approach uses a simplified treatment in which satellite retrievals are assimilated as point-scale observations. Multi-scale data assimilation has been widely developed to address this issue (De Lannoy et al. 2012; Sahoo et al. 2013; Vergopolan et al. 2020), and is operationally implemented in systems such as the SMAP Level-4 product. These frameworks account for the spatial footprint of observations and their associated error structures, either by including spatially correlated updates or by assimilating observations in observation space. The present system relies on retrieved soil moisture products and does not include a three-dimensional observation operator, which limits the effectiveness of soil moisture assimilation. In addition, a finer resolution of remotely sensed soil moisture datasets has been demonstrated to offer a more accurate representation of local hydrological conditions, such as the effects of intensive precipitation events, and therefore can contribute more to improve land surface model simulations (Lievens et al. 2017b; Lu et al. 2019). The newly pre-operational soil moisture product at 1 km resolution by Sentinel-1 might benefit the assimilation. Active microwave observations are strongly affected by vegetation structure and water content, and surface roughness (Kim et al. 2018; Rahmati et al. 2026; Vreugdenhil et al. 2018), which can degrade the accuracy of soil moisture retrievals. Similar limitations are already evident in ASCAT-based products, as shown in Chapter 5. A more robust approach would be to assimilate microwave observations directly (e.g., brightness temperature or backscatter) and combine them with improved vegetation modeling and radiative transfer schemes to better represent the interaction between land-surface states and satellite signals.

A spatially uniform observation error was applied to remotely sensed soil moisture, although spatial and temporal variability is known to exist with respect to land cover and vegetation condition in reality (Dorigo et al. 2010; Draper et al. 2013). Such a simplified error specification can degrade assimilation performance, as the observation error covariance directly controls the relative weighting between observations and model background through the Kalman gain (Degelia et al. 2020; Fielding et al. 2019; Minamide et al. 2017). The observation errors in theory include uncertainty due to systematic errors, instrument errors (random observation noise), and representation errors (e.g., scale mismatch between observed and modelled variable) (Fowler et al. 2013; Janjić et al. 2018). Accurate estimation of observation errors can improve the benefits of assimilating remote sensing datasets (Degelia et al. 2023; Terasaki et al. 2024). Further studies should focus on the spatial patterns of the different microwave soil moisture retrievals to quantify

their observational errors and take into account their different sensitivities to vegetation and other atmospheric conditions. Approaches such as TC analysis and adaptive estimation within the assimilation system offer promising ways to better quantify and dynamically update observation uncertainties in different microwave soil moisture products.

Another limitation of the work in this PhD dissertation is the small study area, relatively short simulation period and limited number of in situ measurements for verification. In situ information is important to evaluate the high-resolution models and to understand the influence of complicated topography and vegetation cover on model uncertainties. Further improvements can be achieved by increasing the ensemble size and using a longer DA period with multiple data types in the models. However, this points to the need to improve computational efficiency for the complex coupled land surface and subsurface models. For example, future studies can focus on the use of GPUs (graphical processing units) to speed up simulations. A further possibility is the development, implementation, and use of surrogate models (emulators) (Baker et al. 2022; Olson et al. 2024; Tran et al. 2021) that can approximate the full model's behaviors with significantly reduced computational cost and more powerful supercomputers.

Bibliography

Ahmad, Jawairia A, Barton A Forman, and Sujay V Kumar (2022). "Soil moisture estimation in South Asia via assimilation of SMAP retrievals". In: *Hydrology and Earth System Sciences* 26.8, pp. 2221–2243.

Ajami, Hoori, Matthew F McCabe, Jason P Evans, and Simon Stisen (2014). "Assessing the impact of model spin-up on surface water-groundwater interactions using an integrated hydrologic model". In: *Water Resources Research* 50.3, pp. 2636–2656.

Albergel, C, J-C Calvet, P De Rosnay, G Balsamo, W Wagner, S Hasenauer, V Naeimi, E Martin, E Bazile, F Bouyssel, et al. (2010). "Cross-evaluation of modelled and remotely sensed surface soil moisture with in situ data in southwestern France". In: *Hydrology and Earth System Sciences* 14.11, pp. 2177–2191.

Albergel, Clement, Patricia De Rosnay, Claire Gruhier, Joaquin Muñoz-Sabater, Stefan Hasenauer, Lars Isaksen, Yann Kerr, and Wolfgang Wagner (2012). "Evaluation of remotely sensed and modelled soil moisture products using global ground-based in situ observations". In: *Remote Sensing of Environment* 118, pp. 215–226.

Albergel, Clement, Emanuel Dutra, Simon Munier, Jean-Christophe Calvet, Joaquin Munoz-Sabater, Patricia de Rosnay, and Gianpaolo Balsamo (2018). "ERA-5 and ERA-Interim driven ISBA land surface model simulations: which one performs better?" In: *Hydrology and Earth System Sciences* 22.6, pp. 3515–3532.

Albergel, Clément, Simon Munier, Delphine Jennifer Leroux, Hélène Dewaele, David Fairbairn, Alina Lavinia Barbu, Emiliano Gelati, Wouter Dorigo, Stéphanie Faroux, Catherine Meurey, et al. (2017). "Sequential assimilation of satellite-derived vegetation and soil moisture products using SURFEX_v8. 0: LDAS-Monde assessment over the Euro-Mediterranean area". In: *Geoscientific Model Development* 10.10, pp. 3889–3912.

Alkhaier, F, RJ Schotting, and Zhongbo Su (2009). "A qualitative description of shallow groundwater effect on surface temperature of bare soil". In: *Hydrology and Earth System Sciences* 13.9, pp. 1749–1756.

Alkhaier, F., G. N. Flerchinger, and Z. Su (2012). "Shallow groundwater effect on land surface temperature and surface energy balance under bare soil conditions: modeling and description". In: *Hydrology and Earth System Sciences* 16.7, pp. 1817–1831. DOI: 10.5194/hess-16-1817-2012. URL: https://hess.copernicus.org/articles/16/1817/2012/.

Anderson, WB, BF Zaitchik, CR Hain, MC Anderson, MT Yilmaz, J Mecikalski, and L Schultz (2012). "Towards an integrated soil moisture drought monitor for East Africa". In: *Hydrology and Earth System Sciences* 16.8, pp. 2893–2913.

Andreadis, Konstantinos M, Dean F Meason, Barbara Höck, Priscilla Lad, and Narendra Das (2022). "Evaluation of Multiscale SMAP Soil Moisture Products in Forested Environments". In: *IEEE Geoscience and Remote Sensing Letters* 19, pp. 1–5.

Appels, Willemijn M, Patrick W Bogaart, and Sjoerd EATM van der Zee (2017). "Feedbacks between shallow groundwater dynamics and surface topography on runoff generation in flat fields". In: *Water Resources Research* 53.12, pp. 10336–10353.

Ashby, Steven F and Robert D Falgout (1996). "A parallel multigrid preconditioned conjugate gradient algorithm for groundwater flow simulations". In: *Nuclear science and engineering* 124.1, pp. 145–159.

Ayres, Edward, Andreas Colliander, Michael H Cosh, Joshua A Roberti, Sam Simkin, and Melissa A Genazzio (2021). "Validation of SMAP soil moisture at terrestrial National Ecological Observatory Network (NEON) sites show potential for soil moisture retrieval in forested areas". In: *IEEE journal of selected topics in applied earth observations and remote sensing* 14, pp. 10903–10918.

Baatz, R, HR Bogena, H-J Hendricks Franssen, JA Huisman, W Qu, C Montzka, and H Vereecken (2014). "Calibration of a catchment scale cosmic-ray probe network: A comparison of three parameterization methods". In: *Journal of Hydrology* 516, pp. 231–244.

Baatz, R, HR Bogena, H-J Hendricks Franssen, JA Huisman, C Montzka, and H Vereecken (2015). "An empirical vegetation correction for soil water content quantification using cosmic ray probes". In: *Water Resources Research* 51.4, pp. 2030–2046.

Baatz, Roland, Harrie-Jan Hendricks Franssen, Xujun Han, Tim Hoar, Heye Reemt Bogena, and Harry Vereecken (2017). "Evaluation of a cosmic-ray neutron sensor network for improved land surface model prediction". In: *Hydrology and Earth System Sciences* 21.5, pp. 2509–2530.

Babaeian, Ebrahim, Sidike Paheding, Nahian Siddique, Vijay K Devabhaktuni, and Markus Tuller (2021). "Estimation of root zone soil moisture from ground and remotely sensed soil information with multisensor data fusion and automated machine learning". In: *Remote Sensing of Environment* 260, p. 112434.

Babaeian, Ebrahim, Morteza Sadeghi, Scott B Jones, Carsten Montzka, Harry Vereecken, and Markus Tuller (2019). "Ground, proximal, and satellite remote sensing of soil moisture". In: *Reviews of Geophysics* 57.2, pp. 530–616.

Baker, Evan, Anna B Harper, Daniel Williamson, and Peter Challenor (2022). "Emulation of high-resolution land surface models using sparse Gaussian processes with application to JULES". In: *Geoscientific Model Development* 15.5, pp. 1913–1929.

Baldauf, Michael, Axel Seifert, Jochen Förstner, Detlev Majewski, Matthias Raschendorfer, and Thorsten Reinhardt (2011). "Operational convective-scale numerical weather prediction with the COSMO model: Description and sensitivities". In: *Monthly Weather Review* 139.12, pp. 3887–3905.

Barrett, Brian W, Edward Dwyer, and Pádraig Whelan (2009). "Soil moisture retrieval from active spaceborne microwave observations: An evaluation of current techniques". In: *Remote Sensing* 1.3, pp. 210–242.

Bartalis, Zoltan, Wolfgang Wagner, Vahid Naeimi, Stefan Hasenauer, Klaus Scipal, Hans Bonekamp, Julia Figa, and Craig Anderson (2007). "Initial soil moisture retrievals from the METOP-A Advanced Scatterometer (ASCAT)". In: *Geophysical Research Letters* 34.20.

Bastidas, Luis A, Hoshin V Gupta, Kuo-Lin Hsu, and Soroosh Sorooshian (2003). "Parameter, structure, and model performance evaluation for land-surface schemes". In: *Calibration of watershed models* 6, pp. 229–237.

Batchu, Vishal, Grey Nearing, and Varun Gulshan (2023). "A Deep Learning Data Fusion Model using Sentinel-1/2, SoilGrids, SMAP-USDA, and GLDAS for Soil Moisture Retrieval". In: *Journal of Hydrometeorology*.

Batjes, NH (1997). "A world dataset of derived soil properties by FAO–UNESCO soil unit for global modelling". In: *Soil use and management* 13.1, pp. 9–16.

Batjes, Niels H, Eloi Ribeiro, Ad Van Oostrum, Johan Leenaars, Tom Hengl, and Jorge Mendes de Jesus (2017). "WoSIS: providing standardised soil profile data for the world". In: *Earth System Science Data* 9.1, pp. 1–14.

Baur, Martin, Thomas Jagdhuber, Moritz Link, Maria Piles, Ruzbeh Akbar, and Dara Entekhabi (2018). "Multi-Frequency Estimation of Canopy Penetration Depths from SMAP/AMSR2 Radiometer and IceSAT Lidar Data". In: *IGARSS 2018-2018 IEEE International Geoscience and Remote Sensing Symposium*. IEEE, pp. 365–368.

Bayat, Aida Taghavi, Sarah Schönbrodt-Stitt, Paolo Nasta, Nima Ahmadian, Christopher Conrad, Heye R Bogena, Harry Vereecken, Jannis Jakobi, Roland Baatz, and Nunzio Romano (2020). "Mapping near-surface soil moisture in a Mediterranean agroforestry ecosystem using Cosmic-Ray Neutron Probe and Sentinel-1 Data". In: *2020 IEEE International Workshop on Metrology for Agriculture and Forestry (MetroAgriFor)*. IEEE, pp. 201–206.

Bayat, Bagher, Fernando Camacho, Jaime Nickeson, Michael Cosh, John Bolten, Harry Vereecken, and Carsten Montzka (2021). "Toward operational validation systems for global satellite-based terrestrial essential climate variables". In: *International Journal of Applied Earth Observation and Geoinformation* 95, p. 102240.

Berg, Alexis, Benjamin R Lintner, Kirsten L Findell, Sergey Malyshev, Paul C Loikith, and Pierre Gentine (2014). "Impact of soil moisture–atmosphere interactions on surface temperature distribution". In: *Journal of Climate* 27.21, pp. 7976–7993.

Beven, Keith J and Michael J Kirkby (1979). "A physically based, variable contributing area model of basin hydrology/Un modèle à base physique de zone d'appel variable de l'hydrologie du bassin versant". In: *Hydrological sciences journal* 24.1, pp. 43–69.

Bi, Haiyun, Jianwen Ma, Wenjun Zheng, and Jiangyuan Zeng (2016). "Comparison of soil moisture in GLDAS model simulations and in situ observations over the Tibetan Plateau". In: *Journal of Geophysical Research: Atmospheres* 121.6, pp. 2658–2678.

Bierkens, Marc FP, Victoria A Bell, Peter Burek, Nathaniel Chaney, Laura E Condon, Cédric H David, Ad de Roo, Petra Döll, Niels Drost, James S Famiglietti, et al. (2015). "Hyper-resolution global hydrological modelling: what is next? "Everywhere and locally relevant"". In: *Hydrological processes* 29.2, pp. 310–320.

Blankenship, Clay B, Jonathan L Case, Bradley T Zavodsky, and William L Crosson (2016). "Assimilation of SMOS retrievals in the Land Information System". In: *IEEE Transactions on Geoscience and Remote Sensing* 54.11, pp. 6320–6332.

Blyth, Eleanor M, Vivek K Arora, Douglas B Clark, Simon J Dadson, Martin G De Kauwe, David M Lawrence, Joe R Melton, Julia Pongratz, Rachael H Turton, Kei Yoshimura, et al. (2021). "Advances in land surface modelling". In: *Current Climate Change Reports* 7.2, pp. 45–71.

Blyverket, Jostein, Paul D Hamer, Laurent Bertino, Clément Albergel, David Fairbairn, and William A Lahoz (2019). "An Evaluation of the EnKF vs. EnOI and the Assimilation of SMAP, SMOS and ESA CCI Soil Moisture Data over the Contiguous US". In: *Remote Sensing* 11.5, p. 478.

Bogena, Heye Reemt (2016). "TERENO: German network of terrestrial environmental observatories". In: *Journal of large-scale research facilities JLSRF* 2, A52–A52.

Bogena, Heye Reemt, Martin Schrön, Jannis Jakobi, Patrizia Ney, Steffen Zacharias, Mie Andreasen, Roland Baatz, David Boorman, Mustafa Berk Duygu, Miguel Angel Eguibar-Galán, et al. (2022). "COSMOS-Europe: a European network of cosmic-ray neutron soil moisture sensors". In: *Earth System Science Data* 14.3, pp. 1125–1151.

Bogena, HR, JA Huisman, R Baatz, H-J Hendricks Franssen, and H Vereecken (2013). "Accuracy of the cosmic-ray soil water content probe in humid forest ecosystems: The worst case scenario". In: *Water Resources Research* 49.9, pp. 5778–5791.

Bogena, HR, C Montzka, JA Huisman, A Graf, M Schmidt, M Stockinger, C Von Hebel, HJ Hendricks-Franssen, J Van der Kruk, W Tappe, et al. (2018). "The TERENO-Rur hydrological observatory: A multiscale multi-compartment research platform for the advancement of hydrological science". In: *Vadose Zone Journal* 17.1, pp. 1–22.

Bollmeyer, Christoph, Jan Keller, Christian Ohlwein, Andreas Hense, Michael Borsche, Deborah Niermann, Frank Kaspar, and Martin Schupfner (2024). *Regional Reanalysis COSMO-REA6 - Standardised Parameters*. dataset. Version 1.0. Accessed: 2025-03-15. DOI: https://doi.org/10.26050/WDCC/CR6_EU6. URL: https://www.wdc-climate.de/ui/entry?acronym=CR6_EU6.

Bollmeyer, Christoph, JD Keller, Christian Ohlwein, Sabrina Wahl, Susanne Crewell, P Friederichs, A Hense, J Keune, S Kneifel, IJQJotRMS Pscheidt, et al. (2015). "Towards a high-resolution regional reanalysis for the European CORDEX domain". In: *Quarterly Journal of the Royal Meteorological Society* 141.686, pp. 1–15.

Bonan, Gordon B (1998). "The land surface climatology of the NCAR Land Surface Model coupled to the NCAR Community Climate Model". In: *Journal of Climate* 11.6, pp. 1307–1326.

Bonan, Gordon B, Samuel Levis, Stephen Sitch, Mariana Vertenstein, and Keith W Oleson (2003). "A dynamic global vegetation model for use with climate models: concepts and description of simulated vegetation dynamics". In: *Global Change Biology* 9.11, pp. 1543–1566.

Bonan, Gordon B, Edward G Patton, Ian N Harman, Keith W Oleson, John J Finnigan, Yaqiong Lu, and Elizabeth A Burakowski (2018). "Modeling canopy-induced turbulence in the Earth system: A unified parameterization of turbulent exchange within plant canopies and the roughness sublayer (CLM-ml v0)". In: *Geoscientific Model Development* 11.4, pp. 1467–1496.

Borowik, A and J Wyszkowska (2016). "Soil moisture as a factor affecting the microbiological and biochemical activity of soil". In: *Plant, Soil and Environment* 62.6, pp. 250–255.

Brandhorst, N, D Erdal, and I Neuweiler (2017). "Soil moisture prediction with the ensemble Kalman filter: Handling uncertainty of soil hydraulic parameters". In: *Advances in Water Resources* 110, pp. 360–370.

Brandhorst, N. and I. Neuweiler (2023). "Impact of parameter updates on soil moisture assimilation in a 3D heterogeneous hillslope model". In: *Hydrology and Earth System Sciences* 27.6, pp. 1301–1323. DOI: 10.5194/hess-27-1301-2023. URL: https://hess.copernicus.org/articles/27/1301/2023/.

Brandhorst, Natascha and Insa Neuweiler (2022). "Impact of parameter updates on soil moisture assimilation in a 3D heterogeneous hillslope model". In: *Hydrology and Earth System Sciences Discussions* 2022, pp. 1–34.

Brocca, Luca, Wade T Crow, Luca Ciabatta, Christian Massari, Patricia De Rosnay, Markus Enenkel, Sebastian Hahn, Giriraj Amarnath, Stefania Camici, Angelica Tarpanelli, et al. (2017). "A review of the applications of ASCAT soil moisture products". In: *IEEE Journal of Selected Topics in Applied Earth Observations and Remote Sensing* 10.5, pp. 2285–2306.

Brocca, Luca, F Melone, T Moramarco, Wolfgang Wagner, Vahid Naeimi, Zoltan Bartalis, and Stefan Hasenauer (2010). "Improving runoff prediction through the assimilation of the ASCAT soil moisture product". In: *Hydrology and Earth System Sciences* 14.10, pp. 1881–1893.

Brocca, Luca, Tommaso Moramarco, Florisa Melone, Wolfgang Wagner, Stefan Hasenauer, and Sebastian Hahn (2011). "Assimilation of surface-and root-zone ASCAT soil moisture products into rainfall–runoff modeling". In: *IEEE Transactions on Geoscience and Remote Sensing* 50.7, pp. 2542–2555.

Burgin, Mariko S, Andreas Colliander, Eni G Njoku, Steven K Chan, Francois Cabot, Yann H Kerr, Rajat Bindlish, Thomas J Jackson, Dara Entekhabi, and Simon H Yueh (2017). "A comparative study of the SMAP passive soil moisture product with existing satellite-based soil moisture products". In: *IEEE Transactions on Geoscience and Remote Sensing* 55.5, pp. 2959–2971.

Caires, S and A Sterl (2003). "Validation of ocean wind and wave data using triple collocation". In: *Journal of geophysical research: oceans* 108.C3.

Celia, Michael A, Efthimios T Bouloutas, and Rebecca L Zarba (1990). "A general mass-conservative numerical solution for the unsaturated flow equation". In: *Water resources research* 26.7, pp. 1483–1496.

Chakrabarti, Subit, Tara Bongiovanni, Jasmeet Judge, Lincoln Zotarelli, and Cimelio Bayer (2014). "Assimilation of SMOS soil moisture for quantifying drought impacts on crop yield in agricultural regions". In: *IEEE Journal of Selected Topics in Applied Earth Observations and Remote Sensing* 7.9, pp. 3867–3879.

Chakravorty, Aniket, Bhagu Ram Chahar, Om Prakash Sharma, and CT Dhanya (2016). "A regional scale performance evaluation of SMOS and ESA-CCI soil moisture products over India with simulated soil moisture from MERRA-Land". In: *Remote Sensing of Environment* 186, pp. 514–527.

Chan, S, Rajat Bindlish, Peggy O'Neill, T Jackson, Julian Chaubell, Jeffrey Piepmeier, S Dunbar, Andreas Colliander, Fan Chen, Dara Entekhabi, et al. (2017). "Development and validation of the SMAP enhanced passive soil moisture product". In: *2017 IEEE International Geoscience and Remote Sensing Symposium (IGARSS)*. IEEE, pp. 2539–2542.

Chan, Steven K, Rajat Bindlish, Peggy O'Neill, Thomas Jackson, Eni Njoku, Scott Dunbar, Julian Chaubell, Jeffrey Piepmeier, Simon Yueh, Dara Entekhabi, et al. (2018). "Development and assessment of the SMAP enhanced passive soil moisture product". In: *Remote sensing of environment* 204, pp. 931–941.

Chaudhuri, A, H-J Hendricks Franssen, and M Sekhar (2018). "Iterative filter based estimation of fully 3D heterogeneous fields of permeability and Mualem-van Genuchten parameters". In: *Advances in water resources* 122, pp. 340–354.

Chen, Fan, Wade T Crow, Rajat Bindlish, Andreas Colliander, Mariko S Burgin, Jun Asanuma, and Kentaro Aida (2018). "Global-scale evaluation of SMAP, SMOS and ASCAT soil moisture products using triple collocation". In: *Remote Sensing of Environment* 214, pp. 1–13.

Chen, Fan, Wade T Crow, Andreas Colliander, Michael H Cosh, Thomas J Jackson, Rajat Bindlish, Rolf H Reichle, Steven K Chan, David D Bosch, Patrick J Starks, et al. (2016). "Application of triple collocation in ground-based validation of soil moisture active/passive (SMAP) level 2 data products". In: *IEEE Journal of Selected Topics in Applied Earth Observations and Remote Sensing* 10.2, pp. 489–502.

Chen, Fan, Wade T Crow, Patrick J Starks, and Daniel N Moriasi (2011). "Improving hydrologic predictions of a catchment model via assimilation of surface soil moisture". In: *Advances in Water Resources* 34.4, pp. 526–536.

Chen, Quan, Jiangyuan Zeng, Chenyang Cui, Zhen Li, Kun-Shan Chen, Xiaojing Bai, and Jia Xu (2017a). "Soil moisture retrieval from SMAP: a validation and error analysis study using ground-based observations over the little Washita watershed". In: *IEEE Transactions on Geoscience and Remote Sensing* 56.3, pp. 1394–1408.

Chen, Xi and Qi Hu (2004). "Groundwater influences on soil moisture and surface evaporation". In: *Journal of Hydrology* 297.1-4, pp. 285–300.

Chen, Yingying, Kun Yang, Jun Qin, Qian Cui, Hui Lu, Zhu La, Menglei Han, and Wenjun Tang (2017b). "Evaluation of SMAP, SMOS, and AMSR2 soil moisture retrievals against observations from two networks on the Tibetan Plateau". In: *Journal of Geophysical Research: Atmospheres* 122.11, pp. 5780–5792.

Clapp, Roger B and George M Hornberger (1978). "Empirical equations for some soil hydraulic properties". In: *Water resources research* 14.4, pp. 601–604.

Clark, DB, LM Mercado, S Sitch, CD Jones, N Gedney, MJ Best, M Pryor, GG Rooney, RLH Essery, E Blyth, et al. (2011). "The Joint UK Land Environment Simulator (JULES), model description–Part 2: carbon fluxes and vegetation dynamics". In: *Geoscientific Model Development* 4.3, pp. 701–722.

Clewley, Daniel, Jane B Whitcomb, Ruzbeh Akbar, Agnelo R Silva, Aaron Berg, Justin R Adams, Todd Caldwell, Dara Entekhabi, and Mahta Moghaddam (2017). "A method for upscaling in situ soil moisture measurements to satellite footprint scale using random forests". In: *IEEE Journal of Selected Topics in Applied Earth Observations and Remote Sensing* 10.6, pp. 2663–2673.

Colliander, Andreas, Thomas J Jackson, Rajat Bindlish, S Chan, N Das, SB Kim, MH Cosh, RS Dunbar, L Dang, L Pashaian, et al. (2017). "Validation of SMAP surface soil moisture products with core validation sites". In: *Remote sensing of environment* 191, pp. 215–231.

Colliander, Andreas, Rolf H Reichle, Wade T Crow, Michael H Cosh, Fan Chen, Steven Chan, Narendra Narayan Das, Rajat Bindlish, Julian Chaubell, Seungbum Kim, et al. (2021). "Validation of soil moisture data products from the NASA SMAP mission". In: *IEEE Journal of selected topics in applied earth observations and remote sensing* 15, pp. 364–392.

Condon, Laura E and Reed M Maxwell (2013). "Implementation of a linear optimization water allocation algorithm into a fully integrated physical hydrology model". In: *Advances in Water Resources* 60, pp. 135–147.

– (2014). "Groundwater-fed irrigation impacts spatially distributed temporal scaling behavior of the natural system: a spatio-temporal framework for understanding water management impacts". In: *Environmental Research Letters* 9.3, p. 034009.

– (2015). "Evaluating the relationship between topography and groundwater using outputs from a continental-scale integrated hydrology model". In: *Water Resources Research* 51.8, pp. 6602–6621.

– (2019). "Simulating the sensitivity of evapotranspiration and streamflow to large-scale groundwater depletion". In: *Science Advances* 5.6, eaav4574.

Cosby, BJ, GM Hornberger, RB Clapp, and ToR Ginn (1984). "A statistical exploration of the relationships of soil moisture characteristics to the physical properties of soils". In: *Water resources research* 20.6, pp. 682–690.

Crow, Wade T, Aaron A Berg, Michael H Cosh, Alexander Loew, Binayak P Mohanty, Rocco Panciera, Patricia de Rosnay, Dongryeol Ryu, and Jeffrey P Walker (2012). "Upscaling sparse ground-based soil moisture observations for the validation of coarse-resolution satellite soil moisture products". In: *Reviews of Geophysics* 50.2.

Crow, Wade T, Hyunglok Kim, and Sujay Kumar (2024). "Systematic modeling errors undermine the application of land data assimilation systems for hydrological and weather forecasting". In: *Journal of Hydrometeorology* 25.1, pp. 3–26.

Cui, Huizhen, Lingmei Jiang, Jinyang Du, Shaojie Zhao, Gongxue Wang, Zheng Lu, and Jian Wang (2017). "Evaluation and analysis of AMSR-2, SMOS, and SMAP soil moisture products in the Genhe area of China". In: *Journal of Geophysical Research: Atmospheres* 122.16, pp. 8650–8666.

Cuntz, Matthias, Juliane Mai, Luis Samaniego, Martyn Clark, Volker Wulfmeyer, Oliver Branch, Sabine Attinger, and Stephan Thober (2016). "The impact of standard and hard-coded parameters on the hydrologic fluxes in the Noah-MP land surface model". In: *Journal of Geophysical Research: Atmospheres* 121.18, pp. 10–676.

Dai, Yongjiu, Xubin Zeng, Robert E Dickinson, Ian Baker, Gordon B Bonan, Michael G Bosilovich, A Scott Denning, Paul A Dirmeyer, Paul R Houser, Guoyue Niu, et al. (2003). "The common land model". In: *Bulletin of the American Meteorological Society* 84.8, pp. 1013–1024.

De Lannoy, Gabriëlle JM and Rolf H Reichle (2016). "Assimilation of SMOS brightness temperatures or soil moisture retrievals into a land surface model". In: *Hydrology and Earth System Sciences* 20.12, pp. 4895–4911.

De Lannoy, Gabriëlle JM, Rolf H Reichle, Kristi R Arsenault, Paul R Houser, Sujay Kumar, Niko EC Verhoest, and Valentijn RN Pauwels (2012). "Multiscale assimilation of Advanced Microwave Scanning Radiometer–EOS snow water equivalent and Moderate Resolution Imaging Spectroradiometer snow cover fraction observations in northern Colorado". In: *Water Resources Research* 48.1.

De Santis, D, D Biondi, WT Crow, S Camici, S Modanesi, L Brocca, and C Massari (2021). "Assimilation of satellite soil moisture products for river flow prediction: An extensive experiment in over 700 catchments throughout Europe". In: *Water Resources Research* 57.6, e2021WR029643.

Dean, Thomas J, James P Bell, and AJB Baty (1987). "Soil moisture measurement by an improved capacitance technique, Part I. Sensor design and performance". In: *Journal of Hydrology* 93.1-2, pp. 67–78.

Dee, Dick P, S M Uppala, Adrian J Simmons, Paul Berrisford, Paul Poli, Shinya Kobayashi, U Andrae, MA Balmaseda, G Balsamo, d P Bauer, et al. (2011). "The ERA-Interim reanalysis: Configuration and performance of the data assimilation system". In: *Quarterly Journal of the royal meteorological society* 137.656, pp. 553–597.

Degelia, Samuel K and Xuguang Wang (2023). "Impacts of Methods for Estimating the Observation Error Variance for the Frequent Assimilation of Thermodynamic Profilers on Convective-Scale Forecasts". In: *Monthly Weather Review* 151.4, pp. 855–875.

Degelia, Samuel K, Xuguang Wang, David J Stensrud, and David D Turner (2020). "Systematic evaluation of the impact of assimilating a network of ground-based remote sensing profilers for forecasts of nocturnal convection initiation during PECAN". In: *Monthly Weather Review* 148.12, pp. 4703–4728.

Dirmeyer, Paul A (2011). "The terrestrial segment of soil moisture–climate coupling". In: *Geophysical Research Letters* 38.16.

Dobriyal, Pariva, Ashi Qureshi, Ruchi Badola, and Syed Ainul Hussain (2012). "A review of the methods available for estimating soil moisture and its implications for water resource management". In: *Journal of Hydrology* 458, pp. 110–117.

Dobson, M Craig and Fawwaz T Ulaby (1986). "Active microwave soil moisture research". In: *IEEE Transactions on Geoscience and Remote Sensing* 1, pp. 23–36.

Dorigo, Wouter, Wolfgang Wagner, Clement Albergel, Franziska Albrecht, Gianpaolo Balsamo, Luca Brocca, Daniel Chung, Martin Ertl, Matthias Forkel, Alexander Gruber, et al. (2017). "ESA CCI Soil Moisture for improved Earth system understanding: State-of-the art and future directions". In: *Remote Sensing of Environment* 203, pp. 185–215.

Dorigo, Wouter A, Klaus Scipal, Robert M Parinussa, Yi Y Liu, Wolfgang Wagner, Richard AM De Jeu, and Vahid Naeimi (2010). "Error characterisation of global active and passive microwave soil moisture datasets". In: *Hydrology and Earth System Sciences* 14.12, pp. 2605–2616.

Draper, C, J-F Mahfouf, J-C Calvet, E Martin, and W Wagner (2011). "Assimilation of ASCAT near-surface soil moisture into the SIM hydrological model over France". In: *Hydrology and Earth System Sciences* 15.12, pp. 3829–3841.

Draper, Clara, Rolf Reichle, Richard de Jeu, Vahid Naeimi, Robert Parinussa, and Wolfgang Wagner (2013). "Estimating root mean square errors in remotely sensed soil moisture over continental scale domains". In: *Remote Sensing of Environment* 137, pp. 288–298.

Draper, CS, RH Reichle, GJM De Lannoy, and Qing Liu (2012). "Assimilation of passive and active microwave soil moisture retrievals". In: *Geophysical Research Letters* 39.4.

Drought 2018 Team and ICOS Ecosystem Thematic Centre (2019). *Drought-2018 ecosystem eddy covariance flux product in FLUXNET-Archive format - release 2019-1*. DOI: 10.18160/PZDK-EF78. URL: https://meta.icos-cp.eu/collections/UZw8ra7OVilmVjATTCgIimpz.

Du, Jinyang, John S Kimball, Lucas A Jones, Youngwook Kim, Joseph Glassy, and Jennifer D Watts (2017). "A global satellite environmental data record derived from AMSR-E and AMSR2 microwave Earth observations". In: *Earth System Science Data* 9.2, pp. 791–808.

Dubois, Pascale C, Jakob Van Zyl, and Ted Engman (1995). "Measuring soil moisture with imaging radars". In: *IEEE transactions on geoscience and remote sensing* 33.4, pp. 915–926.

Dumedah, Gift and Jeffrey P Walker (2014). "Assessment of land surface model uncertainty: A crucial step towards the identification of model weaknesses". In: *Journal of Hydrology* 519, pp. 1474–1484.

Duygu, Mustafa Berk and Zuhal Akyürek (2019). "Using cosmic-ray neutron probes in validating satellite soil moisture products and land surface models". In: *Water* 11.7, p. 1362.

El Hajj, Mohammad, Nicolas Baghdadi, Mehrez Zribi, Nemesio Rodríguez-Fernández, Jean Pierre Wigneron, Amen Al-Yaari, Ahmad Al Bitar, Clément Albergel, and Jean-Christophe Calvet (2018). "Evaluation of SMOS, SMAP, ASCAT and Sentinel-1 soil moisture products at sites in Southwestern France". In: *Remote Sensing* 10.4, p. 569.

Eltahir, Elfatih AB (1998). "A soil moisture–rainfall feedback mechanism: 1. Theory and observations". In: *Water resources research* 34.4, pp. 765–776.

Engdahl, Nicholas B and Reed M Maxwell (2015). "Quantifying changes in age distributions and the hydrologic balance of a high-mountain watershed from climate induced variations in recharge". In: *Journal of Hydrology* 522, pp. 152–162.

Engman, Edwin T (1991). "Applications of microwave remote sensing of soil moisture for water resources and agriculture". In: *Remote Sensing of Environment* 35.2-3, pp. 213–226.

Entekhabi, Dara, Eni G Njoku, Peggy E O'neill, Kent H Kellogg, Wade T Crow, Wendy N EdeMein, Jared K Entin, Shawn D Goodman, Thomas J Jackson, Joel Johnson, et al. (2010a). "The soil moisture active passive (SMAP) mission". In: *Proceedings of the IEEE* 98.5, pp. 704–716.

Entekhabi, Dara, Rolf H Reichle, Randal D Koster, and Wade T Crow (2010b). "Performance metrics for soil moisture retrievals and application requirements". In: *Journal of Hydrometeorology* 11.3, pp. 832–840.

Entekhabi, Dara, Ignacio Rodriguez-Iturbe, and Fabio Castelli (1996). "Mutual interaction of soil moisture state and atmospheric processes". In: *Journal of Hydrology* 184.1-2, pp. 3–17.

Escorihuela, Maria-José, Andre Chanzy, Jean-Pierre Wigneron, and Yann H Kerr (2010). "Effective soil moisture sampling depth of L-band radiometry: A case study". In: *Remote Sensing of Environment* 114.5, pp. 995–1001.

Evensen, Geir (1994). "Sequential data assimilation with a nonlinear quasi-geostrophic model using Monte Carlo methods to forecast error statistics". In: *Journal of Geophysical Research: Oceans* 99.C5, pp. 10143–10162.

– (2003). "The ensemble Kalman filter: Theoretical formulation and practical implementation". In: *Ocean dynamics* 53, pp. 343–367.

Fairbairn, D, AL Barbu, J-F Mahfouf, J-C Calvet, and E Gelati (2015). "Comparing the ensemble and extended Kalman filters for in situ soil moisture assimilation with contrasting conditions". In: *Hydrology and Earth System Sciences* 19.12, pp. 4811–4830.

Fairbairn, David, Alina Lavinia Barbu, Adrien Napoly, Clément Albergel, Jean-François Mahfouf, and Jean-Christophe Calvet (2017). "The effect of satellite-derived surface soil moisture and leaf area index land data assimilation on streamflow simulations over France". In: *Hydrology and Earth System Sciences* 21.4, pp. 2015–2033.

Falloon, Pete, Chris D Jones, Melanie Ades, and Keryn Paul (2011). "Direct soil moisture controls of future global soil carbon changes: An important source of uncertainty". In: *Global Biogeochemical Cycles* 25.3.

Fersch, Benjamin, Thomas Jagdhuber, Martin Schrön, Ingo Völksch, and Marc Jäger (2018). "Synergies for soil moisture retrieval across scales from airborne polarimetric SAR, cosmic ray neutron roving, and an in situ sensor network". In: *Water Resources Research* 54.11, pp. 9364–9383.

Fielding, MD and O Stiller (2019). "Characterizing the representativity error of cloud profiling observations for data assimilation". In: *Journal of Geophysical Research: Atmospheres* 124.7, pp. 4086–4103.

Fisher, Rosie A, Charles D Koven, William RL Anderegg, Bradley O Christoffersen, Michael C Dietze, Caroline E Farrior, Jennifer A Holm, George C Hurtt, Ryan G Knox, Peter J Lawrence, et al. (2018). "Vegetation demographics in Earth System Models: A review of progress and priorities". In: *Global change biology* 24.1, pp. 35–54.

Ford, Trent W and Steven M Quiring (2019). "Comparison of contemporary in situ, model, and satellite remote sensing soil moisture with a focus on drought monitoring". In: *Water Resources Research* 55.2, pp. 1565–1582.

Forrester, Mary M and Reed M Maxwell (2020). "Impact of lateral groundwater flow and subsurface lower boundary conditions on atmospheric boundary layer development over complex terrain". In: *Journal of Hydrometeorology* 21.6, pp. 1133–1160.

Fowler, Alison and Peter Jan Van Leeuwen (2013). "Observation impact in data assimilation: the effect of non-Gaussian observation error". In: *Tellus A: Dynamic Meteorology and Oceanography* 65.1, p. 20035.

Franz, TE, M Zreda, R Rosolem, and TPA Ferre (2013). "A universal calibration function for determination of soil moisture with cosmic-ray neutrons". In: *Hydrology and Earth System Sciences* 17.2, pp. 453–460.

Franz, Trenton E, M Zreda, TPA Ferre, R Rosolem, C Zweck, S Stillman, X Zeng, and WJ Shuttleworth (2012a). "Measurement depth of the cosmic ray soil moisture probe affected by hydrogen from various sources". In: *Water Resources Research* 48.8.

Franz, Trenton E, M Zreda, R Rosolem, and TPA Ferre (2012b). "Field validation of a cosmic-ray neutron sensor using a distributed sensor network". In: *Vadose Zone Journal* 11.4, vzj2012–0046.

Furusho-Percot, Carina, Klaus Goergen, Carl Hartick, Ketan Kulkarni, Jessica Keune, and Stefan Kollet (2019). "Pan-European groundwater to atmosphere terrestrial systems climatology from a physically consistent simulation". In: *Scientific data* 6.1, p. 320.

Gaspari, Gregory and Stephen E Cohn (1999). "Construction of correlation functions in two and three dimensions". In: *Quarterly Journal of the Royal Meteorological Society* 125.554, pp. 723–757.

Gavahi, Keyhan, Peyman Abbaszadeh, Hamid Moradkhani, Xiwu Zhan, and Christopher Hain (2020). "Multivariate assimilation of remotely sensed soil moisture and evapotranspiration for drought monitoring". In: *Journal of Hydrometeorology* 21.10, pp. 2293–2308.

Gebler, S, W Kurtz, VRN Pauwels, SJ Kollet, H Vereecken, and H-J Hendricks Franssen (2019). "Assimilation of high-resolution soil moisture data into an integrated terrestrial model for a small-scale head-water catchment". In: *Water resources research* 55.12, pp. 10358–10385.

Gebler, Sebastian, H-J Hendricks Franssen, SJ Kollet, Wei Qu, and H Vereecken (2017). "High resolution modelling of soil moisture patterns with TerrSysMP: A comparison with sensor network data". In: *Journal of hydrology* 547, pp. 309–331.

Gevaert, Anouk I, Luigi J Renzullo, Albert IJM Van Dijk, Hans J Van Der Woerd, Albrecht H Weerts, and Richard AM De Jeu (2018). "Joint assimilation of soil moisture retrieved from multiple passive microwave frequencies increases robustness of soil moisture state estimation". In: *Hydrology and Earth System Sciences* 22.9, pp. 4605–4619.

Gleeson, Tom and Andrew H Manning (2008). "Regional groundwater flow in mountainous terrain: Three-dimensional simulations of topographic and hydrogeologic controls". In: *Water Resources Research* 44.10.

Gleeson, Tom, Leslie Smith, Nils Moosdorf, Jens Hartmann, Hans H Dürr, Andrew H Manning, Ludovicus PH van Beek, and A Mark Jellinek (2011). "Mapping permeability over the surface of the Earth". In: *Geophysical Research Letters* 38.2.

Green, Julia K, Sonia I Seneviratne, Alexis M Berg, Kirsten L Findell, Stefan Hagemann, David M Lawrence, and Pierre Gentine (2019). "Large influence of soil moisture on long-term terrestrial carbon uptake". In: *Nature* 565.7740, pp. 476–479.

Grillakis, Manolis G (2019). "Increase in severe and extreme soil moisture droughts for Europe under climate change". In: *Science of the Total Environment* 660, pp. 1245–1255.

Gruber, Alexander, Gabrielle De Lannoy, Clément Albergel, Amen Al-Yaari, Luca Brocca, J-C Calvet, Andreas Colliander, Michael Cosh, Wade Crow, Wouter Dorigo, et al. (2020). "Validation practices for satellite soil moisture retrievals: What are (the) errors?" In: *Remote sensing of environment* 244, p. 111806.

Gruber, Alexander, Wouter Arnoud Dorigo, Wade Crow, and Wolfgang Wagner (2017). "Triple collocation-based merging of satellite soil moisture retrievals". In: *IEEE Transactions on Geoscience and Remote Sensing* 55.12, pp. 6780–6792.

Gruber, Alexander, Tracy Scanlon, Robin van der Schalie, Wolfgang Wagner, and Wouter Dorigo (2019). "Evolution of the ESA CCI Soil Moisture climate data records and their underlying merging methodology". In: *Earth System Science Data* 11.2, pp. 717–739.

Gruber, Alexander, C-H Su, Simon Zwieback, Wade Crow, Wouter Dorigo, and Wolfgang Wagner (2016). "Recent advances in (soil moisture) triple collocation analysis". In: *International Journal of Applied Earth Observation and Geoinformation* 45, pp. 200–211.

H2020_eLTER_Project Team (2019). *Vielsalm Terrestrial Observatory - Regional climate model data from EURO-CORDEX for the eLTER project*. Data set. DOI: 10.23728/B2SHARE.FD9504653B6D4D0292A351C9E38C4530. URL: https://b2share.eudat.eu.

Haitjema, Henk M and Sherry Mitchell-Bruker (2005). "Are water tables a subdued replica of the topography?" In: *Groundwater* 43.6, pp. 781–786.

Han, Xujun, Harrie-Jan Hendricks Franssen, Carsten Montzka, and Harry Vereecken (2014). "Soil moisture and soil properties estimation in the Community Land Model with synthetic brightness temperature observations". In: *Water resources research* 50.7, pp. 6081–6105.

Han, Xujun, Harrie-Jan Hendricks Franssen, Xin Li, Yanlin Zhang, Carsten Montzka, and Harry Vereecken (2013). "Joint assimilation of surface temperature and L-band microwave brightness temperature in land data assimilation". In: *Vadose Zone Journal* 12.3, vzj2012–0072.

Hanson, Blaine (2009). "Field Estimation of Soil Water Content: A Practical Guide to Methods, Instrumentation and Sensor Technology". In: *Vadose Zone Journal* 8.3, pp. 628–628. DOI: https://doi.org/10.2136/vzj2008.0171. eprint: https://acsess.onlinelibrary.wiley.com/doi/pdf/10.2136/vzj2008.0171. URL: https://acsess.onlinelibrary.wiley.com/doi/abs/10.2136/vzj2008.0171.

Hartley, AJ, N MacBean, Goran Georgievski, and Sophie Bontemps (2017). "Uncertainty in plant functional type distributions and its impact on land surface models". In: *Remote Sensing of Environment* 203, pp. 71–89.

Hasan, Sayeh, Carsten Montzka, Christoph Rüdiger, Muhammad Ali, Heye R Bogena, and Harry Vereecken (2014). "Soil moisture retrieval from airborne L-band passive microwave using high resolution multispectral data". In: *ISPRS journal of photogrammetry and remote sensing* 91, pp. 59–71.

Havranek, Wilhelm Manfred and Udo Benecke (1978). "The influence of soil moisture on water potential, transpiration and photosynthesis of conifer seedlings". In: *Plant and Soil* 49, pp. 91–103.

Henderson-Sellers, A (1996). "Soil moisture: A critical focus for global change studies". In: *Global and Planetary Change* 13.1-4, pp. 3–9.

Hendricks Franssen, Harrie-Jan and W Kinzelbach (2008). "Real-time groundwater flow modeling with the ensemble Kalman filter: Joint estimation of states and parameters and the filter inbreeding problem". In: *Water resources research* 44.9.

Hengl, Tomislav, Jorge Mendes De Jesus, Robert A MacMillan, Niels H Batjes, Gerard BM Heuvelink, Eloi Ribeiro, Alessandro Samuel-Rosa, Bas Kempen, Johan GB Leenaars, Markus G Walsh, et al. (2014). "SoilGrids1km–global soil information based on automated mapping". In: *PloS one* 9.8, e105992.

Hengl, Tomislav, Jorge Mendes de Jesus, Gerard BM Heuvelink, Maria Ruiperez Gonzalez, Milan Kilibarda, Aleksandar Blagotić, Wei Shangguan, Marvin N Wright, Xiaoyuan Geng, Bernhard Bauer-Marschallinger, et al. (2017). "SoilGrids250m: Global gridded soil information based on machine learning". In: *PLoS one* 12.2, e0169748.

Herrmann, Frank, Luise Keller, Ralf Kunkel, Harry Vereecken, and Frank Wendland (2015). "Determination of spatially differentiated water balance components including groundwater recharge on the Federal State level–A case study using the mGROWA model in North Rhine-Westphalia (Germany)". In: *Journal of Hydrology: Regional Studies* 4, pp. 294–312.

Heyvaert, Zdenko, Samuel Scherrer, Wouter Dorigo, Michel Bechtold, and Gabriëlle De Lannoy (2024). "Joint assimilation of satellite-based surface soil moisture and vegetation conditions into the Noah-MP land surface model". In: *Science of Remote Sensing* 9, p. 100129.

Hidayat, Hidayat, Adriaan J Teuling, Bart Vermeulen, Muh Taufik, Karl Kastner, Tjitske J Geertsema, Dinja CC Bol, Dirk H Hoekman, Gadis Sri Haryani, Henny AJ Van Lanen, et al. (2017). "Hydrology of inland tropical lowlands: The Kapuas and Mahakam wetlands". In: *Hydrology and earth system sciences* 21.5, pp. 2579–2594.

Hochreiter, Sepp and Jürgen Schmidhuber (1997). "Long Short-Term Memory". In: *Neural Computation* 9.8, pp. 1735–1780.

Holtzman, Nataniel M, Tamlin M Pavelsky, Jonathan S Cohen, Melissa L Wrzesien, and Jonathan D Herman (2020). "Tailoring WRF and Noah-MP to improve process representation of Sierra Nevada runoff: Diagnostic evaluation and applications". In: *Journal of Advances in Modeling Earth Systems* 12.3, e2019MS001832.

Hossain, Faisal and Emmanouil N Anagnostou (2005). "Numerical investigation of the impact of uncertainties in satellite rainfall estimation and land surface model parameters on simulation of soil moisture". In: *Advances in Water Resources* 28.12, pp. 1336–1350.

Hostache, Renaud, Dominik Rains, Kaniska Mallick, Marco Chini, Ramona Pelich, Hans Lievens, Fabrizio Fenicia, Giovanni Corato, Niko EC Verhoest, and Patrick Matgen (2020). "Assimilation of Soil Moisture and Ocean Salinity (SMOS) brightness temperature into a large-scale distributed conceptual hydrological model to improve soil moisture predictions: the Murray–Darling basin in Australia as a test case". In: *Hydrology and Earth System Sciences* 24.10, pp. 4793–4812.

Houser, Paul R, W James Shuttleworth, James S Famiglietti, Hoshin V Gupta, Kamran H Syed, and David C Goodrich (1998). "Integration of soil moisture remote sensing and hydrologic modeling using data assimilation". In: *Water resources research* 34.12, pp. 3405–3420.

Houtekamer, Peter L and Herschel L Mitchell (1998). "Data assimilation using an ensemble Kalman filter technique". In: *Monthly Weather Review* 126.3, pp. 796–811.

Howells, Owen D, George P Petropoulos, Prashant K Srivastava, Dimitrios Triantakonstantis, and Ionut Sandric (2021). "Exploring the potential of SCAT-SAR SWI for soil moisture retrievals at selected COSMOS-UK sites". In: *International Journal of Remote Sensing* 42.23, pp. 9155–9169.

Huang, Chunlin, Weijing Chen, Yan Li, Huanfeng Shen, and Xin Li (2016). "Assimilating multi-source data into land surface model to simultaneously improve estimations of soil moisture, soil temperature, and surface turbulent fluxes in irrigated fields". In: *Agricultural and Forest Meteorology* 230, pp. 142–156.

Huang, Chunlin, Xin Li, Ling Lu, and Juan Gu (2008). "Experiments of one-dimensional soil moisture assimilation system based on ensemble Kalman filter". In: *Remote sensing of environment* 112.3, pp. 888–900.

Hubbell, JM and JB Sisson (1998). "Advanced tensiometer for shallow or deep soil water potential measurements". In: *Soil Science* 163.4, pp. 271–277.

Hung, Ching Pui, Bernd Schalge, Gabriele Baroni, Harry Vereecken, and Harrie-Jan Hendricks Franssen (2022). "Assimilation of Groundwater Level and Soil Moisture Data in an Integrated Land Surface-Subsurface Model for Southwestern Germany". In: *Water Resources Research* 58.6, e2021WR031549.

Hunt, Brian R, Eric J Kostelich, and Istvan Szunyogh (2007). "Efficient data assimilation for spatiotemporal chaos: A local ensemble transform Kalman filter". In: *Physica D: Nonlinear Phenomena* 230.1-2, pp. 112–126.

Imaoka, K, M Kachi, M Kasahara, N Ito, K Nakagawa, and T Oki (2010). "Instrument performance and calibration of AMSR-E and AMSR2". In: *International archives of the photogrammetry, remote sensing and spatial information science* 38.8, pp. 13–18.

Imaoka, Keiji, Takashi Maeda, Misako Kachi, Marehito Kasahara, Norimasa Ito, and Keizo Nakagawa (2012). "Status of AMSR2 instrument on GCOM-W1". In: *Earth observing missions and sensors: Development, implementation, and characterization II*. Vol. 8528. SPIE, pp. 201–206.

Jackson, Thomas J, J Schmugge, and ET Engman (1996). "Remote sensing applications to hydrology: soil moisture". In: *Hydrological Sciences Journal* 41.4, pp. 517–530.

Jafarpour, Behnam and Mohammadali Tarrahi (2011). "Assessing the performance of the ensemble Kalman filter for subsurface flow data integration under variogram uncertainty". In: *Water Resources Research* 47.5.

Jakobi, J, JA Huisman, H Vereecken, B Diekkrüger, and HR Bogena (2018). "Cosmic ray neutron sensing for simultaneous soil water content and biomass quantification in drought conditions". In: *Water Resources Research* 54.10, pp. 7383–7402.

Janjić, Tijana, Niels Bormann, Marc Bocquet, JA Carton, Stephen E Cohn, Sarah L Dance, Svetlana N Losa, Nancy K Nichols, Roland Potthast, Joanne A Waller, et al. (2018). "On the representation error in data assimilation". In: *Quarterly Journal of the Royal Meteorological Society* 144.713, pp. 1257–1278.

Jha, Madan K, Alivia Chowdhury, VM Chowdary, and Stefan Peiffer (2007). "Groundwater management and development by integrated remote sensing and geographic information systems: prospects and constraints". In: *Water resources management* 21, pp. 427–467.

Ji, Peng, Xing Yuan, and Xin-Zhong Liang (2017). "Do lateral flows matter for the hyperresolution land surface modeling?" In: *Journal of Geophysical Research: Atmospheres* 122.22, pp. 12–077.

Ji, Xinye, Chaopeng Shen, and William J Riley (2015). "Temporal evolution of soil moisture statistical fractal and controls by soil texture and regional groundwater flow". In: *Advances in Water Resources* 86, pp. 155–169.

Johnson, Eduardo, José Yáñez, Cristian Ortiz, and José Muñoz (2010). "Evaporation from shallow groundwater in closed basins in the Chilean Altiplano". In: *Hydrological Sciences Journal–Journal des Sciences Hydrologiques* 55.4, pp. 624–635.

Kang, Jian, Rui Jin, and Xin Li (2021). "An advanced framework for merging remotely sensed soil moisture products at the regional scale supported by error structure analysis: A case study on the Tibetan Plateau". In: *IEEE Journal of Selected Topics in Applied Earth Observations and Remote Sensing* 14, pp. 3614–3624.

Karthikeyan, L and Ashok K Mishra (2021). "Multi-layer high-resolution soil moisture estimation using machine learning over the United States". In: *Remote Sensing of Environment* 266, p. 112706.

Karthikeyan, L, Ming Pan, Niko Wanders, D Nagesh Kumar, and Eric F Wood (2017). "Four decades of microwave satellite soil moisture observations: Part 1. A review of retrieval algorithms". In: *Advances in Water Resources* 109, pp. 106–120.

Kerr, Yann H, Philippe Waldteufel, J-P Wigneron, JAMJ Martinuzzi, Jordi Font, and Michael Berger (2001). "Soil moisture retrieval from space: The Soil Moisture and Ocean Salinity (SMOS) mission". In: *IEEE transactions on Geoscience and remote sensing* 39.8, pp. 1729–1735.

Kerr, Yann H, Philippe Waldteufel, Jean-Pierre Wigneron, Steven Delwart, François Cabot, Jacqueline Boutin, Maria-José Escorihuela, Jordi Font, Nicolas Reul, Claire Gruhier, et al. (2010). "The SMOS mission: New tool for monitoring key elements ofthe global water cycle". In: *Proceedings of the IEEE* 98.5, pp. 666–687.

Khaki, M, H-J Hendricks Franssen, and SC Han (2020). "Multi-mission satellite remote sensing data for improving land hydrological models via data assimilation". In: *Scientific reports* 10.1, p. 18791.

Kim, Hyunglok, Robert Parinussa, Alexandra G Konings, Wolfgang Wagner, Michael H Cosh, Venkat Lakshmi, Muhammad Zohaib, and Minha Choi (2018). "Global-scale assessment and combination of SMAP with ASCAT (active) and AMSR2 (passive) soil moisture products". In: *Remote Sensing of Environment* 204, pp. 260–275.

Kim, Jonggun and Binayak P Mohanty (2017). "A physically based hydrological connectivity algorithm for describing spatial patterns of soil moisture in the unsaturated zone". In: *Journal of Geophysical Research: Atmospheres* 122.4, pp. 2096–2114.

Kim, Seokhyeon, Robert M Parinussa, Yi Y Liu, Fiona M Johnson, and Ashish Sharma (2015). "A framework for combining multiple soil moisture retrievals based on maximizing temporal correlation". In: *Geophysical Research Letters* 42.16, pp. 6662–6670.

– (2016). "Merging alternate remotely-sensed soil moisture retrievals using a non-static model combination approach". In: *Remote Sensing* 8.6, p. 518.

Kim, Seokhyeon, Hung T Pham, Yi Y Liu, Lucy Marshall, and Ashish Sharma (2020). "Improving the combination of satellite soil moisture data sets by considering error cross correlation: A comparison between triple collocation (TC) and extended double instrumental variable (EIVD) alternatives". In: *IEEE transactions on Geoscience and remote sensing* 59.9, pp. 7285–7295.

Koch, Julian, Thomas Cornelissen, Zhufeng Fang, Heye Bogena, Bernd Diekkrüger, Stefan Kollet, and Simon Stisen (2016). "Inter-comparison of three distributed hydrological models with respect to seasonal variability of soil moisture patterns at a small forested catchment". In: *Journal of hydrology* 533, pp. 234–249.

Köhli, M, M Schrön, M Zreda, U Schmidt, P Dietrich, and S Zacharias (2015). "Footprint characteristics revised for field-scale soil moisture monitoring with cosmic-ray neutrons". In: *Water Resources Research* 51.7, pp. 5772–5790.

Kolassa, Jana, RH Reichle, and Clara S Draper (2017a). "Merging active and passive microwave observations in soil moisture data assimilation". In: *Remote sensing of environment* 191, pp. 117–130.

Kolassa, Jana, Rolf H Reichle, Qing Liu, Michael Cosh, David D Bosch, Todd G Caldwell, Andreas Colliander, Chandra Holifield Collins, Thomas J Jackson, Stan J Livingston, et al.

(2017b). “Data assimilation to extract soil moisture information from SMAP observations”. In: *Remote Sensing* 9.11, p. 1179.

Kollet, Stefan J and Reed M Maxwell (2006). “Integrated surface–groundwater flow modeling: A free-surface overland flow boundary condition in a parallel groundwater flow model”. In: *Advances in Water Resources* 29.7, pp. 945–958.

– (2008). “Capturing the influence of groundwater dynamics on land surface processes using an integrated, distributed watershed model”. In: *Water Resources Research* 44.2.

Kollet, Stefan J, Reed M Maxwell, Carol S Woodward, Steve Smith, Jan Vanderborght, Harry Vereecken, and Clemens Simmer (2010). “Proof of concept of regional scale hydrologic simulations at hydrologic resolution utilizing massively parallel computer resources”. In: *Water resources research* 46.4.

Konings, Alexandra G, Maria Piles, Narendra Das, and Dara Entekhabi (2017). “L-band vegetation optical depth and effective scattering albedo estimation from SMAP”. In: *Remote Sensing of Environment* 198, pp. 460–470.

Koster, Randal D, Paul A Dirmeyer, Zhichang Guo, Gordon Bonan, Edmond Chan, Peter Cox, CT Gordon, Shinjiro Kanae, Eva Kowalczyk, David Lawrence, et al. (2004). “Regions of strong coupling between soil moisture and precipitation”. In: *Science* 305.5687, pp. 1138–1140.

Koster, Randal D, Qing Liu, Sarith PP Mahanama, and Rolf H Reichle (2018). “Improved hydrological simulation using SMAP data: Relative impacts of model calibration and data assimilation”. In: *Journal of Hydrometeorology* 19.4, pp. 727–741.

Kreklow, Jennifer, Björn Tetzlaff, Benjamin Burkhard, and Gerald Kuhnt (2020). “Radar-based precipitation climatology in Germany–developments, uncertainties and potentials”. In: *Atmosphere* 11.2, p. 217.

Kumar, Sujay, Jana Kolassa, Rolf Reichle, Wade Crow, Gabrielle de Lannoy, Patricia de Rosnay, Natasha MacBean, Manuela Girotto, Andy Fox, Tristan Quaife, et al. (2022). “An agenda for land data assimilation priorities: Realizing the promise of terrestrial water, energy, and vegetation observations from space”. In: *Journal of Advances in Modeling Earth Systems* 14.11, e2022MS003259.

Kumar, Sujay V, Rolf H Reichle, Randal D Koster, Wade T Crow, and Christa D Peters-Lidard (2009). “Role of subsurface physics in the assimilation of surface soil moisture observations”. In: *Journal of hydrometeorology* 10.6, pp. 1534–1547.

Kumar, SV, CD Peters-Lidard, JA Santanello, RH Reichle, CS Draper, RD Koster, G Nearing, and MF Jasinski (2015). “Evaluating the utility of satellite soil moisture retrievals over irrigated areas and the ability of land data assimilation methods to correct for unmodeled processes”. In: *Hydrology and Earth System Sciences* 19.11, pp. 4463–4478.

Kurtz, Wolfgang, Guowei He, Stefan J Kollet, Reed M Maxwell, Harry Vereecken, and Harrie-Jan Hendricks Franssen (2016). “TerrSysMP–PDAF (version 1.0): a modular high-performance data assimilation framework for an integrated land surface–subsurface model”. In: *Geoscientific Model Development* 9.4, pp. 1341–1360.

Laguë, Marysa M, Gordon B Bonan, and Abigail LS Swann (2019). “Separating the impact of individual land surface properties on the terrestrial surface energy budget in both the coupled and uncoupled land–atmosphere system”. In: *Journal of Climate* 32.18, pp. 5725–5744.

Lahmers, Timothy M, Sujay V Kumar, Daniel Rosen, Aubrey Dugger, David J Gochis, Joseph A Santanello, Chandana Gangodagamage, and Rocky Dunlap (2022). “Assimilation of NASA’s Airborne Snow Observatory Snow Measurements for Improved Hydrological Modeling: A Case Study Enabled by the Coupled LIS/WRF-Hydro System”. In: *Water Resources Research* 58.3, e2021WR029867.

Larue, Fanny, Alain Royer, Danielle De Sève, Alexandre Roy, and Emmanuel Cosme (2018). “Assimilation of passive microwave AMSR-2 satellite observations in a snowpack evolution model over northeastern Canada”. In: *Hydrology and Earth System Sciences* 22.11, pp. 5711–5734.

Lawrence, David M, Rosie A Fisher, Charles D Koven, Keith W Oleson, Sean C Swenson, Gordon Bonan, Nathan Collier, Bardan Ghimire, Léo Van Kampenhout, Daniel Kennedy, et al. (2019). “The Community Land Model version 5: Description of new features, benchmarking, and impact of forcing uncertainty”. In: *Journal of Advances in Modeling Earth Systems* 11.12, pp. 4245–4287.

Li, Chengwei, Hui Lu, Kun Yang, Menglei Han, Jonathon S Wright, Yingying Chen, Le Yu, Shiming Xu, Xiaomeng Huang, and Wei Gong (2018a). "The evaluation of SMAP enhanced soil moisture products using high-resolution model simulations and in-situ observations on the Tibetan Plateau". In: *Remote Sensing* 10.4, p. 535.

Li, Fang, Heye Reemt Bogena, Bagher Bayat, Wolfgang Kurtz, and Harrie-Jan Hendricks Franssen (2024). "Can a Sparse Network of Cosmic Ray Neutron Sensors Improve Soil Moisture and Evapotranspiration Estimation at the Larger Catchment Scale?" In: *Water Resources Research* 60.1, e2023WR035056.

Li, Fang, Wolfgang Kurtz, Ching Pui Hung, Harry Vereecken, and Harrie-Jan Hendricks Franssen (2023). "Water table depth assimilation in integrated terrestrial system models at the larger catchment scale". In: *Frontiers in Water* 5, p. 1150999.

Li, Jianduo, Fei Chen, Guo Zhang, Michael Barlage, Yanjun Gan, Yufei Xin, and Chen Wang (2018b). "Impacts of land cover and soil texture uncertainty on land model simulations over the central Tibetan Plateau". In: *Journal of Advances in Modeling Earth Systems* 10.9, pp. 2121–2146.

Li, Liuyang, Qing Zhu, Ya Liu, Xiaoming Lai, and Kaihua Liao (2022). "Fusing satellite-based surface soil moisture products over a typical region with complex land surface characteristics". In: *Journal of Hydrology* 612, p. 128158.

Li, Qinghuan, Richard Kelly, Leena Leppänen, Juho Vehviläinen, Anna Kontu, Juha Lemmetyinen, and Jouni Pulliainen (2019). "The influence of thermal properties and canopy-intercepted snow on passive microwave transmissivity of a scots pine". In: *IEEE Transactions on Geoscience and Remote Sensing* 57.8, pp. 5424–5433.

Liang, Xu, Zhenghui Xie, and Maoyi Huang (2003). "A new parameterization for surface and groundwater interactions and its impact on water budgets with the variable infiltration capacity (VIC) land surface model". In: *Journal of Geophysical Research: Atmospheres* 108.D16.

Lievens, Hans, GJM De Lannoy, A Al Bitar, M Drusch, G Dumedah, H-J Hendricks Franssen, YH Kerr, S Kumar Tomer, Brecht Martens, Olivier Merlin, et al. (2016). "Assimilation of SMOS soil moisture and brightness temperature products into a land surface model". In: *Remote sensing of environment* 180, pp. 292–304.

Lievens, Hans, Brecht Martens, NEC Verhoest, S Hahn, RH Reichle, and D Gonzalez Miralles (2017a). "Assimilation of global radar backscatter and radiometer brightness temperature observations to improve soil moisture and land evaporation estimates". In: *Remote Sensing of Environment* 189, pp. 194–210.

Lievens, Hans, Rolf H Reichle, Qing Liu, Gabrielle JM De Lannoy, R Scott Dunbar, SB Kim, Narendra N Das, M Cosh, Jeffrey P Walker, and Wolfgang Wagner (2017b). "Joint Sentinel-1 and SMAP data assimilation to improve soil moisture estimates". In: *Geophysical research letters* 44.12, pp. 6145–6153.

Lievens, Hans, Sat Kumar Tomer, Ahmad Al Bitar, Gabriëlle JM De Lannoy, Matthias Drusch, Gift Dumedah, H-J Hendricks Franssen, Yann Henry Kerr, Brecht Martens, Ming Pan, et al. (2015). "SMOS soil moisture assimilation for improved hydrologic simulation in the Murray Darling Basin, Australia". In: *Remote Sensing of Environment* 168, pp. 146–162.

Liu, H, TW Lei, J Zhao, CP Yuan, YT Fan, and LQ Qu (2011a). "Effects of rainfall intensity and antecedent soil water content on soil infiltrability under rainfall conditions using the run off-on-out method". In: *Journal of Hydrology* 396.1-2, pp. 24–32.

Liu, Pang-Wei, Tara Bongiovanni, Alejandro Monsivais-Huertero, Jasmeet Judge, Susan Steele-Dunne, Rajat Bindlish, and Thomas J Jackson (2016). "Assimilation of active and passive microwave observations for improved estimates of soil moisture and crop growth". In: *IEEE Journal of Selected Topics in Applied Earth Observations and Remote Sensing* 9.4, pp. 1357–1369.

Liu, Y Y, Wouter A Dorigo, RM Parinussa, Richard AM de Jeu, Wolfgang Wagner, Matthew F McCabe, JP Evans, and AIJM Van Dijk (2012). "Trend-preserving blending of passive and active microwave soil moisture retrievals". In: *Remote sensing of environment* 123, pp. 280–297.

Liu, Yi Y, RM Parinussa, Wouter A Dorigo, Richard AM De Jeu, Wolfgang Wagner, AIJM Van Dijk, Matthew F McCabe, and JP Evans (2011b). "Developing an improved soil moisture dataset by blending passive and active microwave satellite-based retrievals". In: *Hydrology and Earth System Sciences* 15.2, pp. 425–436.

Loizu, Javier, Christian Massari, Jesús Álvarez-Mozos, Angelica Tarpanelli, Luca Brocca, and Javier Casalí (2018). "On the assimilation set-up of ASCAT soil moisture data for improving streamflow catchment simulation". In: *Advances in Water Resources* 111, pp. 86–104.

Lorenz, Ruth, Eric B Jaeger, and Sonia I Seneviratne (2010). "Persistence of heat waves and its link to soil moisture memory". In: *Geophysical Research Letters* 37.9.

Lu, Yang, Jianzhi Dong, and Susan C Steele-Dunne (2019). "Impact of soil moisture data resolution on soil moisture and surface heat flux estimates through data assimilation: a case study in the southern Great Plains". In: *Journal of Hydrometeorology* 20.4, pp. 715–730.

Lu, Yang, Susan C Steele-Dunne, and Gabriëlle JM De Lannoy (2020). "Improving soil moisture and surface turbulent heat flux estimates by assimilation of SMAP brightness temperatures or soil moisture retrievals and GOES land surface temperature retrievals". In: *Journal of Hydrometeorology* 21.2, pp. 183–203.

Ma, Hongliang, Xiaojun Li, Jiangyuan Zeng, Xiang Zhang, Jianzhi Dong, Nengcheng Chen, Lei Fan, Morteza Sadeghi, Frédéric Frappart, Xiangzhuo Liu, et al. (2023). "An assessment of L-band surface soil moisture products from SMOS and SMAP in the tropical areas". In: *Remote Sensing of Environment* 284, p. 113344.

Ma, Hongliang, Jiangyuan Zeng, Nengcheng Chen, Xiang Zhang, Michael H Cosh, and Wei Wang (2019). "Satellite surface soil moisture from SMAP, SMOS, AMSR2 and ESA CCI: A comprehensive assessment using global ground-based observations". In: *Remote Sensing of Environment* 231, p. 111215.

Martens, Brecht, Diego Miralles, Hans Lievens, D Fernández-Prieto, and Niko EC Verhoest (2016). "Improving terrestrial evaporation estimates over continental Australia through assimilation of SMOS soil moisture". In: *International Journal of Applied Earth Observation and Geoinformation* 48, pp. 146–162.

Martínez-de la Torre, Alberto and Gonzalo Miguez-Macho (2019). "Groundwater influence on soil moisture memory and land–atmosphere fluxes in the Iberian Peninsula". In: *Hydrology and Earth System Sciences* 23.12, pp. 4909–4932.

Maxwell, Reed M (2013). "A terrain-following grid transform and preconditioner for parallel, large-scale, integrated hydrologic modeling". In: *Advances in Water Resources* 53, pp. 109–117.

Maxwell, Reed M, Fotini Katopodes Chow, and Stefan J Kollet (2007). "The groundwater–land-surface–atmosphere connection: Soil moisture effects on the atmospheric boundary layer in fully-coupled simulations". In: *Advances in Water Resources* 30.12, pp. 2447–2466.

Maxwell, Reed M and Laura E Condon (2016). "Connections between groundwater flow and transpiration partitioning". In: *Science* 353.6297, pp. 377–380.

Maxwell, Reed M and Norman L Miller (2005). "Development of a coupled land surface and groundwater model". In: *Journal of Hydrometeorology* 6.3, pp. 233–247.

Maxwell, RM, LE Condon, and SJ Kollet (2015). "A high-resolution simulation of groundwater and surface water over most of the continental US with the integrated hydrologic model ParFlow v3". In: *Geoscientific model development* 8.3, pp. 923–937.

McColl, Kaighin A, Jur Vogelzang, Alexandra G Konings, Dara Entekhabi, María Piles, and Ad Stoffelen (2014). "Extended triple collocation: Estimating errors and correlation coefficients with respect to an unknown target". In: *Geophysical research letters* 41.17, pp. 6229–6236.

Ni-Meister, Wenge (2008). "Recent advances on soil moisture data assimilation". In: *Physical Geography* 29.1, pp. 19–37.

Mialon, Arnaud, Laurent Coret, Yann H Kerr, François Sécherre, and Jean-Pierre Wigneron (2008). "Flagging the topographic impact on the SMOS signal". In: *IEEE Transactions on Geoscience and Remote Sensing* 46.3, pp. 689–694.

Milly, PCD (1987). "Estimation of Brooks-Corey parameters from water retention data". In: *Water Resources Research* 23.6, pp. 1085–1089.

Min, Xiaoxiao, Yulin Shangguan, Danlu Li, and Zhou Shi (2022). "Improving the fusion of global soil moisture datasets from SMAP, SMOS, ASCAT, and MERRA2 by considering the non-zero error covariance". In: *International Journal of Applied Earth Observation and Geoinformation* 113, p. 103016.

Minamide, Masashi and Fuqing Zhang (2017). "Adaptive observation error inflation for assimilating all-sky satellite radiance". In: *Monthly Weather Review* 145.3, pp. 1063–1081.

Mishra, Vikalp, W Lee Ellenburg, Robert E Griffin, John R Mecikalski, James F Cruise, Christopher R Hain, and Martha C Anderson (2018). "An initial assessment of a SMAP soil moisture

disaggregation scheme using TIR surface evaporation data over the continental United States". In: *International journal of applied earth observation and geoinformation* 68, pp. 92–104.
Mohanty, Binayak P, Michael H Cosh, Venkat Lakshmi, and Carsten Montzka (2017). "Soil moisture remote sensing: State-of-the-science". In: *Vadose Zone Journal* 16.1, pp. 1–9.
Montzka, Carsten, Heye R Bogena, Michael Herbst, Michael H Cosh, Thomas Jagdhuber, and Harry Vereecken (2020). "Estimating the number of reference sites necessary for the validation of global soil moisture products". In: *IEEE geoscience and remote sensing letters* 18.9, pp. 1530–1534.
Montzka, Carsten, Heye R Bogena, Marek Zreda, Alessandra Monerris, Ross Morrison, Sekhar Muddu, and Harry Vereecken (2017). "Validation of spaceborne and modelled surface soil moisture products with cosmic-ray neutron probes". In: *Remote sensing* 9.2, p. 103.
Montzka, Carsten, Jennifer P Grant, Hamid Moradkhani, Harrie-Jan Hendricks Franssen, Lutz Weihermüller, Matthias Drusch, and Harry Vereecken (2013). "Estimation of radiative transfer parameters from L-band passive microwave brightness temperatures using advanced data assimilation". In: *Vadose Zone Journal* 12.3.
Montzka, Carsten, Thomas Jagdhuber, Ralf Horn, Heye R Bogena, Irena Hajnsek, Andreas Reigber, and Harry Vereecken (2016). "Investigation of SMAP fusion algorithms with airborne active and passive L-band microwave remote sensing". In: *IEEE Transactions on Geoscience and Remote Sensing* 54.7, pp. 3878–3889.
Montzka, Carsten, Hamid Moradkhani, Lutz Weihermüller, Harrie-Jan Hendricks Franssen, Morton Canty, and Harry Vereecken (2011). "Hydraulic parameter estimation by remotely-sensed top soil moisture observations with the particle filter". In: *Journal of hydrology* 399.3-4, pp. 410–421.
Montzka, Carsten, Valentijn RN Pauwels, Harrie-Jan Hendricks Franssen, Xujun Han, and Harry Vereecken (2012). "Multivariate and multiscale data assimilation in terrestrial systems: A review". In: *Sensors* 12.12, pp. 16291–16333.
Mousa, BG and Hong Shu (2020a). "Spatial evaluation and assimilation of SMAP, SMOS, and ASCAT satellite soil moisture products over Africa using statistical techniques". In: *Earth and Space Science* 7.1, e2019EA000841.
Mousa, BG, Hong Shu, Mohamed Freeshah, and Aqil Tariq (2020b). "A novel scheme for merging active and passive satellite soil moisture retrievals based on maximizing the signal to noise ratio". In: *Remote Sensing* 12.22, p. 3804.
Nair, Akhilesh S and J Indu (2019). "Improvement of land surface model simulations over India via data assimilation of satellite-based soil moisture products". In: *Journal of Hydrology* 573, pp. 406–421.
Nair, Akhilesh S, Rohit Mangla, Thiruvengadam P, and J Indu (2022). "Remote sensing data assimilation". In: *Hydrological Sciences Journal* 67.16, pp. 2457–2489.
Naz, Bibi S, Wolfgang Kurtz, Carsten Montzka, Wendy Sharples, Klaus Goergen, Jessica Keune, Huilin Gao, Anne Springer, Harrie-Jan Hendricks Franssen, and Stefan Kollet (2019). "Improving soil moisture and runoff simulations at 3 km over Europe using land surface data assimilation". In: *Hydrology and earth system sciences* 23.1, pp. 277–301.
Naz, Bibi S, Wendy Sharples, Yueling Ma, Klaus Goergen, and Stefan Kollet (2023). "Continental-scale evaluation of a fully distributed coupled land surface and groundwater model, ParFlow-CLM (v3. 6.0), over Europe". In: *Geoscientific Model Development* 16.6, pp. 1617–1639.
Nearing, Grey S, David M Mocko, Christa D Peters-Lidard, Sujay V Kumar, and Youlong Xia (2016). "Benchmarking NLDAS-2 soil moisture and evapotranspiration to separate uncertainty contributions". In: *Journal of hydrometeorology* 17.3, pp. 745–759.
Nearing, Grey S, Benjamin L Ruddell, Martyn P Clark, Bart Nijssen, and Christa Peters-Lidard (2018). "Benchmarking and process diagnostics of land models". In: *Journal of Hydrometeorology* 19.11, pp. 1835–1852.
Nerger, Lars and Wolfgang Hiller (2013). "Software for ensemble-based data assimilation systems-Implementation strategies and scalability". In: *Computers & Geosciences* 55, pp. 110–118.
Nerger, Lars, Wolfgang Hiller, and Jens Schröter (2005). "PDAF-the parallel data assimilation framework: experiences with Kalman filtering". In: *Use of high performance computing in meteorology*. World Scientific, pp. 63–83.
Nguyen, Thu Thuy, Huu Hao Ngo, Wenshan Guo, Soon Woong Chang, Dinh Duc Nguyen, Chi Trung Nguyen, Jian Zhang, Shuang Liang, Xuan Thanh Bui, and Ngoc Bich Hoang (2022).

"A low-cost approach for soil moisture prediction using multi-sensor data and machine learning algorithm". In: *Science of The Total Environment* 833, p. 155066.

Nie, Wanshu, Sujay V Kumar, Kristi R Arsenault, Christa D Peters-Lidard, Iliana E Mladenova, Karim Bergaoui, Abheera Hazra, Benjamin F Zaitchik, Sarith P Mahanama, Rachael McDonnell, et al. (2022). "Towards effective drought monitoring in the Middle East and North Africa (MENA) region: implications from assimilating leaf area index and soil moisture into the Noah-MP land surface model for Morocco". In: *Hydrology and Earth System Sciences* 26.9, pp. 2365–2386.

Niu, Guo-Yue, Claudio Paniconi, Peter A Troch, Russell L Scott, Matej Durcik, Xubin Zeng, Travis Huxman, and David C Goodrich (2014a). "An integrated modelling framework of catchment-scale ecohydrological processes: 1. Model description and tests over an energy-limited watershed". In: *Ecohydrology* 7.2, pp. 427–439.

– (2014b). "An integrated modelling framework of catchment-scale ecohydrological processes: 1. Model description and tests over an energy-limited watershed". In: *Ecohydrology* 7.2, pp. 427–439.

Niu, Guo-Yue, Peter A Troch, Claudio Paniconi, Russell L Scott, Matej Durcik, Xubin Zeng, Travis Huxman, David Goodrich, and Jon Pelletier (2014c). "An integrated modelling framework of catchment-scale ecohydrological processes: 2. The role of water subsidy by overland flow on vegetation dynamics in a semi-arid catchment". In: *Ecohydrology* 7.2, pp. 815–827.

Njoku, Eni G, Thomas J Jackson, Venkat Lakshmi, Tsz K Chan, and Son V Nghiem (2003). "Soil moisture retrieval from AMSR-E". In: *IEEE transactions on Geoscience and remote sensing* 41.2, pp. 215–229.

Nousu, Jari-Pekka, Kersti Leppä, Hannu Marttila, Pertti Ala-Aho, Giulia Mazzotti, Terhikki Manninen, Mika Korkiakoski, Mika Aurela, Annalea Lohila, and Samuli Launiainen (2024). "Multi-scale soil moisture data and process-based modeling reveal the importance of lateral groundwater flow in a subarctic catchment". In: *Hydrology and Earth System Sciences* 28.20, pp. 4643–4666.

O'neill, Mary MF, Danielle T Tijerina, Laura E Condon, and Reed M Maxwell (2021). "Assessment of the ParFlow–CLM CONUS 1.0 integrated hydrologic model: evaluation of hyper-resolution water balance components across the contiguous United States". In: *Geoscientific Model Development* 14.12, pp. 7223–7254.

O'Neill, P. E., S. Chan, E. G. Njoku, T. Jackson, R. Bindlish, J. Chaubell, and A. Colliander (2021). *SMAP Enhanced L3 Radiometer Global and Polar Grid Daily 9 km EASE-Grid Soil Moisture, Version 5*. Accessed Jul.1,2023. DOI: 10.5067/4DQ54OUIJ9DL. URL: https://nsidc.org/data/SPL3SMP%5C_E/versions/5.

O'Neill, Peggy, S Chan, Rajat Bindlish, T Jackson, Andreas Colliander, S Dunbar, Fan Chen, Jeffrey Piepmeier, Simon Yueh, Dara Entekhabi, et al. (2017). "Assessment of version 4 of the SMAP passive soil moisture standard product". In: *2017 IEEE International Geoscience and Remote Sensing Symposium (IGARSS)*. IEEE, pp. 3941–3944.

O'Neill, Peggy, Dara Entekhabi, Eni Njoku, and Kent Kellogg (2010). "The NASA soil moisture active passive (SMAP) mission: Overview". In: *2010 IEEE International Geoscience and Remote Sensing Symposium*. IEEE, pp. 3236–3239.

Ochoa, Carlos G, Alexander G Fernald, Steven J Guldan, and Manoj K Shukla (2009). "Water movement through a shallow vadose zone: A field irrigation experiment". In: *Vadose Zone Journal* 8.2, pp. 414–425.

Oleson, Keith, Yongjiu Dai, B Bonan, Mike Bosilovichm, Robert Dickinson, Paul Dirmeyer, Forrest Hoffman, Paul Houser, Samuel Levis, Guo-Yue Niu, et al. (2004). "Technical description of the community land model (CLM)". In: *NCAR Tech. Note NCAR/TN-478+ STR*.

Oleson, Keith W, David M Lawrence, GB Bonan, Beth Drewniak, Maoyi Huang, CD Koven, Samuel Levis, Fang Li, William J Riley, Zachary M Subin, et al. (2010). "Technical description of version 4.0 of the Community Land Model (CLM)". In: *NCAR Tech. Note NCAR/TN-478+ STR* 257, pp. 1–257.

Oleson, KW, G-Y Niu, Z-L Yang, DM Lawrence, PE Thornton, PJ Lawrence, R Stöckli, RE Dickinson, GB Bonan, Samuel Levis, et al. (2008). "Improvements to the Community Land Model and their impact on the hydrological cycle". In: *Journal of Geophysical Research: Biogeosciences* 113.G1.

Olson, Roman, Tomoko Nitta, and Kei Yoshimura (2024). "A fast physically-guided emulator of MATSIRO land surface model". In: *Journal of Hydrology* 634, p. 131093.

Ott, Edward, Brian R Hunt, Istvan Szunyogh, Aleksey V Zimin, Eric J Kostelich, Matteo Corazza, Eugenia Kalnay, DJ Patil, and James A Yorke (2004). "A local ensemble Kalman filter for atmospheric data assimilation". In: *Tellus A: Dynamic Meteorology and Oceanography* 56.5, pp. 415–428.

Owe, Manfred and Richard de Jeu (2014). *AMSR2/GCOM-W1 surface soil moisture (LPRM) L3 1 day 25 km x 25 km descending V001, Edited by Goddard Earth Sciences Data and Information Services Center (GES DISC) (Bill Teng)*. Accessed Jul.1,2023. DOI: 10.5067/CGDEOBASZ178. URL: https://disc.gsfc.nasa.gov/datasets/LPRM%5C_AMSR2%5C_D%5C_SOILM3%5C_001/summary.

Owe, Manfred, Richard de Jeu, and Thomas Holmes (2008). "Multisensor historical climatology of satellite-derived global land surface moisture". In: *Journal of Geophysical Research: Earth Surface* 113.F1.

Pan, Ming, Xitian Cai, Nathaniel W Chaney, Dara Entekhabi, and Eric F Wood (2016). "An initial assessment of SMAP soil moisture retrievals using high-resolution model simulations and in situ observations". In: *Geophysical Research Letters* 43.18, pp. 9662–9668.

Parinussa, Robert M, Thomas RH Holmes, Niko Wanders, Wouter A Dorigo, and Richard AM de Jeu (2015). "A preliminary study toward consistent soil moisture from AMSR2". In: *Journal of Hydrometeorology* 16.2, pp. 932–947.

Park, Chang-Hwan, Carsten Montzka, Thomas Jagdhuber, François Jonard, Gabrielle De Lannoy, Jinkyu Hong, Thomas J Jackson, and Volker Wulfmeyer (2019). "A dielectric mixing model accounting for soil organic matter". In: *Vadose Zone Journal* 18.1, p. 190036.

Pastorello, Gilberto, Carlo Trotta, Eleonora Canfora, Housen Chu, Danielle Christianson, You-Wei Cheah, Cristina Poindexter, Jiquan Chen, Abdelrahman Elbashandy, Marty Humphrey, et al. (2020). "The FLUXNET2015 dataset and the ONEFlux processing pipeline for eddy covariance data". In: *Scientific data* 7.1, pp. 1–27.

Pathiraja, Sahani, Daniela Anghileri, Paolo Burlando, Ashish Sharma, Lucy Marshall, and Hamid Moradkhani (2018). "Insights on the impact of systematic model errors on data assimilation performance in changing catchments". In: *Advances in Water Resources* 113, pp. 202–222.

Patil, Amol and RAAJ Ramsankaran (2018). "Improved streamflow simulations by coupling soil moisture analytical relationship in EnKF based hydrological data assimilation framework". In: *Advances in Water Resources* 121, pp. 173–188.

Peng, Jian, Maliko Tanguy, Emma L Robinson, Ewan Pinnington, Jonathan Evans, Rich Ellis, Elizabeth Cooper, Jamie Hannaford, Eleanor Blyth, and Simon Dadson (2021). "Estimation and evaluation of high-resolution soil moisture from merged model and Earth observation data in the Great Britain". In: *Remote Sensing of Environment* 264, p. 112610.

Peters-Lidard, Christa D, Sujay V Kumar, David M Mocko, and Yudong Tian (2011). "Estimating evapotranspiration with land data assimilation systems". In: *Hydrological Processes* 25.26, pp. 3979–3992.

Pinnington, Ewan, Javier Amezcua, Elizabeth Cooper, Simon Dadson, Rich Ellis, Jian Peng, Emma Robinson, Ross Morrison, Simon Osborne, and Tristan Quaife (2021). "Improving soil moisture prediction of a high-resolution land surface model by parameterising pedotransfer functions through assimilation of SMAP satellite data". In: *Hydrology and Earth System Sciences* 25.3, pp. 1617–1641.

Pinnington, Ewan, Tristan Quaife, and Emily Black (2018). "Impact of remotely sensed soil moisture and precipitation on soil moisture prediction in a data assimilation system with the JULES land surface model". In: *Hydrology and Earth System Sciences* 22.4, pp. 2575–2588.

Pleim, Jonathan E and Aijun Xiu (2003). "Development of a land surface model. Part II: Data assimilation". In: *Journal of Applied Meteorology* 42.12, pp. 1811–1822.

Poggio, Laura, Luis M De Sousa, Niels H Batjes, Gerard Heuvelink, Bas Kempen, Eloi Ribeiro, and David Rossiter (2021). "SoilGrids 2.0: producing soil information for the globe with quantified spatial uncertainty". In: *Soil* 7.1, pp. 217–240.

Prakash, Ved and Vimal Mishra (2023). "Soil moisture and streamflow data assimilation for streamflow prediction in the Narmada River Basin". In: *Journal of Hydrometeorology* 24.8, pp. 1377–1392.

Preimesberger, Wolfgang, Tracy Scanlon, Chun-Hsu Su, Alexander Gruber, and Wouter Dorigo (2020). "Homogenization of structural breaks in the global ESA CCI soil moisture multisatellite climate data record". In: *IEEE Transactions on Geoscience and Remote Sensing* 59.4, pp. 2845–2862.

R.B.Myneni, Y.Knyazikhin, T. Park. (2015). *MCD15A2H MODIS/Terra+Aqua Leaf Area Index/FPAR 8-day L4 Global 500m SIN Grid V006 [Data set]*. Accessed Jul.1,2023. DOI: 10.5067/MODIS/MCD15A2H.006. URL: https://doi.org/10.5067/MODIS/MCD15A2H.006.

Rahman, Azbina, Viviana Maggioni, Xinxuan Zhang, Paul Houser, Timothy Sauer, and David M Mocko (2022). "The joint assimilation of remotely sensed leaf area index and surface soil moisture into a land surface model". In: *Remote Sensing* 14.3, p. 437.

Rahman, M, M Sulis, and SJ Kollet (2015). "The subsurface–land surface–atmosphere connection under convective conditions". In: *Advances in water resources* 83, pp. 240–249.

Rahmati, Mehdi, Anna Balenzano, Michel Bechtold, Luca Brocca, Anke Fluhrer, Thomas Jagdhuber, Kleanthis Karamvasis, David Mengen, Rolf H Reichle, Seung-bum Kim, et al. (2026). "Soil moisture retrieval from Sentinel-1: Lessons learned after more than a decade in orbit". In: *Remote Sensing of Environment* 333, p. 115146.

Rajkai, K_ and BE Ryden (1992). "Measuring areal soil moisture distribution with the TDR method". In: *Geoderma* 52.1-2, pp. 73–85.

Reichle, RH, WT Crow, RD Koster, HO Sharif, and SPP Mahanama (2008a). "Contribution of soil moisture retrievals to land data assimilation products". In: *Geophysical Research Letters* 35.1.

Reichle, Rolf H (2008). "Data assimilation methods in the Earth sciences". In: *Advances in water resources* 31.11, pp. 1411–1418.

Reichle, Rolf H, Wade T Crow, and Christian L Keppenne (2008b). "An adaptive ensemble Kalman filter for soil moisture data assimilation". In: *Water resources research* 44.3.

Reichle, Rolf H, Gabrielle JM De Lannoy, Qing Liu, Joseph V Ardizzone, Andreas Colliander, Austin Conaty, Wade Crow, Thomas J Jackson, Lucas A Jones, John S Kimball, et al. (2017). "Assessment of the SMAP level-4 surface and root-zone soil moisture product using in situ measurements". In: *Journal of hydrometeorology* 18.10, pp. 2621–2645.

Reichle, Rolf H and Randal D Koster (2003). "Assessing the impact of horizontal error correlations in background fields on soil moisture estimation". In: *Journal of Hydrometeorology* 4.6, pp. 1229–1242.

– (2004). "Bias reduction in short records of satellite soil moisture". In: *Geophysical Research Letters* 31.19.

Reichle, Rolf H, Sujay V Kumar, Sarith PP Mahanama, Randal D Koster, and Qing Liu (2010). "Assimilation of satellite-derived skin temperature observations into land surface models". In: *Journal of Hydrometeorology* 11.5, pp. 1103–1122.

Reichle, Rolf H, Dennis B McLaughlin, and Dara Entekhabi (2002). "Hydrologic data assimilation with the ensemble Kalman filter". In: *Monthly Weather Review* 130.1, pp. 103–114.

Renzullo, Luigi J, AIJM Van Dijk, J-M Perraud, D Collins, B Henderson, H Jin, AB Smith, and DL McJannet (2014). "Continental satellite soil moisture data assimilation improves root-zone moisture analysis for water resources assessment". In: *Journal of Hydrology* 519, pp. 2747–2762.

Riley, WJ and C Shen (2014). "Characterizing coarse-resolution watershed soil moisture heterogeneity using fine-scale simulations". In: *Hydrology and Earth System Sciences* 18.7, pp. 2463–2483.

Robinson, David A, Colin S Campbell, Jan W Hopmans, Brian K Hornbuckle, Scott B Jones, Rosemary Knight, Fred Ogden, John Selker, and Ole Wendroth (2008). "Soil moisture measurement for ecological and hydrological watershed-scale observatories: A review". In: *Vadose zone journal* 7.1, pp. 358–389.

Robock, Alan, Konstantin Y Vinnikov, Govindarajalu Srinivasan, Jared K Entin, Steven E Hollinger, Nina A Speranskaya, Suxia Liu, and A Namkhai (2000). "The global soil moisture data bank". In: *Bulletin of the American Meteorological Society* 81.6, pp. 1281–1300.

Roebeling, RA, ELA Wolters, JF Meirink, and H Leijnse (2012). "Triple collocation of summer precipitation retrievals from SEVIRI over Europe with gridded rain gauge and weather radar data". In: *Journal of hydrometeorology* 13.5, pp. 1552–1566.

Rummler, Thomas, Joel Arnault, David Gochis, and Harald Kunstmann (2019). "Role of lateral terrestrial water flow on the regional water cycle in a complex terrain region: Investigation

with a fully coupled model system". In: *Journal of Geophysical Research: Atmospheres* 124.2, pp. 507–529.

Ryu, Dongryeol, Wade T Crow, Xiwu Zhan, and Thomas J Jackson (2009). "Correcting unintended perturbation biases in hydrologic data assimilation". In: *Journal of hydrometeorology* 10.3, pp. 734–750.

Saf, H (2021). *Metop ASCAT surface soil moisture climate data record v7 12.5 km sampling (H119)*. Accessed Jul.1,2023. DOI: 10.15770/EUM_SAF_H_0009. URL: http://doi.org/10.15770/EUM%5C_SAF%5C_H%5C_0009.

Sahoo, Alok Kumar, Gabriëlle JM De Lannoy, Rolf H Reichle, and Paul R Houser (2013). "Assimilation and downscaling of satellite observed soil moisture over the Little River Experimental Watershed in Georgia, USA". In: *Advances in Water Resources* 52, pp. 19–33.

Salcedo-Sanz, Sancho, Pedram Ghamisi, María Piles, Martin Werner, Lucas Cuadra, A Moreno-Martínez, Emma Izquierdo-Verdiguier, Jordi Muñoz-Marí, Amirhosein Mosavi, and Gustau Camps-Valls (2020). "Machine learning information fusion in Earth observation: A comprehensive review of methods, applications and data sources". In: *Information Fusion* 63, pp. 256–272.

Sawada, Yohei (2020). "Do surface lateral flows matter for data assimilation of soil moisture observations into hyperresolution land models?" In: *Hydrology and Earth System Sciences* 24.8, pp. 3881–3898.

Sawada, Yohei, Toshio Koike, and Jeffrey P Walker (2015). "A land data assimilation system for simultaneous simulation of soil moisture and vegetation dynamics". In: *Journal of Geophysical Research: Atmospheres* 120.12, pp. 5910–5930.

Schaap, Marcel G, Feike J Leij, and Martinus Th Van Genuchten (2001). "Rosetta: A computer program for estimating soil hydraulic parameters with hierarchical pedotransfer functions". In: *Journal of hydrology* 251.3-4, pp. 163–176.

Scherrer, Samuel, Gabriëlle De Lannoy, Zdenko Heyvaert, Michel Bechtold, Clement Albergel, Tarek S El-Madany, and Wouter Dorigo (2023). "Bias-blind and bias-aware assimilation of leaf area index into the Noah-MP land surface model over Europe". In: *Hydrology and Earth System Sciences* 27.22, pp. 4087–4114.

Schmugge, Td (1978). "Remote sensing of surface soil moisture". In: *Journal of Applied Meteorology (1962-1982)*, pp. 1549–1557.

Schmugge, Thomas, Peggy E O'Neill, and James R Wang (1986). "Passive microwave soil moisture research". In: *IEEE Transactions on Geoscience and Remote Sensing* 1, pp. 12–22.

Schrön, M, M Köhli, L Scheiffele, J Iwema, HR Bogena, L Lv, E Martini, G Baroni, R Rosolem, J Weimar, et al. (2017a). "Spatial sensitivity of cosmic-ray neutron sensors applied to improve calibration and validation". In: *Hydrol. Earth Syst. Sci* 21, pp. 5009–5030.

Schrön, Martin, Markus Köhli, Lena Scheiffele, Joost Iwema, Heye R Bogena, Ling Lv, Edoardo Martini, Gabriele Baroni, Rafael Rosolem, Jannis Weimar, et al. (2017b). "Improving calibration and validation of cosmic-ray neutron sensors in the light of spatial sensitivity". In: *Hydrology and Earth System Sciences* 21.10, pp. 5009–5030.

Schwingshackl, Clemens, Martin Hirschi, and Sonia I Seneviratne (2017). "Quantifying spatiotemporal variations of soil moisture control on surface energy balance and near-surface air temperature". In: *Journal of Climate* 30.18, pp. 7105–7124.

Scipal, K, T Holmes, R De Jeu, V Naeimi, and W Wagner (2008). "A possible solution for the problem of estimating the error structure of global soil moisture data sets". In: *Geophysical Research Letters* 35.24.

Scipal, Klaus, Wouter Dorigo, and Richard deJeu (2010). "Triple collocation–A new tool to determine the error structure of global soil moisture products". In: *2010 IEEE International Geoscience and Remote Sensing Symposium*. IEEE, pp. 4426–4429.

Sellers, Piers J, RE Dickinson, DA Randall, Alan K Betts, Forrest G Hall, Joseph A Berry, GJ Collatz, AS Denning, Harold Alfred Mooney, Carlos A Nobre, et al. (1997). "Modeling the exchanges of energy, water, and carbon between continents and the atmosphere". In: *Science* 275.5299, pp. 502–509.

Senatore, Alfonso, Giuseppe Mendicino, David J Gochis, Wei Yu, David N Yates, and Harald Kunstmann (2015). "Fully coupled atmosphere-hydrology simulations for the central M editerranean: Impact of enhanced hydrological parameterization for short and long time scales". In: *Journal of Advances in Modeling Earth Systems* 7.4, pp. 1693–1715.

Seneviratne, Sonia I, Thierry Corti, Edouard L Davin, Martin Hirschi, Eric B Jaeger, Irene Lehner, Boris Orlowsky, and Adriaan J Teuling (2010). "Investigating soil moisture–climate interactions in a changing climate: A review". In: *Earth-Science Reviews* 99.3-4, pp. 125–161.

Seo, Eunkyo, Myong-In Lee, and Rolf H Reichle (2021). "Assimilation of SMAP and ASCAT soil moisture retrievals into the JULES land surface model using the Local Ensemble Transform Kalman Filter". In: *Remote sensing of Environment* 253, p. 112222.

Shen, Chaopeng, Jie Niu, and Mantha S Phanikumar (2013). "Evaluating controls on coupled hydrologic and vegetation dynamics in a humid continental climate watershed using a subsurface-land surface processes model". In: *Water Resources Research* 49.5, pp. 2552–2572.

Shi, Yuning, Kenneth J Davis, Christopher J Duffy, and Xuan Yu (2013). "Development of a coupled land surface hydrologic model and evaluation at a critical zone observatory". In: *Journal of Hydrometeorology* 14.5, pp. 1401–1420.

Shrestha, P, W Kurtz, G Vogel, J-P Schulz, M Sulis, H-J Hendricks Franssen, S Kollet, and C Simmer (2018). "Connection between root zone soil moisture and surface energy flux partitioning using modeling, observations, and data assimilation for a temperate grassland site in Germany". In: *Journal of Geophysical Research: Biogeosciences* 123.9, pp. 2839–2862.

Shrestha, P, M Sulis, M Masbou, S Kollet, and C Simmer (2014). "A scale-consistent terrestrial systems modeling platform based on COSMO, CLM, and ParFlow". In: *Monthly weather review* 142.9, pp. 3466–3483.

Siami-Namini, Sima, Neda Tavakoli, and Akbar Siami Namin (2018). "A comparison of ARIMA and LSTM in forecasting time series". In: *2018 17th IEEE international conference on machine learning and applications (ICMLA)*. IEEE, pp. 1394–1401.

Singh, Abhilash, Kumar Gaurav, Gaurav Kailash Sonkar, and Cheng-Chi Lee (2023). "Strategies to measure soil moisture using traditional methods, automated sensors, remote sensing, and machine learning techniques: review, bibliometric analysis, applications, research findings, and future directions". In: *IEEE Access*.

Small, Eric E and Shirley A Kurc (2003). "Tight coupling between soil moisture and the surface radiation budget in semiarid environments: Implications for land-atmosphere interactions". In: *Water Resources Research* 39.10.

Soltani, Samira Sadat, Marwan Fahs, Ahmad Al Bitar, and Behzad Ataie-Ashtiani (2022). "Improvement of soil moisture and groundwater level estimations using a scale-consistent river parameterization for the coupled ParFlow-CLM hydrological model: A case study of the Upper Rhine Basin". In: *Journal of hydrology* 610, p. 127991.

Soulis, Eric D, Kenneth R Snelgrove, Nicholas Kouwen, Frank Seglenieks, and Diana L Verseghy (2000). "Towards closing the vertical water balance in Canadian atmospheric models: coupling of the land surface scheme CLASS with the distributed hydrological model WATFLOOD". In: *Atmosphere-ocean* 38.1, pp. 251–269.

Sridhar, Venkataramana, Mirza M Billah, and John W Hildreth (2018). "Coupled surface and groundwater hydrological modeling in a changing climate". In: *Groundwater* 56.4, pp. 618–635.

Stillman, Susan and Xubin Zeng (2018). "Evaluation of SMAP soil moisture relative to five other satellite products using the climate reference network measurements over USA". In: *IEEE Transactions on Geoscience and Remote Sensing* 56.11, pp. 6296–6305.

Stoffelen, Ad (1998). "Toward the true near-surface wind speed: Error modeling and calibration using triple collocation". In: *Journal of geophysical research: oceans* 103.C4, pp. 7755–7766.

Strebel, Lukas, Heye Bogena, Harry Vereecken, Mie Andreasen, Sergio Aranda-Barranco, and Harrie-Jan Hendricks Franssen (2024). "Evapotranspiration prediction for European forest sites does not improve with assimilation of in situ soil water content data". In: *Hydrology and Earth System Sciences* 28.4, pp. 1001–1026.

Su, Chun-Hsu, Dongryeol Ryu, Wade T Crow, and Andrew W Western (2014). "Beyond triple collocation: Applications to soil moisture monitoring". In: *Journal of Geophysical Research: Atmospheres* 119.11, pp. 6419–6439.

Su, Zhongbo, J Wen, Laura Dente, R Van Der Velde, Lin Wang, Yaoming Ma, Kun Yang, and Zhengguo Hu (2011). "The Tibetan Plateau observatory of plateau scale soil moisture and soil temperature (Tibet-Obs) for quantifying uncertainties in coarse resolution satellite and model products". In: *Hydrology and earth system sciences* 15.7, pp. 2303–2316.

Sulis, Mauro, J Keune, P Shrestha, C Simmer, and SJ Kollet (2018). "Quantifying the impact of subsurface-land surface physical processes on the predictive skill of subseasonal mesoscale

atmospheric simulations". In: *Journal of Geophysical Research: Atmospheres* 123.17, pp. 9131–9151.

Sulis, Mauro, John L Williams, Prabhakar Shrestha, Malte Diederich, Clemens Simmer, Stefan J Kollet, and Reed M Maxwell (2017). "Coupling groundwater, vegetation, and atmospheric processes: A comparison of two integrated models". In: *Journal of Hydrometeorology* 18.5, pp. 1489–1511.

Talone, Marco, Adriano Camps, Alessandra Monerris, Mercè Vall-Llossera, Paolo Ferrazzoli, and Mara Piles (2007). "Surface topography and mixed-pixel effects on the simulated L-band brightness temperatures". In: *IEEE transactions on geoscience and remote sensing* 45.7, pp. 1996–2003.

Tangdamrongsub, Natthachet, Shin-Chan Han, In-Young Yeo, Jianzhi Dong, Susan C Steele-Dunne, Garry Willgoose, and Jeffrey P Walker (2020). "Multivariate data assimilation of GRACE, SMOS, SMAP measurements for improved regional soil moisture and groundwater storage estimates". In: *Advances in Water Resources* 135, p. 103477.

Terasaki, Koji and Takemasa Miyoshi (2024). "Including the horizontal observation error correlation in the ensemble Kalman filter: idealized experiments with NICAM-LETKF". In: *Monthly Weather Review* 152.1, pp. 277–293.

Teuling, AJ, Sonia I Seneviratne, C Williams, and PA Troch (2006). "Observed timescales of evapotranspiration response to soil moisture". In: *Geophysical Research Letters* 33.23.

Tian, Jiaxin, Jun Qin, Kun Yang, Long Zhao, Yingying Chen, Hui Lu, Xin Li, and Jiancheng Shi (2022). "Improving surface soil moisture retrievals through a novel assimilation algorithm to estimate both model and observation errors". In: *Remote Sensing of Environment* 269, p. 112802.

Tian, W, X Li, G-D Cheng, X-S Wang, and BX Hu (2012). "Coupling a groundwater model with a land surface model to improve water and energy cycle simulation". In: *Hydrology and Earth System Sciences* 16.12, pp. 4707–4723.

Tian, Zhengchao, Zizhong Li, Gang Liu, Baoguo Li, and Tusheng Ren (2016). "Soil water content determination with cosmic-ray neutron sensor: Correcting aboveground hydrogen effects with thermal/fast neutron ratio". In: *Journal of Hydrology* 540, pp. 923–933.

Tiemann, Lisa K and Sharon A Billings (2011). "Changes in variability of soil moisture alter microbial community C and N resource use". In: *Soil Biology and Biochemistry* 43.9, pp. 1837–1847.

Tran, Hoang, Elena Leonarduzzi, Luis De la Fuente, Robert Bruce Hull, Vineet Bansal, Calla Chennault, Pierre Gentine, Peter Melchior, Laura E Condon, and Reed M Maxwell (2021). "Development of a deep learning emulator for a distributed groundwater–surface water model: ParFlow-ML". In: *Water* 13.23, p. 3393.

Trugman, AT, D Medvigy, JS Mankin, and WRL Anderegg (2018). "Soil moisture stress as a major driver of carbon cycle uncertainty". In: *Geophysical Research Letters* 45.13, pp. 6495–6503.

Uebel, M and A Bott (2018). "Influence of complex terrain and anthropogenic emissions on atmospheric CO2 patterns–a high-resolution numerical analysis". In: *Quarterly Journal of the Royal Meteorological Society* 144.710, pp. 34–47.

Ukkola, Anna M, Ned Haughton, Martin G De Kauwe, Gab Abramowitz, and Andy J Pitman (2017). "FluxnetLSM R package (v1. 0): A community tool for processing FLUXNET data for use in land surface modelling". In: *Geoscientific Model Development* 10.9, pp. 3379–3390.

Ulaby, FT, RK Moore, and AK Fung (1982). *Microwave remote sensing: Active and passive. Volume 2-Radar remote sensing and surface scattering and emission theory.* Artech House.

Valcke, S (2013). "The OASIS3 coupler: A European climate modelling community software". In: *Geoscientific Model Development* 6.2, pp. 373–388.

Van Genuchten, M Th (1980). "A closed-form equation for predicting the hydraulic conductivity of unsaturated soils". In: *Soil science society of America journal* 44.5, pp. 892–898.

Vergopolan, Noemi, Nathaniel W Chaney, Hylke E Beck, Ming Pan, Justin Sheffield, Steven Chan, and Eric F Wood (2020). "Combining hyper-resolution land surface modeling with SMAP brightness temperatures to obtain 30-m soil moisture estimates". In: *Remote Sensing of Environment* 242, p. 111740.

Vreugdenhil, Mariette, Wolfgang Wagner, Bernhard Bauer-Marschallinger, Isabella Pfeil, Irene Teubner, Christoph Rüdiger, and Peter Strauss (2018). "Sensitivity of Sentinel-1 backscatter to vegetation dynamics: An Austrian case study". In: *Remote Sensing* 10.9, p. 1396.

Wagner, Wolfgang, Sebastian Hahn, Richard Kidd, Thomas Melzer, Zoltan Bartalis, Stefan Hasenauer, Julia Figa, Patricia De Rosnay, Alexander Jann, Stefan Schneider, et al. (2013). "The ASCAT soil moisture product: a review of its". In: *Meteorologische Zeitschrift* 22.1, pp. 1–29.

Walker, Jeffrey P, Garry R Willgoose, and Jetse D Kalma (2004). "In situ measurement of soil moisture: a comparison of techniques". In: *Journal of Hydrology* 293.1-4, pp. 85–99.

Walker, Victoria A, Brian K Hornbuckle, Michael H Cosh, and John H Prueger (2019). "Seasonal evaluation of SMAP soil moisture in the US corn belt". In: *Remote Sensing* 11.21, p. 2488.

Wallace, Jim, Craig Macfarlane, Dave McJannet, Tim Ellis, Andrew Grigg, and Albert Van Dijk (2013). "Evaluation of forest interception estimation in the continental scale Australian Water Resources Assessment–Landscape (AWRA-L) model". In: *Journal of Hydrology* 499, pp. 210–223.

Wanders, Niko, Marc FP Bierkens, Steven M de Jong, Ad de Roo, and Derek Karssenberg (2014). "The benefits of using remotely sensed soil moisture in parameter identification of large-scale hydrological models". In: *Water resources research* 50.8, pp. 6874–6891.

Wang, JR and BJ Choudhury (1981). "Remote sensing of soil moisture content, over bare field at 1.4 GHz frequency". In: *Journal of Geophysical Research: Oceans* 86.C6, pp. 5277–5282.

Wang, Yi, Wenke Wang, Zhitong Ma, Ming Zhao, Wanxin Li, Xinyue Hou, Jie Li, Fei Ye, and Wenjing Ma (2023). "A deep learning approach based on physical constraints for predicting soil moisture in unsaturated zones". In: *Water Resources Research* 59.11, e2023WR035194.

Wang, Zengyan, Tao Che, Tianjie Zhao, Liyun Dai, Xiaojun Li, and Jean-Pierre Wigneron (2021). "Evaluation of SMAP, SMOS, and AMSR2 soil moisture products based on distributed ground observation network in cold and arid regions of China". In: *IEEE Journal of Selected Topics in Applied Earth Observations and Remote Sensing* 14, pp. 8955–8970.

Wang, Zhuangji, Dennis Timlin, Mikhail Kouznetsov, David Fleisher, Sanai Li, Katherine Tully, and Vangimalla Reddy (2020). "Coupled model of surface runoff and surface-subsurface water movement". In: *Advances in Water Resources* 137, p. 103499.

Wigneron, J-P, TJ Jackson, P O'neill, Gabrielle De Lannoy, Patricia de Rosnay, JP Walker, P Ferrazzoli, V Mironov, Simone Bircher, JP Grant, et al. (2017). "Modelling the passive microwave signature from land surfaces: A review of recent results and application to the L-band SMOS & SMAP soil moisture retrieval algorithms". In: *Remote Sensing of Environment* 192, pp. 238–262.

Will, Bianca and Ilona Rolfes (2013). "Comparative study of moisture measurements by time domain transmissometry". In: *SENSORS, 2013 IEEE*. IEEE, pp. 1–4.

Wood, Eric F, Joshua K Roundy, Tara J Troy, LPH Van Beek, Marc FP Bierkens, Eleanor Blyth, Ad de Roo, Petra Döll, Mike Ek, James Famiglietti, et al. (2011). "Hyperresolution global land surface modeling: Meeting a grand challenge for monitoring Earth's terrestrial water". In: *Water Resources Research* 47.5.

Xie, Qiuxia, Li Jia, Massimo Menenti, and Guangcheng Hu (2022). "Global soil moisture data fusion by Triple Collocation Analysis from 2011 to 2018". In: *Scientific Data* 9.1, p. 687.

Xu, Xiaoyong and Steven K Frey (2021). "Validation of SMOS, SMAP, and ESA CCI soil moisture over a Humid Region". In: *IEEE Journal of Selected Topics in Applied Earth Observations and Remote Sensing* 14, pp. 10784–10793.

Xu, Xiaoyong, Bryan A Tolson, Jonathan Li, and Bruce Davison (2017). "Comparison of X-band and L-band soil moisture retrievals for land data assimilation". In: *IEEE Journal of Selected Topics in Applied Earth Observations and Remote Sensing* 10.9, pp. 3850–3860.

Xu, Xiaoyong, Bryan A Tolson, Jonathan Li, Ralf M Staebler, Frank Seglenieks, Amin Haghnegahdar, and Bruce Davison (2015). "Assimilation of SMOS soil moisture over the Great Lakes basin". In: *Remote Sensing of Environment* 169, pp. 163–175.

Xu, Zexuan, Erica R Siirila-Woodburn, Alan M Rhoades, and Daniel Feldman (2023). "Sensitivities of subgrid-scale physics schemes, meteorological forcing, and topographic radiation in atmosphere-through-bedrock integrated process models: a case study in the Upper Colorado River basin". In: *Hydrology and Earth System Sciences* 27.9, pp. 1771–1789.

Al-Yaari, Amen, J-P Wigneron, Agnès Ducharne, Yann Kerr, Patricia De Rosnay, Richard De Jeu, Ajit Govind, A Al Bitar, Clément Albergel, Joaquin Munoz-Sabater, et al. (2014). "Global-scale evaluation of two satellite-based passive microwave soil moisture datasets (SMOS and AMSR-E) with respect to Land Data Assimilation System estimates". In: *Remote Sensing of Environment* 149, pp. 181–195.

Yair, A (2008). "Effects of surface runoff and subsurface flow on the spatial variability of water resources in longitudinal dunes". In: *Arid Dune Ecosystems: The Nizzana Sands in the Negev Desert*. Springer, pp. 251–269.

Yang, Kun, La Zhu, Yingying Chen, Long Zhao, Jun Qin, Hui Lu, Wenjun Tang, Menglei Han, Baohong Ding, and Nan Fang (2016). "Land surface model calibration through microwave data assimilation for improving soil moisture simulations". In: *Journal of Hydrology* 533, pp. 266–276.

Yang, Yanqing, Jianyun Zhang, Zhenxin Bao, Tianqi Ao, Guoqing Wang, Houfa Wu, and Jie Wang (2021a). "Evaluation of multi-source soil moisture datasets over central and eastern agricultural area of China using in situ monitoring network". In: *Remote Sensing* 13.6, p. 1175.

Yang, Zhao, Maoyi Huang, Larry K Berg, Yun Qian, William I Gustafson, Yuanhao Fang, Ying Liu, Jerome D Fast, Koichi Sakaguchi, and Sheng-Lun Tai (2021b). "Impact of lateral flow on surface water and energy budgets over the Southern Great Plains-A modeling study". In: *Journal of Geophysical Research: Atmospheres* 126.12, e2020JD033659.

Yetbarek, Ephrem, Saurabh Kumar, and Richa Ojha (2020). "Effects of soil heterogeneity on subsurface water movement in agricultural fields: A numerical study". In: *Journal of Hydrology* 590, p. 125420.

Yilmaz, M Tugrul and Wade T Crow (2014). "Evaluation of assumptions in soil moisture triple collocation analysis". In: *Journal of Hydrometeorology* 15.3, pp. 1293–1302.

Yilmaz, MT, WT Crow, MC Anderson, and C Hain (2012). "An objective methodology for merging satellite-and model-based soil moisture products". In: *Water Resources Research* 48.11.

Yin, Jifu, Xiwu Zhan, Youfei Zheng, Christopher R Hain, Jicheng Liu, and Li Fang (2015). "Optimal ensemble size of ensemble Kalman filter in sequential soil moisture data assimilation". In: *Geophysical Research Letters* 42.16, pp. 6710–6715.

Yongjiu, Dai and Zeng Qingcun (1997). "A land surface model (IAP94) for climate studies part I: Formulation and validation in off-line experiments". In: *Advances in Atmospheric Sciences* 14.4, pp. 433–460.

Zacharias, Steffen, Heye Bogena, Luis Samaniego, Matthias Mauder, Roland Fuß, Thomas Pütz, Mark Frenzel, Mike Schwank, Cornelia Baessler, Klaus Butterbach-Bahl, et al. (2011). "A network of terrestrial environmental observatories in Germany". In: *Vadose zone journal* 10.3, pp. 955–973.

Zamani, Ahmadreza, Ahmadreza Azimian, Arnold Heemink, and Dimitri Solomatine (2010). "Non-linear wave data assimilation with an ANN-type wind-wave model and Ensemble Kalman Filter (EnKF)". In: *Applied Mathematical Modelling* 34.8, pp. 1984–1999.

Zhang, Hongjuan, Wolfgang Kurtz, Stefan Kollet, Harry Vereecken, and Harrie-Jan Hendricks Franssen (2018). "Comparison of different assimilation methodologies of groundwater levels to improve predictions of root zone soil moisture with an integrated terrestrial system model". In: *Advances in water resources* 111, pp. 224–238.

Zhang, Ke, Li-jun Chao, Qing-qing Wang, Ying-chun Huang, Rong-hua Liu, Yang Hong, Yong Tu, Wei Qu, and Jin-yin Ye (2019a). "Using multi-satellite microwave remote sensing observations for retrieval of daily surface soil moisture across China". In: *Water Science and Engineering* 12.2, pp. 85–97.

Zhang, Lanhui, Chansheng He, Mingmin Zhang, and Yi Zhu (2019b). "Evaluation of the SMOS and SMAP soil moisture products under different vegetation types against two sparse in situ networks over arid mountainous watersheds, Northwest China". In: *Science China Earth Sciences* 62, pp. 703–718.

Zhang, Ning, Steven M Quiring, and Trent W Ford (2021a). "Blending Noah, SMOS, and in situ soil moisture using multiple weighting and sampling schemes". In: *Journal of Hydrometeorology* 22.7, pp. 1835–1854.

Zhang, Runze, Seokhyeon Kim, and Ashish Sharma (2019c). "A comprehensive validation of the SMAP Enhanced Level-3 Soil Moisture product using ground measurements over varied climates and landscapes". In: *Remote sensing of environment* 223, pp. 82–94.

Zhang, Yonggen and Marcel G Schaap (2017). "Weighted recalibration of the Rosetta pedotransfer model with improved estimates of hydraulic parameter distributions and summary statistics (Rosetta3)". In: *Journal of Hydrology* 547, pp. 39–53.

Zhang, Zhenyu, Joel Arnault, Patrick Laux, Ning Ma, Jianhui Wei, Shasha Shang, and Harald Kunstmann (2021b). "Convection-permitting fully coupled WRF-Hydro ensemble simulations in high mountain environment: impact of boundary layer-and lateral flow parameterizations on land–atmosphere interactions". In: *Climate Dynamics*, pp. 1–22.

Zhao, Haojin, Carsten Montzka, Roland Baatz, Harry Vereecken, and Harrie-Jan Hendricks Franssen (2021a). "The Importance of Subsurface Processes in Land Surface Modeling over a Temperate Region: An Analysis with SMAP, Cosmic Ray Neutron Sensing and Triple Collocation Analysis". In: *Remote Sensing* 13.16, p. 3068.

Zhao, Haojin, Carsten Montzka, Harry Vereecken, and Harrie-Jan Hendricks Franssen (2024). "A comparative analysis of remote sensing soil moisture datasets fusion methods: novel LSTM approach versus widely used triple collocation technique". In: *IEEE Journal of Selected Topics in Applied Earth Observations and Remote Sensing* 17, pp. 16659–16671.

Zhao, Hong, Yijian Zeng, Xujun Han, and Zhongbo Su (2023). "Retrieving Soil Physical Properties by Assimilating SMAP Brightness Temperature Observations into the Community Land Model". In: *Sensors* 23.5, p. 2620.

Zhao, Tianjie, Jiancheng Shi, Dara Entekhabi, Thomas J Jackson, Lu Hu, Zhiqing Peng, Panpan Yao, Shangnan Li, and Chuen Siang Kang (2021b). "Retrievals of soil moisture and vegetation optical depth using a multi-channel collaborative algorithm". In: *Remote Sensing of Environment* 257, p. 112321.

Zhao, Tianjie, Jiancheng Shi, Liqing Lv, Hongxin Xu, Deqing Chen, Qian Cui, Thomas J Jackson, Guangjian Yan, Li Jia, Liangfu Chen, et al. (2020). "Soil moisture experiment in the Luan River supporting new satellite mission opportunities". In: *Remote Sensing of Environment* 240, p. 111680.

Zheng, Donghai, Xin Wang, Rogier Van Der Velde, Paolo Ferrazzoli, Jun Wen, Zuoliang Wang, Mike Schwank, Andreas Colliander, Rajat Bindlish, and Zhongbo Su (2018). "Impact of surface roughness, vegetation opacity and soil permittivity on L-band microwave emission and soil moisture retrieval in the third pole environment". In: *Remote sensing of environment* 209, pp. 633–647.

Zhou, Jianhong, Wade T Crow, Zhiyong Wu, Jianzhi Dong, Hai He, and Huihui Feng (2021). "A triple collocation-based 2D soil moisture merging methodology considering spatial and temporal non-stationary errors". In: *Remote Sensing of Environment* 263, p. 112509.

– (2022). "Improving soil moisture assimilation efficiency via model calibration using SMAP surface soil moisture climatology information". In: *Remote Sensing of Environment* 280, p. 113161.

Zhou, Jianhong, Zhiyong Wu, Wade T Crow, Jianzhi Dong, and Hai He (2020). "Improving spatial patterns prior to land surface data assimilation via model calibration using SMAP surface soil moisture data". In: *Water Resources Research* 56.10, e2020WR027770.

Zhou, Jingwei, Adriaan J Teuling, Sonia I Seneviratne, and Annette L Hirsch (2024). "Soil moisture-temperature coupling increases population exposure to future heatwaves". In: *Earth's Future* 12.7, e2024EF004697.

Zhu, Luyao, Hongquan Wang, Cheng Tong, Wenbin Liu, and Benxu Du (2019). "Evaluation of ESA active, passive and combined soil moisture products using upscaled ground measurements". In: *Sensors* 19.12, p. 2718.

Zhu, Xuchao, Ming'an Shao, Chen Zeng, Xiaoxu Jia, Laiming Huang, Yangjian Zhang, and Juntao Zhu (2016). "Application of cosmic-ray neutron sensing to monitor soil water content in an alpine meadow ecosystem on the northern Tibetan Plateau". In: *Journal of Hydrology* 536, pp. 247–254.

Zipper, Samuel C, Mehmet Evren Soylu, Eric G Booth, and Steven P Loheide (2015). "Untangling the effects of shallow groundwater and soil texture as drivers of subfield-scale yield variability". In: *Water Resources Research* 51.8, pp. 6338–6358.

Zreda, Marek, Darin Desilets, TPA Ferré, and Russell L Scott (2008). "Measuring soil moisture content non-invasively at intermediate spatial scale using cosmic-ray neutrons". In: *Geophysical research letters* 35.21.

Zreda, Marek, WJ Shuttleworth, Xubin Zeng, Chris Zweck, D Desilets, T Franz, and R Rosolem (2012). "COSMOS: The cosmic-ray soil moisture observing system". In: *Hydrology and Earth System Sciences* 16.11, pp. 4079–4099.

Acknowledgments

First and foremost, I am grateful to my supervisor, Prof.Dr.Harrie-Jan Hendricks Franssen, for his guidance and expertise throughout my PhD studies. We had many meetings and discussions, and he gave me loads of great ideas and solutions. He always made me think about things in a different way and made me work harder to be the best I can be. I am also grateful to the China Scholarship Council (CSC) for providing me with financial support for work and life. I would like to extend my thanks to Dr. Carsten Montzka for sharing his vast knowledge of remote sensing and to Dr. Johannes Keller for his instrumental help in navigating the TSMP-PDAF framework on HPCs.

I would like to acknowledge:

Prof. Dr. Harry Vereecken for fostering a supportive scientific environment for my PhD studies. His kind suggestions and feedback on PhD reports were very helpful.

Dr. Roland Baatz for his help in improving my research papers.

Dr. Heye Bogena and Dr. Alexander Graf for providing the CRNS and EC measurement data, which were crucial for my research.

A special thanks to my colleagues at The IBG-3 for the great time working together over the past five years.

I am also grateful to the Juelich Supercomputer Centre for providing the computational and storage resources on JUWELS and JURECA that were essential for this research. My gratitude also extends to the Dragon5 cooperation between ESA and the Ministry of Science and Technology (MOST) of P.R. China.

Last but not least, I would like to express my deepest gratitude to my parents for their love and support throughout this journey. And to my amazing husband, Zhaolin, thank you for always having my back when I am not at my best and joining me in the adventure of creating our own.

Band / Volume 711
No-Regret-Maßnahmen der integrierten Netzplanung mit Fokus auf Wasserstoff
T. G. Busch (2026), xx, 325 pp
ISBN: 978-3-95806-922-0 (Print)
ISBN: 978-3-95806-923-7 (E-Book)

Band / Volume 712
Data-Driven Modeling for Digital Representations in Energy Systems
M. C. Zimmer (2026), xv, 166 pp
ISBN: 978-3-95806-926-8 (Print)
ISBN: 978-3-95806-927-5 (E-Book)

Band / Volume 713
Towards integrated PV applications: development of lightweight silicon heterojunction solar modules and their damp-heat and UV stability
K. Zhang (2026), iii, 179 pp
ISBN: 978-3-95806-928-2 (Print)
ISBN: 978-3-95806-929-9 (E-Book)

Band / Volume 714
Zinc-Based Catalysts for the Electrochemical CO_2 Reduction
I. Stamatelos (2026), vii, 136 pp
ISBN: 978-3-95806-932-9 (Print)
ISBN: 978-3-95806-933-6 (E-Book)

Band / Volume 715
Charakterisierung innovativer keramischer Materialien für Elektrolysezellen
L. P. Wehner (2026), xiv, 110 pp
ISBN: 978-3-95806-936-7 (Print)
ISBN: 978-3-95806-937-4 (E-Book)

Band / Volume 716
Process Optimization and Scale-Up for $Ba(Zr,Ce,Y)O_{3-\delta}$-Based Proton-Conducting Electrolysis Half-Cells
L.-A. Schäfer (2026), iv, 141 pp
ISBN: 978-3-95806-940-4 (Print)
ISBN: 978-3-95806-941-1 (E-Book)

Schriften des Forschungszentrums Jülich
Reihe Energie & Umwelt / Energy & Environment

Band / Volume 717
Kostenoptimale Energieausfälle in erneuerbaren Energiesystemen
D. Franzmann (2026), xix, 235 pp
ISBN: 978-3-95806-942-8 (Print)
ISBN: 978-3-95806-943-5 (E-Book)

Band / Volume 718
***Semiclassical Thermodynamics* of Metal-Solution Interfaces: A Density-Potential Functional Theory Study**
Z. Zhang (2026), 143 pp
ISBN: 978-3-95806-946-6 (Print)
ISBN: 978-3-95806-947-3 (E-Book)

Band / Volume 719
Development and Characterization of the Airborne Chemical Ionization Mass Spectrometer FunMass-C for Atmospheric Trace Gas Measurements
S. Alber (2026), xli, 265 pp
ISBN: 978-3-95806-948-0 (Print)
ISBN: 978-3-95806-949-7 (E-Book)

Band / Volume 720
Material design and stability of All-Solid-State Lithium batteries
F. H. Al-Jaljouli (2026), xv, 174 pp
ISBN: 978-3-95806-950-3 (Print)
ISBN: 978-3-95806-951-0 (E-Book)

Band / Volume 721
Towards improved representation of the hydrological cycle by assimilating multi-source remotely sensed soil moisture data in terrestrial system models
H. Zhao (2026), XVI, 139 pp
ISBN: 978-3-95806-952-7 (Print)
ISBN: 978-3-95806-953-4 (E-Book)

Weitere ***Schriften des Verlags im Forschungszentrum Jülich*** unter
http://wwwzb1.fz-juelich.de/verlagextern1/index.asp

Energie & Umwelt / Energy & Environment
Band / Volume 721
ISBN 978-3-95806-953-4

Mitglied der Helmholtz-Gemeinschaft

JÜLICH
Forschungszentrum